DEVELOPING EXOCOUNTER PLATFORM FOR THE DETECTION OF PLACENTA SMALL EXTRACELLULAR VESICLE (psEV) IN SERUM/PLASMA FROM NORMAL PREGNANCY AND PREECLAMPSIA PATIENTS AND DISSECTING THE POTENTIAL ROLE OF psEV ON THE RENAL FUNCTION



Shuhan Jiang

Green Templeton College

A thesis submitted for the degree of Doctor of Philosophy

Trinity term 2023

45,938 words

This thesis is submitted to the University of Oxford in partial fulfilment of the Doctor of Philosophy degree requirements.

The thesis is my work and describes my research, except where otherwise stated.

Copyright © Shuhan Jiang
All rights reserved

Acknowledgements

Looking back to where I started my DPhil journey 4 years ago, I realise how much I have grown and evolved. This personal development is largely due to the incredible people I encountered throughout this journey, who have supported me in countless ways.

First and foremost, I would like to express my deepest gratitude to my supervisors Prof. Manu Vatish and Dr. Wei Zhang, who have guided, supported, and nurtured me throughout my DPhil journey, much like caring parents. Manu has consistently believed in my research ideas and never doubted my capacity to achieve my goals. Wei has not only supported my research but also embraced me as a family member, generously sharing the produce from her garden. Manu and Wei' expertise, mentorship, and genuine interest in my success have been instrumental in shaping my research and inspiring me to pursue my academic goals with passion and dedication.

I would also like to extend my appreciation to my amazing colleagues: Maryam Rahbar, Prassana Logentheran, Carolina Motta Mejia, William Cooke, Emily Mazey, Emily Hyde, Gabriel Jones, Faheem Seedat, Catarina Dos Palmos, Yushi Abe, Qing Cao, and Qian Chen. Additionally, I am grateful to the research midwives Fenella Roseman and Lotoyah Carty, as well as everyone who kindly provided samples for this project.

My heartfelt thanks go to my boyfriend Dr Jiayu Wang who has done an amazing job looking after me and providing valuable insights into my research. Without his amazing cooking for these 4 years, I could have been slimmer. I would like to thank my father Xiaoming Jiang, my mother Bing Ling, and my grandma Yuhua Tan, for their financial and mental support. I am

very grateful to have my gym and volleyball buddies - Jia Wei, Qingze Gu, Hanwen Zhang, Jiaqi Zheng, Jinlin Chen, Emilien Dupont and Julie Lin - for enriching my leisure time.

I would like to thank extraordinary researchers who have generously invested a lot of their time in my research. Dr Katherine Bull supported me for my Transfer and Confirmation viva and has also kindly agreed to my final DPhil viva examiner. Her insights and support have significantly influenced my work. Prof Harpal Randeva has graciously agreed to examine my thesis and will dedicate a lot of time to reviewing my work. I am also grateful to Prof Helen Townley for her involvement in my Transfer viva and Dr Kevin Coward for my Confirmation viva.

Finally, I would like to thank my funding body China Scholarship Council – Fazheng Group – University of Oxford Scholarship for funding my study. I also want to recognize my own hard work during these four years, filled with challenging cycling from Oxford city centre to the JR hospital and the typical rainy UK weather.

List of abbreviations

ACE	Acetate
ALIX	ALG-2 interacting protein X
AFM	Atomic force microscopy
ANOVA	Analysis of variance
BCA	Bicinchonic assay
BG	Background
C19MC	Chromosome 19 microRNA cluster
cDNA	Complementary deoxyribonucleic acid
DEP	Differentially expressed proteins
DLS	Dynamic light scattering
ECL	Chemiluminescence
eNOS	Endothelial nitric oxide synthase
EOPE	Early onset preeclampsia
ESCRT	Endosomal sorting complexes required for transport
EV	Extracellular vesicles
fPBS	Filtered phosphate buffered saline
GEnCs	Glomerular endothelial cells
GFB	Glomerular filtration barrier
HELLP	Haemolysis elevated liver enzymes and low platelets
HUVEC	Human umbilical vein endothelial cells
ILV	Intraluminal vesicle
iNTA	Interferometric nanoparticle tracking analysis

ISEV	International Society for Extracellular Vesicles
LOPE	Late onset preeclampsia
MESF	Molecules of equivalent soluble fluorochrome
mg	Milligrams
mL	Millilitres
m/lEV	Medium/large extracellular vesicle
MVE	Multivesicular endosomes
MVB	Multivesicular bodies
NEP	Neprilysin
NP	Normal pregnancy
NTA	Nanoparticle tracking analysis
PV	Peripheral vein
PBS	phosphate buffered saline
PBST	Phosphate buffered saline with Tween-20
PC	Phosphatidylcholine
PCA	Principle component analysis
PE	Preeclampsia
PEG	Polyethylene glycol
PLAP	Placenta alkaline phosphatase
PL	Placenta lysate
PFP	Platelet free plasma
PS	Phosphatidylserine
psEV	Placental small extracellular vesicles
PPI	Protein-Protein Interaction
PVDF	Polyvinylidene difluoride

RBC	Red blood cell
RNA	Ribonucleic acid
RS	Raman spectroscopy
RT-qPCR	Reverse transcription (quantitative) polymerase chain reaction
SEC	Size exclusion chromatography
sEV	Small extracellular vesicles
sEng	Soluble endoglin
SD	Standard deviation
sFlt-1	Soluble fms-like tyrosine kinase 1
SM	Sphingomyelin
SPR	Surface plasmon resonance
SP-IRIS	Single particle – interferometric reflectance imaging sensor
STB	Syncytiotrophoblast
TBST	Tris-buffered saline with Tween-20
TEM	Transmission electron microscopy
TRIM23	Tripartite motif containing 23
TRPS	Tuneable resistive pulse sensing
TSG101	Tumour susceptibility gene 101
UC	Ultracentrifugation
UF	Ultrafiltration
UV	Uterine vein
WB	Western blot
WWD-EOPE	Women who developed early onset preeclampsia
WWD-LOPE	Women who developed late onset preeclampsia
μg	Micrograms

μL	Microlitres
mL	Millilitre

Abstract

Title: Developing ExoCounter platform for the detection of placenta small extracellular vesicle (psEV) in serum/plasma from normal pregnancy and preeclampsia patients and dissecting the potential role of psEV on the renal function

Name and college: Shuhan Jiang, Green Templeton Colledge

Degree: DPhil in Women's & Reproductive Health

Term and year of submission: Trinity term 2023

Introduction: Preeclampsia (PE) is a complication of pregnancy that affects 2-8% of women worldwide. It is one of the leading causes of maternal deaths and premature birth. PE is characterised by high blood pressure, proteinuria, and/or end-organ damage after 20 weeks of gestation. The placenta is believed to play a crucial role in the development of PE, with altered extracellular vesicle (pEV) being released into the maternal circulation. However, the potential diagnostic utility of pEV for early detection of PE remains unclear. Furthermore, the impact of pEV on renal functions, specifically regarding proteinuria and reduced renal function in PE, is not fully understood. This thesis aims to address these questions and shed light on the involvement of pEV in PE pathogenesis.

Aim: My research investigates the potential of utilizing pEV as a diagnostic tool for early detection of preeclampsia, while also examining the impact of pEV on renal functions in individuals with normal pregnancy (NP) and PE.

Methodology: I have investigated the potential diagnostic value of pEV for early detection of PE, using a novel EV characterising device named ExoCounter. Additionally, I conducted

comprehensive studies to understand the functional and proteomics effects of pEV derived from NP and PE on podocytes, a type of renal cells.

Results: The serum of women who developed early onset preeclampsia (WWD-EOPE) during the first trimester showed significantly higher counts of CD10-placental alkaline phosphatase (PLAP) and CD63-PLAP placental small extracellular vesicle (psEV) compared to normal pregnancy (NP). While previous studies have demonstrated that the levels of CD10-PLAP and CD63-PLAP placental extracellular vesicles (pEV) are elevated in PE compared to NP in the third trimester, this is the first study to report that this elevation can also be detected as early as the first trimester. These psEV can serve as biomarkers to identify patients at risk of developing EOPE, allowing for early intervention. Additionally, psEV isolated from ex vivo placental dual-lobe perfusion were found to be internalized by podocytes. Flow cytometry analysis revealed no significant difference in the levels of podocyte-internalized EV from NP psEV and PE psEV. NP psEV induced increased migration ability in podocytes, potentially through mechanisms involving enhanced nephrin expression and strengthened cytoskeleton filamentous F-actin. On the other hand, PE psEV impaired podocyte adhesion ability and did not stimulate migration, potentially due to the formation of stressed F-actin. Subsequent analysis using proteomics analysis and functional enrichment revealed that differentially expressed proteins (DEPs) in podocytes treated with NP psEV were found to be associated with cellular component organization or biogenesis, intracellular transport, and mitochondrial functions. Conversely, DEPs in podocytes treated with PE psEV were potentially involved in metabolic processes, nitrogen compound metabolic processes, and gene expression.

Conclusions: The findings presented in this thesis have advanced the knowledge of psEV in the context of preeclampsia, offering insights into their diagnostic potential and proposing effective methodologies for their evaluation. Furthermore, the examination of NP and PE

psEV's impact on podocyte functions has provided valuable insights that could guide the development of future therapeutic strategies to enhance maternal and fetal well-being.

Table of Contents

Chapter 1

1.1 Abstract....16

1.2 Extracellular vesicles....17

1.2.1 Biogenesis & Classification....17

1.2.2. The contents of EV's cargo....22

1.2.3 The uptake of EV by recipient cells....24

1.2.4 The diagnostic and therapeutic values of EV....27

1.2.5 The isolation methods of EV....31

Differential Ultracentrifugation (UC)....31
Size exclusion chromatography (SEC)....33
Ultrafiltration....34
Precipitation....34
Affinity-based isolation of EV....35
Isolation placenta-derived EV....36

1.2.6 The EV characterisation methods....38

Protein, DNA/RNA, and total lipids concentration....38
Western blot....39
Single particle tracking analysis....40
Non-cryogenic and cryogenic electron microscopy (EM)....42
Flow cytometry (FCM)....43
Atomic force microscopy (AFM)....45
Surface plasmon resonance (SPR)....46
Raman spectroscopy (RS)....46
Single particle – interferometric reflectance imaging sensor (SP-IRIS)....47
Future of EV characterisation....48

1.3 Placenta biology, preeclampsia (PE) and roles of EV in PE....48

1.4 Glomerular filtration barrier and renal damage in PE....51

1.5 The possible roles of placental EV in renal damage in PE....55

1.7 Conclusion....58

1.8 Reference....59

Chapter 2

2.1 Abstract....84

2.2 Introduction....85

2.3 Aims....88

2.4 Methods....89

2.4.1 Human Subjects and Ethic Approval....89

2.4.2 Isolation of psEV by placental dual-lobe perfusion and serial ultracentrifugation.....90
2.4.3 Plasma sample preparation.....90
2.4.4 Serum sample collection.....91
2.4.5 Western Blot.....92
2.4.6 Transmission Electron Microscopy (TEM).....93
2.4.7 Nanoparticle Tracking Analysis (NTA).....93
2.5.8 Identifying PLAP-associated antigens by MACSPlex Exosome Kit.....94
2.5.9 ExoCounter.....94
2.5.10 Experimental design and flow.....98
2.5.11 Statistical Analysis.....99
2.5 Results.....100
2.5.1 psEV Characterisation.....100
2.5.2 Antibody coating and blocking buffer optimisation for ExoCounter assay using psEV 101
2.5.3 CD63 is determined by MACSPlex kit and confirmed by ExoCounter as the most abundant tetraspanin on psEV.....103
2.5.4 Identify the optimal coating and detecting antibody combination for ExoCounter psEV quantification.....106
2.5.5 ExoCounter assay optimisation for plasma samples.....107
2.5.6 ExoCounter detected higher placenta specific CD63-PLAP sEV counts in uterine vein (UV) compared to paired peripheral vein (PV).....110
2.5.7 The unique psEV profile of WWD-EOPE compared to NP and WWD-LOPE could be observed as early as the first trimester.....110
2.5.8 Counts of psEV detected by ExoCounter were highly consistent in serum and plasma samples from the same donor.....113
2.5.9 Significant higher counts of CD10-PLAP and CD63-PLAP sEV were detected by ExoCounter in WWD-WOPE compared to WWD-LOPE and NP in the first trimester serum samples.....114
2.6 Discussion & Future work.....117
2.7 Reference.....122

Chapter 3

3.1 Abstract.....129
3.2 Introduction.....131
3.3 Aims.....133
3.4 Methods.....133
3.4.1 Human Subjects and Ethic Approval.....133
3.4.2 Placenta perfusion and psEV isolation & characterisation.....134
3.4.3 Western Blot.....134
3.4.4 Podocyte Culture and Differentiation.....134

3.4.5 PKH26 staining of psEV and time course assessment of internalisation of EV by podocyte via flow cytometry and confocal microscopy....135
3.4.6 F-actin staining....137
3.4.7 Podocyte Migration assay....137
3.4.8 Podocyte Adhesion assay....138
3.4.9 Podocyte Viability Assay....138
3.4.10 Podocyte RNA Extraction and quantitative polymerase chain reaction (qPCR)....139
3.4.11 ExoCounter....139
3.4.12 Isolation of Urine EV and Removal of Uromodulin....140
3.4.13 Isolation of red blood cell (RBC) EV by differential ultracentrifugation (UC)....142
3.4.14 Statistical Analysis....143
3.5 Results....144
3.5.1 NaCl is the better method to remove uromodulin in urine....144
3.5.2 The presence of psEV in urine from both NP and PE....146
3.5.3 Podocyte Differentiation....148
3.5.4 RBC sEV characterisation as control for the experiment....150
3.5.5 psEV internalisation by podocytes....151
3.5.6 The influence of psEV on podocytes upon internalisation....155
3.5.7 The mechanism of psEV influence podocytes migration and adhesion ability....157
3.6 Discussion & Future work....160
3.7 Reference....164

Chapter 4

4.1 Abstract....171
4.2 Introduction....173
4.3 Aims....174
4.4 Methods....175
4.4.1 Proteomics experimental design....175
4.4.2 Data cleaning (distribution, missing value, normalization, imputation)....176
4.4.3 Differentially expressed proteins (DEPs) using outlier significance A/B test....176
4.4.4 Protein-protein interaction (PPI) and functional enrichment analysis....177
4.4.5 Western blot....178
4.4.6 Statistical Analysis....179
4.5 Results....180
4.5.1 The initial data cleaning....180
4.5.2 Data imputation....182
4.5.3 Principal component analysis (PCA) plot and cluster analysis....184
4.5.4 Differentially expressed proteins (DEPs)....186

4.5.5 Protein-protein-interaction (PPI) and functional enrichment analysis.....193
4.5.6 DEPs validation through western blot.....202
4.6 Discussion & Future work.....205
4.7 References.....210
Chapter 5
5.1 Final summary.....216
5.2 Limitations.....218
5.3 Future studies.....219
5.4 A step forward.....221
5.6 Final discussion.....229
5.7 Reference.....230
Appendix.....231

CHAPTER 1

Introduction &
Literature Review

Table of contents

1.1 Abstract....16

1.2 Extracellular vesicles....17

1.2.1 Biogenesis & Classification....17

1.2.2. The contents of EV's cargo....22

1.2.3 The uptake of EV by recipient cells....24

1.2.4 The diagnostic and therapeutic values of EV....27

1.2.5 The isolation methods of EV....31

Differential Ultracentrifugation (UC)....31
Size exclusion chromatography (SEC)....33
Ultrafiltration....34
Precipitation....34
Affinity-based isolation of EV....35
Isolation placenta-derived EV....36

1.2.6 The EV characterisation methods....38

Protein, DNA/RNA, and total lipids concentration....38
Western blot....39
Single particle tracking analysis....40
Non-cryogenic and cryogenic electron microscopy (EM)....42
Flow cytometry (FCM)....43
Atomic force microscopy (AFM)....45
Surface plasmon resonance (SPR)....46
Raman spectroscopy (RS)....46
Single particle – interferometric reflectance imaging sensor (SP-IRIS)....47
Future of EV characterisation....48

1.3 Placenta biology, preeclampsia (PE) and roles of EV in PE....48

1.4 Glomerular filtration barrier and renal damage in PE....51

1.5 The possible roles of placental EV in renal damage in PE....55

1.7 Conclusion....58

1.8 Reference....59

1.1 Abstract

Preeclampsia (PE) is a hypertension disorder and the renal system is frequently involved. Renal injury and proteinuria are very common symptoms in PE while the underlying mechanism is not clear. Placenta, as the centre of the pathology of PE, releases extracellular vesicles (EV) into the maternal circulation to influence the functions of the recipient cells. In order to unveil the mechanism of placenta-derived EV on renal functions, reliable methods are needed to isolate and characterise placental EV.

In this chapter, I first did a thorough literature review on EV biogenesis, EV cargos, and EV uptake by the recipient cells. Then I further reviewed the EV isolation and characterisation methods, including methods used for placental EV isolation. Together, this helped to understand the experimental tools I used for EV investigation in my thesis. Next, I have also explored EV's diagnostic and therapeutic value. Then, I reviewed the renal pathology in PE, emphasizing microscopic findings and recent *in vivo* and *in vitro* experimental evidence. Lastly, I explored the possible roles of placental EV on cells forming the glomerular filtration barrier (GFB) and suggested the possible mechanisms of how placental EV influence GFB.

1.2 Extracellular vesicles

1.2.1 Biogenesis & Classification

Extracellular vesicle (EV) are cell-derived lipid bilayer membrane enclosed particles containing diverse biological cargos[1]. EV is a term, which collectively includes microvesicles, exosomes and apoptotic vesicles. Each of these derive through distinct biogenesis pathways. Microvesicles (also known as ectosomes) are formed by outward budding of the plasma membranes, while exosomes are generated by several orderly steps including the internal budding of endosomes, forming of multivesicular bodies (MVBs, also known as late endosomes) and fusion of MVBs with cell plasma membranes to release exosomes (Figure 1)[2]. Apoptotic vesicles (0.5-5μm, also known as apoptotic bodies) are formed during apoptosis by budding of the plasma membranes, which is proved to be a highly regulated process including biochemical steps[3,4] with corresponding characteristic morphological changes. Unique to the apoptotic vesicles are the presence of closely packed organelles, histone complexes and de-granulated genetic material[5]. Apoptotic vesicles fall outside the scope of this thesis, and thus will not be extensively discussed.

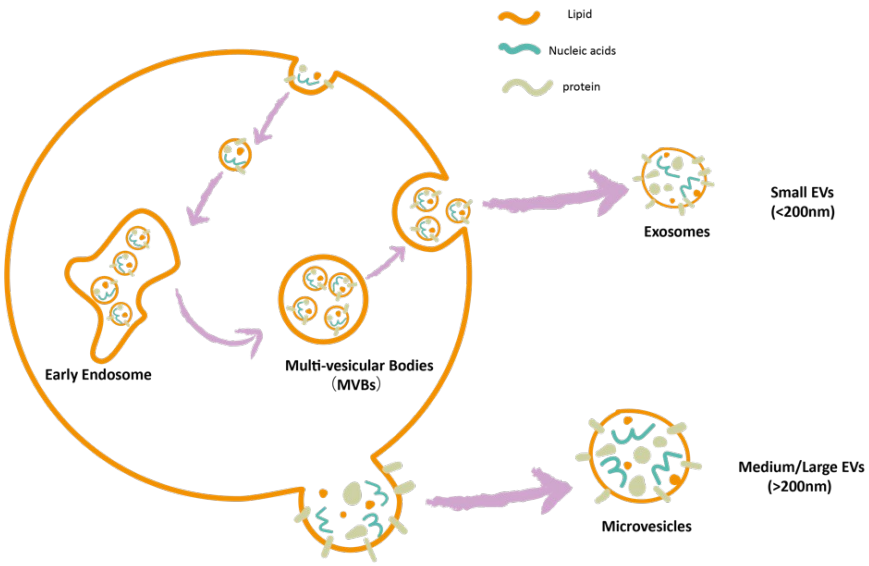


Figure 1. The biogenesis of microvesicles and exosomes. The microvesicles are formed via outward budding of the plasma membrane while exosomes are generated by the internal budding of endosomes, forming of multivesicular bodies, and fusion of MVBs with plasma membranes to release exosomes.

It's important to note that different cell types may use common or different machinery for the microvesicle and exosome biogenesis[6]. The biogenesis described here is the common machinery that most cells share. Several crucial steps are involved in the biogenesis of both microvesicles and exosomes, such as the plasma membrane redistribution, cytoskeleton rearrangement and cargo sorting.

The biogenesis of microvesicles starts with exposure to stimulus such as inflammatory cytokines[7], growth factors[8], shear stress[9], and hypoxia[10] which leads to Ca^{2+} influx. The influx then initiates a dynamic phospholipid redistribution and cytoskeletal protein contraction to form microvesicles. Cell membrane keeps asymmetry to maintain their functions by keeping the phosphatidylcholine (PC) and sphingomyelin (SM) on the outer layer while the

phosphatidylserine (PS) and phosphatidylethanolamine (PE) on the inner layer[11]. Under the Ca^{2+}-dependent pathway, the microvesicles start to bleb on the specific site of the membrane where it recruits and activates Ca^{2+}-dependent enzymes such as scramblase, flippase and floppase. Flippase is responsible for PS translocation and keeps PS sequestered from the cell surface[12]. Floppase is an ATP-dependent protein that can translocate PS from the inner layer to the out layer, and it is responsible for the disruption of asymmetry cell membrane associated lipid distribution when cells are activated[13]. Scramblase is a bidirectional lipid transporter which can translocate phospholipids flow according to the concentration difference, thus it's important for membrane randomization[13]. Upon stimulation or apoptosis, the change of membrane asymmetry is done by stimulating scramblase and floppase activities and concomitantly inhibiting the flippase[14]. This results in the exposure of the inner layer of phospholipid PS during the resting status to the external layer[14]. In the meantime, the Ca^{2+} influx can also induce the cytoskeleton rearrangement and actin-myosin contractility through Rho/ROCK signal pathway which is important for the blebbing[15-17].

For the microvesicle cargo sorting, the complex named endosomal sorting complex required for transport (ESCRT), is an important player. ESCRT is essential for endosomal trafficking via membrane deformation, cargo recognition and sorting, and interacting within ESCRT proteins themselves[18]. ESCRT consists of four protein complexes which are ESCRT-0, ESCRT-I, ESCRT-II, ESCRTIII and other accessory proteins[19]. The ESCRT proteins catalyse the key events of cellular membrane fission, such as intraluminal vesicle formation, vesicle budding from plasma membrane and abscission of the intercellular bridge[20]. The ESCRT-dependent pathway is stepwise and it starts with ESCRT-0 recognising mono-ubiquitinated proteins, and then recruiting ESCRT-I and ESCRT-II to deform the membrane for the preparation of budding to allow cargo to be sorted into endosomal invaginations[21]. Finally,

under the recruitment of subunits of ESCRT-II and ESCRT-III complexes, the membrane is further invaginated to close the nascent vesicle[21].

In an ESCRT-dependent microvesicle formation, which is believed to be the major pathway for microvesicles biogenesis, ESCRT-0 and ESCRT-I have been shown to be required for the early stages of microvesicle formation[22]. ESCRT-I subunit tumour susceptibility gene 101 (TSG101) can interact with Alix and arrestin domain-containing protein 1 (ARRDC1). The late endosome surface TSG101 can be recruited by ARRDC1 to the plasma membrane to produce microvesicles[23]. ESCRT-III is important for the release of microvesicles[24]. It has been suggested that microvesicles can also be formed by ESCRT-independent pathways. This is supported by the fact that knockdown of ESCRT proteins did not result in a completely suppression of the microvesicles release [22]. However, more studies are needed to resemble a clear picture of the ESCRT-independent pathway for the biogenesis of microvesicles.

Microvesicles have a multifaceted role in both health and disease states, largely attributed to their ability to transfer their content, which includes proteins, lipids, and nucleic acids, to recipient cells. This process can alter the behaviour and phenotype of these cells. One of their key roles is in the modulation of immune responses. The effect can be either immune-enhancing or immune-suppressing, contingent on the specific nature of their cargo[25]. They also have a regulatory role in blood clotting. For instance, platelet-derived microvesicles can facilitate coagulation by offering a surface for clotting factor complex assembly[26]. In addition, microvesicles have an impact on angiogenesis, with those originating from endothelial cells known to stimulate the creation of new blood vessels. Microvesicles are also important in tumour progression. In cancer, tumour-derived microvesicles can promote tumour growth, metastasis, and immune evasion[27].

The knowledge of exosomes biogenesis is more comprehensive than microvesicles. It involves sorting cargos into multivesicular bodies (MVB), MVB formation, transporting of MVBs and MVB-plasma membrane fusion[28]. Upon the plasma membrane invagination, the cell-surface proteins or other extracellular content are endocytosed to form the early endosome[29]. By further inward invagination of the endosomal limiting membrane, the early endosome matures into late endosomes (also known as MVBs) and forms intraluminal vesicles (ILVs)[30]. The late endosomes can be targeted to fuse with lysosomes or with autophagosomes for degradation and recycling, or fuse with the plasma membrane to release the exosomes into extra-cellular space (Figure 1)[31].

For the cargo sorting for exosomes, ESCRT pathway is expected to be involved since exosomes originate as MVB vesicles. By screening 23 components of ESCRT through RNA interference in major histocompatibility complex class II (MHCII) – expressing Hela (HeLa-CIITA) cells, the functions of ESCRT components on exosome biogenesis has been suggested[32]. The loss of function of 23 ESCRT proteins, HRS, STAM1, TSG101 and ALIX decreased and VPS4B increased the exosomes secretion, implicating the different roles of ESCRT in the biogenesis[32]. Apart from ESCRT-dependent pathway, the biogenesis of exosomes can also be ESCRT-independent and rely on the ceramide pathway or tetraspanins pathway. Under the ceramide pathway, the microdomains of the endosomal membrane are enriched for sphingolipid from which ceramides are formed[33,34]. Ceramides then induce the coalescence of small microdomains into larger domains to promote domain-induced budding[34]. These findings are supported by observations that the lipid composition of exosomes closely mirrored lipid rafts, with a significant enrichment of ceramide[34]. The crucial role of ceramide in exosome biogenesis is further supported by the substantial

reduction in exosome release when neutral sphingomyelinase (nSMase) - an enzyme involved in ceramide production – is inhibited, and by an increase of exosome budding via treating the cells with nSMase[34]. Tetraspanins such as CD9, CD63, CD81 and CD82 have been shown to play important roles in the ESCRT-independent biogenesis of exosomes through the formation of a molecular web of interactions among tetraspanins and with other targets[35-38]. These observations are obtained either by the enhanced exosome secretion via overexpression of tetraspanins[36,37] or by reduced exosome secretion via tetraspanins knockout models[35,37].

It is important to note that the boundary between exosomes and microvesicles is not always clear-cut, as their sizes can overlap and they can carry similar types of cargo. The current method to distinguish these two types of EV are solely based on the biogenesis. Furthermore, the specific functions of exosomes and microvesicles can greatly depend on their cell of origin and the physiological or pathological context. However, there are some differences between exosomes and microvesicles. For example, due to the different biogenesis, exosomes often carry a specific set of proteins, lipids, and RNA molecules that reflect their endosomal origin, while microvesicles contain a broader range of cytoplasmic and surface proteins from their parent cell[30]. As a result, they might interact with different types of target cells and exert different biological effects. More research is needed to fully understand their distinct roles. As the precise EV classification according to their biogenesis remains a challenge, International Society for Extracellular Vesicles (ISEV) has recommended an EV classification based on the size of the EV, where EV can be classified into medium/large EV (m/lEV, >200nm) and small EV (sEV, <200nm)[39].

1.2.2. The contents of EV’s cargo

The EV cargo, consists of proteins, lipids and nucleic acids, varies depending on EV originating cell types and biogenesis. By using an omics approach, a comprehensive profiling of the cargo of different types of EV can be established[40-43]. Collective efforts have resulted in several omics databases with selective focus on proteins, lipids, RNA or metabolites, such as Vesiclepedia (http://microvesicles.org/) and ExoCarta (http://www.exocarta.org/), ExoBCD (https://exobcd.liumwei.org/), EV-TRACK (https://evtrack.org/). Recently, a manually curated database, EV-ADD (https://www.evdnadatabase.com/) has also been established for EV-associated DNA in human biofluids[44]. Apart from omics studies, systemic reviews serve as valuable resource to study EV cargos and their roles as biomarkers for different diseases[45,46].

The protein cargo of EVs includes both commonly shared proteins and proteins indicative of their cellular origin. The majority are commonly shared proteins, including the proteins associated with the biogenesis such as ESCRT proteins, tetraspanins, small GTPase Rab family, proteins responsible for signal transduction, antigen presentation, enzymatic process and cytoskeleton[29]. The other category proteins are those shared between EV and their parent cells. For instance, adiponectin is specific for adipocyte-derived exosomes and placental alkaline phosphate (PLAP) is specific for placenta-derived exosomes[47,48].

In terms of EV lipid cargos, the common lipids include fatty acid, cholesterol, glycerides, sphingolipids, PS, PC and ceramide[49]. Using lipidomic profiling, a more comprehensive lipid profile of EV can be identified. For example, more than 100 species of lipid can be found in EV excreted in urine[50] or from prostate cancer cell lines[51]. More importantly, different lipidomic profiles of EV can be found between health status and disease status which can assist in biomarker discoveries as well as development of new therapeutic tools[52].

Nucleic acids are another important EV cargo. EV contain DNA and RNA while the RNA concentration is 20-30 fold higher than DNA concentration in exosomes[53]. RNA is the better studied cargos where both coding and non-coding species have been identified. It has been suggested to categorise EV-RNA into three types including: 1) intact mRNAs and miRNAs (confirmed to be functional in recipient cells); 2) intact RNAs (predicted to be functional); 3) fragments of RNAs[54]. The RNA cargos of EV are important in cell-cell communication and has been shown to actively influence the recipient cells' functions[55,56]. The functions of RNA cargos of EV have been extensively reviewed elsewhere[54]. DNA cargo has also been studied and both nuclear DNA and mitochondrial DNA has been found in EV[57]. Interestingly, DNA can be encapsulated by EV or attached to the surface of the EV[58]. EV's DNA cargo is important for cellular homeostasis[59], DNA transfer and modulation of recipient cells[60] and regulation of immune response[61]. The current studies of EV-DNA are under the umbrella of cell-free DNA (cfDNA). In pregnancy, cfDNA is exceptionally important because this technique has been used as a non-invasive clinical test to detect foetal gender and chromosomal abnormalities[62]. cfDNA is fragmented with the majority peaking at 162 bp in length and over 90% of cfDNA in plasma is located in exosomes with the DNA length in exosome being similar to cfDNA [53]. Due to the protection of the EV membrane, cfDNA in the EV has an extra peak at longer length (421 bp) which indicates the cfDNA in the EV might represent a distinct biological characteristic[63]. More evidence has shown EV-associated DNAs can reflect the health of foetus and work as biomarkers for a variety of pregnancy-related disease. For example, decreased cfDNA integrity within maternal plasma EVs has been observed in cases of aneuploid foetuses compared to euploid foetuses[63]. This offers a promising screening biomarker for non-invasive antenatal testing. In preeclampsia, incomplete restructuring of maternal spiral arteries leads to compromised placental blood supply, resulting in placental ischemia, hypoxia, and escalated oxidative stress. These adverse

conditions can provoke an increased discharge of EVs from the placenta into the maternal bloodstream. It has been observed that the concentration of DNA associated with EVs is higher in the plasma of women with preeclampsia at term, which could potentially signal a dysfunction in the extravillous cytotrophoblasts[64].

1.2.3 The uptake of EV by recipient cells

EV can be uptake by recipient cells by endocytosis or directly fusing with the plasma membrane (Figure 2). Under the direct plasma membrane fusion pathway, EV first come in tight contact with the plasma membrane and then initiates lipid reorganization, protein restructuring and membrane dimpling. This is followed by the hemifusion of the EV membrane with the recipient cell membrane where the initial pore has formed. The fusion induces the insertion of the EV membrane to recipient plasma membrane and releases of the EV cargos into the cell.

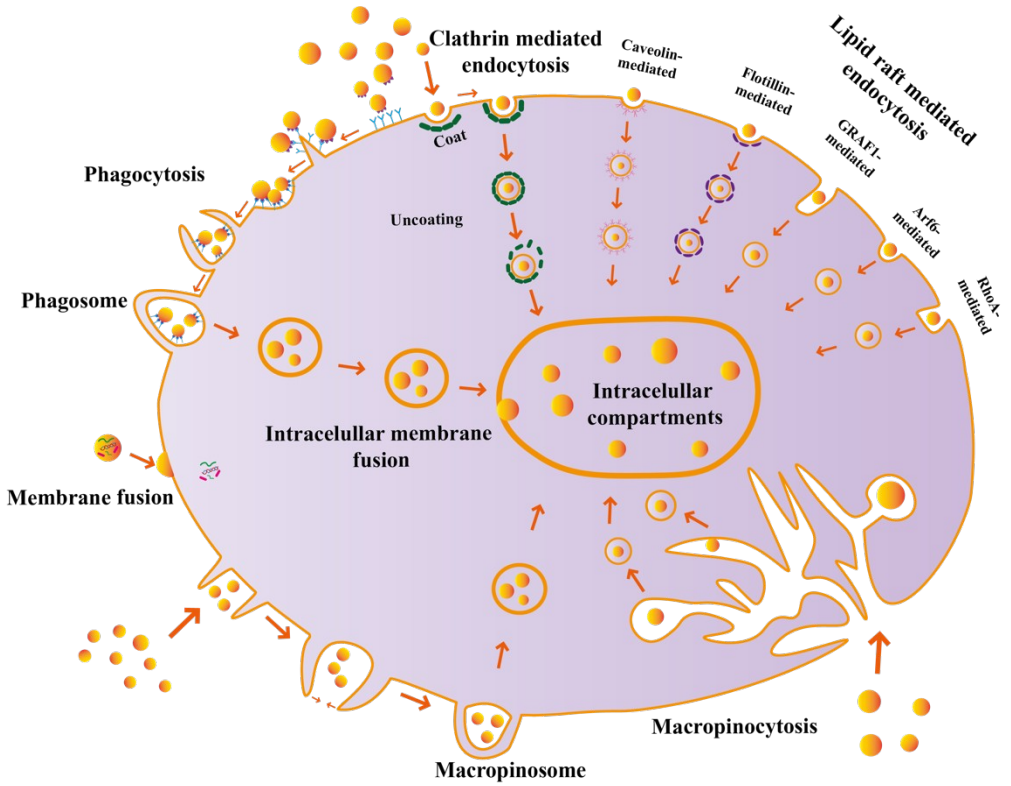


Figure 2. The EV uptake by recipient cells via membrane fusion, endocytosis (no lipid rafts involved, only lipid rafts involved, both non-lipid and lipid rafts involved), micropinocytosis, phagocytosis.

The EV endocytosis pathway can be further divided based on the involvedness of the lipid rafts as 1) no lipid rafts involved (clathrin-mediated endocytosis); 2) taking place in lipid rafts (caveolin-mediated/filipin-mediated/GTPase regulator associated with focal adhesion kinase-1 (GRAF1)-mediated/adenosine diphosphate-ribosylation factor 6 (Arf6)-mediated/RohA-dependent endocytosis); 3) pathways involves lipid rafts and non-raft membrane domains (micropinocytosis and phagocytosis) (Figure 2)[65]. Lipid rafts are membrane microdomains enriched in cholesterol, sphingolipids and glycosylphosphatidylinositol (GPI)-anchored proteins. These domains have lower fluidity and higher saturated lipids than the rest of the plasma membrane[66].

The clathrin-mediated endocytosis is a lipid rafts independent process. It requires endocytic coat proteins to form from the cytosol and after EV have been internalized, the coat proteins then promote the membrane bending and continue with the scission process where the neck of the membrane is cut. This is followed by an uncoating process in which EV are released to fuse with the endosome[67].

For the lipid-rafts-based endocytosis, the well-studied is the caveolin-mediated endocytosis. There are small cave-like invaginations on the plasma membrane enriched in cholesterol, sphingolipids and caveolins called caveolae[68]. After ligands are triggered, caveolar endocytosis is initiated in a highly regulated way and once caveolae pinch off from the plasma membrane, they can be directed to the classical endocytotic pathway[68]. Other lipid-

raft mediated endocytosis such as Flotillin-mediated endocytosis[69,70] and RohA-dependent endocytosis[71] have also been utilised by recipient cells for EV uptake. GRAF1-mediated endocytosis is also an important endocytosis pathway while research on EV internalization via this route is also scarce. Finally, Arf6 has been implied to regulate the biogenesis of EV, however, their roles in the exosomes uptake by cells are still not clear[72].

Macropinocytosis is another common way to internalize cargo in a nonspecific way. This process starts with the highly ruffled plasma membrane forming around a region of extracellular fluid and subsequently internalizes the whole region. EV can be internalised by the ruffled extensions which protrude from the plasma membrane inwards towards the basal membrane to form macropinosomes[73,74]. Then macropinosomes pinch off from the membrane and are internalised[75]. There is evidence supporting EV's uptake in this way and there is also contradicting evidence, which may suggest this internalisation method only occurs on certain cell types[76,77].

EV can also be internalised by phagocytosis and phagocytosis usually happens in the internalization of large particles (> 0.5 μm)[78]. Unlike macropinocytosis, EV internalised by phagocytosis is a specific way which requires the phagocytic receptors of the recipient cells to be bound by the EV associated ligands[78]. Highly efficient phagocytosis is typically restricted to specialised professional phagocytes while non-phagocytic cells show low-efficiency phagocytosis[79]. After the recognition, the plasma membrane changes its lipid composition and remodels the actin cytoskeleton to generate the membrane protrusions to engulf the EV and engage in sequential order to form phagosomes and be internalized by cells[80]

The processes of EV uptake by recipient cells that have been described so far are studied in various cell types, each of which may employ the same or different pathways for EV internalization. To the best of my understanding, studies directly investigating EV uptake in glomerular cells are rather limited. Therefore, further research is necessary to uncover the specific mechanisms through which these cells internalize EVs.

1.2.4 The diagnostic and therapeutic values of EV

EV bears diagnostic value because EV contains information from parent cells and the EV contents such as proteins, nucleic acid and lipids can be shifted from the healthy status compared to diseases. EV can be released into biofluids available to be sampled with minimally invasive methods. The fact that EV are present in various biofluids such as blood, urine, saliva, breast milk, cerebrospinal fluid, and amniotic fluid[43,81-84], has made them attractive candidates for biomarkers discovery. By characterising the EV profiles in the biofluid, EV-based diagnostic markers have been found in various diseases such as cancers, cardiovascular diseases, nervous system diseases, kidney diseases, and liver disease[85-90]. Specificly for preeclampsia (PE), EV-based biomarkers also show a promising future in assisting diagnosis (Table 1). Unique to PE and other pregnancy-related disease, diagnosis in the early trimester is critical to create a window for early intervention. For this reason, research to identify EV-based biomarkers in early pregnancy is clinically important.

Source	Biomarkers	Size	Trimester	Isolation method	Detection method	Ref
Plasma	miR-486-1-5p miR-486-2-5p	40-130 nm (NTA)	Early (12 weeks); Mid (23 weeks); Late (33 weeks)	Density gradient UC	Small RNA sequencing	91
Plasma	10miRNAs upregulated; 10 miRNAs	Mean size	<18 weeks	Density gradient	Small RNA	92

	downregulated	95 ± 25 nm (NTA)		UC	sequencing	
Plasma	miR-855-5p	NM	35 weeks	UC	RT-PCR	[93]
Plasma	miR-15a-5p	50-200 nm (NTA)	Second and third trimester	Density gradient UC	RT-PCR	[94]
Plasma	miRNA-136 miRNA-494 miRNA-495	<100nm (TEM)	Second and third trimester	UC	RT-PCR	[95]
Plasma	miR-517-5p miR-520-5p miR-525-5p	NM	First trimester	miRCURY Exosome Isolation Kit	RT-PCR	[96]
Plasma	miR-134 miR-196b miR-302c miR-346 miR-376c miR-486-3p miR-590-5p miR-618	NM	First trimester to the third trimester	ExoQuick Exosome Kit	microRNA-arrays	[97]
Plasma	IL-10 IL-2 TNF-α	20-130 nm (NTA)	Third trimester	Density gradient UC	Bead-based multiplex assay	[98]
Plasma	IL-21 IL-22 TGF-α	Mode size 150nm (PE)* 100nm (NP)* (TRPS)	Second trimester	qEV size exclusion columns	ELISA	[99]
Plasma	Neprilysin (NEP)	NM	Third trimester	qEV size exclusion columns	Flow cytometry; NEP activity kit	[48]
Plasma	CTB-TIMP AV-PAI PlGF	NM	Third trimester (28-32 weeks)	Immunomagnetic	ELISA	[100]
Plasma	Syncytin-1	Peak < 100nm (NTA)	Third trimester	Size exclusion columns	WB; RT-PCR	[101]

Plasma	HLA-DR	NM	Third trimester	UC	Flow cytometry	[102]
Serum	miR-31-5p	NM	NM	UC	RT-PCT	[103]
Serum	miR-155-5p	NM	Second trimester (17-28 weeks)	Immunomagnetic	RNA sequencing	[104]
Serum	Syncytin-2	Mean size 100 nm (TEM & NTA)	24 & 36 weeks	ExoQuick Precipitation	ELISA	[105]
Urine	Podocin Nephrin	152 ± 62 nm (NTA)	NM	Total EV isolation kit (precipitation)	Electrochemical immunoassay	[106]
Urine	NKCC2 ENaC	NM	Third trimester	UC	WB	[107]
Urine	C9 neoantigen Plasmin	NM	Second & Third trimester	UC	WB	[108]
Amniotic fluid	CD105 (endoglin)	221.8 ± 6.2 nm (NTA)	Third trimester	UC; SEC (for ExoView)	WB; IRIS	[109]

Table 1. EV biomarkers found to be differentially regulated in PE. * Speculated from the figures in the original manuscript. NM denotes not mentioned. CTB, cholera toxin B chain; AV, annexin V; PlGF, placental growth factor; NEP, neprilysin; NKCC2, Na-Cl2-K co-transporter 2; ENaC, epithelial sodium channel; HLA-DR, human leukocyte antigen-DR isotype; UC, ultracentrifuge; NTA, nanoparticle tracking analysis; WB, western blot; IRIS, Interferometry reflectance imaging sensing; TEM, transmission electron microscopy.

There is a huge therapeutic potential for EV because of EV's advantages. 1) Due to the protection of the bilayer of the membrane, EV cargo/drugs can be protected from degradation[110]. 2) EV can be derived from the owner's cells which offers biocompatibility and low immunogenicity[110]. 3) EV can be engineered to deliver to target cells which can largely

reduce the side effect[111]. 4) EV can also pass through tissue barriers such as the blood-brain barrier which can overcome the inaccessibility of certain drugs[112].

Purified EV can be engineered and loaded with functioning nucleic acids, enzymes or proteins. There are different approaches to engineering EV as therapeutic tools including the passive or active cargo-loading methods. The passive loading methods include loading cargo into EV by directly incubating desired cargo with EV[113] or by incubating drugs with cells or by transfecting cells to overexpress therapeutic molecules and then isolating drug-bore EV from cells[114,115]. The limitation of the passive loading method is its low loading capacity and toxicity and safety concerns regarding the transfection reagents. Different from the passive methods, the active methods normally use physical or chemical tools to compromise the membrane integrity to increase the drug loading[116]. Commonly used methods include sonication[117], extrusion (using a syringe-based lipid extruder to disrupt EV membrane)[118], freeze and thaw cycles (at least 3 cycles)[119], electroporation (electrical current to disrupt the membrane)[120] and membrane permeabilizers (e.g. saponin)[118]. Other than these methods, using chemical modification or antibody-based methods to anchor molecules into the lipid bilayer of EV can also engineer EV into effective therapeutics agent[121,122]. Click chemistry has been used for direct conjugation to chemically modify the EV's surface molecules via covalent bounds[121]. Nanobodies, small variable domains derived from heavy-chain antibodies, can be anchored on the surface of EV via glycosylphosphatidylinositol (GPI) and alter the target cells' behaviour[122]. Notably, pH gradient modification can also load functional miRNA cargo into EV[123]. This method utilises the ion trapping phenomenon where a weakly unionised miRNA can be entered, ionised and trapped in the aqueous centre of EV[123,124]. The advantages of this method are that it doesn't require expensive equipment and the unloaded miRNA can be reused[123].

When considering the half-life, liposomes, which are artificially created vesicles composed of a lipid bilayer, appear to be more durable with a half-life of several hours compared to the half-life of extracellular vesicles (EVs), which is around 30 minutes[125]. This extended duration makes liposomes a more attractive candidate for drug delivery. Nonetheless, it's important to note that the reported half-life of injected EVs in vivo can range from 30 minutes (when labelled by Gaussia luciferase) to several days (when labelled by PKH membrane dye), indicating a need for further studies to accurately compare EVs and liposomes using equivalent labelling methodologies[126].

1.2.5 The isolation methods of EV

The main purpose of EV isolation is to increase the yield over a period of time while keeping purity and reducing contamination. The current methods to isolate EV all have their own merits and demerits which will be thoroughly discussed here.

Differential Ultracentrifugation (UC)

Differential UC is the most frequently used method to isolate EV by itself or combined with other methods[127]. Differential UC works based on the buoyant density of EV. It starts with low-speed (e.g., 1,500g) centrifuge to remove cell and debris, which is followed by a 10,000g centrifuge to remove aggregates of apoptotic bodies, biopolymers and other structures whose buoyant density are higher than small EV (sEV)[128]. Finally, a classic 100,000g is applied to concentrate sEV (40-100 nm); and other contaminating proteins can be removed by repeated UC[129]. Differential UC has been considered a gold standard to isolate EV because of its several merits. UC has good reproducibility and it is easy to handle[130]. Furthermore, UC can handle a wide volume ranging from 2.5 mL to large volume > 600 mL can all be applied

using UC while other methods are limited when the volume is large[130]. Importantly, it is believed that UC induces less undesirable impact on EV except for gravitational force[128].

However, UC is not suitable for all sample types. According to the survey conducted by ISEV in 2019, blood/plasma is the most popular sample type[127]. However, UC is the least appropriate method for EV isolation from plasma, since only a minority of EV can be isolated from plasma using UC[131]. Apart from the sample type, other contaminants such as lipoproteins, which can influence the downstream analysis, may also be co-sedimented by UC. In plasma, the level of lipoproteins is estimated to be 10^7-10^9 folds higher than EV which will inevitably be a contaminant when isolating EV[132]. Apart from lipoproteins, other soluble proteins can also be a problem for UC. Uromodulin is one such example. Uromodulin is major protein in the urine samples, which when untreated can be co-sediment and become a major contaminant in isolate urine EV using UC. Uromodulin can form mesh-like structures that trap large numbers of EV and other soluble proteins during low-speed centrifugation. Several methods, including adding β-mercaptoethanol (β-ME), dithiothreitol (DTT), NaCl and $ZnSO_4$ either prior to isolation or after acquiring the pellet, have been developed and proven to be effective[133-136].

Other methods, such as sucrose density gradient UC have been utilised to combine with UC in order to achieve a better purity and recovery rate during EV isolation. For example, after the classic differential UC, a better purification of EV can be achieved by washing the pellet using a 30% sucrose cushion[137]. Though, this method does improve the purity of the EV, EV might be ruptured and lost after a high-velocity UC[138].

Size exclusion chromatography (SEC)

More and more researchers use SEC to isolate EV[127]. SEC isolates EV based on their size distribution and an SEC system is made of a porous stationary phase for chromatographic separation[139]. The basic principle is that solutes with high molecular weight or size penetrate the column first, while solutes with low molecular weight or size will penetrate or partition into the pores of the packing and elute later[140]. By collecting different fractions from the elute, EV are not only separated by sizes but also from soluble proteins[139].

There are several unique advantages of using SEC to isolate EV. First, SEC can efficiently remove unwanted soluble proteins such as serum albumin co-existing in the starting materials with EV [131]. Second, the EV isolated by SEC is functionally improved compared to the ones isolated by UC[141]. This is probably due to the buffer SEC normally uses for isolating EV is PBS which is more physiological than sucrose which is used in density gradient UC, and the EV's shape can be well kept in SEC isolation compared to fused EV normally seen after UC [139,141,142].

However, other proteins such as chylomicrons and low-density lipoproteins (VLDL) are in a similar size to exosomes[132] and such particles are likely to be co-isolated with EV by SEC[143]. It has been suggested that other methods such as immunoprecipitation should be utilized to further purify EV after SEC isolation. Another major shortcoming of SEC is that the sample can be diluted, and it will be difficult to perform the downstream analysis such as western blot.

Ultrafiltration

Ultrafiltration (UF) is a simple-to-use technique where EV can be isolated by their size and mass using a molecular weight cut-off membrane of centrifugal filters[144]. The most used type is regenerated cellulose with a pore size of 100kDa and there are around 18% of researchers utilise this method to isolate EV[144,145]. It is worth noting that UF is normally combined with other isolation methods such as SEC to either concentrate a large volume of starting material or concentrate EV after isolation[144,146,147]. However, the filtration membrane tends to be clogged during large-volume filtration which may result in longer filtration time[148]. UF may also lead to low EV yield due to the EV adhesion to the membranes[149]. More importantly, it's necessary to check the influence of different centrifugal filters for specific sample type in order to prevent significant EV loss[144]. It has been shown that 10kDa Amicon filters have better performance than 100kDa Amicon filters when isolating plasma and urine EV[144]. This is probably due to less adhesion of EV to the membrane when 10kDa filters are chosen.

Precipitation

By using a polymer solution, the water molecules of a sample bind to the polymers thus decreasing the EV's solubility, which then allows the isolation of EV by low-speed centrifugation. Polyethylene glycol (PEG) is the most common used polymer in the isolation of EV[150]. There are several commercial kits available such as ExoQuick, ExoSpin, OptiPrep and Total Exosome Isolation Kit[150,151]. The biggest advantages of this method are that it is easy to achieve using a bench-top centrifuge and it has high reproducibility and short processing time makes it ideal for clinical application[138]. The limitation of this approach is that the co-precipitated polymers as well as other non-EV components such as albumin and lipoproteins can influence the downstream analysis such as mass spectrometry[151]. Combining precipitate methods with SEC to remove the PEG and other co-precipitated proteins may be

necessary[152]. Furthermore, the commercially available precipitation kits are expensive which can cost 4 dollars/mL of sample[153]. A simple salt solution containing PEG, at a cost of less than 0.01 dollars/mL of sample, has been shown to lead to a high EV yield with high quality. EV isolated using this method showed good performance in downstream mass spectrometry analysis[154]. Other precipitation methods using protamine and sodium acetate are also shown to be cost effective ways of EV isolation[155,156]. Given that EV carry a negative charge, they can be aggregated and isolated from biological fluids using protamine, which is positively[156]. Sodium acetate can mediate the removal of the exosome hydration layer that promotes hydrophobic interactions which then lead to precipitation[155].

Affinity-based isolation of EV

Affinity-based isolation utilises antibodies or aptamer against either the generic EV's surface proteins such as CD63, CD9 and CD81, or known specific EV surface proteins such as tumour-associated markers to isolate tetraspanin expressing EV or specific EV populations[157]. Using antibody-coated magnetic beads to isolate EV is one example of this method. After the isolation, subsequent identification of proteins, such as by western blot, on magnetic beads isolated EV can be used as evidence of protein co-existence [157]. Though, the immunomagnetic based method is not suitable for large-volume samples due to the required EV concentration and high cost[129], application of immunomagnetic based isolation for large sample volume can be achieved when combined with a concentration step using methods such as ultrafiltration to reduce the starting sample volume [157]. Antibody-based methods are compatible with downstream analysis using flow cytometry, western blot and electron microscopy when the removal of the antibodies is not required[129]. However, when the antibody removal is needed, an alkaline or acidic elution buffer is normally applied during the elution process which can damage the integrity and functionality of EV[158]. Aptamer-based methods have been

developed to overcome this limitation. Aptamers are small oligonucleotide molecules of RNA or single-stranded DNA, which can bind to the target molecules on the EV with high specificity[159]. The high chemical stability of aptamers, along with their ease of synthesis and modification, makes them an attractive alternative to antibodies[158]. A cleavable linker between Aptamer and magnetic beads allows EV to be released in their intact state after magnetic beads isolation[160]. Another commonly used affinity-based isolation is the membrane-based method which can also offer the benefit of isolating EV in their intact state. This method isolates EV based on a generic biochemical characteristic[158]. There are commercially available kits for this method including ExoEasy kit (QIAGEN). ExoEasy has been recognised as the easiest method to perform which only requires 30mins for isolation[161]. However, this method can co-isolate some non-EV components[162]. When it comes to RNA analysis, it's necessary to use some detergents such as proteinase K and RNase A to eliminate non-vesicle RNA after isolation with ExoEasy[162].

Isolation of placenta-derived EV

The aforementioned methods are available to isolate placenta derived EV. The choice of methods to isolate placenta-derived EV largely depends on the experiment itself. There are three main sources to acquire placenta EV: 1) placental EV from biofluids such as plasma, serum, amnion fluid, and urine[109,163,164]. 2) placental EV from *in vitro* culture systems under different culture conditions, such as explant culture[165]. 3) placental EV from placenta perfusion[48] or placenta homogenate[166], where EV from normal/disease placentas are harvested within a short time of placenta retrieval. There are several important factors that need to be considered when choosing the right isolation methods. First, the isolation method relies on the volume of the starting material and the sample type. Placenta ex vivo perfusion normally generates 500 – 1000 mL perfusate which requires the isolation methods can effectively

isolate EV in a reasonable time length. In such situation, ultracentrifuge-based isolation is preferred. While the starting volume is small, such as blood samples which can be less than 5 mL, affinity-based or precipitation approaches can also be used. Second, the choice of isolation method must consider the impact of co-isolated contaminations on the downstream analysis. For example, lipoproteins are more enriched in blood samples compared to other sample types that the level of lipoproteins in plasma is estimated to be 10^7-10^9 folds higher than EV[132]. In such cases, a single isolation technique cannot yield the desired purity of EV. Combining two techniques, such as SEC and immunoprecipitation, can largely reduce the contaminants. Thirdly, the isolation methods should be compatible with the downstream analysis. The polymers used in precipitation can be co-precipitated which can interfere the downstream analysis, such as mass spectrometry[151]. Therefore, such isolation methods should be avoided when mass spectrometry is considered. Current published isolation methods to acquire placenta derived EV are summarized in Table 2.

Sample Type	Method	Volume	Isolation Method
placenta	Placenta ex vivo perfusion	500-1000 mL	UC[48]
	Explant culture	< 50 mL	UC[165,167]
	Placental homogenate	< 500 mL	Isolated by UC, purified by SEC[166]
	Trophoblast cell culture	< 500 mL	Concentrated by UF, isolated by SEC[168] Density gradient UC[169]
Blood	plasma	< 5 mL	SEC[99] Precipitation[170] Density gradient UC[163]
	serum	< 5 mL	Precipitation[105,170] UC[171]
Urine	urine	5 – 150 mL	SEC[164]
Amnion fluid	Amnion fluid	20 mL	UC[109]

Table 2. Published isolation methods to acquire total EV containing placenta-derived EV.

1.2.6 The EV characterisation methods

As recommended by ISEV, multiple complementary methods and in total a minimum of 3 methods must be employed to perform the EV characterisation[39]. The complementary methods should include an EV image, one single particle characterisation (not electron microscope-based), and one from biochemical characterisation such as western blot. The physical characterisation methods such as transmission electron microscopy (TEM), and/or nanoparticle tracking analysis (NTA), and/or tuneable resistive pulse sensing (TRPS), and/or dynamic light scattering (DLS) and/or atomic force microscopy (AFM); and biochemical composition analysis such as Raman spectroscopy, and/or western blot, and/or flow cytometry and/or plasmon resonance imaging.

Protein, DNA/RNA, and total lipids concentration

As mentioned, EV consist of complexed biological materials including proteins, lipids and nucleic acids. Each of these has been used as surrogate marker to achieve an estimation of EV quantities. Protein concentration estimation is the most commonly employed method. Protein concentration of EV-enriched samples can be estimated using a protein quantification assay such as bicinchoninic acid (BCA) assay. However, because lysed EV contains lipids which are not present in the bovine serum albumin used to generate the standard curve, such protein quantitation provides an estimate rather absolute quantitation. Contaminants in the samples, such as co-isolated lipoproteins can also compromise the accuracy of the measurement[39,172]. In case where the available sample is scarce, Nanodrop or other methods requires small sample input can also be used. It is important to note that the comparison between samples should only be made when the same method was used for measurement.

Total lipid that can be quantified by sulfo-phospho-vanillin (SPV) assay or by measuring the fluoresce of phospholipid dyes such as DiR has also been used for EV quantitation[39,173]. However, the contamination of lipoproteins during EV isolation may also result in the overestimation of the EV quantity[39,49].

EV contain RNA cargos which are enriched in small non-coding RNA[54]. The types of RNAs EV contain largely depend on the origin and in physiological/pathological state of cells where they are derived from[54]. The quantification and characterisation of RNA content in EV can be done via Bioanalyzer, next generation sequencing and RT-qPCR[174]. However, the concordance among quantification methods is poor due to the low numbers of RNA per vesicle and the profiling method[39,54,174]. Also, other contaminations such as lipoproteins, ribonucleoproteins and exosmeres (non-membranous nanovesicles ≤ 50 nm) can also be the origin of the isolated RNA[39].

EV carries a variety of DNA types, which include single-stranded DNA (ssDNA)[175], double-stranded DNA (dsDNA)[176], mitochondrial DNA (mtDNA)[177] and viral DNA[178]. These DNA encapsulated in EV play crucial roles in cellular homeostasis, genome integration and immune regulation[57,59,179,180]. Similar to EV RNA, the measurement of EV DNA can be done via bioanalyzer, NanoDrop, sequencing and PCR[57].

Western blot

Using western blot to show the isolated EV expressing EV markers is an essential method in bulk EV characterisation. According to ISEV's recommendation, at least 3 categories of markers must be evaluated. These include transmembrane/lipid-bound protein (category 1),

cytosolic protein (category 2) and negative marker (category 3)[39]. In the case of identifying EV of a specific cell-origin, a cell-type specific marker is also required (category 4)[39]. Finally, secreted or luminal proteins that are related to EV binding to specific receptors (category 5) are needed for EV functional activities[39].

Single particle tracking analysis

Nanoparticle tracking analysis (NTA)

Nanoparticle tracking analysis (NTA) is developed based on the Brownian motion of particles in suspension[181]. The samples are injected with a fixed flow rate while exposed to a narrow laser beam[182]. The light scattered from illuminated particles in the samples is recorded by a highly sensitive camera and the particle size can be estimated using Stoke Einstein's Equation with the known temperature and liquid viscosity[181]. Based on the volume assessed, the particle concentration can also be calculated[183]. NTA can measure particles from 30 nm to 1-2 μm[181].

As one of early technologies developed for EV analysis, NTA is one of the top 2 most popular EV characterisation approach because of its several favourable advantages[145]. First, the process for preparing samples for EV assessment using NTA is straightforward, typically involving the resuspension of EV in phosphate-buffered saline (PBS) buffer[184]. Second, the recording of the video and the computation of results using built-in algorithms is a quick process, usually taking only takes a few minutes. Additionally, it is possible to detect the antigen expressed on EV stained with fluorescent antibodies using the fluorescent NTA.

However, NTA has its limitations. First, evidence has shown the day-to-day variation ranges from 1% to 16% for the size measurement and 1%-25% for concentration measurement using

the same software setting and the same sample measured on different days[183]. The instrument-instrument variation is also noticeble[183]. When using un-processed urine, the variation can reach 47% of the same sample calculated by area under the curve (AUC) of 20nm - 100nm distribution[185]. These observations have made the reproducibility of NTA questionable. Second, though it is possible to detect fluorophore-conjugated antibody labelled EV, it normally requires an increase in the camera level to detect the fluorescent particles[186,187]. Such adjustment may lead to the detection of only large and bright particles and the small particles may be indistinguishable from the background[186]. More importantly, it's necessary to remove the dyes by ultracentrifugation or size exclusion filtration before the measurement in order to remove dye aggregates and to achieve a proper signal-to-noise ratio[187,188]. The use of immunofluorescent NTA, for instance, with Quantum dots – photostable and bright semiconductor nanocrystals with diameters ranging between 10-30 nm - enables conjugation to EV and allows for the characterisation of their immunophenotypic properties[189,190]. Third, a proper sample dilution to avoid overlapping effect is required to achieve a proper NTA measurement. The recommended concentration is 2 -10 x 10^8 particles/mL[187]. Considering the concentration of the particles is unknown for most of the samples measured the first time, it usually takes several attempts to achieve the right concentration.

Dynamic light scattering (DLS)

Similar to NTA, Dynamic light scattering (DLS) is also based on the Brownian motion of dispersed particles. And it uses scattered light intensity to estimate the size of EV[191]. Different to NTA, DLS does not visualize the particles and the scattering intensity can be influenced by the large particles present in the samples[192]. As a result, DLS is more suitable to measure homogenous samples while NTA is able to work with heterogenous samples[192,193]. However, because it is easy to use and it does not require sample dilution within a certain particle

concentration range (particles/mL) as required by NTA, the results from DLS are found to be more reproducible[193].

Tuneable resistive pulse sensing (TRPS)

In TRPS, a single conical-shaped nanopore is created in the middle of two fluid cells and a current is applied and monitored through the nanopore[194]. Each time when an EV pass through the nanopore, the resistance of the current is measured and the extent of resistance is proportional to the volume of the EV[195]. Thus, the size of the EV can be measured. In the past, the pore size is not changeable due to the materials they are made of[196]. Clogging of the nanopore by large EV has been a commonly reported issue. However, with material technology development, a stretchable nanopore is created to fulfil a broad size measurement[196]. It has been reported that the lower size detection limit of commercially available instrument qNano is 55-60nm similar to NTA [197]. However, it's worth noting that the size range of EV that qNano can measure is subject to the pore size. Therefore, selecting the right pore size is critical for an accurate measurement.

Non-cryogenic and cryogenic electron microscopy (EM)

Transmission electron microscopy (TEM) and cryo-electron microscopy (cryo-EM) have been widely used in the EV characterisation because they provide critical morphological information with high resolution (the imaging resolution can be down to 1nm)[198]. EM does not only provide morphology information it can also couple with immunogold labelling to reveal the biochemical properties of EV[198]. TEM utilises a beam of accelerated electrons to pass through the thin samples and the spread fraction of the beam is transmitted by the objective lens and projected on the projector lens[199]. With the help of magnetic lenses, the spatial changes of the sample can be magnified[199]. EV shows a characteristic cup shape under negative staining as revealed by TEM. However, the samples must be fixed or dehydrated

before the TEM measurement, in addition, the accelerated electron may irritate the biological samples[182]. Therefore, cyro-EM has been developed which does not require dehydration and fixation and it can be done at low temperatures which reduce the irritation caused by electrons[182]. Furthermore, cryo-EM can provide 3D reconstructions which shows exosomes are spherical rather than the cup-shape under TEM[200].

Flow cytometry (FCM)

Unlike western blot, TEM, NTA, and other techniques mentioned in this chapter, which perform bulk analysis, FCM is able to offer single-EV characterisation. However, there were also several technical obstacles that need to be tackled. Conventional FCM is first developed to characterise cells in the circulation which are much larger than EV[201]. The size range of EV is 30 nm -1 μm while the size of cells is in the range of 5 to 20 μm which is hundreds of times larger than EV[202,203]. Due to the small size of EV, light scatter property alone cannot distinguish the signals from the background noise by most conventional FCMs. In fact, it has been shown that among the 46 FCMs tested, only 32 FCMs (70%) are sensitive enough to detect signals below 400nm using polystyrene beads. Among these 32 FCMs, only 6 FCMs (19%) could measure platelet EV below 600nm[204]. The revelation of EV when they are fluorescent can be separated from background noises has led to the development of various techniques for generic EV labelling. For example, several lipophilic and cytoplasmic fluorophores have been developed for EV generic labelling. The most extensively used dye is the PKH lipophilic dyes which interact with the lipid bilayer of EV and promote long-term dye retention and stable fluorescence[205]. Other lipophilic dyes such as DiI, DiR, DiD and FM are also used to label EV[206-209]. There is, however, a lack of well-designed studies sharing consensus on details such as titration of dyes and the necessity of post-staining free dye removals.

In addition to difficulty in achieving EV separation from noise based on their scatter light property, the small surface area of EV and consequently limited numbers of antigens available for binding of fluorochrome conjugated antibody is another challenge[210]. For EV to be recognised as being positively labelled, the number of fluorochromes per EV must be above the detection sensitivity/threshold of the prospective channel. Detection sensitivity/threshold is measured by molecules of equivalent of soluble fluorochrome (MESF). According to BD's product specification, BD's LSR-II has a detection sensitivity of 30 and 80 MESF for the PE and FITC channels respectively. This means when a PE conjugated antibody is used to label an antigen expressed by an EV, the number of PE fluorochromes on that EV must be higher than 30 MESF for it to be detectable by the machine. Conversely, an EV, which does bear PE fluorochromes but less than 30 MESF, is considered negative. In reality detection, sensitivity is often considerably lower than the product specification. Taken together, it is possible to analyse EV when their fluorescence is above machines' detection threshold. This is true for EV generic dye labelling or by fluorochrome conjugated antibody labelling.

Large beads (normally ≥ 4μm) to couple with EV has also been developed to detect EV's signals from conventional FCM[211]. This approach allows researchers to detect the signals from multiple EV, but it can provide semi-quantification of the number of EV in the biofluid[212,213]. By pre-loading 4.8μm carboxylated polystyrene beads with varying amounts of 2 dyes, a commercially available kit, MACSPlex exosome kit, has been developed to detect 37 different EV populations by conventional flow cytometry[214].

Apart from these methods, efforts have been put into developing high-resolution FCM. These high-resolution FCMs have much higher 488 nm laser power, wider forward scatter detection and lower sample acquisition speed compared to conventional FCMs leading to the possibility to detect weak signals from EV[215-217]. Such configurations have led to the birth of several commercially available high-resolution FCM, such as dedicated EV flow cytometer nanoFCM, or Cytometer with adds on for EV analysis, such as CytoFLEX system, NovoCyte flow cytometer[217-219]. Performance and limitations of these new generation flow cytometers are awaited to be validated.

Atomic force microscopy (AFM)

AFM is a microscopic technique which utilises the tip of a cantilever to probe the surface of the samples and the tip deflection can be registered by a laser beam reflected onto a photodiode[220]. By scanning the biological samples with the tip, the images of the cells can be constructed as well as the stiffness and elasticity of sample can be measured by the force between the tip and the sample surface[221]. Depending on the interaction of the tips with the surface of the samples, different imaging modes of AFM have been developed. The contact mode, which was developed the earliest, involves the constant contact of the tip with the surface of the samples, which is not suitable for biological samples due to unwanted friction and irreversible deformations[222]. Later on, tapping mode AFM is established with an oscillating tip to scan a sample. Due to the simple use and less perturbation to the samples, tapping mode AFM was once the most commonly used for extracellular vesicles characterisation[222]. Non-contact mode AFM uses a feedback loop to keep the oscillation near the surface rather than contacting it is the latest development[222]. In order to perform the EV characterization using AFM, EV need to be attached to a surface such as mica sheets[223,224]. AFM can be used in different acquisition modes which are air or liquid mode. While air mode

AFM offers more stability, it has the drawback of potentially causing sample drying. Therefore, researchers often opt for liquid-mode AFM, which can prevent the liquid evaporation and allows for preservation of samples in physiological conditions[223]. When combined with antibody labelling, EV markers can also be assessed by AFM[223]. Several antigens on a single EV can be simultaneously assessed by fluorescence AFM by incubating EV with a cocktail of different fluorescent antibodies[225]. AFM has been utilised for characterisation of EV from various origins such as erythrocyte, saliva, blood, and synovial fluid[224,226-228]. However, AFM does have its own limitations that EV needs to be stably attached on substrate, it has low throughput, the requirement of specific skills and costly equipment, and the results largely depend on the types of tip and scanning speed[172,222,224].

Surface plasmon resonance (SPR)

SPR is a label-free and real-time assay that can detect the ligand binding to target receptors immobilized on a sensing surface via the changes of the local index of retraction upon absoption[229,230]. The theory behind this is that when plane polarized light illuminates the surface, it can excite a global resonance of surface-confined free electrons under certain conditions[231]. The conditions depend on the effective refractive index in close proximity to the sensor surface, while the binding process can induce temporal changes in the refractive index which can be monitored[231]. SPR not only can measure the concentration and the size of the EV, but it can also measure the total mass of EV including lipids, proteins and nucleotides[231]. When a transmission mode is applied, SPR can detect 12 exosomal markers within 30mins and the sensor can be in repeated use[232]. SPR has been shown to be superior in performance than flow cytometry in detecting EV's surface antigens[233]. More studies are required before an objective conclusion is made.

Raman spectroscopy (RS)

Raman spectroscopy (RS) is a label-free technique that utilises laser irradiation to induce the inelastic scattering of light from analytes[234]. The photons from the laser light interact with the molecules of the sample so that only a small portion of the scattered photons don't have the same energy as the incident photons while the majority have the same energy[234]. The shifted energy can be measured to reveal the vibrational energy difference from the molecular bonds of the components of samples measured[234]. The intensity is proportional to the concentration of the molecular constituents that make the bands[235]. Because RS is a non-destructive approach, it has been utilised in assisting in cancer diagnosis and locating the precise range of cancer tissues during surgery and therapeutic effects of drug nanocarriers[234,235]. RS has also been successfully utilised in the characterisation and quantification of EV as well as the content of EV such as microRNA[236-239]. Combined with robust analysis, the comprehensive signals obtained from the EV via RS can be further clearly identified[240]. There are several limitations to RS. The signals obtained are too comprehensive to interpret if heterogenous EV exist in biological samples such as urine and blood[240]. More importantly, PEG or other polymers in the commercial precipitation kits and sucrose used by density gradient ultracentrifugation may interfere with the RS analysis, which restricts the use of RS[241].

Single particle – interferometric reflectance imaging sensor (SP-IRIS)

Interferometric reflectance imaging sensor (RIS) is novel sensing technology where enables via label-free quantification of molecules[242]. SP-IRIS has been specially developed to measure single particles in solution[242]. It can measure and quantify EV via the interference between the scattered field from the particle and reference field reflected off the interface of the layered substrate[242]. A platform, ExoView, has been developed based on this technology to quantify EV in plasma and cell culture medium without isolation[243,244] and protein cargo

loading efficiency[245]. By using specific antibodies, a subpopulation of EV can be quantified via SP-IRIS[243].

Future of EV characterisation

Though each of the techniques has its advantages and limitations, combining the current technologies may be a suitable solution to overcome the current obstacles each technique faces. For example, interferometric nanoparticle tracking analysis (iNTA) where interferometric detection of scattering combines with NTA can let researchers distinguish lipoproteins from EV with a label-free method[246,247]. This is not achievable using NTA alone. Similarly, combining fluorescence imaging with Raman spectroscopy can allow researchers to distinguish the subpopulation of EV[248] while combining brightfield microscopy with Raman spectroscopy can allow researchers to gain size information[249].

1.3 Placenta biology, preeclampsia (PE) and roles of EV in PE

The placenta is the maternal-fetal vascular interface responsible for the gas and nutrient exchange during pregnancy[250]. Healthy development of the placenta is the foundation of a healthy pregnancy.

After fertilization, the embryo moves from the oviduct towards the uterus for implantation[251]. During this process, the embryo undergoes continuous cleavage and development to reach the morula stage and later the blastocyst stage[252]. Blastocyst has the first cell lineage division that differentiates totipotent morula into two cell types called inner cell mass and trophoblast[252].

The trophoblast gives rise to the placenta while the inner cell mass will eventually become fetus[252]. The trophoblasts continue to form the maternal-fetal junction and further proliferate and differentiate into two cell types, cytotrophoblast (inner layer) and syncytiotrophoblast (outer layer)[253]. The syncytiotrophoblast (STB) layer then invades the decidua and creates the lacunae inside this layer[253]. The erosion causes the release of maternal blood and gland contents of the maternal capillaries and endometrial glands[253,254]. The STB layer continues to grow during the pregnancy by cell-cell fusion of the underlying cytotrophoblast and this layer can reach 10 m^2 at term[255,256]. This continuous and multinucleated layer is in direct contact with the maternal blood[257] and releases multiple factors into the maternal circulation including pro-inflammatory cytokines, angiogenic factors, cell-free fetal DNA and extracellular vesicles, which can altered in the disease status[258].

Preeclampsia (PE) is a major cause of maternal and foetal morbidity and mortality, and it is characterized by new onset hypertension, proteinuria and other end organ dysfunction after 20 weeks of gestation[259]. With the renal system being the primary target, its clinical manifestations can be diverse involving in neurological, haematological, cardiorespiratory, and liver dysfunctions[259]. PE can also induce fetal complications such as fetal growth restriction (FGR), stillbirth and neonatal death[260]. Depend on the disease onset, PE has two subtypes which can be categorized as early-onset preeclampsia (EOPE, <34 weeks of gestation) and late-onset preeclampsia (LOPE, ≥ 34 weeks of gestation). The overall PE incidence rate is around 3.1% of all pregnancy while the LOPE consists of 2.72% and EOPE makes up 0.37%[261]. The only effective treatment of PE is to terminate the pregnancy. The fact that delivery of the placenta cues PE suggests the maternal pathology of PE is driven by the placenta[262]. The fact that PE also happens in molar pregnancies, which are characterised by abnormal trophoblast proliferation, further supports the idea that placenta drives PE[263].

Though the pathophysiology of preeclampsia is complex, the two stages hypothesis remains popular to date. According to this hypothesis, the first stage is the pre-clinical stage where the placenta manifests poor development and then leads to the second stage where the symptoms are shown[264]. The maldevelopment of the placenta in PE patients could be attributed to the insufficient invasion of trophoblast, which manifests as the reduced number of extravillous trophoblast number in the spiral artery and insufficient muscle destruction[265]. In the normal pregnancy, the placenta and foetus exist in a low oxygen environment (pO_2 < 20 mmHg) during early pregnancy before the intervillous blood flow is established[266]. With the extravillous cytotrophoblasts invading, the highly contractile muscular spiral arteries have been converted into dilated ducts to provide enough blood supply from the mother to the fetus[267]. By the end of the first trimester, the oxygen level undergoes a steep increase ($pO_2 \approx$ 50 mmHg) along with the increased antioxidant level[266]. In preeclampsia, the insufficient invasion directly results in inadequate placental perfusion and further induces oxidative stress, which leads to the release of multiple factors and contributes to various maternal symptoms[268]. For example, soluble fms-like tyrosine kinase 1 (sFlt-1), acting as a decoy receptor and hindering vascular endothelial growth factor (VEGF) and placental growth factor (PlGF) signalling, is increased in the circulation of PE pregnancies. Delivering sflt-1 producing adenoviruses into pregnant mice induced endothelial dysfunction, hypertension and proteinuria in a dose dependent manner but not in controls[269]. This data suggests a direct causal relationship between quantity of sflt-1 and endothelium disfunction. Soluble endoglin (sEng) is another elevated factor found to be increased in the circulation of PE patients[270]. These factors are released far earlier than the maternal symptoms show up[267].

Similarly, EV is another elevated factor released by the placenta earlier than the manifestation of maternal symptoms in PE[271]. The placenta-derived EV (pEV) have been detected as early as the 6 weeks of gestation and its level in circulation has been shown a

gestational age related incremental increase[272,273]. The pEV internalization and induced various functional changes on the recipient cells have been demonstrated[271]. In PE, the content or number of pEV cargos can be different compared to the pEV from NP, which may tribute to endothelial damage[48], inflammation[274,275], and abnormal coagulation[276] as shown in different experiment models.

1.4 Glomerular filtration barrier and renal damage in PE

Proteinuria is a common symptom of PE. Though proteinuria is not in the diagnosis requirement, the majority of the patients still suffer from it[277]. In non-pregnant women, the urine is almost free of protein and the total protein secretion is less than 150 mg per 24h[277]. In normal pregnancy, a physiological increase in urine protein excretion is expected and significant protein excretion is defined as ≥ 300 mg per 24h[277,278]. This increased protein excretion is due to a 50% increased glomerular filtration rate (GFR) resulting from 30% - 80 % increase in blood volume passing glomeruli and an altered tubular reabsorption[279,280]. In PE, a one-third reduction in estimated GFR (eGFR) can be observed compared to NP controls[281]. The proteinuria of PE generally involves proteins with high molecular weight such as albumin[277], though studies investigate whether the proteinuria in PE is selective or non-selective are scarce. Available evidence pointed out the protein selectivity was in an “intermediate range” and selective and non-selective proteins both exists in PE[282].

The glomerular filtration barrier (GFB) is the most important structure in the kidney to prevent the leakage of protein into the urine. This barrier consists of two types of cells, namely glomerular endothelial cells and podocytes, and a layer of the glomerular basement membrane (GBM) jointly secreted by these two types of cells (Figure 3A). In the glomerular endothelial cell layer, there are transcytoplasmic holes called fenestrae together with a layer

of negatively charged glycocalyx covering the fenestrated and interfenestral domains to maintain the glomerular barrier functions[283]. GBM, rich in type IV collagens, proteoglycans and laminins, are considered to be important in forming a size-selective and charge-selective barrier in the kidney[284]. Podocytes are terminally differentiated cells with lots of digit-like foot processes connected by slit diaphragm which is another important structure to the barrier functions[285]. Irreplaceable functions of podocytes include 1) supporting structures to the capillary loop and counteracting the glomerular capillary hydrostatic pressure[286], 2) removing proteins and immunoglobulins that may clog the filter[287], 3) participating in the synthesis and repair of GBM[288] and 4) interact with glomerular endothelial cells and mesangial cells to maintain their functions[289].

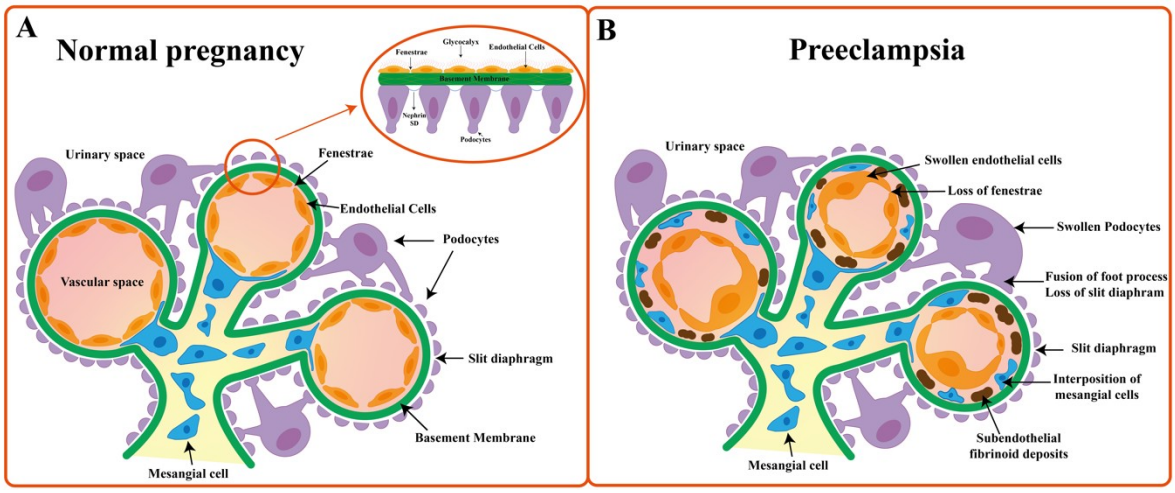


Figure 3. The schematic illustration of the glomerulus and glomerular filtration barrier in normal pregnancy (A) and preeclampsia (B). In preeclampsia, swollen endothelial cells and mesangial cells (glomerular capillary endotheliosis) are seen, which results in the loss of density and size of fenestrate, increased subendothelial fibrinoid deposits and interposition of mesangial cells (“double contour” of basement membrane). Segmental foot process fusion, slightly reduced number of the slit diaphragm (SD), and swollen podocytes are also observed in PE.

Under microscopic examinations (Figure 3), the glomeruli are enlarged and solidified due to the narrowness and occlusion of capillary lumens by the swollen endothelial cells and mesangial cells[290]. This has resulted in the glomerulus appearing 'bloodless' which is a hallmark feature of PE, though it can also appear in other hypertensive disorders[290]. This observation is first defined as glomerular capillary endotheliosis by Spargo *et al*[291]. Due to the swollen endothelial cells, the density and size of the fenestrate between the glomerular endothelial cells are reduced[292]. Furthermore, the increased subendothelial fibrinoid deposits as well as the interposition of mesangial cells further reduce the permeability of the GFB. The interposition of mesangial cells into the capillaries has resulted in a "double contoured" appearance of the basement membrane[293]. Interestingly, a constant debate about whether the GBM is thickened in PE hasn't come to a consensus. Some studies have supported a thickened basement membrane[293,294] while more recent studies didn't support such observations[292,295,296]. More studies are required to elucidate this observation. Other than the change of thickness, evidence has shown a decreased negative charge of the basement membrane has weakened the charge selectivity of the filtration barrier in PE[296]. Later evidence has pointed out that endotheliosis can also appear in normal pregnant women's kidneys[297]. This has brought the role of podocytes in the renal pathology of preeclampsia into the focus of attention [277]. However, historical microscopic examinations have not find significant structural or quantity changes in podocytes[292,296,298]. Only some segmental foot process fusion[296], a slightly reduced number of the slit diaphragm (1264 *per mm* GBM in NP vs 1133 *per mm* GBM in PE)[292], and swollen podocytes (in 18% PE patients) were seen in PE[299]. Nevertheless, gaining renal biopsies to perform microscopic examinations in the time of disease is not always possible and some microscopic evidence is from postpartum which weakens the strength of the evidence[296].

Other evidence has emerged to support the importance of podocytes in the renal pathology of PE. Podocytes are exposed to the constant fluid flow, which increases their possibility of detachment compared to other static cells. Indeed, by doing urinalysis, more podocytes were found in the PE urine when compared to NP and the level of podocyturia is positively correlated to the level of proteinuria[300]. The shedding of podocytes implies adhesion ability of the podocytes is reduced in PE. The reduced podocyte adhesion ability is further supported by the loss of nephrin on podocytes in PE. Nephrin, as an essential component of the slit diaphragm, is responsible for regulating actin filament network and focal adhesion dynamics including lamellipodia formation[301,302]. The reduced expression of nephrin in PE compared to normotensive or chronic hypertensive pregnancies has been well established using kidney tissue sections[303,304]. Additionally, excessive nephrin excretion in urine is also found in the PE compared to NP[305-307] and this increased level of nephrin excretion has shown a direct positively correlation with the degree of proteinuria[308,309]. The reduced number of podocytes may further lead to the impaired barrier functions in PE patients and lead to the development of proteinuria[310]. Podocytes, as terminally differentiated cells, cannot renew themselves[311]. The potential replenishment of lost podocytes has been associated with local pluripotent progenitor cells, including parietal epithelial cells (PECs), Cells of Renin Lineage (CoRL), or bone marrow-derived stem cells that might differentiate into podocytes in response to local signals[311-313]. However, the exact mechanisms underlying podocyte replacement continue to be the subject of ongoing scientific debate. In PE, if the podocytes are constantly detached from GFB, it would be reasonable to assume that podocyte replenish should have been increased as a recovery process–after delivery. Indeed, increased intraglomerular cell proliferation and more activated parietal epithelial cells on a podocyte location are found in PE compared to NP or hypertensive controls[299].

Angiogenic factors are playing important roles in the renal pathology of PE. Increasing sFlt-1 in the maternal circulation is a hallmark of preeclamptic patients sFlt-1 can bind and antagonize VEGF and placental growth factor (PlGF) which can lead to vasoconstriction and endothelial dysfunctions[258]. Excessive sFlt-1 in the maternal circulation can be both harmful to glomerular endothelial cells and podocytes. For glomerular endothelial cells, sFlt-1 has been shown to cause rapid glomerular endothelial cell detachment, cell damage and hypertrophy in a mice model[314]. For podocytes, sFlt-1 can induce the loss of slit diaphragms and the reduction of nephrin expression[314]. Injecting excessive sFlt-1 into mice can induce classic preeclampsia symptoms including hypertension, proteinuria and glomerular injury which can be rescued by exogenous VEGF and PlGF[269,314]. Similar to sFlt-1, soluble endoglin (sEng), another soluble factor released in increased quantity by diseased placenta, can bind and antagonize transforming growth factor β(TGF-β)[270]. Excessive sEng can also induce hypertension, proteinuria and glomerular injury (endotheliosis) in mice[315]. Direct evidence of how sEng influences podocytes is lacking, but it has been suggested sEng may cause podocyte detachment through the impaired binding of integrin α3β1 to laminin-521 on the GBM[316].

1.5 The possible roles of placental EV in renal damage in PE

Placental EV can be detected in the maternal circulation as early as 6 weeks of gestation[272]. Some *in vivo* evidence has shed light on how placenta EV can influence kidney functions. Injecting mice with placental EV isolated from injured placenta induce preeclampsia symptoms such as hypertension and proteinuria and kidneys displaying vascular leakage and fibrin deposition in the glomerular capillaries[317]. These effects can be rescued by the

microvesicle-scavenging factor lactadherin[317]. *Chang et al* also studied the effect of injecting placental EV isolated from plasma into mice[318]. Injecting placental EV isolated from PE plasma induced PE-like symptoms such as hypertension as well as elevated sFlt-1 and sEng levels[318]. However, they didn't find any glomerular injury by immunohistochemistry and the mice didn't develop proteinuria[318].

Placenta EV from preeclamptic patients carry excessive sFlg-1 and sEng which can impair angiogenesis and reduce the proliferation and migration of human umbilical vein endothelial cells (HUVEC)[318]. Similarly, placental EV from preeclampsia can impair human aortic endothelial cells (HAECs) migration ability, barrier integrity and endothelial-dependent vasodilator function, such as the endothelial cells' response to acetylcholine-induced relaxation and downregulation of eNOS[319]. The coronary artery endothelial cells (HCAEC) can also be influenced by placental EV via transferring placenta-specific miRNAs into the endoplasmic reticulum and mitochondria, and downregulating PE-associated genes such as FLT1[320].

Evidence on how placental EV influence podocytes is scarce. Under healthy conditions, it's generally accepted that, molecules smaller than 2 nm can freely traverse the GFB, while those larger than 4.2 nm face considerable restriction[321]. Molecules between these sizes experience varying levels of filtration[321]. Given the substantial size of EVs, ranging from 10 nm to 1 μm, their traversal across the GFB seems unlikely. However, in vivo evidence has shed light on the possibility of EV to transverse GFB in healthy status. A study showed that fluorescence labelled EV injected into the rat circulation can reach the urine[322]. This suggests a high likelihood that these injected EV interact with podocytes as they pass through the GFB to the urinary system. Detection of the fluorescence-labelled placenta EV in kidney tissues also

implicate the possibility of placenta EV come in contact with podocytes as part of the journey leaving the circulation[323]. It is also possible that the placental EV can be translocated by glomerular endothelial cells into the podocytes. This is supported by the evidence that when endocytosis takes place in endothelial cells, the cargo may undergo transcytosis across the endothelial cell to the underlying tissue[324]. However, given the complexity of the mechanisms dictating how molecules traverse the GFB – involving a dynamic interplay among glomerular endothelial cells, the basement membrane, and podocytes – further research is needed to elucidate the precise route EVs take through the GFB. In the pathological condition, the filtration slits of podocytes may widen, potentially allowing even larger EV to pass through[325]. Placenta EV has a variety range of size and certain placenta EV might be capable of traversing the GFB and entering the urine.

Considering the evidence presented above, I aim to investigate the potential of placental EV to pass through GFB and be internalised by podocytes. Furthermore, I am interested in understanding the impact that these placental EV might have on podocytes.

1.7 Conclusion

Placenta-derived EV carrying proteins, nucleic acids and lipids, with PE disease specific alterations, could be important contributors to the pathogenic mechanisms of glomerular damage. In addition, these EV can also be valuable biomarkers to diagnose or stratify the disease severity. However, in order to unveil the roles of EV, novel and reliable isolation and characterisation methods are required.

Furthermore, renal injury and proteinuria are frequently observed in PE, but the underlying mechanisms causing these conditions remain largely unknown. It is critical to deepen our understanding of the factors contributing to these symptoms, including the potential influence of placental EV. Given the complexity of these processes, further research and a multi-faceted approach will be necessary to elucidate these mechanisms fully. This could potentially lead to more effective prevention strategies, diagnostic tools, and treatments for PE in the future.

In this thesis, I first investigate a novel, clinically-applicable device for characterizing small EV, with the aim of using small placental extracellular vesicle (psEV) to aid in the early diagnosis of preeclampsia. Following this, I delve into a thorough analysis of the functional impact of psEV from normal pregnancies and those affected by preeclampsia on podocytes.

Finally, leveraging bioinformatics tools, I provide an extensive exploration of the influence exerted by psEV on podocytes.

1.8 Reference

1. Schorey JS, Cheng Y, Singh PP, Smith VL. Exosomes and other extracellular vesicles in host-pathogen interactions. *EMBO Rep*. 2015;16:24-43. doi: 10.15252/embr.201439363
2. van Niel G, D'Angelo G, Raposo G. Shedding light on the cell biology of extracellular vesicles. *Nat Rev Mol Cell Biol*. 2018;19:213-228. doi: 10.1038/nrm.2017.125
3. Poon IKH, Chiu Y-H, Armstrong AJ, Kinchen JM, Juncadella IJ, Bayliss DA, Ravichandran KS. Unexpected link between an antibiotic, pannexin channels and apoptosis. *Nature*. 2014;507:329-334. doi: 10.1038/nature13147
4. Atkin-Smith GK, Tixeira R, Paone S, Mathivanan S, Collins C, Liem M, Goodall KJ, Ravichandran KS, Hulett MD, Poon IKH. A novel mechanism of generating extracellular vesicles during apoptosis via a beads-on-a-string membrane structure. *Nature Communications*. 2015;6:7439. doi: 10.1038/ncomms8439
5. Saraste A, Pulkki K. Morphologic and biochemical hallmarks of apoptosis. *Cardiovascular Research*. 2000;45:528-537. doi: 10.1016/s0008-6363(99)00384-3
6. Urbanelli L, Magini A, Buratta S, Brozzi A, Sagini K, Polchi A, Tancini B, Emiliani C. Signaling Pathways in Exosomes Biogenesis, Secretion and Fate. *Genes*. 2013;4:152-170.
7. Colombo F, Bastoni M, Nigro A, Podini P, Finardi A, Casella G, Ramesh M, Farina C, Verderio C, Furlan R. Cytokines Stimulate the Release of Microvesicles from Myeloid Cells Independently from the P2X7 Receptor/Acid Sphingomyelinase Pathway. *Front Immunol*. 2018;9:204. doi: 10.3389/fimmu.2018.00204
8. Lopatina T, Bruno S, Tetta C, Kalinina N, Porta M, Camussi G. Platelet-derived growth factor regulates the secretion of extracellular vesicles by adipose mesenchymal stem cells and enhances their angiogenic potential. *Cell Communication and Signaling*. 2014;12:26. doi: 10.1186/1478-811X-12-26
9. Vion A-C, Ramkhelawon B, Loyer X, Chironi G, Devue C, Loirand G, Tedgui A, Lehoux S, Boulanger CM. Shear Stress Regulates Endothelial Microparticle Release. *Circulation Research*. 2013;112:1323-1333. doi: doi:10.1161/CIRCRESAHA.112.300818
10. Wang T, Gilkes DM, Takano N, Xiang L, Luo W, Bishop CJ, Chaturvedi P, Green JJ, Semenza GL. Hypoxia-inducible factors and RAB22A mediate formation of microvesicles that stimulate breast cancer invasion and metastasis. *Proceedings of the National Academy of Sciences*. 2014;111:E3234-E3242. doi: doi:10.1073/pnas.1410041111

11. Morita S-y, Ikeda Y. Regulation of membrane phospholipid biosynthesis in mammalian cells. *Biochemical Pharmacology*. 2022;206:115296. doi: https://doi.org/10.1016/j.bcp.2022.115296
12. Daleke DL. Regulation of transbilayer plasma membrane phospholipid asymmetry. *Journal of Lipid Research*. 2003;44:233-242. doi: 10.1194/jlr.R200019-JLR200
13. Bevers EM, Comfurius P, Dekkers DWC, Zwaal RFA. Lipid translocation across the plasma membrane of mammalian cells. *Biochimica et Biophysica Acta (BBA) - Molecular and Cell Biology of Lipids*. 1999;1439:317-330. doi: https://doi.org/10.1016/S1388-1981(99)00110-9
14. Hugel B, Martínez MC, Kunzelmann C, Freyssinet J-M. Membrane Microparticles: Two Sides of the Coin. *Physiology*. 2005;20:22-27. doi: 10.1152/physiol.00029.2004
15. Yu X, Xu J, Liu W, Xu W. Bubbles Induce Endothelial Microparticle Formation via a Calcium-Dependent Pathway Involving Flippase Inactivation and Rho Kinase Activation. *Cellular Physiology and Biochemistry*. 2018;46:965-974. doi: 10.1159/000488825
16. Sebbagh M, Renvoizé C, Hamelin J, Riché N, Bertoglio J, Bréard J. Caspase-3-mediated cleavage of ROCK I induces MLC phosphorylation and apoptotic membrane blebbing. *Nat Cell Biol*. 2001;3:346-352. doi: 10.1038/35070019
17. Coleman ML, Sahai EA, Yeo M, Bosch M, Dewar A, Olson MF. Membrane blebbing during apoptosis results from caspase-mediated activation of ROCK I. *Nat Cell Biol*. 2001;3:339-345. doi: 10.1038/35070009
18. Henne WM, Buchkovich NJ, Emr SD. The ESCRT pathway. *Dev Cell*. 2011;21:77-91. doi: 10.1016/j.devcel.2011.05.015
19. Avalos-Padilla Y, Georgiev VN, Lantero E, Pujals S, Verhoef R, N. Borgheti-Cardoso L, Albertazzi L, Dimova R, Fernàndez-Busquets X. The ESCRT-III machinery participates in the production of extracellular vesicles and protein export during Plasmodium falciparum infection. *PLOS Pathogens*. 2021;17:e1009455. doi: 10.1371/journal.ppat.1009455
20. McCullough J, Colf LA, Sundquist WI. Membrane fission reactions of the mammalian ESCRT pathway. *Annu Rev Biochem*. 2013;82:663-692. doi: 10.1146/annurev-biochem-072909-101058
21. Raiborg C, Stenmark H. The ESCRT machinery in endosomal sorting of ubiquitylated membrane proteins. *Nature*. 2009;458:445-452. doi: 10.1038/nature07961
22. Wehman AM, Poggioli C, Schweinsberg P, Grant BD, Nance J. The P4-ATPase TAT-5 inhibits the budding of extracellular vesicles in C. elegans embryos. *Curr Biol*. 2011;21:1951-1959. doi: 10.1016/j.cub.2011.10.040
23. Nabhan JF, Hu R, Oh RS, Cohen SN, Lu Q. Formation and release of arrestin domain-containing protein 1-mediated microvesicles (ARMMs) at plasma membrane by recruitment of TSG101 protein. *Proc Natl Acad Sci U S A*. 2012;109:4146-4151. doi: 10.1073/pnas.1200448109
24. Nabhan JF, Hu R, Oh RS, Cohen SN, Lu Q. Formation and release of arrestin domain-containing protein 1-mediated microvesicles (ARMMs) at plasma membrane by recruitment of TSG101 protein. *Proceedings of the National Academy of Sciences*. 2012;109:4146-4151. doi: doi:10.1073/pnas.1200448109
25. Robbins PD, Morelli AE. Regulation of immune responses by extracellular vesicles. *Nat Rev Immunol*. 2014;14:195-208. doi: 10.1038/nri3622
26. Melki I, Tessandier N, Zufferey A, Boilard E. Platelet microvesicles in health and disease. *Platelets*. 2017;28:214-221. doi: 10.1080/09537104.2016.1265924
27. Pfeiler S, Thakur M, Grünauer P, Megens RTA, Joshi U, Coletti R, Samara V, Müller-Stoy G, Ishikawa-Ankerhold H, Stark K, et al. CD36-triggered cell invasion

and persistent tissue colonization by tumor microvesicles during metastasis. *Faseb j*. 2019;33:1860-1872. doi: 10.1096/fj.201800985R
28. Han QF, Li WJ, Hu KS, Gao J, Zhai WL, Yang JH, Zhang SJ. Exosome biogenesis: machinery, regulation, and therapeutic implications in cancer. *Mol Cancer*. 2022;21:207. doi: 10.1186/s12943-022-01671-0
29. Abels ER, Breakefield XO. Introduction to Extracellular Vesicles: Biogenesis, RNA Cargo Selection, Content, Release, and Uptake. *Cell Mol Neurobiol*. 2016;36:301-312. doi: 10.1007/s10571-016-0366-z
30. Akers JC, Gonda D, Kim R, Carter BS, Chen CC. Biogenesis of extracellular vesicles (EV): exosomes, microvesicles, retrovirus-like vesicles, and apoptotic bodies. *J Neurooncol*. 2013;113:1-11. doi: 10.1007/s11060-013-1084-8
31. Kalluri R, LeBleu VS. The biology, function, and biomedical applications of exosomes. *Science*. 2020;367:eaau6977. doi: doi:10.1126/science.aau6977
32. Colombo M, Moita C, van Niel G, Kowal J, Vigneron J, Benaroch P, Manel N, Moita LF, Théry C, Raposo G. Analysis of ESCRT functions in exosome biogenesis, composition and secretion highlights the heterogeneity of extracellular vesicles. *J Cell Sci*. 2013;126:5553-5565. doi: 10.1242/jcs.128868
33. Kitatani K, Idkowiak-Baldys J, Hannun YA. The sphingolipid salvage pathway in ceramide metabolism and signaling. *Cell Signal*. 2008;20:1010-1018. doi: 10.1016/j.cellsig.2007.12.006
34. Trajkovic K, Hsu C, Chiantia S, Rajendran L, Wenzel D, Wieland F, Schwille P, Brügger B, Simons M. Ceramide Triggers Budding of Exosome Vesicles into Multivesicular Endosomes. *Science*. 2008;319:1244-1247. doi: doi:10.1126/science.1153124
35. Hurwitz SN, Conlon MM, Rider MA, Brownstein NC, Meckes DG, Jr. Nanoparticle analysis sheds budding insights into genetic drivers of extracellular vesicle biogenesis. *J Extracell Vesicles*. 2016;5:31295. doi: 10.3402/jev.v5.31295
36. Böker KO, Lemus-Diaz N, Rinaldi Ferreira R, Schiller L, Schneider S, Gruber J. The Impact of the CD9 Tetraspanin on Lentivirus Infectivity and Exosome Secretion. *Mol Ther*. 2018;26:634-647. doi: 10.1016/j.ymthe.2017.11.008
37. Chairoungdua A, Smith DL, Pochard P, Hull M, Caplan MJ. Exosome release of β-catenin: a novel mechanism that antagonizes Wnt signaling. *J Cell Biol*. 2010;190:1079-1091. doi: 10.1083/jcb.201002049
38. Andreu Z, Yáñez-Mó M. Tetraspanins in extracellular vesicle formation and function. *Front Immunol*. 2014;5:442. doi: 10.3389/fimmu.2014.00442
39. Théry C, Witwer KW, Aikawa E, Alcaraz MJ, Anderson JD, Andriantsitohaina R, Antoniou A, Arab T, Archer F, Atkin-Smith GK, et al. Minimal information for studies of extracellular vesicles 2018 (MISEV2018): a position statement of the International Society for Extracellular Vesicles and update of the MISEV2014 guidelines. *J Extracell Vesicles*. 2018;7:1535750. doi: 10.1080/20013078.2018.1535750
40. Conde-Vancells J, Rodriguez-Suarez E, Embade N, Gil D, Matthiesen R, Valle M, Elortza F, Lu SC, Mato JM, Falcon-Perez JM. Characterization and comprehensive proteome profiling of exosomes secreted by hepatocytes. *J Proteome Res*. 2008;7:5157-5166. doi: 10.1021/pr8004887
41. Muraoka S, DeLeo AM, Sethi MK, Yukawa-Takamatsu K, Yang Z, Ko J, Hogan JD, Ruan Z, You Y, Wang Y, et al. Proteomic and biological profiling of extracellular vesicles from Alzheimer's disease human brain tissues. *Alzheimers Dement*. 2020;16:896-907. doi: 10.1002/alz.12089

42. Nunez Lopez YO, Iliuk A, Petrilli AM, Glass C, Casu A, Pratley RE. Proteomics and Phosphoproteomics of Circulating Extracellular Vesicles Provide New Insights into Diabetes Pathobiology. *Int J Mol Sci*. 2022;23. doi: 10.3390/ijms23105779
43. Almeida A, Gabriel M, Firlej V, Martin-Jaular L, Lejars M, Cipolla R, Petit F, Vogt N, San-Roman M, Dingli F, et al. Urinary extracellular vesicles contain mature transcriptome enriched in circular and long noncoding RNAs with functional significance in prostate cancer. *J Extracell Vesicles*. 2022;11:e12210. doi: 10.1002/jev2.12210
44. Tsering T, Li M, Chen Y, Nadeau A, Laskaris A, Abdouh M, Bustamante P, Burnier JV. EV-ADD, a database for EV-associated DNA in human liquid biopsy samples. *J Extracell Vesicles*. 2022;11:e12270. doi: 10.1002/jev2.12270
45. Alonso-Alonso ML, García-Posadas L, Diebold Y. Extracellular Vesicles from Human Adipose-Derived Mesenchymal Stem Cells: A Review of Common Cargos. *Stem Cell Rev Rep*. 2022;18:854-901. doi: 10.1007/s12015-021-10155-5
46. Monteiro-Reis S, Carvalho-Maia C, Bart G, Vainio SJ, Pedro J, Silva ER, Sales G, Henrique R, Jerónimo C. Secreted Extracellular Vesicle Molecular Cargo as a Novel Liquid Biopsy Diagnostics of Central Nervous System Diseases. *Int J Mol Sci*. 2021;22. doi: 10.3390/ijms22063267
47. Phoonsawat W, Aoki-Yoshida A, Tsuruta T, Sonoyama K. Adiponectin is partially associated with exosomes in mouse serum. *Biochemical and Biophysical Research Communications*. 2014;448:261-266. doi: https://doi.org/10.1016/j.bbrc.2014.04.114
48. Gill M, Motta-Mejia C, Kandzija N, Cooke W, Zhang W, Cerdeira AS, Bastie C, Redman C, Vatish M. Placental Syncytiotrophoblast-Derived Extracellular Vesicles Carry Active NEP (Neprilysin) and Are Increased in Preeclampsia. *Hypertension*. 2019;73:1112-1119. doi: 10.1161/hypertensionaha.119.12707
49. Skotland T, Sagini K, Sandvig K, Llorente A. An emerging focus on lipids in extracellular vesicles. *Advanced Drug Delivery Reviews*. 2020;159:308-321. doi: https://doi.org/10.1016/j.addr.2020.03.002
50. Skotland T, Ekroos K, Kauhanen D, Simolin H, Seierstad T, Berge V, Sandvig K, Llorente A. Molecular lipid species in urinary exosomes as potential prostate cancer biomarkers. *European Journal of Cancer*. 2017;70:122-132. doi: https://doi.org/10.1016/j.ejca.2016.10.011
51. Brzozowski JS, Jankowski H, Bond DR, McCague SB, Munro BR, Predebon MJ, Scarlett CJ, Skelding KA, Weidenhofer J. Lipidomic profiling of extracellular vesicles derived from prostate and prostate cancer cell lines. *Lipids in Health and Disease*. 2018;17:211. doi: 10.1186/s12944-018-0854-x
52. Nishida-Aoki N, Izumi Y, Takeda H, Takahashi M, Ochiya T, Bamba T. Lipidomic Analysis of Cells and Extracellular Vesicles from High- and Low-Metastatic Triple-Negative Breast Cancer. *Metabolites*. 2020;10. doi: 10.3390/metabo10020067
53. Fernando MR, Jiang C, Krzyzanowski GD, Ryan WL. New evidence that a large proportion of human blood plasma cell-free DNA is localized in exosomes. *PLoS One*. 2017;12:e0183915. doi: 10.1371/journal.pone.0183915
54. O'Brien K, Breyne K, Ughetto S, Laurent LC, Breakefield XO. RNA delivery by extracellular vesicles in mammalian cells and its applications. *Nat Rev Mol Cell Biol*. 2020;21:585-606. doi: 10.1038/s41580-020-0251-y
55. Pan Y, Hui X, Hoo RLC, Ye D, Chan CYC, Feng T, Wang Y, Lam KSL, Xu A. Adipocyte-secreted exosomal microRNA-34a inhibits M2 macrophage polarization to promote obesity-induced adipose inflammation. *J Clin Invest*. 2019;129:834-849. doi: 10.1172/jci123069

56. Chaiwangyen W, Murrieta-Coxca JM, Favaro RR, Photini SM, Gutiérrez-Samudio RN, Schleussner E, Markert UR, Morales-Prieto DM. MiR-519d-3p in Trophoblastic Cells: Effects, Targets and Transfer to Allogeneic Immune Cells via Extracellular Vesicles. *Int J Mol Sci*. 2020;21. doi: 10.3390/ijms21103458
57. Elzanowska J, Semira C, Costa-Silva B. DNA in extracellular vesicles: biological and clinical aspects. *Mol Oncol*. 2021;15:1701-1714. doi: 10.1002/1878-0261.12777
58. Tutanov O, Shtam T, Grigor'eva A, Tupikin A, Tsentalovich Y, Tamkovich S. Blood Plasma Exosomes Contain Circulating DNA in Their Crown. *Diagnostics (Basel)*. 2022;12. doi: 10.3390/diagnostics12040854
59. Takahashi A, Okada R, Nagao K, Kawamata Y, Hanyu A, Yoshimoto S, Takasugi M, Watanabe S, Kanemaki MT, Obuse C, et al. Exosomes maintain cellular homeostasis by excreting harmful DNA from cells. *Nat Commun*. 2017;8:15287. doi: 10.1038/ncomms15287
60. Seo W, Gao Y, He Y, Sun J, Xu H, Feng D, Park SH, Cho YE, Guillot A, Ren T, et al. ALDH2 deficiency promotes alcohol-associated liver cancer by activating oncogenic pathways via oxidized DNA-enriched extracellular vesicles. *J Hepatol*. 2019;71:1000-1011. doi: 10.1016/j.jhep.2019.06.018
61. Kitai Y, Kawasaki T, Sueyoshi T, Kobiyama K, Ishii KJ, Zou J, Akira S, Matsuda T, Kawai T. DNA-Containing Exosomes Derived from Cancer Cells Treated with Topotecan Activate a STING-Dependent Pathway and Reinforce Antitumor Immunity. *J Immunol*. 2017;198:1649-1659. doi: 10.4049/jimmunol.1601694
62. Konečná B, Tóthová Ľ, Repiská G. Exosomes-Associated DNA-New Marker in Pregnancy Complications? *Int J Mol Sci*. 2019;20. doi: 10.3390/ijms20122890
63. Pan M, Lu J, Liu Z, Shi H, Bai Y, Chen P, Ge Q. Integrity of cell-free DNA in maternal plasma extracellular vesicles as a potential biomarker for non-invasive prenatal testing. *Int J Gynaecol Obstet*. 2022;158:406-417. doi: 10.1002/ijgo.13976
64. Orozco AF, Jorgez CJ, Ramos-Perez WD, Popek EJ, Yu X, Kozinetz CA, Bischoff FZ, Lewis DE. Placental release of distinct DNA-associated micro-particles into maternal circulation: reflective of gestation time and preeclampsia. *Placenta*. 2009;30:891-897. doi: 10.1016/j.placenta.2009.06.012
65. Lajoie P, Nabi IR. Regulation of raft-dependent endocytosis. *J Cell Mol Med*. 2007;11:644-653. doi: 10.1111/j.1582-4934.2007.00083.x
66. Magee AI, Parmryd I. Detergent-resistant membranes and the protein composition of lipid rafts. *Genome Biology*. 2003;4:234. doi: 10.1186/gb-2003-4-11-234
67. Kaksonen M, Roux A. Mechanisms of clathrin-mediated endocytosis. *Nature Reviews Molecular Cell Biology*. 2018;19:313-326. doi: 10.1038/nrm.2017.132
68. Kiss AL, Botos E. Endocytosis via caveolae: alternative pathway with distinct cellular compartments to avoid lysosomal degradation? *J Cell Mol Med*. 2009;13:1228-1237. doi: 10.1111/j.1582-4934.2009.00754.x
69. de Gassart A, Géminard C, Février B, Raposo G, Vidal M. Lipid raft-associated protein sorting in exosomes. *Blood*. 2003;102:4336-4344. doi: https://doi.org/10.1182/blood-2003-03-0871
70. Staubach S, Razawi H, Hanisch FG. Proteomics of MUC1-containing lipid rafts from plasma membranes and exosomes of human breast carcinoma cells MCF-7. *Proteomics*. 2009;9:2820-2835. doi: 10.1002/pmic.200800793
71. Costa Verdera H, Gitz-Francois JJ, Schiffelers RM, Vader P. Cellular uptake of extracellular vesicles is mediated by clathrin-independent endocytosis and macropinocytosis. *Journal of Controlled Release*. 2017;266:100-108. doi: https://doi.org/10.1016/j.jconrel.2017.09.019

72. Ghossoub R, Lembo F, Rubio A, Gaillard CB, Bouchet J, Vitale N, Slavík J, Machala M, Zimmermann P. Syntenin-ALIX exosome biogenesis and budding into multivesicular bodies are controlled by ARF6 and PLD2. *Nat Commun*. 2014;5:3477. doi: 10.1038/ncomms4477
73. Means N, Elechalawar CK, Chen WR, Bhattacharya R, Mukherjee P. Revealing macropinocytosis using nanoparticles. *Molecular Aspects of Medicine*. 2022;83:100993. doi: https://doi.org/10.1016/j.mam.2021.100993
74. Doherty GJ, McMahon HT. Mechanisms of endocytosis. *Annu Rev Biochem*. 2009;78:857-902. doi: 10.1146/annurev.biochem.78.081307.110540
75. Swanson JA. Shaping cups into phagosomes and macropinosomes. *Nat Rev Mol Cell Biol*. 2008;9:639-649. doi: 10.1038/nrm2447
76. Feng D, Zhao WL, Ye YY, Bai XC, Liu RQ, Chang LF, Zhou Q, Sui SF. Cellular internalization of exosomes occurs through phagocytosis. *Traffic*. 2010;11:675-687. doi: 10.1111/j.1600-0854.2010.01041.x
77. Fitzner D, Schnaars M, van Rossum D, Krishnamoorthy G, Dibaj P, Bakhti M, Regen T, Hanisch UK, Simons M. Selective transfer of exosomes from oligodendrocytes to microglia by macropinocytosis. *J Cell Sci*. 2011;124:447-458. doi: 10.1242/jcs.074088
78. Uribe-Querol E, Rosales C. Phagocytosis: Our Current Understanding of a Universal Biological Process. *Front Immunol*. 2020;11:1066. doi: 10.3389/fimmu.2020.01066
79. Feng D, Zhao W-L, Ye Y-Y, Bai X-C, Liu R-Q, Chang L-F, Zhou Q, Sui S-F. Cellular Internalization of Exosomes Occurs Through Phagocytosis. *Traffic*. 2010;11:675-687. doi: https://doi.org/10.1111/j.1600-0854.2010.01041.x
80. Botelho RJ, Grinstein S. Phagocytosis. *Curr Biol*. 2011;21:R533-538. doi: 10.1016/j.cub.2011.05.053
81. Ebert B, Rai AJ. Isolation and Characterization of Amniotic Fluid-Derived Extracellular Vesicles for Biomarker Discovery. *Methods Mol Biol*. 2019;1885:287-294. doi: 10.1007/978-1-4939-8889-1_19
82. Hu Y, Thaler J, Nieuwland R. Extracellular Vesicles in Human Milk. *Pharmaceuticals (Basel)*. 2021;14. doi: 10.3390/ph14101050
83. Chiabotto G, Gai C, Deregibus MC, Camussi G. Salivary Extracellular Vesicle-Associated exRNA as Cancer Biomarker. *Cancers (Basel)*. 2019;11. doi: 10.3390/cancers11070891
84. Krušić Alić V, Malenica M, Biberić M, Zrna S, Valenčić L, Šuput A, Kalagac Fabris L, Wechtersbach K, Kojc N, Kurtjak M, et al. Extracellular Vesicles from Human Cerebrospinal Fluid Are Effectively Separated by Sepharose CL-6B-Comparison of Four Gravity-Flow Size Exclusion Chromatography Methods. *Biomedicines*. 2022;10. doi: 10.3390/biomedicines10040785
85. Øverbye A, Skotland T, Koehler CJ, Thiede B, Seierstad T, Berge V, Sandvig K, Llorente A. Identification of prostate cancer biomarkers in urinary exosomes. *Oncotarget*. 2015;6:30357-30376. doi: 10.18632/oncotarget.4851
86. Bryzgunova OE, Zaripov MM, Skvortsova TE, Lekchnov EA, Grigor'eva AE, Zaporozhchenko IA, Morozkin ES, Ryabchikova EI, Yurchenko YB, Voitsitskiy VE, et al. Comparative Study of Extracellular Vesicles from the Urine of Healthy Individuals and Prostate Cancer Patients. *PLOS ONE*. 2016;11:e0157566. doi: 10.1371/journal.pone.0157566
87. Fu S, Zhang Y, Li Y, Luo L, Zhao Y, Yao Y. Extracellular vesicles in cardiovascular diseases. *Cell Death Discov*. 2020;6:68. doi: 10.1038/s41420-020-00305-y
88. Mazurskyy A, Howitt J. Extracellular Vesicles in Neurological Disorders. *Subcell Biochem*. 2021;97:411-436. doi: 10.1007/978-3-030-67171-6_16

89. Grange C, Bussolati B. Extracellular vesicles in kidney disease. *Nature Reviews Nephrology*. 2022;18:499-513. doi: 10.1038/s41581-022-00586-9
90. Szabo G, Momen-Heravi F. Extracellular vesicles in liver disease and potential as biomarkers and therapeutic targets. *Nat Rev Gastroenterol Hepatol*. 2017;14:455-466. doi: 10.1038/nrgastro.2017.71
91. Salomon C, Guanzon D, Scholz-Romero K, Longo S, Correa P, Illanes SE, Rice GE. Placental Exosomes as Early Biomarker of Preeclampsia: Potential Role of Exosomal MicroRNAs Across Gestation. *J Clin Endocrinol Metab*. 2017;102:3182-3194. doi: 10.1210/jc.2017-00672
92. Wu L, Zhou H, Lin H, Qi J, Zhu C, Gao Z, Wang H. Circulating microRNAs are elevated in plasma from severe preeclamptic pregnancies. *Reproduction*. 2012;143:389-397. doi: 10.1530/rep-11-0304
93. Sandrim VC, Luizon MR, Palei AC, Tanus-Santos JE, Cavalli RC. Circulating microRNA expression profiles in pre-eclampsia: evidence of increased miR-885-5p levels. *Bjog*. 2016;123:2120-2128. doi: 10.1111/1471-0528.13903
94. Wang Y, Du X, Wang J. Transfer of miR-15a-5p by placental exosomes promotes pre-eclampsia progression by regulating PI3K/AKT signaling pathway via CDK1. *Mol Immunol*. 2020;128:277-286. doi: 10.1016/j.molimm.2020.10.019
95. Motawi TMK, Sabry D, Maurice NW, Rizk SM. Role of mesenchymal stem cells exosomes derived microRNAs; miR-136, miR-494 and miR-495 in pre-eclampsia diagnosis and evaluation. *Arch Biochem Biophys*. 2018;659:13-21. doi: 10.1016/j.abb.2018.09.023
96. Hromadnikova I, Dvorakova L, Kotlabova K, Krofta L. The Prediction of Gestational Hypertension, Preeclampsia and Fetal Growth Restriction via the First Trimester Screening of Plasma Exosomal C19MC microRNAs. *Int J Mol Sci*. 2019;20. doi: 10.3390/ijms20122972
97. Devor E, Santillan D, Scroggins S, Warrier A, Santillan M. Trimester-specific plasma exosome microRNA expression profiles in preeclampsia. *J Matern Fetal Neonatal Med*. 2020;33:3116-3124. doi: 10.1080/14767058.2019.1569614
98. Pillay P, Moodley K, Vatish M, Moodley J, Duarte R, Mackraj I. Exosomal Th1/Th2 cytokines in preeclampsia and HIV-positive preeclamptic women on highly active anti-retroviral therapy. *Cytokine*. 2020;125:154795. doi: https://doi.org/10.1016/j.cyto.2019.154795
99. Chen HY, Wang XY, Lu KM, Yu CH, Su MT, Kang L, Hsu KF, Chen PF, Lin SH. Maternal Th17/Treg Cytokines and Small Extracellular Vesicles in Plasma as Potential Biomarkers for Preeclampsia. *Int J Med Sci*. 2022;19:1672-1679. doi: 10.7150/ijms.71047
100. Tan KH, Tan SS, Ng MJ, Tey WS, Sim WK, Allen JC, Lim SK. Extracellular vesicles yield predictive pre-eclampsia biomarkers. *J Extracell Vesicles*. 2017;6:1408390. doi: 10.1080/20013078.2017.1408390
101. Levine L, Habertheuer A, Ram C, Korutla L, Schwartz N, Hu RW, Reddy S, Freas A, Zielinski PD, Harmon J, et al. Syncytiotrophoblast extracellular microvesicle profiles in maternal circulation for noninvasive diagnosis of preeclampsia. *Sci Rep*. 2020;10:6398. doi: 10.1038/s41598-020-62193-7
102. Tersigni C, Lucchetti D, Franco R, Colella F, Neri C, Crispino L, Sgambato A, Lanzone A, Scambia G, Vatish M, et al. Circulating Placental Vesicles Carry HLA-DR in Pre-Eclampsia: A New Potential Marker of the Syndrome. *Front Immunol*. 2021;12:717879. doi: 10.3389/fimmu.2021.717879

103. Zou G, Ji Q, Geng Z, Du X, Jiang L, Liu T. miR-31-5p from placental and peripheral blood exosomes is a potential biomarker to diagnose preeclampsia. *Hereditas*. 2022;159:35. doi: 10.1186/s41065-022-00250-z
104. Srinivasan S, Treacy R, Herrero T, Olsen R, Leonardo TR, Zhang X, DeHoff P, To C, Poling LG, Fernando A, et al. Discovery and Verification of Extracellular miRNA Biomarkers for Non-invasive Prediction of Pre-eclampsia in Asymptomatic Women. *Cell Rep Med*. 2020;1. doi: 10.1016/j.xcrm.2020.100013
105. Vargas A, Zhou S, Éthier-Chiasson M, Flipo D, Lafond J, Gilbert C, Barbeau B. Syncytin proteins incorporated in placenta exosomes are important for cell uptake and show variation in abundance in serum exosomes from patients with preeclampsia. *Faseb j*. 2014;28:3703-3719. doi: 10.1096/fj.13-239053
106. Lee S, Gonzalez-Suarez AM, Huang X, Calvo-Lozano O, Suvakov S, Lechuga LM, Garovic VD, Stybayeva G, Revzin A. Using Electrochemical Immunoassay in a Novel Microtiter Plate to Detect Surface Markers of Preeclampsia on Urinary Extracellular Vesicles. *ACS Sens*. 2022. doi: 10.1021/acssensors.2c02077
107. Hu CC, Katerelos M, Choy SW, Crossthwaite A, Walker SP, Pell G, Lee M, Cook N, Mount PF, Paizis K, et al. Pre-eclampsia is associated with altered expression of the renal sodium transporters NKCC2, NCC and ENaC in urinary extracellular vesicles. *PLoS One*. 2018;13:e0204514. doi: 10.1371/journal.pone.0204514
108. Isaksson GL, Nielsen LH, Palarasah Y, Jensen DM, Andersen LLT, Madsen K, Bistrup C, Jørgensen JS, Ovesen PG, Jensen BL. Urine excretion of C3dg and sC5b-9 coincide with proteinuria and development of preeclampsia in pregnant women with type-1 diabetes. *J Hypertens*. 2023;41:223-232. doi: 10.1097/hjh.0000000000003288
109. Gebara N, Scheel J, Skovronova R, Grange C, Marozio L, Gupta S, Giorgione V, Caicci F, Benedetto C, Khalil A, et al. Single extracellular vesicle analysis in human amniotic fluid shows evidence of phenotype alterations in preeclampsia. *J Extracell Vesicles*. 2022;11:e12217. doi: 10.1002/jev2.12217
110. Tang TT, Wang B, Lv LL, Liu BC. Extracellular vesicle-based Nanotherapeutics: Emerging frontiers in anti-inflammatory therapy. *Theranostics*. 2020;10:8111-8129. doi: 10.7150/thno.47865
111. Wang Z, Mo H, He Z, Chen A, Cheng P. Extracellular vesicles as an emerging drug delivery system for cancer treatment: Current strategies and recent advances. *Biomedicine & Pharmacotherapy*. 2022;153:113480. doi: https://doi.org/10.1016/j.biopha.2022.113480
112. Alvarez-Erviti L, Seow Y, Yin H, Betts C, Lakhal S, Wood MJA. Delivery of siRNA to the mouse brain by systemic injection of targeted exosomes. *Nature Biotechnology*. 2011;29:341-345. doi: 10.1038/nbt.1807
113. Sun D, Zhuang X, Xiang X, Liu Y, Zhang S, Liu C, Barnes S, Grizzle W, Miller D, Zhang HG. A novel nanoparticle drug delivery system: the anti-inflammatory activity of curcumin is enhanced when encapsulated in exosomes. *Mol Ther*. 2010;18:1606-1614. doi: 10.1038/mt.2010.105
114. Pascucci L, Coccè V, Bonomi A, Ami D, Ceccarelli P, Ciusani E, Viganò L, Locatelli A, Sisto F, Doglia SM, et al. Paclitaxel is incorporated by mesenchymal stromal cells and released in exosomes that inhibit in vitro tumor growth: a new approach for drug delivery. *J Control Release*. 2014;192:262-270. doi: 10.1016/j.jconrel.2014.07.042
115. Mizrak A, Bolukbasi MF, Ozdener GB, Brenner GJ, Madlener S, Erkan EP, Ströbel T, Breakefield XO, Saydam O. Genetically engineered microvesicles carrying suicide mRNA/protein inhibit schwannoma tumor growth. *Mol Ther*. 2013;21:101-108. doi: 10.1038/mt.2012.161

116. Luan X, Sansanaphongpricha K, Myers I, Chen H, Yuan H, Sun D. Engineering exosomes as refined biological nanoplatforms for drug delivery. *Acta Pharmacologica Sinica*. 2017;38:754-763. doi: 10.1038/aps.2017.12
117. Kim MS, Haney MJ, Zhao Y, Mahajan V, Deygen I, Klyachko NL, Inskoe E, Piroyan A, Sokolsky M, Okolie O, et al. Development of exosome-encapsulated paclitaxel to overcome MDR in cancer cells. *Nanomedicine: Nanotechnology, Biology and Medicine*. 2016;12:655-664. doi: https://doi.org/10.1016/j.nano.2015.10.012
118. Fuhrmann G, Serio A, Mazo M, Nair R, Stevens MM. Active loading into extracellular vesicles significantly improves the cellular uptake and photodynamic effect of porphyrins. *J Control Release*. 2015;205:35-44. doi: 10.1016/j.jconrel.2014.11.029
119. Sato YT, Umezaki K, Sawada S, Mukai SA, Sasaki Y, Harada N, Shiku H, Akiyoshi K. Engineering hybrid exosomes by membrane fusion with liposomes. *Sci Rep*. 2016;6:21933. doi: 10.1038/srep21933
120. Lamichhane TN, Raiker RS, Jay SM. Exogenous DNA Loading into Extracellular Vesicles via Electroporation is Size-Dependent and Enables Limited Gene Delivery. *Molecular Pharmaceutics*. 2015;12:3650-3657. doi: 10.1021/acs.molpharmaceut.5b00364
121. Wang M, Altinoglu S, Takeda YS, Xu Q. Integrating Protein Engineering and Bioorthogonal Click Conjugation for Extracellular Vesicle Modulation and Intracellular Delivery. *PLOS ONE*. 2015;10:e0141860. doi: 10.1371/journal.pone.0141860
122. Kooijmans SA, Aleza CG, Roffler SR, van Solinge WW, Vader P, Schiffelers RM. Display of GPI-anchored anti-EGFR nanobodies on extracellular vesicles promotes tumour cell targeting. *J Extracell Vesicles*. 2016;5:31053. doi: 10.3402/jev.v5.31053
123. Jeyaram A, Lamichhane TN, Wang S, Zou L, Dahal E, Kronstadt SM, Levy D, Parajuli B, Knudsen DR, Chao W, et al. Enhanced Loading of Functional miRNA Cargo via pH Gradient Modification of Extracellular Vesicles. *Mol Ther*. 2020;28:975-985. doi: 10.1016/j.ymthe.2019.12.007
124. Cave G, Kee R, Harvey M, Wu Z. pH Gradient Liposomes Extract Protein Bound Amitriptyline in Peritoneal Dialysis—Exploratory Work. *International Journal of Molecular Sciences*. 2022;23:11577.
125. Herrmann IK, Wood MJA, Fuhrmann G. Extracellular vesicles as a next-generation drug delivery platform. *Nature Nanotechnology*. 2021;16:748-759. doi: 10.1038/s41565-021-00931-2
126. Lai CP, Mardini O, Ericsson M, Prabhakar S, Maguire C, Chen JW, Tannous BA, Breakefield XO. Dynamic biodistribution of extracellular vesicles in vivo using a multimodal imaging reporter. *ACS Nano*. 2014;8:483-494. doi: 10.1021/nn404945r
127. Royo F, Théry C, Falcón-Pérez JM, Nieuwland R, Witwer KW. Methods for Separation and Characterization of Extracellular Vesicles: Results of a Worldwide Survey Performed by the ISEV Rigor and Standardization Subcommittee. *Cells*. 2020;9. doi: 10.3390/cells9091955
128. Konoshenko MY, Lekchnov EA, Vlassov AV, Laktionov PP. Isolation of Extracellular Vesicles: General Methodologies and Latest Trends. *Biomed Res Int*. 2018;2018:8545347. doi: 10.1155/2018/8545347
129. Théry C, Amigorena S, Raposo G, Clayton A. Isolation and characterization of exosomes from cell culture supernatants and biological fluids. *Curr Protoc Cell Biol*. 2006;Chapter 3:Unit 3.22. doi: 10.1002/0471143030.cb0322s30

130. Ramírez-Bajo MJ, Banon-Maneus E, Rovira J, Campistol JM, Diekmann F. Isolation of Extracellular Vesicles Derived from Mesenchymal Stromal Cells by Ultracentrifugation. *Bio Protoc*. 2020;10:e3860. doi: 10.21769/BioProtoc.3860
131. Baranyai T, Herczeg K, Onódi Z, Voszka I, Módos K, Marton N, Nagy G, Mäger I, Wood MJ, El Andaloussi S, et al. Isolation of Exosomes from Blood Plasma: Qualitative and Quantitative Comparison of Ultracentrifugation and Size Exclusion Chromatography Methods. *PLoS One*. 2015;10:e0145686. doi: 10.1371/journal.pone.0145686
132. Simonsen JB. What Are We Looking At? Extracellular Vesicles, Lipoproteins, or Both? *Circ Res*. 2017;121:920-922. doi: 10.1161/circresaha.117.311767
133. Santucci L, Bruschi M, Del Zotto G, Antonini F, Ghiggeri GM, Panfoli I, Candiano G. Biological surface properties in extracellular vesicles and their effect on cargo proteins. *Sci Rep*. 2019;9:13048. doi: 10.1038/s41598-019-47598-3
134. Fernández-Llama P, Khositseth S, Gonzales PA, Star RA, Pisitkun T, Knepper MA. Tamm-Horsfall protein and urinary exosome isolation. *Kidney Int*. 2010;77:736-742. doi: 10.1038/ki.2009.550
135. Yao C, Chen X, Xu Y, Wang F, Ji J, Xu H, He J, Wang L, Li Y. Comparing pretreatment strategies to increase the yield and purity of human urinary extracellular vesicles. *J Chromatogr B Analyt Technol Biomed Life Sci*. 2022;1206:123359. doi: 10.1016/j.jchromb.2022.123359
136. Liu Z, Cauvi DM, Bernardino EMA, Lara B, Lizardo RE, Hawisher D, Bickler S, De Maio A. Isolation and characterization of human urine extracellular vesicles. *Cell Stress Chaperones*. 2018;23:943-953. doi: 10.1007/s12192-018-0902-5
137. Webber J, Clayton A. How pure are your vesicles? *Journal of Extracellular Vesicles*. 2013;2:19861. doi: 10.3402/jev.v2i0.19861
138. Caradec J, Kharmate G, Hosseini-Beheshti E, Adomat H, Gleave M, Guns E. Reproducibility and efficiency of serum-derived exosome extraction methods. *Clin Biochem*. 2014;47:1286-1292. doi: 10.1016/j.clinbiochem.2014.06.011
139. Liangsupree T, Multia E, Riekkola M-L. Modern isolation and separation techniques for extracellular vesicles. *Journal of Chromatography A*. 2021;1636:461773. doi: https://doi.org/10.1016/j.chroma.2020.461773
140. Mori S, Barth HG. *Size exclusion chromatography*. Springer Science & Business Media; 1999.
141. Mol EA, Goumans M-J, Doevendans PA, Sluijter JPG, Vader P. Higher functionality of extracellular vesicles isolated using size-exclusion chromatography compared to ultracentrifugation. *Nanomedicine: Nanotechnology, Biology and Medicine*. 2017;13:2061-2065. doi: https://doi.org/10.1016/j.nano.2017.03.011
142. Linares R, Tan S, Gounou C, Arraud N, Brisson AR. High-speed centrifugation induces aggregation of extracellular vesicles. *Journal of extracellular vesicles*. 2015;4:29509.
143. Sódar BW, Kittel Á, Pálóczi K, Vukman KV, Osteikoetxea X, Szabó-Taylor K, Németh A, Sperlágh B, Baranyai T, Giricz Z, et al. Low-density lipoprotein mimics blood plasma-derived exosomes and microvesicles during isolation and detection. *Sci Rep*. 2016;6:24316. doi: 10.1038/srep24316
144. Vergauwen G, Dhondt B, Van Deun J, De Smedt E, Berx G, Timmerman E, Gevaert K, Miinalainen I, Cocquyt V, Braems G, et al. Confounding factors of ultrafiltration and protein analysis in extracellular vesicle research. *Scientific Reports*. 2017;7:2704. doi: 10.1038/s41598-017-02599-y

145. Gardiner C, Di Vizio D, Sahoo S, Théry C, Witwer KW, Wauben M, Hill AF. Techniques used for the isolation and characterization of extracellular vesicles: results of a worldwide survey. *J Extracell Vesicles*. 2016;5:32945. doi: 10.3402/jev.v5.32945
146. Shu S, Allen CL, Benjamin-Davalos S, Koroleva M, MacFarland D, Minderman H, Ernstoff MS. A Rapid Exosome Isolation Using Ultrafiltration and Size Exclusion Chromatography (REIUS) Method for Exosome Isolation from Melanoma Cell Lines. *Methods Mol Biol*. 2021;2265:289-304. doi: 10.1007/978-1-0716-1205-7_22
147. Benedikter BJ, Bouwman FG, Vajen T, Heinzmann ACA, Grauls G, Mariman EC, Wouters EFM, Savelkoul PH, Lopez-Iglesias C, Koenen RR, et al. Ultrafiltration combined with size exclusion chromatography efficiently isolates extracellular vesicles from cell culture media for compositional and functional studies. *Scientific Reports*. 2017;7:15297. doi: 10.1038/s41598-017-15717-7
148. Carnino JM, Lee H, Jin Y. Isolation and characterization of extracellular vesicles from Broncho-alveolar lavage fluid: a review and comparison of different methods. *Respiratory Research*. 2019;20:240. doi: 10.1186/s12931-019-1210-z
149. Lucchetti D, Fattorossi A, Sgambato A. Extracellular Vesicles in Oncology: Progress and Pitfalls in the Methods of Isolation and Analysis. *Biotechnology Journal*. 2019;14:1700716. doi: https://doi.org/10.1002/biot.201700716
150. Tiwari S, Kumar V, Randhawa S, Verma SK. Preparation and characterization of extracellular vesicles. *Am J Reprod Immunol*. 2021;85:e13367. doi: 10.1111/aji.13367
151. Zhu L, Sun HT, Wang S, Huang SL, Zheng Y, Wang CQ, Hu BY, Qin W, Zou TT, Fu Y, et al. Isolation and characterization of exosomes for cancer research. *J Hematol Oncol*. 2020;13:152. doi: 10.1186/s13045-020-00987-y
152. Taylor DD, Shah S. Methods of isolating extracellular vesicles impact down-stream analyses of their cargoes. *Methods*. 2015;87:3-10. doi: 10.1016/j.ymeth.2015.02.019
153. Niu Z, Pang RTK, Liu W, Li Q, Cheng R, Yeung WSB. Polymer-based precipitation preserves biological activities of extracellular vesicles from an endometrial cell line. *PLOS ONE*. 2017;12:e0186534. doi: 10.1371/journal.pone.0186534
154. Rider MA, Hurwitz SN, Meckes DG, Jr. ExtraPEG: A Polyethylene Glycol-Based Method for Enrichment of Extracellular Vesicles. *Sci Rep*. 2016;6:23978. doi: 10.1038/srep23978
155. Brownlee Z, Lynn KD, Thorpe PE, Schroit AJ. A novel "salting-out" procedure for the isolation of tumor-derived exosomes. *J Immunol Methods*. 2014;407:120-126. doi: 10.1016/j.jim.2014.04.003
156. Deregibus MC, Figliolini F, D'Antico S, Manzini PM, Pasquino C, De Lena M, Tetta C, Brizzi MF, Camussi G. Charge-based precipitation of extracellular vesicles. *Int J Mol Med*. 2016;38:1359-1366. doi: 10.3892/ijmm.2016.2759
157. Momen-Heravi F, Balaj L, Alian S, Mantel PY, Halleck AE, Trachtenberg AJ, Soria CE, Oquin S, Bonebreak CM, Saracoglu E, et al. Current methods for the isolation of extracellular vesicles. *Biol Chem*. 2013;394:1253-1262. doi: 10.1515/hsz-2013-0141
158. Ströhle G, Gan J, Li H. Affinity-based isolation of extracellular vesicles and the effects on downstream molecular analysis. *Analytical and Bioanalytical Chemistry*. 2022;414:7051-7067. doi: 10.1007/s00216-022-04178-1
159. Ma H, Liu J, Ali MM, Mahmood MAI, Labanieh L, Lu M, Iqbal SM, Zhang Q, Zhao W, Wan Y. Nucleic acid aptamers in cancer research, diagnosis and therapy. *Chemical Society Reviews*. 2015;44:1240-1256. doi: 10.1039/C4CS00357H
160. Chang M, Wang Q, Qin W, Shi X, Xu G. Rational Synthesis of Aptamer-Functionalized Polyethylenimine-Modified Magnetic Graphene Oxide Composites for Highly Efficient Enrichment and Comprehensive Metabolomics Analysis of

Exosomes. *Analytical Chemistry*. 2020;92:15497-15505. doi: 10.1021/acs.analchem.0c03374
161. Veerman RE, Teeuwen L, Czarnewski P, Güclüler Akpinar G, Sandberg A, Cao X, Pernemalm M, Orre LM, Gabrielsson S, Eldh M. Molecular evaluation of five different isolation methods for extracellular vesicles reveals different clinical applicability and subcellular origin. *Journal of Extracellular Vesicles*. 2021;10:e12128. doi: https://doi.org/10.1002/jev2.12128
162. Gutiérrez García G, Galicia García G, Zalapa Soto J, Izquierdo Medina A, Rotzinger-Rodríguez M, Casas Aguilar GA, López Pacheco CP, Aguayo Á, Aguilar-Hernandez MM. Analysis of RNA yield in extracellular vesicles isolated by membrane affinity column and differential ultracentrifugation. *PLOS ONE*. 2020;15:e0238545. doi: 10.1371/journal.pone.0238545
163. Li H, Ouyang Y, Sadovsky E, Parks WT, Chu T, Sadovsky Y. Unique microRNA Signals in Plasma Exosomes from Pregnancies Complicated by Preeclampsia. *Hypertension*. 2020;75:762-771. doi: 10.1161/hypertensionaha.119.14081
164. Herrera-Van Oostdam AS, Toro-Ortíz JC, López JA, Noyola DE, García-López DA, Durán-Figueroa NV, Martínez-Martínez E, Portales-Pérez DP, Salgado-Bustamante M, López-Hernández Y. Placental exosomes isolated from urine of patients with gestational diabetes exhibit a differential profile expression of microRNAs across gestation. *Int J Mol Med*. 2020;46:546-560. doi: 10.3892/ijmm.2020.4626
165. Tong M, Kleffmann T, Pradhan S, Johansson CL, DeSousa J, Stone PR, James JL, Chen Q, Chamley LW. Proteomic characterization of macro-, micro- and nano-extracellular vesicles derived from the same first trimester placenta: relevance for feto-maternal communication. *Human Reproduction*. 2016;31:687-699. doi: 10.1093/humrep/dew004
166. Burkova EE, Dmitrenok PS, Bulgakov DV, Vlassov VV, Ryabchikova EI, Nevinsky GA. Exosomes from human placenta purified by affinity chromatography on sepharose bearing immobilized antibodies against CD81 tetraspanin contain many peptides and small proteins. *IUBMB Life*. 2018;70:1144-1155. doi: https://doi.org/10.1002/iub.1928
167. Ayala-Ramírez P, Machuca-Acevedo C, Gámez T, Quijano S, Barreto A, Silva JL, Olaya CM, García-Robles R. Assessment of Placental Extracellular Vesicles-Associated Fas Ligand and TNF-Related Apoptosis-Inducing Ligand in Pregnancies Complicated by Early and Late Onset Preeclampsia. *Front Physiol*. 2021;12:708824. doi: 10.3389/fphys.2021.708824
168. Godakumara K, Ord J, Lättekivi F, Dissanayake K, Viil J, Boggavarapu NR, Faridani OR, Jääger K, Velthut-Meikas A, Jaakma Ü, et al. Trophoblast derived extracellular vesicles specifically alter the transcriptome of endometrial cells and may constitute a critical component of embryo-maternal communication. *Reproductive Biology and Endocrinology*. 2021;19:115. doi: 10.1186/s12958-021-00801-5
169. Ouyang Y, Bayer A, Chu T, Tyurin VA, Kagan VE, Morelli AE, Coyne CB, Sadovsky Y. Isolation of human trophoblastic extracellular vesicles and characterization of their cargo and antiviral activity. *Placenta*. 2016;47:86-95. doi: 10.1016/j.placenta.2016.09.008
170. Hussein S, Ju W, Pizzella S, Flory M, Chu C, Wang Y, Zhong N. Reduced expression in preterm birth of sFLT-1 and PlGF with a high sFLT-1/PlGF ratio in extracellular vesicles suggests a potential biomarker. *Front Endocrinol (Lausanne)*. 2022;13:1024587. doi: 10.3389/fendo.2022.1024587
171. Gillet V, Ouellet A, Stepanov Y, Rodosthenous RS, Croft EK, Brennan K, Abdelouahab N, Baccarelli A, Takser L. miRNA Profiles in Extracellular Vesicles

From Serum Early in Pregnancies Complicated by Gestational Diabetes Mellitus. *J Clin Endocrinol Metab*. 2019;104:5157-5169. doi: 10.1210/jc.2018-02693
172. Hartjes TA, Mytnyk S, Jenster GW, van Steijn V, van Royen ME. Extracellular Vesicle Quantification and Characterization: Common Methods and Emerging Approaches. *Bioengineering (Basel)*. 2019;6. doi: 10.3390/bioengineering6010007
173. Visnovitz T, Osteikoetxea X, Sódar BW, Mihály J, Lőrincz P, Vukman KV, Tóth EÁ, Koncz A, Székács I, Horváth R, et al. An improved 96 well plate format lipid quantification assay for standardisation of experiments with extracellular vesicles. *Journal of Extracellular Vesicles*. 2019;8:1565263. doi: 10.1080/20013078.2019.1565263
174. Mateescu B, Kowal EJ, van Balkom BW, Bartel S, Bhattacharyya SN, Buzás EI, Buck AH, de Candia P, Chow FW, Das S, et al. Obstacles and opportunities in the functional analysis of extracellular vesicle RNA - an ISEV position paper. *J Extracell Vesicles*. 2017;6:1286095. doi: 10.1080/20013078.2017.1286095
175. Vagner T, Spinelli C, Minciacchi VR, Balaj L, Zandian M, Conley A, Zijlstra A, Freeman MR, Demichelis F, De S, et al. Large extracellular vesicles carry most of the tumour DNA circulating in prostate cancer patient plasma. *Journal of Extracellular Vesicles*. 2018;7:1505403. doi: https://doi.org/10.1080/20013078.2018.1505403
176. Lee TH, Chennakrishnaiah S, Audemard E, Montermini L, Meehan B, Rak J. Oncogenic ras-driven cancer cell vesiculation leads to emission of double-stranded DNA capable of interacting with target cells. *Biochem Biophys Res Commun*. 2014;451:295-301. doi: 10.1016/j.bbrc.2014.07.109
177. Guescini M, Genedani S, Stocchi V, Agnati LF. Astrocytes and Glioblastoma cells release exosomes carrying mtDNA. *J Neural Transm (Vienna)*. 2010;117:1-4. doi: 10.1007/s00702-009-0288-8
178. Saari H, Turunen T, Lõhmus A, Turunen M, Jalasvuori M, Butcher SJ, Ylä-Herttuala S, Viitala T, Cerullo V, Siljander PRM, et al. Extracellular vesicles provide a capsid-free vector for oncolytic adenoviral DNA delivery. *Journal of Extracellular Vesicles*. 2020;9:1747206. doi: 10.1080/20013078.2020.1747206
179. Torralba D, Baixauli F, Villarroya-Beltri C, Fernández-Delgado I, Latorre-Pellicer A, Acín-Pérez R, Martín-Cófreces NB, Jaso-Tamame Á L, Iborra S, Jorge I, et al. Priming of dendritic cells by DNA-containing extracellular vesicles from activated T cells through antigen-driven contacts. *Nat Commun*. 2018;9:2658. doi: 10.1038/s41467-018-05077-9
180. Malkin EZ, Bratman SV. Bioactive DNA from extracellular vesicles and particles. *Cell Death & Disease*. 2020;11:584. doi: 10.1038/s41419-020-02803-4
181. Longjohn MN, Christian SL. Characterizing Extracellular Vesicles Using Nanoparticle-Tracking Analysis. *Methods Mol Biol*. 2022;2508:353-373. doi: 10.1007/978-1-0716-2376-3_23
182. Szatanek R, Baj-Krzyworzeka M, Zimoch J, Lekka M, Siedlar M, Baran J. The Methods of Choice for Extracellular Vesicles (EVs) Characterization. *Int J Mol Sci*. 2017;18. doi: 10.3390/ijms18061153
183. Vestad B, Llorente A, Neurauter A, Phuyal S, Kierulf B, Kierulf P, Skotland T, Sandvig K, Haug KBF, Øvstebø R. Size and concentration analyses of extracellular vesicles by nanoparticle tracking analysis: a variation study. *Journal of Extracellular Vesicles*. 2017;6:1344087. doi: 10.1080/20013078.2017.1344087
184. Buzás EI, Gardiner C, Lee C, Smith ZJ. Single particle analysis: Methods for detection of platelet extracellular vesicles in suspension (excluding flow cytometry). *Platelets*. 2017;28:249-255. doi: 10.1080/09537104.2016.1260704

185. Oosthuyzen W, Sime NE, Ivy JR, Turtle EJ, Street JM, Pound J, Bath LE, Webb DJ, Gregory CD, Bailey MA, et al. Quantification of human urinary exosomes by nanoparticle tracking analysis. *J Physiol*. 2013;591:5833-5842. doi: 10.1113/jphysiol.2013.264069
186. Midekessa G, Godakumara K, Dissanayake K, Hasan MM, Reshi QUA, Rinken T, Fazeli A. Characterization of Extracellular Vesicles Labelled with a Lipophilic Dye Using Fluorescence Nanoparticle Tracking Analysis. *Membranes*. 2021;11:779.
187. Gardiner C, Ferreira YJ, Dragovic RA, Redman CWG, Sargent IL. Extracellular vesicle sizing and enumeration by nanoparticle tracking analysis. *Journal of Extracellular Vesicles*. 2013;2:19671. doi: 10.3402/jev.v2i0.19671
188. Dehghani M, Gulvin SM, Flax J, Gaborski TR. Systematic Evaluation of PKH Labelling on Extracellular Vesicle Size by Nanoparticle Tracking Analysis. *Scientific Reports*. 2020;10:9533. doi: 10.1038/s41598-020-66434-7
189. Thane KE, Davis AM, Hoffman AM. Improved methods for fluorescent labeling and detection of single extracellular vesicles using nanoparticle tracking analysis. *Scientific Reports*. 2019;9:12295. doi: 10.1038/s41598-019-48181-6
190. Carnell-Morris P, Tannetta D, Siupa A, Hole P, Dragovic R. Analysis of Extracellular Vesicles Using Fluorescence Nanoparticle Tracking Analysis. *Methods Mol Biol*. 2017;1660:153-173. doi: 10.1007/978-1-4939-7253-1_13
191. Khan MA, Anand S, Deshmukh SK, Singh S, Singh AP. Determining the Size Distribution and Integrity of Extracellular Vesicles by Dynamic Light Scattering. *Methods Mol Biol*. 2022;2413:165-175. doi: 10.1007/978-1-0716-1896-7_17
192. Gurunathan S, Kang MH, Jeyaraj M, Qasim M, Kim JH. Review of the Isolation, Characterization, Biological Function, and Multifarious Therapeutic Approaches of Exosomes. *Cells*. 2019;8. doi: 10.3390/cells8040307
193. Filipe V, Hawe A, Jiskoot W. Critical evaluation of Nanoparticle Tracking Analysis (NTA) by NanoSight for the measurement of nanoparticles and protein aggregates. *Pharm Res*. 2010;27:796-810. doi: 10.1007/s11095-010-0073-2
194. Maas SL, Broekman ML, de Vrij J. Tunable Resistive Pulse Sensing for the Characterization of Extracellular Vesicles. *Methods Mol Biol*. 2017;1545:21-33. doi: 10.1007/978-1-4939-6728-5_2
195. Bayley H, Martin CR. Resistive-Pulse Sensing-From Microbes to Molecules. *Chem Rev*. 2000;100:2575-2594. doi: 10.1021/cr980099g
196. Roberts GS, Kozak D, Anderson W, Broom MF, Vogel R, Trau M. Tunable Nano/Micropores for Particle Detection and Discrimination: Scanning Ion Occlusion Spectroscopy. *Small*. 2010;6:2653-2658. doi: https://doi.org/10.1002/smll.201001129
197. Maas SL, de Vrij J, van der Vlist EJ, Geragousian B, van Bloois L, Mastrobattista E, Schiffelers RM, Wauben MH, Broekman ML, Nolte-'t Hoen EN. Possibilities and limitations of current technologies for quantification of biological extracellular vesicles and synthetic mimics. *J Control Release*. 2015;200:87-96. doi: 10.1016/j.jconrel.2014.12.041
198. Cizmar P, Yuana Y. Detection and Characterization of Extracellular Vesicles by Transmission and Cryo-Transmission Electron Microscopy. *Methods Mol Biol*. 2017;1660:221-232. doi: 10.1007/978-1-4939-7253-1_18
199. Grover A, Sinha R, Jyoti D, Faggio C. Imperative role of electron microscopy in toxicity assessment: A review. *Microsc Res Tech*. 2022;85:1976-1989. doi: 10.1002/jemt.24029
200. Coleman BM, Hanssen E, Lawson VA, Hill AF. Prion-infected cells regulate the release of exosomes with distinct ultrastructural features. *Faseb j*. 2012;26:4160-4173. doi: 10.1096/fj.11-202077

201. Fulwyler MJ. Electronic Separation of Biological Cells by Volume. *Science*. 1965;150:910-911. doi: 10.1126/science.150.3698.910
202. Doyle LM, Wang MZ. Overview of Extracellular Vesicles, Their Origin, Composition, Purpose, and Methods for Exosome Isolation and Analysis. *Cells*. 2019;8. doi: 10.3390/cells8070727
203. Guertin DA, Sabatini DM. 12 - Cell Growth. In: Mendelsohn J, Gray JW, Howley PM, Israel MA, Thompson CB, eds. *The Molecular Basis of Cancer (Fourth Edition)*. Philadelphia: W.B. Saunders; 2015:179-190.e171.
204. van der Pol E, Sturk A, van Leeuwen T, Nieuwland R, Coumans F. Standardization of extracellular vesicle measurements by flow cytometry through vesicle diameter approximation. *J Thromb Haemost*. 2018;16:1236-1245. doi: 10.1111/jth.14009
205. Pužar Dominkuš P, Stenovec M, Sitar S, Lasič E, Zorec R, Plemenitaš A, Žagar E, Kreft M, Lenassi M. PKH26 labeling of extracellular vesicles: Characterization and cellular internalization of contaminating PKH26 nanoparticles. *Biochimica et Biophysica Acta (BBA) - Biomembranes*. 2018;1860:1350-1361. doi: https://doi.org/10.1016/j.bbamem.2018.03.013
206. Wiklander OP, Nordin JZ, O'Loughlin A, Gustafsson Y, Corso G, Mäger I, Vader P, Lee Y, Sork H, Seow Y, et al. Extracellular vesicle in vivo biodistribution is determined by cell source, route of administration and targeting. *J Extracell Vesicles*. 2015;4:26316. doi: 10.3402/jev.v4.26316
207. Gupta D, Liang X, Pavlova S, Wiklander OPB, Corso G, Zhao Y, Saher O, Bost J, Zickler AM, Piffko A, et al. Quantification of extracellular vesicles in vitro and in vivo using sensitive bioluminescence imaging. *J Extracell Vesicles*. 2020;9:1800222. doi: 10.1080/20013078.2020.1800222
208. Grange C, Tapparo M, Bruno S, Chatterjee D, Quesenberry PJ, Tetta C, Camussi G. Biodistribution of mesenchymal stem cell-derived extracellular vesicles in a model of acute kidney injury monitored by optical imaging. *Int J Mol Med*. 2014;33:1055-1063. doi: 10.3892/ijmm.2014.1663
209. Pospichalova V, Svoboda J, Dave Z, Kotrbova A, Kaiser K, Klemova D, Ilkovics L, Hampl A, Crha I, Jandakova E, et al. Simplified protocol for flow cytometry analysis of fluorescently labeled exosomes and microvesicles using dedicated flow cytometer. *J Extracell Vesicles*. 2015;4:25530. doi: 10.3402/jev.v4.25530
210. Gul B, Syed F, Khan S, Iqbal A, Ahmad I. Characterization of extracellular vesicles by flow cytometry: Challenges and promises. *Micron*. 2022;161:103341. doi: https://doi.org/10.1016/j.micron.2022.103341
211. Morales-Kastresana A, Jones JC. Flow Cytometric Analysis of Extracellular Vesicles. *Methods Mol Biol*. 2017;1545:215-225. doi: 10.1007/978-1-4939-6728-5_16
212. Suárez H, Gámez-Valero A, Reyes R, López-Martín S, Rodríguez MJ, Carrascosa JL, Cabañas C, Borràs FE, Yáñez-Mó M. A bead-assisted flow cytometry method for the semi-quantitative analysis of Extracellular Vesicles. *Scientific Reports*. 2017;7:11271. doi: 10.1038/s41598-017-11249-2
213. Cvjetkovic A, Jang SC, Konečná B, Höög JL, Sihlbom C, Lässer C, Lötvall J. Detailed Analysis of Protein Topology of Extracellular Vesicles–Evidence of Unconventional Membrane Protein Orientation. *Scientific Reports*. 2016;6:36338. doi: 10.1038/srep36338
214. Koliha N, Wiencek Y, Heider U, Jüngst C, Kladt N, Krauthäuser S, Johnston IC, Bosio A, Schauss A, Wild S. A novel multiplex bead-based platform highlights the diversity of extracellular vesicles. *J Extracell Vesicles*. 2016;5:29975. doi: 10.3402/jev.v5.29975

215. Nolte-'t Hoen EN, van der Vlist EJ, Aalberts M, Mertens HC, Bosch BJ, Bartelink W, Mastrobattista E, van Gaal EV, Stoorvogel W, Arkesteijn GJ, et al. Quantitative and qualitative flow cytometric analysis of nanosized cell-derived membrane vesicles. *Nanomedicine*. 2012;8:712-720. doi: 10.1016/j.nano.2011.09.006
216. van der Vlist EJ, Nolte-'t Hoen ENM, Stoorvogel W, Arkesteijn GJA, Wauben MHM. Fluorescent labeling of nano-sized vesicles released by cells and subsequent quantitative and qualitative analysis by high-resolution flow cytometry. *Nature Protocols*. 2012;7:1311-1326. doi: 10.1038/nprot.2012.065
217. Danielson KM, Estanislau J, Tigges J, Toxavidis V, Camacho V, Felton EJ, Khoory J, Kreimer S, Ivanov AR, Mantel PY, et al. Diurnal Variations of Circulating Extracellular Vesicles Measured by Nano Flow Cytometry. *PLoS One*. 2016;11:e0144678. doi: 10.1371/journal.pone.0144678
218. Ender F, Zamzow P, von Bubnoff N, Gieseler F. Detection and Quantification of Extracellular Vesicles via FACS: Membrane Labeling Matters! *International Journal of Molecular Sciences*. 2020;21:291.
219. Choi D, Montermini L, Jeong H, Sharma S, Meehan B, Rak J. Mapping Subpopulations of Cancer Cell-Derived Extracellular Vesicles and Particles by Nano-Flow Cytometry. *ACS Nano*. 2019;13:10499-10511. doi: 10.1021/acsnano.9b04480
220. Lekka M. Discrimination Between Normal and Cancerous Cells Using AFM. *Bionanoscience*. 2016;6:65-80. doi: 10.1007/s12668-016-0191-3
221. Rosenhek-Goldian I, Abou Karam P, Regev-Rudzki N, Rojas A. Imaging of Extracellular Vesicles Derived from Plasmodium falciparum-Infected Red Blood Cells Using Atomic Force Microscopy. *Methods Mol Biol*. 2022;2470:133-145. doi: 10.1007/978-1-0716-2189-9_12
222. Sharma S, LeClaire M, Gimzewski JK. Ascent of atomic force microscopy as a nanoanalytical tool for exosomes and other extracellular vesicles. *Nanotechnology*. 2018;29:132001. doi: 10.1088/1361-6528/aaab06
223. Hardij J, Cecchet F, Berquand A, Gheldof D, Chatelain C, Mullier F, Chatelain B, Dogné JM. Characterisation of tissue factor-bearing extracellular vesicles with AFM: comparison of air-tapping-mode AFM and liquid Peak Force AFM. *J Extracell Vesicles*. 2013;2. doi: 10.3402/jev.v2i0.21045
224. Sebaihi N, De Boeck B, Yuana Y, Nieuwland R, Pétry J. Dimensional characterization of extracellular vesicles using atomic force microscopy. *Measurement Science and Technology*. 2017;28:034006. doi: 10.1088/1361-6501/28/3/034006
225. Cavallaro S, Pevere F, Stridfeldt F, Görgens A, Paba C, Sahu SS, Mamand DR, Gupta D, El Andaloussi S, Linnros J, et al. Multiparametric Profiling of Single Nanoscale Extracellular Vesicles by Combined Atomic Force and Fluorescence Microscopy: Correlation and Heterogeneity in Their Molecular and Biophysical Features. *Small*. 2021;17:e2008155. doi: 10.1002/smll.202008155
226. Sharma S, Rasool HI, Palanisamy V, Mathisen C, Schmidt M, Wong DT, Gimzewski JK. Structural-Mechanical Characterization of Nanoparticle Exosomes in Human Saliva, Using Correlative AFM, FESEM, and Force Spectroscopy. *ACS Nano*. 2010;4:1921-1926. doi: 10.1021/nn901824n
227. György B, Módos K, Pállinger É, Pálóczi K, Pásztói M, Misják P, Deli MA, Sipos Á, Szalai A, Voszka I, et al. Detection and isolation of cell-derived microparticles are compromised by protein complexes resulting from shared biophysical parameters. *Blood*. 2011;117:e39-e48. doi: 10.1182/blood-2010-09-307595
228. Ashcroft BA, de Sonneville J, Yuana Y, Osanto S, Bertina R, Kuil ME, Oosterkamp TH. Determination of the size distribution of blood microparticles directly in plasma

using atomic force microscopy and microfluidics. *Biomed Microdevices*. 2012;14:641-649. doi: 10.1007/s10544-012-9642-y
229. Im H, Yang K, Lee H, Castro CM. Characterization of Extracellular Vesicles by Surface Plasmon Resonance. *Methods Mol Biol*. 2017;1660:133-141. doi: 10.1007/978-1-4939-7253-1_11
230. Lee HJ, Nedelkov D, Corn RM. Surface Plasmon Resonance Imaging Measurements of Antibody Arrays for the Multiplexed Detection of Low Molecular Weight Protein Biomarkers. *Analytical Chemistry*. 2006;78:6504-6510. doi: 10.1021/ac060881d
231. Rupert DLM, Lässer C, Eldh M, Block S, Zhdanov VP, Lotvall JO, Bally M, Höök F. Determination of Exosome Concentration in Solution Using Surface Plasmon Resonance Spectroscopy. *Analytical Chemistry*. 2014;86:5929-5936. doi: 10.1021/ac500931f
232. Im H, Shao H, Park YI, Peterson VM, Castro CM, Weissleder R, Lee H. Label-free detection and molecular profiling of exosomes with a nano-plasmonic sensor. *Nat Biotechnol*. 2014;32:490-495. doi: 10.1038/nbt.2886
233. Gool EL, Stojanovic I, Schasfoort RBM, Sturk A, van Leeuwen TG, Nieuwland R, Terstappen L, Coumans FAW. Surface Plasmon Resonance is an Analytically Sensitive Method for Antigen Profiling of Extracellular Vesicles. *Clin Chem*. 2017;63:1633-1641. doi: 10.1373/clinchem.2016.271049
234. Canetta E. Current and Future Advancements of Raman Spectroscopy Techniques in Cancer Nanomedicine. *Int J Mol Sci*. 2021;22. doi: 10.3390/ijms222313141
235. Auner GW, Koya SK, Huang C, Broadbent B, Trexler M, Auner Z, Elias A, Mehne KC, Brusatori MA. Applications of Raman spectroscopy in cancer diagnosis. *Cancer and Metastasis Reviews*. 2018;37:691-717. doi: 10.1007/s10555-018-9770-9
236. Pang Y, Wang C, Lu L, Wang C, Sun Z, Xiao R. Dual-SERS biosensor for one-step detection of microRNAs in exosome and residual plasma of blood samples for diagnosing pancreatic cancer. *Biosens Bioelectron*. 2019;130:204-213. doi: 10.1016/j.bios.2019.01.039
237. Tian YF, Ning CF, He F, Yin BC, Ye BC. Highly sensitive detection of exosomes by SERS using gold nanostar@Raman reporter@nanoshell structures modified with a bivalent cholesterol-labeled DNA anchor. *Analyst*. 2018;143:4915-4922. doi: 10.1039/c8an01041b
238. Kamińska A, Roman M, Wróbel A, Gala-Błądzińska A, Małecki MTP, Paluszkiewicz C, Stępień EŁ P. Raman spectroscopy of urinary extracellular vesicles to stratify patients with chronic kidney disease in type 2 diabetes. *Nanomedicine*. 2022;39:102468. doi: 10.1016/j.nano.2021.102468
239. Osei EB, Paniushkina L, Wilhelm K, Popp J, Nazarenko I, Krafft C. Surface-Enhanced Raman Spectroscopy to Characterize Different Fractions of Extracellular Vesicles from Control and Prostate Cancer Patients. *Biomedicines*. 2021;9. doi: 10.3390/biomedicines9050580
240. Shin H, Jeong H, Park J, Hong S, Choi Y. Correlation between Cancerous Exosomes and Protein Markers Based on Surface-Enhanced Raman Spectroscopy (SERS) and Principal Component Analysis (PCA). *ACS Sens*. 2018;3:2637-2643. doi: 10.1021/acssensors.8b01047
241. Gualerzi A, Kooijmans SAA, Niada S, Picciolini S, Brini AT, Camussi G, Bedoni M. Raman spectroscopy as a quick tool to assess purity of extracellular vesicle preparations and predict their functionality. *Journal of Extracellular Vesicles*. 2019;8:1568780. doi: 10.1080/20013078.2019.1568780

242. Avci O, Ünlü NL, Özkumur AY, Ünlü MS. Interferometric Reflectance Imaging Sensor (IRIS)--A Platform Technology for Multiplexed Diagnostics and Digital Detection. *Sensors (Basel)*. 2015;15:17649-17665. doi: 10.3390/s150717649
243. Breitwieser K, Koch LF, Tertel T, Proestler E, Burgers LD, Lipps C, Adjaye J, Fürst R, Giebel B, Saul MJ. Detailed Characterization of Small Extracellular Vesicles from Different Cell Types Based on Tetraspanin Composition by ExoView R100 Platform. *Int J Mol Sci*. 2022;23. doi: 10.3390/ijms23158544
244. Khan NZ, Cao T, He J, Ritzel RM, Li Y, Henry RJ, Colson C, Stoica BA, Faden AI, Wu J. Spinal cord injury alters microRNA and CD81+ exosome levels in plasma extracellular nanoparticles with neuroinflammatory potential. *Brain Behav Immun*. 2021;92:165-183. doi: 10.1016/j.bbi.2020.12.007
245. Silva AM, Lázaro-Ibáñez E, Gunnarsson A, Dhande A, Daaboul G, Peacock B, Osteikoetxea X, Salmond N, Friis KP, Shatnyeva O, et al. Quantification of protein cargo loading into engineered extracellular vesicles at single-vesicle and single-molecule resolution. *J Extracell Vesicles*. 2021;10:e12130. doi: 10.1002/jev2.12130
246. Kashkanova AD, Blessing M, Gemeinhardt A, Soulat D, Sandoghdar V. Precision size and refractive index analysis of weakly scattering nanoparticles in polydispersions. *Nature Methods*. 2022;19:586-593. doi: 10.1038/s41592-022-01460-z
247. Anna DK, Martin B, Marie R, Andreas SB, Vahid S, Jan Van D. Interferometric nanoparticle tracking analysis enables label-free discrimination of extracellular vesicles from large lipoproteins. *bioRxiv*. 2022:2022.2011.2011.515605. doi: 10.1101/2022.11.11.515605
248. Carney RP, Hazari S, Colquhoun M, Tran D, Hwang B, Mulligan MS, Bryers JD, Girda E, Leiserowitz GS, Smith ZJ, et al. Multispectral Optical Tweezers for Biochemical Fingerprinting of CD9-Positive Exosome Subpopulations. *Analytical Chemistry*. 2017;89:5357-5363. doi: 10.1021/acs.analchem.7b00017
249. Kruglik SG, Royo F, Guigner JM, Palomo L, Seksek O, Turpin PY, Tatischeff I, Falcón-Pérez JM. Raman tweezers microspectroscopy of circa 100 nm extracellular vesicles. *Nanoscale*. 2019;11:1661-1679. doi: 10.1039/c8nr04677h
250. Maltepe E, Fisher SJ. Placenta: the forgotten organ. *Annu Rev Cell Dev Biol*. 2015;31:523-552. doi: 10.1146/annurev-cellbio-100814-125620
251. Li S, Winuthayanon W. Oviduct: roles in fertilization and early embryo development. *J Endocrinol*. 2017;232:R1-r26. doi: 10.1530/joe-16-0302
252. Boss AL, Chamley LW, James JL. Placental formation in early pregnancy: how is the centre of the placenta made? *Hum Reprod Update*. 2018;24:750-760. doi: 10.1093/humupd/dmy030
253. Silva JF, Serakides R. Intrauterine trophoblast migration: A comparative view of humans and rodents. *Cell Adh Migr*. 2016;10:88-110. doi: 10.1080/19336918.2015.1120397
254. Gamage TK, Chamley LW, James JL. Stem cell insights into human trophoblast lineage differentiation. *Hum Reprod Update*. 2016;23:77-103. doi: 10.1093/humupd/dmw026
255. Bischof P, Irminger-Finger I. The human cytotrophoblastic cell, a mononuclear chameleon. *The International Journal of Biochemistry & Cell Biology*. 2005;37:1-16. doi: https://doi.org/10.1016/j.biocel.2004.05.014
256. Biswas S, Ghosh SK, Chhabra S. Surface area of chorionic villi of placentas: an index of intrauterine growth restriction of fetuses. *J Obstet Gynaecol Res*. 2008;34:487-493. doi: 10.1111/j.1447-0756.2008.00719.x

257. Benirschke K, Burton GJ, Baergen RN. Basic Structure of the Villous Trees. In: Benirschke K, Burton GJ, Baergen RN, eds. *Pathology of the Human Placenta*. Berlin, Heidelberg: Springer Berlin Heidelberg; 2012:55-100.
258. Burton GJ, Redman CW, Roberts JM, Moffett A. Pre-eclampsia: pathophysiology and clinical implications. *Bmj*. 2019;366:l2381. doi: 10.1136/bmj.l2381
259. Mol BWJ, Roberts CT, Thangaratinam S, Magee LA, de Groot CJM, Hofmeyr GJ. Pre-eclampsia. *Lancet*. 2016;387:999-1011. doi: 10.1016/s0140-6736(15)00070-7
260. Phipps EA, Thadhani R, Benzing T, Karumanchi SA. Pre-eclampsia: pathogenesis, novel diagnostics and therapies. *Nat Rev Nephrol*. 2019;15:275-289. doi: 10.1038/s41581-019-0119-6
261. Lisonkova S, Joseph K. Incidence of preeclampsia: risk factors and outcomes associated with early-versus late-onset disease. *American journal of obstetrics and gynecology*. 2013;209:544. e541-544. e512.
262. Amaral LM, Wallace K, Owens M, LaMarca B. Pathophysiology and Current Clinical Management of Preeclampsia. *Curr Hypertens Rep*. 2017;19:61. doi: 10.1007/s11906-017-0757-7
263. Jung E, Romero R, Yeo L, Gomez-Lopez N, Chaemsaithong P, Jaovisidha A, Gotsch F, Erez O. The etiology of preeclampsia. *Am J Obstet Gynecol*. 2022;226:S844-s866. doi: 10.1016/j.ajog.2021.11.1356
264. Redman CW. Preeclampsia: a multi-stress disorder. *Rev Med Interne*. 2011;32 Suppl 1:S41-44. doi: 10.1016/j.revmed.2011.03.331
265. Lyall F, Robson SC, Bulmer JN. Spiral artery remodeling and trophoblast invasion in preeclampsia and fetal growth restriction: relationship to clinical outcome. *Hypertension*. 2013;62:1046-1054. doi: 10.1161/hypertensionaha.113.01892
266. Jauniaux E, Watson AL, Hempstock J, Bao YP, Skepper JN, Burton GJ. Onset of maternal arterial blood flow and placental oxidative stress. A possible factor in human early pregnancy failure. *Am J Pathol*. 2000;157:2111-2122. doi: 10.1016/s0002-9440(10)64849-3
267. Levine RJ, Maynard SE, Qian C, Lim KH, England LJ, Yu KF, Schisterman EF, Thadhani R, Sachs BP, Epstein FH, et al. Circulating angiogenic factors and the risk of preeclampsia. *N Engl J Med*. 2004;350:672-683. doi: 10.1056/NEJMoa031884
268. Gebara N, Correia Y, Wang K, Bussolati B. Angiogenic Properties of Placenta-Derived Extracellular Vesicles in Normal Pregnancy and in Preeclampsia. *Int J Mol Sci*. 2021;22. doi: 10.3390/ijms22105402
269. Maynard SE, Min JY, Merchan J, Lim KH, Li J, Mondal S, Libermann TA, Morgan JP, Sellke FW, Stillman IE, et al. Excess placental soluble fms-like tyrosine kinase 1 (sFlt1) may contribute to endothelial dysfunction, hypertension, and proteinuria in preeclampsia. *J Clin Invest*. 2003;111:649-658. doi: 10.1172/jci17189
270. Leaños-Miranda A, Navarro-Romero CS, Sillas-Pardo LJ, Ramírez-Valenzuela KL, Isordia-Salas I, Jiménez-Trejo LM. Soluble Endoglin As a Marker for Preeclampsia, Its Severity, and the Occurrence of Adverse Outcomes. *Hypertension*. 2019;74:991-997. doi: doi:10.1161/HYPERTENSIONAHA.119.13348
271. Awoyemi T, Cerdeira AS, Zhang W, Jiang S, Rahbar M, Logenthiran P, Redman C, Vatish M. Preeclampsia and syncytiotrophoblast membrane extracellular vesicles (STB-EVs). *Clin Sci (Lond)*. 2022;136:1793-1807. doi: 10.1042/cs20220149
272. Sarker S, Scholz-Romero K, Perez A, Illanes SE, Mitchell MD, Rice GE, Salomon C. Placenta-derived exosomes continuously increase in maternal circulation over the first trimester of pregnancy. *J Transl Med*. 2014;12:204. doi: 10.1186/1479-5876-12-204
273. Salomon C, Torres MJ, Kobayashi M, Scholz-Romero K, Sobrevia L, Dobierzewska A, Illanes SE, Mitchell MD, Rice GE. A gestational profile of placental exosomes in

maternal plasma and their effects on endothelial cell migration. *PLoS One*. 2014;9:e98667. doi: 10.1371/journal.pone.0098667
274. Gupta AK, Rusterholz C, Holzgreve W, Hahn S. Syncytiotrophoblast micro-particles do not induce apoptosis in peripheral T lymphocytes, but differ in their activity depending on the mode of preparation. *J Reprod Immunol*. 2005;68:15-26. doi: 10.1016/j.jri.2005.05.003
275. Collett GP, Redman CW, Sargent IL, Vatish M. Endoplasmic reticulum stress stimulates the release of extracellular vesicles carrying danger-associated molecular pattern (DAMP) molecules. *Oncotarget*. 2018;9:6707-6717. doi: 10.18632/oncotarget.24158
276. Tannetta DS, Hunt K, Jones CI, Davidson N, Coxon CH, Ferguson D, Redman CW, Gibbins JM, Sargent IL, Tucker KL. Syncytiotrophoblast Extracellular Vesicles from Pre-Eclampsia Placentas Differentially Affect Platelet Function. *PLoS One*. 2015;10:e0142538. doi: 10.1371/journal.pone.0142538
277. Fishel Bartal M, Lindheimer MD, Sibai BM. Proteinuria during pregnancy: definition, pathophysiology, methodology, and clinical significance. *Am J Obstet Gynecol*. 2022;226:S819-s834. doi: 10.1016/j.ajog.2020.08.108
278. ACOG practice bulletin. Diagnosis and management of preeclampsia and eclampsia. Number 33, January 2002. *Obstet Gynecol*. 2002;99:159-167. doi: 10.1016/s0029-7844(01)01747-1
279. Sturgiss SN, Dunlop W, Davison JM. 1 Renal haemodynamics and tubular function in human pregnancy. *Baillière's Clinical Obstetrics and Gynaecology*. 1994;8:209-234. doi: https://doi.org/10.1016/S0950-3552(05)80319-0
280. Ouzounian JG, Elkayam U. Physiologic Changes During Normal Pregnancy and Delivery. *Cardiology Clinics*. 2012;30:317-329. doi: https://doi.org/10.1016/j.ccl.2012.05.004
281. Moran P, Lindheimer MD, Davison JM. The renal response to preeclampsia. *Seminars in Nephrology*. 2004;24:588-595. doi: https://doi.org/10.1016/j.semnephrol.2004.07.008
282. Conrad KP, Gaber LW, Lindheimer MD. Chapter 17 - The Kidney in Normal Pregnancy and Preeclampsia. In: Lindheimer MD, Roberts JM, Gary Cunningham F, eds. *Chesley's Hypertensive Disorders in Pregnancy (Third Edition)*. San Diego: Academic Press; 2009:297-334.
283. Satchell SC, Braet F. Glomerular endothelial cell fenestrations: an integral component of the glomerular filtration barrier. *Am J Physiol Renal Physiol*. 2009;296:F947-956. doi: 10.1152/ajprenal.90601.2008
284. Suh JH, Miner JH. The glomerular basement membrane as a barrier to albumin. *Nature Reviews Nephrology*. 2013;9:470-477. doi: 10.1038/nrneph.2013.109
285. Trimarchi H. Podocyturia: What is in a name? *J Transl Int Med*. 2015;3:51-56. doi: 10.1515/jtim-2015-0003
286. Jefferson JA, Alpers CE, Shankland SJ. Podocyte biology for the bedside. *Am J Kidney Dis*. 2011;58:835-845. doi: 10.1053/j.ajkd.2011.03.033
287. Akilesh S, Huber TB, Wu H, Wang G, Hartleben B, Kopp JB, Miner JH, Roopenian DC, Unanue ER, Shaw AS. Podocytes use FcRn to clear IgG from the glomerular basement membrane. *Proc Natl Acad Sci U S A*. 2008;105:967-972. doi: 10.1073/pnas.0711515105
288. Byron A, Randles MJ, Humphries JD, Mironov A, Hamidi H, Harris S, Mathieson PW, Saleem MA, Satchell SC, Zent R, et al. Glomerular Cell Cross-Talk Influences Composition and Assembly of Extracellular Matrix. *Journal of the American Society of Nephrology*. 2014;25.

289. Bartlett CS, Jeansson M, Quaggin SE. Vascular Growth Factors and Glomerular Disease. *Annu Rev Physiol*. 2016;78:437-461. doi: 10.1146/annurev-physiol-021115-105412
290. Gaber LW, Spargo BH, Lindheimer MD. 12 Renal pathology in pre-eclampsia. *Baillière's Clinical Obstetrics and Gynaecology*. 1987;1:971-995. doi: https://doi.org/10.1016/S0950-3552(87)80045-7
291. Spargo BH, Lichtig C, Luger AM, Katz AI, Lindheimer MD. The renal lesion in preeclampsia. *Perspect Nephrol Hypertens*. 1976;5:129-137.
292. Lafayette RA, Druzin M, Sibley R, Derby G, Malik T, Huie P, Polhemus C, Deen WM, Myers BD. Nature of glomerular dysfunction in pre-eclampsia11See Editorial by Chapman, p. 1394. *Kidney International*. 1998;54:1240-1249. doi: https://doi.org/10.1046/j.1523-1755.1998.00097.x
293. Gaber LW, Spargo BH, Lindheimer MD. Renal pathology in pre-eclampsia. *Baillieres Clin Obstet Gynaecol*. 1987;1:971-995. doi: 10.1016/s0950-3552(87)80045-7
294. Bell ET. Renal Lesions in the Toxemias of Pregnancy. *Am J Pathol*. 1932;8:1-42.45.
295. Sheehan HL. Renal morphology in preeclampsia. *Kidney Int*. 1980;18:241-252. doi: 10.1038/ki.1980.132
296. Naicker T, Randeree IGH, Moodley J. Glomerular Basement Membrane Changes in African Women with Early-Onset Preeclampsia. *Hypertension in Pregnancy*. 1995;14:371-378. doi: 10.3109/10641959509015683
297. Strevens H, Wide-Swensson D, Hansen A, Horn T, Ingemarsson I, Larsen S, Willner J, Olsen S. Glomerular endotheliosis in normal pregnancy and pre-eclampsia. *Bjog*. 2003;110:831-836.
298. Stillman IE, Karumanchi SA. The Glomerular Injury of Preeclampsia. *Journal of the American Society of Nephrology*. 2007;18:2281. doi: 10.1681/ASN.2007020255
299. Penning ME, Bloemenkamp KW, van der Zon T, Zandbergen M, Schutte JM, Bruijn JA, Bajema IM, Baelde HJ. Association of preeclampsia with podocyte turnover. *Clin J Am Soc Nephrol*. 2014;9:1377-1385. doi: 10.2215/cjn.12811213
300. Zhai T, Furuta I, Akaishi R, Ishikawa S, Morikawa M, Yamada T, Koyama T, Minakami H. Alteration of podocyte phenotype in the urine of women with preeclampsia. *Sci Rep*. 2016;6:24258. doi: 10.1038/srep24258
301. Venkatareddy M, Cook L, Abuarquob K, Verma R, Garg P. Nephrin regulates lamellipodia formation by assembling a protein complex that includes Ship2, filamin and lamellipodin. *PLoS One*. 2011;6:e28710. doi: 10.1371/journal.pone.0028710
302. Zhu J, Sun N, Aoudjit L, Li H, Kawachi H, Lemay S, Takano T. Nephrin mediates actin reorganization via phosphoinositide 3-kinase in podocytes. *Kidney Int*. 2008;73:556-566. doi: 10.1038/sj.ki.5002691
303. Zhao S, Gu X, Groome LJ, Wang Y. Decreased nephrin and GLEPP-1, but increased VEGF, Flt-1, and nitrotyrosine, expressions in kidney tissue sections from women with preeclampsia. *Reprod Sci*. 2009;16:970-979. doi: 10.1177/1933719109338630
304. Garovic VD, Wagner SJ, Petrovic LM, Gray CE, Hall P, Sugimoto H, Kalluri R, Grande JP. Glomerular expression of nephrin and synaptopodin, but not podocin, is decreased in kidney sections from women with preeclampsia. *Nephrol Dial Transplant*. 2007;22:1136-1143. doi: 10.1093/ndt/gfl711
305. Ozdemir F, Tayyar AT, Acmaz G, Aksoy H, Erturk G, Muhtaroglu S, Tayyar M. Comparison of blood and urine nephrin levels in preeclampsia and intrauterine growth retardation. *Pak J Med Sci*. 2016;32:40-43. doi: 10.12669/pjms.321.8865
306. Kostovska I, Tosheska Trajkovska K, Kostovski O, Labudovic D. Urinary Nephrin and Podocalyxin Levels as Predictors of Pre-eclampsia in High-Risk Pregnant Women. *Folia Med (Plovdiv)*. 2021;63:948-957. doi: 10.3897/folmed.63.e60055

307. Jung YJ, Cho HY, Cho S, Kim YH, Jeon JD, Kim YJ, Lee S, Park J, Kim HY, Park YW, et al. The Level of Serum and Urinary Nephrin in Normal Pregnancy and Pregnancy with Subsequent Preeclampsia. *Yonsei Med J*. 2017;58:401-406. doi: 10.3349/ymj.2017.58.2.401
308. Son GH, Kwon JY, Lee S, Park J, Kim YJ, Yun B, Park JH. Comparison of serum and urinary nephrin levels between normal pregnancies and severe preeclampsia. *Eur J Obstet Gynecol Reprod Biol*. 2013;166:139-144. doi: 10.1016/j.ejogrb.2012.10.011
309. Furuta I, Zhai T, Ishikawa S, Umazume T, Nakagawa K, Yamada T, Morikawa M, Minakami H. Association between nephrinuria, podocyturia, and proteinuria in women with pre-eclampsia. *J Obstet Gynaecol Res*. 2017;43:34-41. doi: 10.1111/jog.13180
310. Henao DE, Cadavid AP, Saleem MA. Exogenous vascular endothelial growth factor supplementation can restore the podocyte barrier-forming capacity disrupted by sera of preeclamptic women. *J Obstet Gynaecol Res*. 2013;39:46-52. doi: 10.1111/j.1447-0756.2012.01889.x
311. Shankland SJ, Freedman BS, Pippin JW. Can podocytes be regenerated in adults? *Curr Opin Nephrol Hypertens*. 2017;26:154-164. doi: 10.1097/mnh.0000000000000311
312. Becker JU, Hoerning A, Schmid KW, Hoyer PF. Immigrating progenitor cells contribute to human podocyte turnover. *Kidney Int*. 2007;72:1468-1473. doi: 10.1038/sj.ki.5002524
313. Prodromidi EI, Poulsom R, Jeffery R, Roufosse CA, Pollard PJ, Pusey CD, Cook HT. Bone marrow-derived cells contribute to podocyte regeneration and amelioration of renal disease in a mouse model of Alport syndrome. *Stem Cells*. 2006;24:2448-2455. doi: 10.1634/stemcells.2006-0201
314. Sugimoto H, Hamano Y, Charytan D, Cosgrove D, Kieran M, Sudhakar A, Kalluri R. Neutralization of circulating vascular endothelial growth factor (VEGF) by anti-VEGF antibodies and soluble VEGF receptor 1 (sFlt-1) induces proteinuria. *J Biol Chem*. 2003;278:12605-12608. doi: 10.1074/jbc.C300012200
315. Venkatesha S, Toporsian M, Lam C, Hanai J-i, Mammoto T, Kim YM, Bdolah Y, Lim K-H, Yuan H-T, Libermann TA, et al. Soluble endoglin contributes to the pathogenesis of preeclampsia. *Nature Medicine*. 2006;12:642-649. doi: 10.1038/nm1429
316. Roque L, Lopez-Novoa J. Soluble endoglin: a biomarker or a protagonist in the pathogenesis of preeclampsia? *Portuguese Journal of Nephrology & Hypertension*. 2014;28:185-192.
317. Han C, Wang C, Chen Y, Wang J, Xu X, Hilton T, Cai W, Zhao Z, Wu Y, Li K, et al. Placenta-derived extracellular vesicles induce preeclampsia in mouse models. *Haematologica*. 2020;105:1686-1694. doi: 10.3324/haematol.2019.226209
318. Chang X, Yao J, He Q, Liu M, Duan T, Wang K. Exosomes From Women With Preeclampsia Induced Vascular Dysfunction by Delivering sFlt (Soluble Fms-Like Tyrosine Kinase)-1 and sEng (Soluble Endoglin) to Endothelial Cells. *Hypertension*. 2018;72:1381-1390. doi: doi:10.1161/HYPERTENSIONAHA.118.11706
319. Murugesan S, Hussey H, Saravanakumar L, Sinkey RG, Sturdivant AB, Powell MF, Berkowitz DE. Extracellular Vesicles From Women With Severe Preeclampsia Impair Vascular Endothelial Function. *Anesthesia & Analgesia*. 2022;134.
320. Cronqvist T, Tannetta D, Mörgelin M, Belting M, Sargent I, Familari M, Hansson SR. Syncytiotrophoblast derived extracellular vesicles transfer functional placental miRNAs to primary human endothelial cells. *Scientific Reports*. 2017;7:4558. doi: 10.1038/s41598-017-04468-0

321. Koeppen BM, Stanton BA. 3 - Glomerular Filtration and Renal Blood Flow. In: Koeppen BM, Stanton BA, eds. *Renal Physiology (Fifth Edition)*. Philadelphia: Mosby; 2013:27-43.
322. Cheng Y, Wang X, Yang J, Duan X, Yao Y, Shi X, Chen Z, Fan Z, Liu X, Qin S, et al. A translational study of urine miRNAs in acute myocardial infarction. *J Mol Cell Cardiol*. 2012;53:668-676. doi: 10.1016/j.yjmcc.2012.08.010
323. Tong M, Stanley JL, Chen Q, James JL, Stone PR, Chamley LW. Placental Nano-vesicles Target to Specific Organs and Modulate Vascular Tone In Vivo. *Hum Reprod*. 2017;32:2188-2198. doi: 10.1093/humrep/dex310
324. Simionescu M, Popov D, Sima A. Endothelial transcytosis in health and disease. *Cell and Tissue Research*. 2009;335:27-40. doi: 10.1007/s00441-008-0688-3
325. Tyagi I, Agrawal U, Amitabh V, Jain AK, Saxena S. Thickness of glomerular and tubular basement membranes in preclinical and clinical stages of diabetic nephropathy. *Indian J Nephrol*. 2008;18:64-69. doi: 10.4103/0971-4065.42336

CHAPTER 2

ExoCounter assays identify women who may develop early-onset preeclampsia from 12.5 μL first trimester serum by characterising placental small extracellular vesicle

Table of Contents

2.1 Abstract....84
2.2 Introduction....85
2.3 Aims....88
2.4 Methods....89
2.4.1 Human Subjects and Ethic Approval....89
2.4.2 Isolation of psEV by placental dual-lobe perfusion and serial ultracentrifugation....90
2.4.3 Plasma sample preparation....90
2.4.4 Serum sample collection....91
2.4.5 Western Blot....92
2.4.6 Transmission Electron Microscopy (TEM)....93
2.4.7 Nanoparticle Tracking Analysis (NTA)....93
2.5.8 Identifying PLAP-associated antigens by MACSPlex Exosome Kit....94
2.5.9 ExoCounter....94
2.5.10 Experimental design and flow....98
2.5.11 Statistical Analysis....99
2.5 Results....100
2.5.1 psEV Characterisation....100
2.5.2 Antibody coating and blocking buffer optimisation for ExoCounter assay using psEV 101
2.5.3 CD63 is determined by MACSPlex kit and confirmed by ExoCounter as the most abundant tetraspanin on psEV....103
2.5.4 Identify the optimal coating and detecting antibody combination for ExoCounter psEV quantification....106
2.5.5 ExoCounter assay optimisation for plasma samples....107
2.5.6 ExoCounter detected higher placenta specific CD63-PLAP sEV counts in uterine vein (UV) compared to paired peripheral vein (PV)....110
2.5.7 The unique psEV profile of WWD-EOPE compared to NP and WWD-LOPE could be observed as early as the first trimester....110
2.5.8 Counts of psEV detected by ExoCounter were highly consistent in serum and plasma samples from the same donor....113
2.5.9 Significant higher counts of CD10-PLAP and CD63-PLAP sEV were detected by ExoCounter in WWD-WOPE compared to WWD-LOPE and NP in the first trimester serum samples....114
2.6 Discussion & Future work....117
2.7 Reference....122

2.1 Abstract

Background: Preeclampsia (PE) is a major cause of maternal and perinatal morbidity and mortality worldwide. Identifying women with high risk of developing PE in early pregnancy remains challenging. Extracellular vesicles (EV) released from the placenta offer an attractive biomarker but have been elusive to quantify.

Methods: Here, I tested ExoCounter, a novel device which immunophenotypes size-selected small EV (sEV) <160 nm, for its ability to perform qualitative and quantitative placental sEV (psEV) analysis. To investigate disease- and gestational age-specific changes, we analysed psEV counts in maternal plasma samples taken at each of the three trimesters from women who had a) normal pregnancy (NP, n=3), b) who developed early-onset preeclampsia (WWD-EOPE, n=3) and c) who developed late-onset preeclampsia (WWD-LOPE, n=4) using three antibody pairs, CD10-PLAP, CD10-CD63 and CD63-PLAP. We further validated the findings in first-trimester serum samples among NP (n = 9), WWD-EOPE (n = 7) and WWD-LOPE (n = 8).

Results: I confirmed that CD63 was the major tetraspanin molecule co-expressed with placental alkaline phosphatase (PLAP) – a known placental EV marker on psEV. Higher psEV counts for all three antibody pairs were detected in the plasma of WWD-EOPE than the other two groups in the first trimester which persisted through the second and third trimester. Significantly higher CD10-PLAP ($p<0.01$) and CD63-PLAP ($p<0.01$) psEV counts were validated in the serum of the first trimester of WWD-EOPE compared to NP.

Conclusions: Application of the ExoCounter assay developed here, could identify patients at risk of developing EOPE in the first trimester, thereby providing a window of opportunity for early intervention.

2.2 Introduction

Extracellular vesicle (EV) are cell-derived particles bound by a lipid bilayer, and play important roles in intercellular communication by transferring different cargo including proteins, lipids and genetic material to recipient cells [1]. EV have been detected in various biofluids such as plasma, urine, bile, saliva, breast milk, semen and cerebrospinal fluid[2-8]. So far, small EV (sEV) have been found to play important roles in physiological functions such as angiogenesis, antigen presentation, intercellular signalling[9-11]. sEV are also considered as biomarkers for a variety of diseases, such as cancers, neurodegenerative disease, kidney injuries, hepatitis and cancers [12-17].

Depending on their biogenesis, EV can be classified into endosomal-origin (exosomes) and plasma membrane budding-origin (microvesicles), where the former is formed by inward budding of the endosomal membrane during maturation of multivesicular endosomes (MVEs), and the latter involves directly outward budding at the plasma membrane[1]. As a result, both types of EV share cell plasma membrane associated molecules and genetic makeups of their cell origin although exosomes are preferentially enriched for one or multiple tetraspanins (CD63, CD9 and CD81) in a cell type specific manner[18]. Plasma membrane associated molecules have been instrumental not only in the identification of the cellular origin of EV but also identification of disease-associated molecules, so-called biomarkers. Distinguishing EV phenotype on their biogenesis pathway, however, has been challenging. For this reason, the ISEV (International Society for Extracellular Vesicles) has recommended

an EV classification based on the size of the EV, where EV can be classified into medium/large EV (m/lEV, > 200 nm), small EV (sEV, < 200 nm)[19].

The human placenta, an organ of fetal origin, anchors into the maternal uterus and is responsible for the exchange of nutrients, waste and gases throughout pregnancy[20]. The maternal facing surface of the placenta, the syncytiotrophoblast (STB), is in direct contact with maternal blood and releases placental EV into the maternal circulation[21]. Placental EV carry a unique marker of their origin, placental alkaline phosphatase (PLAP), which has been used to delineate these vesicles from those of other sources. Using PLAP, placental EV have been reported as being detectable in maternal circulation as early as the first trimester in normal pregnancy[22]. It has been shown throughout normal pregnancy, that the level of placental EV in the maternal circulation increases with advancing gestational age [23]. Placental EV have been reported to regulate the functions of maternal endothelial cells, immune cells and hepatocytes [24-26]. Thus, placental EV have the potential to be used as circulating indicators of placental health status.

Preeclampsia (PE) is a pregnancy-specific disorder affecting 3-5% of all pregnancies world-wide[27]. It is a major cause of maternal and neonatal morbidity and mortality [28]. The maternal phenotype of PE is characterized by high blood pressure and damage to another end organ system, which only develops after 20 weeks of gestation[27]. PE has 2 subtypes: early-onset PE (< 34 weeks, EOPE) and late-onset PE (≥ 34 weeks, LOPE)[22,29]. The pathogenesis of these two subtypes is believed to be different. It is hypothesised that EOPE occurs as a result of syncytiotrophoblast stress caused by insufficient trophoblast invasion of maternal spiral arteries in the early stage of pregnancy. LOPE is proposed to result from an interplay between a senescent placenta and maternal predisposition for cardiovascular and metabolic disease [30].

For both subtypes of PE, the only cure is to deliver the placenta which shows that it is both necessary and sufficient for the disease[31]. Predicting PE is challenging: there are no first-trimester laboratory assays for PE used in clinical practice before 20 weeks of gestation[32].

It is well established that plasma placental EV are higher in PE than normal pregnancy (NP), if measured in the second and third trimesters [23,33,34]. There is also evidence that plasma placental EV are more abundant in EOPE than LOPE[34,35]. Additionally, placental EV protein expression changes in PE. Our group has previously shown the upregulation of placental protein 13, siglec-6, and CD10 (neprilysin), and downregulation of eNOS, on placental EV in PE compared to NP[36-39]. However, these quantitative and qualitative differences in placental EV in PE have only been observed after the onset of the disease. While Salomon and colleagues previously discovered an elevation in total placental EVs, present from 11-14 weeks within maternal plasma in PE compared to NP, measured using ELISA with a PLAP antibody[33], it's important to note that to date, no study has conclusively identified alterations in circulating placental EVs expressing a specific disease-related marker, such as CD10, during the first trimester of PE pregnancies.

Most of the current EV analysis platforms, such as nanoparticle tracking analysis, require multiple sample preparation steps. This pre-processing introduces significant pre-analytical variations. Developing a new assay, which allows direct investigation of the markers expressed on the EV with minimal sample preparation, is essential for translation to clinical laboratories. The ExoCounter is a novel semi-automatic EV quantification assay, which allows the investigator to quantify sEV by capture on an optical disc with 160 nm grooves utilizing a combination of up to two different antibodies for sEV adherence and detection [40]. It's important to note, however, that the ExoCounter method has certain limitations.

Specifically, this technique invariably requires a pair of antibodies for EV quantification and presents challenges in downstream isolation of EVs from the disc.

In this study, I first adapted an ExoCounter assay to quantify and characterise placental small EV using placental sEV (psEV) isolated by dual-lobe placental perfusion. I used three different pairs of antibodies (CD10-CD63, CD10-PLAP and CD63-PLAP) to target a PE specific marker (CD10), an EV marker (CD63) and a placental origin marker (PLAP). I applied these assays to detect psEV in longitudinal plasma samples taken from the same women in the first, second and third trimesters, comparing NP (n=3), women who developed EOPE (WWD-EOPE, n=3) and women who developed LOPE (WWD-LOPE, n=4). I validated our findings in a larger sample of first trimester serum samples (NP=9, EOPE=7, LOPE=8), differentiating WWD-EOPE from NP at 10-12 weeks gestation. To my best knowledge, this is the first study reporting both quantitative and qualitative differences in psEV in WWD-EOPE. ExoCounter demonstrates promise as a diagnostic tool to detect disease-specific sEV.

2.3 Aims

The aims of this chapter are to:

1. Isolation & characterization of placental small EV (psEV) from placenta perfusion
2. Determine the optimal experimental conditions for ExoCounter using psEV isolated from placental perfusion
3. Determine the optimal experiment conditions for ExoCounter to quantify psEV using plasma (a complex biofluid)

4. Quantify CD10-CD63, CD10-PLAP and CD63-PLAP psEV via ExoCounter in the first trimester to the third trimester plasma samples from NP, EOPE and LOPE (discovery phase)
5. Quantify CD10-CD63, CD10-PLAP and CD63-PLAP psEV via ExoCounter in the first trimester serum samples from NP, EOPE and LOPE (validation phase)

2.4 Methods

2.4.1 Human Subjects and Ethic Approval

Our group obtained ethical approval from the Central Oxfordshire Research Ethics Committee C (REFS 07/H0607/74 & 07/H0606/148 & 08/H0606/139). For placental perfusion, I prospectively selected pregnant women undergoing elective caesarean sections before labour onset, from the maternity ward at the Women's Centre, John Radcliffe Hospital, Oxford. The placentas were subsequently collected from normotensive (NP) and preeclamptic (PE) women and perfused within 10 to 20 minutes of delivery. The research midwives obtained written informed consent before placenta collection from all participants. Platelet poor plasma taken at the first (10-12 weeks), second (20-21 weeks) and third trimesters (29-31 weeks) were retrieved from our biobank (Ethics as above). Normal pregnancy (NP) was defined as a singleton pregnancy with no history of preeclampsia, hypertensive disorders, or other complications in pregnancy. Patients with preeclampsia were defined as displaying the co-occurrence of *de novo* hypertension (blood pressure >140/90

mmHg) and proteinuria (>300 mg/day) after week 20 of gestation according to the criteria of the International Society for the Study of Hypertension in Pregnancy. The EOPE was defined as the onset before 34 weeks and LOPE was defined as the onset on or after 34 weeks of gestation.

2.4.2 Isolation of psEV by placental dual-lobe perfusion and serial ultracentrifugation

Methods for isolation and enrichment of psEV through ex-vivo dual lobe perfusion have been described in detail in our previous publication [41]. Briefly, a suitable cotyledon was identified devoid of calcifications, ischemia, or rupture. A suitable placental artery and vein were identified and cannulated and the placenta was perfused for three hours at a 4-5 mL/min flow rate to obtain placenta maternal perfusate. The placenta maternal perfusate was centrifuged twice at 1,500g for 10 minutes at 4°C (Beckman Coulter Avanti J-20XP centrifuge using a Beckman Coulter JS-5.3 swing-out rotor) to remove cells and cell debris. The supernatant was carefully pooled and spun at 10,000g (10K) in a swing bucket centrifuge (Beckman Ultracentrifuge SW32 Ti Swinging-Bucket Rotor) at 4 °C for 30 minutes. The post-10K supernatant was filtered through a 0.22 μm Millipore Stericup Filtration Device (Merck, SCVPU11RE), before being spun again at 150,000g for 2 hours (Beckman Ultracentrifuge SW32 Ti Swinging-Bucket Rotor). The post 150K pellet was washed and resuspended in 0.1μm filtered calcium- and magnesium-free phosphate buffer saline PBS (fPBS) to a protein concentration of approximately 2-5μg/μL (measured using a Pierce BCA protein assay), and immediately stored at -80^{0}C as 25-50μL aliquots. All the medium used in placenta perfusion and sample processing were filtered using a 0.1μm filter device before use. A fresh stock of psEV was thawed and then used for subsequent analysis.

2.4.3 Plasma sample preparation

Sodium citrate platelet free plasma (PFP) samples from the first (10-12 weeks), second (20-21 weeks) and third trimester (29-31 weeks), were retrieved from the biobank. All samples had been collected following a standardised plasma sample protocol. In brief, blood was collected into sodium citrate vacutainers (BD Biosciences) and transported to the lab within 30 minutes for sample processing. To obtain plasma, vacutainers were centrifuged at 1,500g for 15 minutes at room temperature in a swing bucket centrifuge (Beckman Coulter Avanti J-20XP centrifuge using a Beckman Coulter JS-5.3 swing-out rotor). Plasma from 0.5cm above the buffy coat layer was collected, aliquoted to Eppendorf tubes and further centrifuged at 13,000g for 2mins in a fixed-angle desktop microfuge. After this last centrifugation, 450 μL of PFP from each Eppendorf tube, was transferred to a new Eppendorf tube leaving behind 50μL of plasma and pellet to minimize platelet contamination. PFP was stored immediately at -80°C. On the day of the experiments, the samples were defrosted and spun at 13,000g for 2mins before investigation on ExoCounter. In total, 3 NPs, 3 EOPEs and 4 LOPEs were analyzed on the ExoCounter.

For the uterine vein (UV) blood and peripheral vein (PV) experiments, the UV blood was collected by the surgeon during the caesarean section before the delivery of the baby, using a 20ml syringe with a 21G needle. The blood was then transferred to a sodium citrate tube. The PV blood was collected using a sodium citrate vacutainer just before the caesarean section. Both UV and PV blood were processed according to the standardised plasma sample protocol as stated above. PFP from these samples was then frozen at -80 °C.

2.4.4 Serum sample collection

The first-trimester serum samples were part of the Newborn Cross Sectional Study. This collection includes a collection of first-trimester serum samples used for the routine triple test from Oxford University Hospitals NHS Foundation Trust, Buckinghamshire Healthcare NHS Trust, and Milton Keynes University Hospital from May 2015 to August 2018. Each sample was retrospectively coded according to the International Classification of Disease (ICD)[42]. For WWD-EOPE and WWD-LOPE, only patients with the code of 0141 indicating severe PE were selected. Severe PE is defined according to ICD as blood pressure over 160/110 mmHg, required hospital admission and without hemolysis elevated liver enzymes and low platelets (HELLP) syndrome. After the blood samples were collected, the blood samples were centrifuged at 3,000g for 5 minutes and the serum was aliquoted into 0.5ml aliquots and stored at -80°C.

2.4.5 Western Blot

Following the guidelines by the International Society for Extracellular Vesicles (ISEV), all the psEV obtained from placenta perfusion were characterised for the presence and absence of a panel of the following markers; PLAP (for syncytiotrophoblast origin, in-house antibody), CD63 (Santa Cruz Biotechnology, Sc-59286), CD9 (Abcam, ab92726), syntenin (Abcam, ab133267) and ALIX (Santa Cruz Biotechnology, Sc-53538, to confirm the presence of extracellular vesicles, all antibodies at 1 in 1000 dilution), and Cytochrome C (as negative EV marker, 1 in 1000 dilution, Santa Cruz Biotechnology, Sc-13156). HEK293 cell lysate and placental tissue lysates each worked as positive and negative controls for EV markers and syncytiotrophoblast marker. Lysates were made using RIPA buffer (ThermoFisher, 89901) and the protein concentrations were determined using Bicinchoninic acid (BCA) assay (ThermoFisher, 23227). In brief, 20μg of protein of placental sEV were mixed with 4X Laemmli buffer with (for PLAP, Cytochrome C, syntenin) or without (for

CD63, CD9, Alix) 5% β-Mercaptoethanol and diluted to 20μL with distilled water. The sample mix was heated at 70°C for 10mins before loading onto a 4%-12% SDS-PAGE 10-well gel (ThermoFisher, NP0321BOX) for electrophoresis. Proteins were transferred onto PVDF membranes (Bio-Rad, 1620177) using a semi-dry transfer system. The membranes were then blocked for 1h in 5**%** Blottto (2BScientific, AD-80402-500) in Tris-Buffered Saline with 0.1% Tween-20 (TBS-T, ThermoFisher) before incubation with primary antibody overnight at 4°C. After further incubation with the appropriate secondary antibody for an hour, chemiluminescence (ECL) (Thermo Fisher, 32106) was used for signal enhancement and developed in a dark room (Hyperfilm ECL, Merck, GE28-9068-35).

2.4.6 Transmission Electron Microscopy (TEM)

psEV isolated from perfusion were diluted with fPBS to achieve a concentration between 0.1-0.3 μg/μL. psEV were fixed with 2% paraformaldehyde to preserve the morphology and internal structure if samples were left overnight before negative staining. 10μL of the psEV solution was applied to freshly glowing discharged carbon formvar 300 mesh copper grids for 2 mins, blotted with filter paper, and stained with 2% uranyl acetate for 10s, then blotted and air-dried. psEV on the grid were negatively stained to enhance the contrast between psEV and the background. The grids were imaged using an FEI Tecnai 12 TEM at 120 kV with a Gatan OneView CMOS camera.

2.4.7 Nanoparticle Tracking Analysis (NTA)

I further characterised the psEV isolated from placenta perfusion by nanoparticle tracking analysis [(NTA) NanoSight NS500 instrument equipped with a 405 nm laser (Malvern UK), sCMOS camera and Nanoparticle Tracking Analysis (NTA) software version 2.3, Build 0033

(Malvern UK)]. Before sample analysis, instrument performance was checked with silica 100 nm microspheres (Polysciences, Inc.). The samples were diluted in fPBS to a range of 1/10,000 to 1/100,000 as determined by the starting concentration. The samples were automatically injected into the sample chamber with a 1ml syringe with the following script used for EV measurements: PRIME, DELAY 5, CAPTURE 60, REPEAT 4. Images of the analyzed samples were captured on camera at a level of 12 (Camera shutter speed; 15 ms and Camera gain; 350) and NTA post-acquisition settings were optimised and kept constant between samples. Each video recording was analysed to infer psEV size and concentration profile.

2.5.8 Identifying PLAP-associated antigens by MACSPlex Exosome Kit

The MACSPlex exosome kit (Miltenyi Biotech, 130-108-813) was used with modification to probe psEV antigens and their association with PLAP. Briefly, 10µg of psEV isolated from placenta perfusion were incubated with MACSPlex Exosome Capture beads following the manufacturer's short protocol for 1.5mL reagent tubes. Samples were washed to remove the non-specific binding and unbound EV at the end of incubation. Instead of using MACSPlex Exosome Detection Reagents (APC-conjugated CD9, CD63 and CD81 antibodies), APC-conjugated PLAP antibody (an in-house mouse IgG1 antibody) at 0.5µg/mL or APC-conjugated IgG1 isotype control (Biolegend) at 1 in 1,000 was added. The remaining incubation and sample washing steps were conducted following the standard manufacturer's protocol. Samples were analyzed using Becton Dickinson LSR-II flow cytometer. For data analysis, the net geometric means of PLAP fluorescence from each capture bead were calculated by subtracting correspondent APC-conjugated IgG1 isotype-stained control tubes from the geometric means fluorescence of the APC-conjugated PLAP antibody stained tubes.

The fluorescent intensity was an indication of PLAP association with antigens captured by capture beads. The higher the fluorescence, the more abundant PLAP antigens.

2.5.9 ExoCounter

The ExoCounter (JVCKENWOOD corp.), can capture and quantify the sEV by sandwich immunoassay using disc and secondary antibodies conjugated to nanobeads (Figure 1). Unique to ExoCounter is that 1) disc is engraved with circular U-shaped trenches 260 nm in width at the top and 160 nm at the bottom. The surface of the disc allows for coating of capturing antibody which permits sEV <160nm to be captured at the bottom of the trench; 2) Captured sEV are further recognized by the secondary antibody conjugated to magnetic nanobeads (FG beads)[43]. The size of the nanobeads is 200nm which permits the beads to enter the trench to bind with sEV while preventing a second bead from entering. This allows one bead to bind to one sEV. The number of beads were counted by an optical pickup equipped with a laser diode, which can illuminate the disc, and a photodetector which can detect the light reflected from the disc. The light from the beads attached to the exosomes was transformed into pulses and counted by a pulse counter circuit. The number of pulses generated by diffraction is therefore equal to the number of captured and labeled sEV; 3) the same or different antibodies can be used in combination giving the flexibility for interrogation of up to two antigens per well. In order to easily describe the experimental antibody layout used for the ExoCounter experiments in the current study, the form of (antibody-1)- (antibody-2) is used to describe the coating antibody (antibody-1, in the groove) and bead-bound antibody (antibody 2). For example, CD63-PLAP denotes CD63 as coating antibody and PLAP as a bead-bound antibody.

This assay has five major steps. First, 90μL of coating antibody (5μg/mL) was applied on a well of the disc to coat for 1h at 37 °C. Next, 200μL of blocking buffer was applied to block non-specific signals for 1h at room temperature. Then, 50μL of samples was applied to the disc and incubated for 2hs at 37 °C on an orbital shaker. For psEV from perfused placentas, psEV were diluted according to the desired concentrations using fPBS up to 50μL. For plasma or serum samples, 12.5μL of plasma or serum samples were diluted in 37.5μL fPBS or PBST to make up to the total 50μL. Next, 50μL of bead-bound antibody solution (20μg/mL) was applied to the disc for 90mins at 37 °C on an orbital shaker. Finally, after the washing and drying steps, the signals were read by the optical system using a Blu-ray laser device and each bead was counted as pulses by the pulse sensing circuit. Between each step, an automatic washer was used to remove the excess reagents and reduce non-specific binding. The washing buffer used was 0.05% Tween-20 in PBS (PBST). The washing program was set to wash the disc with 300μL of PBST 3 times, and an additional wash with 3,000μL deionized water to minimize salt crystal formation before disk drying.

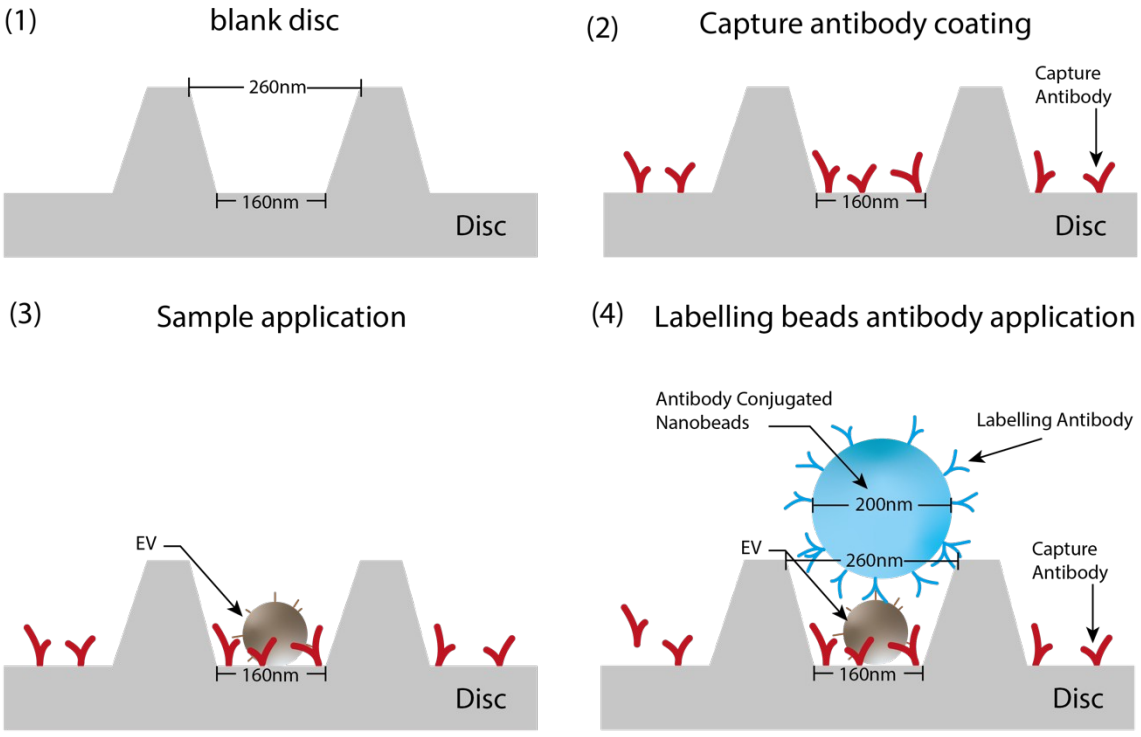


Figure 1. The principle for exosome capture and quantification by ExoCounter. The disc is coated with the capture antibody and then the samples are directly applied to the disc. The target antibody conjugated nanobeads is then added. Beads that specifically bound to exosomes remained after washing step and bead and exosome immobilised on the disc is at one-to-one ratio. The disc is then inserted into a disc-reader where each circular trenches is scanned by a laser in an orderly manner. Each bead will modify a light refraction upon laser excitation. The light refraction signal is captured by a photodetector and converted to pulses. The number of pulses corresponds to the number of beads.

Supplier	Description	Catalog Number	Clone	Assay Concentration
Miltenyi Biotec	CD10 antibody (neprilysin)	130-108-025	97C5	5μg/mL
Biolegend	LEAFTM Purified anti-human CD63	353014	H5C6	5μg/mL
Biolegend	Purified anti-human CD9	312102	HI9a	5μg/mL
In-house	Anti-human placental alkaline phosphatase (PLAP)	N/A	NDOG2	5μg/mL
BioLegend	IgG1	400101	MOPC-21	5μg/mL

Table 1. The information of the antibodies used. N/A denotes not applicable.

For initial assay development, different coating dilution buffer (PBS or Acetate (ACE, 3863)) and disc blocking buffers (1% casein (Thermo Scientific, 37528) or 0.01% casein in PBST) were tested. The coating antibodies used in the experiments were listed in Table 1. Antibody bead conjugation was performed as previously described[40]. For each bead antibody, 50µL of bead antibody solution (20µg/ml) contains approximately 1.6×10^8 FG nanobeads per well. psEV isolated from placental perfusion were used to validate the performance of ExoCounter. In brief, psEV at 3µg/well, 1µg/well, 0.3µg/well, 0.1µg/well and 0.03µg/well were diluted in fPBS and the signals obtained were compared. Each protein concentration was performed in triplicate which resulted in 15 wells being used and the last well (each disc has 16 wells in total) was used as blank well which was treated under identical conditions except no sample was added.

2.5.10 Experimental design and flow

The experimental design for this chapter is shown in Figure 2. First, I isolated and characterised psEV from placenta perfusion. Then, the isolated psEV were used to optimise ExoCounter performance by testing different blocking buffers and antibody diluents. After the optimisation, I measured the assay linearity and repeatability of ExoCounter and compared ExoCounter assay with another qualitative method MACSPlex. Next, I applied the longitudinal first-, second- and third-trimester plasma samples from NP (n = 3), WWD-EOPE (n = 3) and WWD-LOPE (n = 4) on ExoCounter using CD10-PLAP, CD10-CD63 and CD63-PLAP three pairs antibodies to determine if there were disease-specific or gestation-specific psEV profile. Finally, I validated the findings by using a larger sample size of the first-trimester serum samples from NP (n = 9), WWD-EOPE (n = 7) and WWD-LOPE (n = 8).

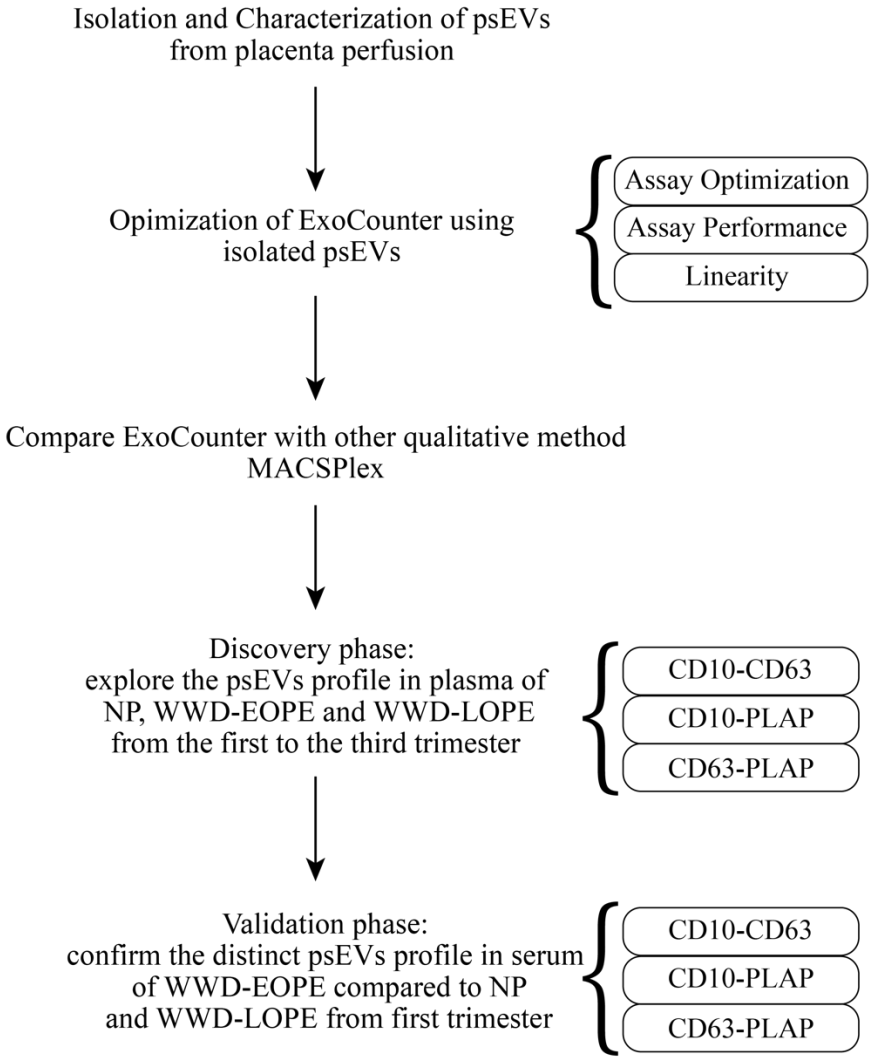


Figure 2. Experimental design and flow chart.

2.5.11 Statistical Analysis

Statistical analysis was performed using GraphPad Prism 9. Continuous variables were compared using the Mann-Whitney test. Categorical variables were compared using the chi-square test. The difference between the uterine vein and peripheral blood was compared using the Wilcoxon test (paired non-parametric test).

2.5 Results

2.5.1 psEV Characterisation

psEV isolated from placental perfusion from NP and EOPE were characterised by TEM, western blot and NTA. psEV expressed syntenin, CD63, Alix, CD9 (exosomal markers), PLAP (the syncytiotrophoblast origin marker), and were negative for cytochrome C (negative control) expression (Figure 3A). Equal amounts of 20μg protein as determined by BCA assays was loaded into each lane. Under TEM, psEV exhibited a characteristic cup shape in negative staining (Figure 3B&C). NTA analysis revealed the mean of the size distribution of psEV was (220.7 ± 90) nm (Figure 3D).

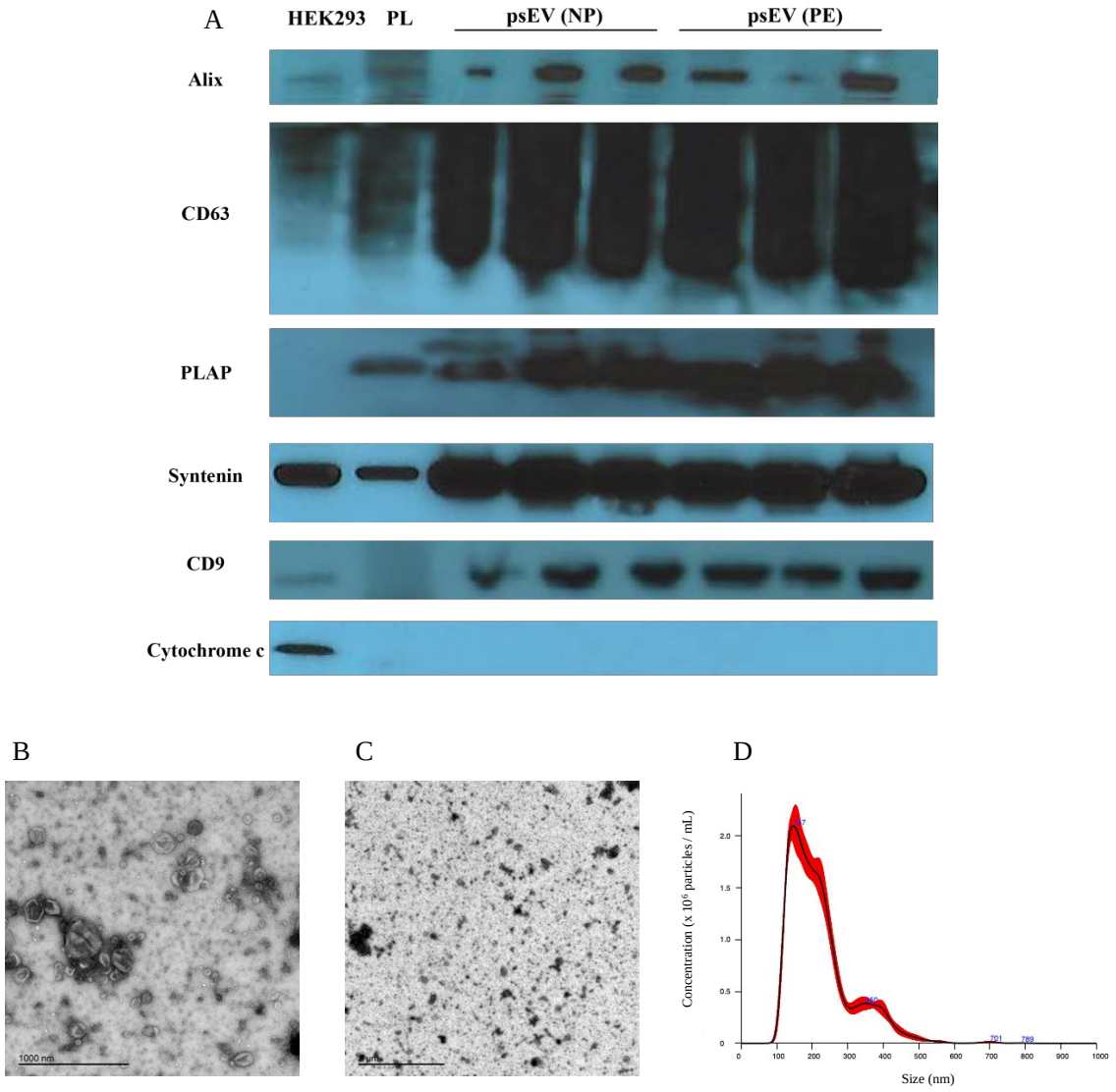


Figure 3. (A) psEV characterized by western blot. PL indicates placenta lysate. HEK293 lysate as negative controls for PLAP and positive control for cytochrome C. The characterization markers were Alix (95kDa), CD63 (30-65kDa), PLAP (66kDa), Syntenin (30kDa), CD9 (23kDa), Cytochrome c (12kDa). (B) Representative pictures of psEV characterised by TEM of higher magnification. Scale bar = 1μm. (C) Representative pictures of psEV characterised by TEM at lower magnification. Scale bar = 5μm. (D) Representative characterisation of psEV by NTA.

2.5.2 Antibody coating and blocking buffer optimisation for ExoCounter assay using psEV

This initial ExoCounter validation on psEV obtained from placental perfusion was to identify the optimal experimental conditions, i.e., an assay condition which could yield the highest specific psEV counts, lowest background and highest assay linearity. For this purpose, different coating antibody diluents and blocking buffers were tested. PLAP coating antibody and PLAP beads antibody were used to detect PLAP-PLAP psEV since PLAP was proven to be abundantly expressed on psEV (Figure 3). ACE or fPBS were tested as coating antibody diluent and 1% Casein or 0.01 % Casein in PBST was tested as blocking buffer. fPBS as coating antibody diluent and 0.01% Casein in PBST as blocking buffer yielded relatively higher counts and lower background signals and the highest $R^2 = 0.9985$ in linear regression analysis compared to other combinations (Figure 4A). Therefore, fPBS was chosen as coating antibody diluent and 0.01% Casein was selected as blocking buffer for psEV isolated from placenta perfusion. Next, with the application of this optimised assay condition, I checked the reproducibility of ExoCounter. This was first done within our Oxford laboratory at different dates using the same psEV samples. Counts of PLAP-PLAP by different operators on different dates (Figure 4B) were highly consistent. PLAP-PLAP psEV counts appeared to

reach the upper plateau phase from 1-3μg but the lower plateau phase was not shown that the counts were still within the linearity range at 0.03 μg (Figure 4B). Therefore, I next performed ExoCounter assay using protein concentration from 0.001-1μg to check and determine the lowest quantifiable linearity range. The same sample was shipped on dry ice to Japan and analysed under the same condition. Counts of PLAP-PLAP psEV obtained in different organisations were again highly consistent (Figure 4C). This data also suggested PLAP-PLAP psEV counts appeared to reach the lower plateau phase from 0.04 μg to 0.001μg. While 0.04 μg is higher than 0.03μg (Figure 4B), 0.03 μg was decided to be the lowest quantifiable linear limit for PLAP-PLAP (Figure 4C).

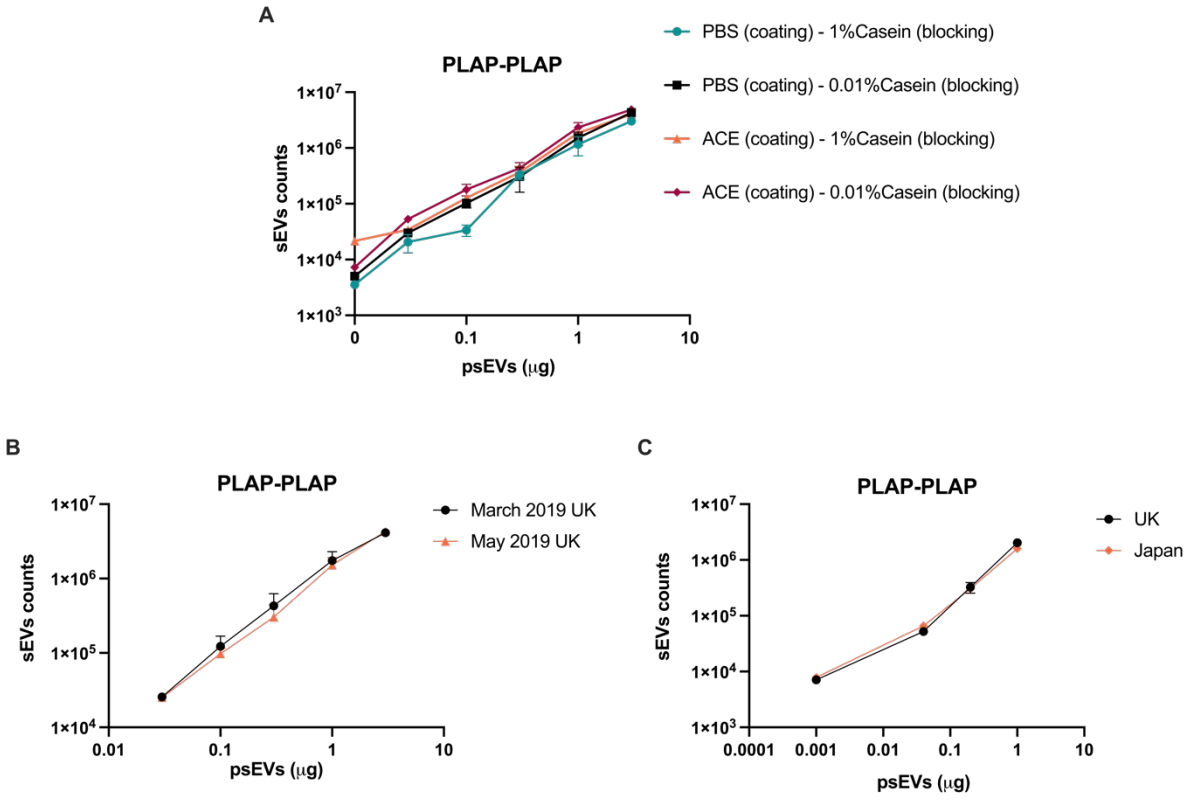


Figure 4. ExoCounter assay optimisation. (A) PBS or ACE was tested as coating antibody diluent, 1% or 0.01% Casein in PBST was tested as blocking buffer. (B) Assay reproducibility and linearity with the application of identified optimal assay conditions on different dates in the same organisation. (C) Assay reproducibility and linearity with the application of identified optimal assay conditions on different dates in different organisations.

PLAP was used as both coating antibody and bead antibody for psEV detection. The amount of protein tested were from 0, 0.03, 0.1, 0.3, 1 and 3 (μg) in Figure (A & B), from 0.001, 0.4, 0.2, and 1 (μg) were tested in (C). For all figures, the x-axis represents the amount of protein tested (μg), the y-axis represents PLAP-PLAP psEV counts detected by ExoCounter with background (A) or after background correction (B&C). PBS as coating antibody diluent and 0.01% Casein in PBST as blocking buffer for both (B) and (C). n=3 for all data points. The error bar of each point was calculated by the standard deviation (SD) and some error bars were invisible due to the size of the error bars being smaller than the symbols.

2.5.3 CD63 is determined by MACSPlex kit and confirmed by ExoCounter as the most abundant tetraspanin on psEV

The MACSPlex kit were used for the identification of major PLAP-associated tetraspanin species on psEV. Tetraspanins have been used as a surrogate marker for sEV. Knowing which one of the tetraspanins is expressed in association with PLAP permits for a more focused analysis of psEV with the ExoCounter. To this end, MACSPlex was used on four psEV samples isolated from placenta perfusion with a modification as specified in the method, the result showed net PLAP fluorescence in association with the 37 markers. Among the three tetraspanins CD9, CD63 and CD81, the highest PLAP fluorescence was found in association with CD63, indicating CD63 was the most common and abundant tetraspanin expressed by psEV (Figure 5). For this reason, CD63 was used as a psEV marker. I also found that CD29 (integrin beta1) and CD105 (endoglin), two markers known to be abundantly expressed by placenta syncytial trophoblasts (REFS), exhibited the highest levels of fluorescence from PLAP labelling (Figure 5). No fluorescence signal was detected from lineage markers for lymphocytes (CD45), for T (CD3, CD4 and CD8) and B (CD19 and

CD20) lymphocytes, for monocyte (CD14 and CD11c). No fluorescence signal was detected from CD1c, CD2, CD24, CD25, CD31, CD40, CD56, CD62P, CD69, CD86, CD133-1, CD142, CD146, CD209, CD326, and HLA-I. These positive and negative labelling together reassured PLAP specificity.

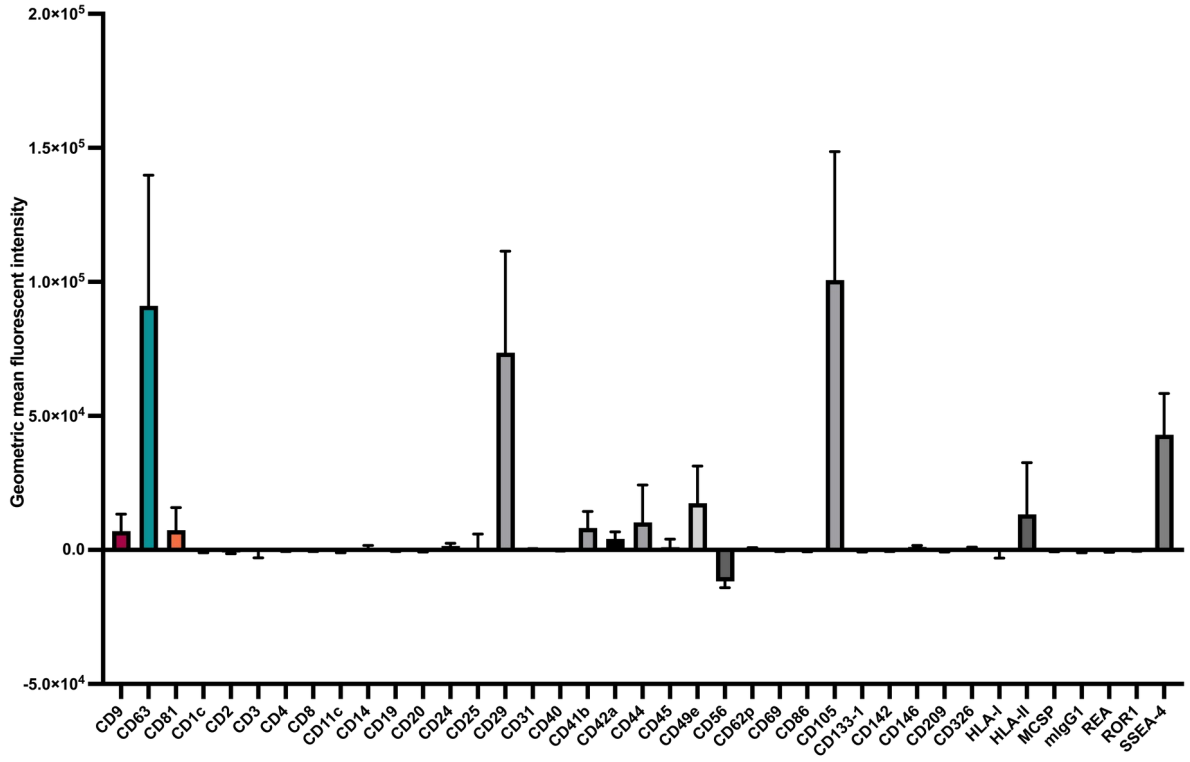


Figure 5. The association of each exosomal or cell lineage markers on psEV with PLAP detected by MACSPlex. Each bar corresponds co-expression of PLAP on each antibody captured sEV populations. Y-axis indicates the geometric mean fluorescent intensity of all the samples measured, n=4.

Having found the differences between CD63 and CD9 in their association with PLAP using the MACSPlex kit, I next tested the association between tetraspanins CD63 or CD9 with placental marker PLAP by ExoCounter. Consistent with the MACSPlex results (Figure 5), counts of psEV by PLAP-CD63 were higher than PLAP-CD9 (Figure 6A). When using PLAP as capturing antibody, the counts of both PLAP-CD63 and PLAP-CD9 increased

proportionally with the increasing psEV protein concentration and the correlation coefficient (Corr) between these two data sets was 0.9972 (Figure 6A). Corr measures the normalised covariance of two data sets with a value of 1 indicating a perfect positive linear relationship. The Corr of PLAP-CD63 and PLAP-CD9 was close to 1 indicating ExoCounter was able to efficiently capture psEV using PLAP as capturing antibody, and differences between PLAP-CD63 and PLAP-CD9 reflected quantitative differences in number of psEV expressing CD63 and/or CD9. Taken together, both ExoCounter and MACSPlex assay consistently showed CD63 is the most abundant tetraspanin molecule co-expressed with PLAP. For this reason, CD63 was chosen to pair with PLAP for ExoCounter assay to represent psEV in the subsequent experiments. In addition, compared to MACSPlex, ExoCounter was able to generate an absolute count of psEV thereby revealing quantitative differences for each protein concentration tested.

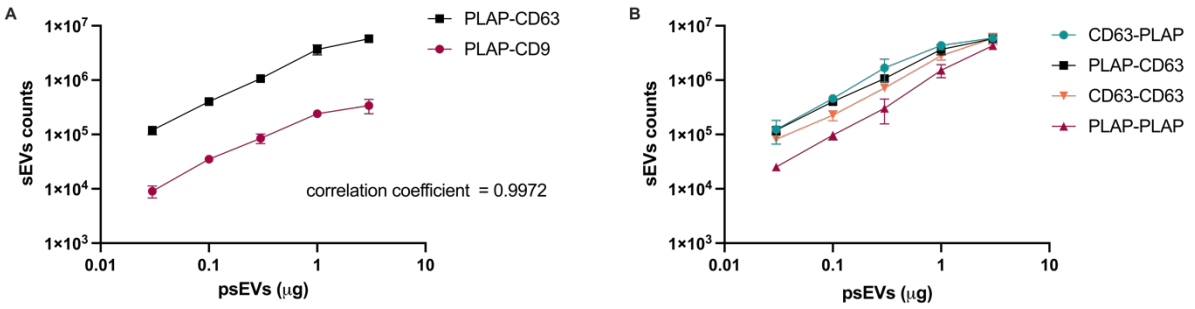


Figure 6. (A) The quantification of psEV isolated from placenta perfusion using PLAP-CD9 and PLAP-CD63 by ExoCounter. The correlation coefficient equals to 0.9972 between PLAP-CD63 and PLAP-CD9, reflecting a consistent difference in counts by PLAP+ psEV bearing CD63 or CD9 regardless of protein concentrations of psEV. (B) The quantification of psEV isolated from placenta perfusion using CD63-PLAP, PLAP-CD63, CD63-CD63 and PLAP-PLAP. The x-axis represents the amount of protein (mg) of psEV tested which includes 0.03, 0.1, 0.3, 1 and 3 mg of psEV. The y-axis represents the absolute counts of

psEV detected by ExoCounter after background correction. The error bar of each point was calculated by the SD of the triplicates and some error bars were invisible due to the size of the error bars being smaller than the symbols.

2.5.4 Identify the optimal coating and detecting antibody combination for ExoCounter psEV quantification

Having established CD63 is the major tetraspannin molecule associated with PLAP, I next tested if counts and backgrounds were affected by switching the same antibody pair from coating antibody to capturing antibody i.e.CD63-PLAP, PLAP-CD63, PLAP-PLAP and CD63-CD63 in ExoCounter assay (Figure 6B). The counts from CD63 (coating)-PLAP (beads) combinations were highly consistent with PLAP (coating)-CD63 (beads) and CD63 (coating)-CD63 (beads). The counts for CD63-PLAP were slightly higher thus this combination was chosen for further experiments. Interestingly, the lowest counts were obtained using PLAP-PLAP combination (Figure 6B). For all the combinations of antibodies tested, psEV counts reached the upper plateau phase when the amount of protein of psEV tested was more than 1μg (Figure 6A & B). This confirmed the highest linear quantifiable limit of psEV was 1μg for the combinations of antibodies tested. Taken together, the quantifiable linear range of the amount of protein of psEV was determined to be 0.03μg to 1μg using ExoCounter. The linear regression formula within the quantifiable linear range for each antibody combination tested in Figure 6B all have R^2 greater than 0.99 (Table 2).

Antibody Combination	Linear Regression Formula	R^2

PLAP-CD9	y = 234,076x + 8,894.3	0.9971
PLAP-CD63	y = 3,667,453.6x + 7,733.9	0.9997
CD63-CD63	y = 2,840,075.7x - 58,911.2	0.9980
PLAP-PLAP	y = 1,567,370.5x - 74,457.8	0.9917
CD63-PLAP	y = 4,294,819.8x + 115,132.7	0.9907

Table 2. The linear regression formula and R^2 for the five different capture and detection marker pairs as shown on Figure 6B.

2.5.5 ExoCounter assay optimisation for plasma samples

When the optimised assay conditions for perfusion generated psEV were applied to plasma samples from pregnant women, the high background signals were observed on ExoCounter. I reasoned, unlike placental perfusion derived psEV, plasma samples contain high levels of immunoglobulin (IgG). Non-specific binding between plasma IgG and beads might be a cause of high background observed. In the past, Tween-20 and casein were shown to be effective to reduce non-specific binding in enzyme-linked immunosorbent assays using plasma[44]. I therefore reassessed casein concentration in the beads antibody diluent for reduction of non-specific binding. To identify the optimal concentration of casein for background reduction, different concentrations of casein (0%, 0.01%, 0.1%, 1%) were added to the beads antibody diluent. Counts from IgG1-CD63, an indication of non-specific binding in plasma samples, were compared. The counts of IgG1-CD63, decreased with increasing concentration of casein in beads diluent with 0.1% casein yielding the lowest background counts (Figure 7A). Next, I checked the effect of casein in the beads antibody diluent on CD63-CD63 specific signals from the same plasma samples. I chose CD63-CD63 instead of

CD63-PLAP since CD63-CD63 was more likely to capture not just psEV but sEV from other cellular sources in plasma samples. Second, I found CD63 antibody conjugated beads generated higher background signals compared to PLAP antibody-conjugated beads (data not shown). After I added casein to the beads diluent, I found CD63-CD63 sEV counts were also decreased with increased concentration of casein (Figure 7B). The highest signal to noise ratios (dividing the counts from CD63-CD63 by IgG1-CD63) were evaluated, and the highest signal to noise ratio was seen when 0.1% casein was used as beads antibody diluent (Figure 7C). Thereafter, 0.1% casein was used in beads diluent for plasma samples.

However, with application of 0.1% casein in beads diluent to the three antibody combinations, CD10-PLAP, CD10-CD63 and CD63-PLAP, to analyze psEV in plasma samples from pregnant women, high background signals from CD10-CD63 were again observed. I next tested if background in plasma could be further reduced by adding 0.05% of Tween 20 to PBS (PBST) and use it as sample diluent instead of just PBS. Furthermore, I also wanted to check if CD10-CD63 sEV were only specific to pregnant women (i.e., only detectable in pregnant plasma samples and not detectable in non-pregnant plasma samples). And if CD10-CD63 sEV were not specific to plasma samples from pregnant women, I next checked if ExoCounter was able to detect the contribution of placenta specific CD10-CD63 sEV signals from plasma samples. For these purposes, I first made a 1 in 4 dilution of plasma samples from non-pregnant women either in PBS or in PBST, and psEV at 4μg/mL were used to spike in non-pregnant plasma samples. If placenta-specific CD10-CD63 signals could be detected, higher counts would have been seen in psEV spiked plasma samples.

Low levels of counts were obtained from IgG1-CD63 regardless of whether PBS or PBST was used as sample diluent, and with or without spiked in psEV (Figure 7D). In contrast,

CD10-CD63 counts in non-spiked samples were 20 times higher than IgG1-CD63 in plasma samples, indicating these CD10-CD63 signals from plasma samples were not pregnancy-specific. After we spiked psEV in the plasma samples, higher counts (1 x 10^5 difference) have been seen in psEV spiked plasma samples compared to samples without spike-in when PBST was used as sample diluent (Figure 7D). These results indicated placenta specific CD10-CD63 psEV from the spiked in were detected above the existing CD10-CD63 sEV signals from plasma samples by ExoCounter. Overall, PBST yielded higher specific signals compared to PBS. Thus, PBST was chosen as plasma diluent in the subsequent experiments.

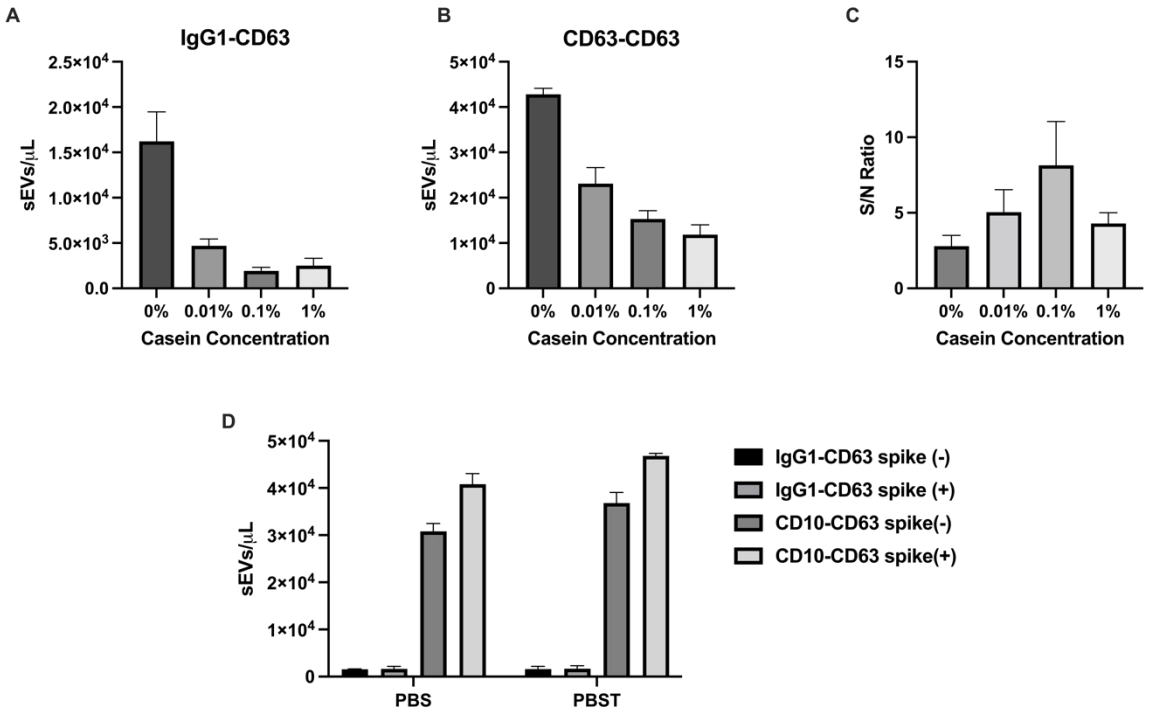


Figure 7. Effect of casein concentration in beads dilution buffer on non-specific signal (IgG1-CD63) (A), specific signal (CD63-CD63) from plasma samples (B) and signal to noise ratio (S/N ratio (C). Effect of PBS or PBST as plasma sample diluent on non-specific signal (IgG1-CD63) and specific signal (CD10-CD63) on spiked and non-spiked plasma samples (D). 4mg/mL psEV isolated from placenta perfusion was spiked into plasma samples from healthy non-pregnant donors as placental specific signals.

2.5.6 ExoCounter detected higher placenta specific CD63-PLAP sEV counts in uterine vein (UV) compared to paired peripheral vein (PV)

After I optimised the assay condition including the optimisation of blocking buffer and sample diluent, I next wanted to see if with application of the optimisation assay conditions 1) sEV counts by CD10-PLAP, CD10-CD63 and CD63-PLAP could be detected in plasma from normal pregnant women; 2) the known psEV gradient between uterine and peripheral vein blood samples from the same donors could be detected by ExoCounter. I chose the combination of CD10, PLAP and CD63 since CD10 is a PE-specific disease marker on sEV [38], PLAP is a placenta-specific marker and CD63 is a sEV marker. The combination of either two markers from these three would give us representatives of placenta-specific or disease-specific sEV signals. Indeed, the representative placenta-specific CD63-PLAP sEV counts were all higher in the UV compared to PV ($P < 0.05$, Figure 6A) in all the 7 pairs of samples tested. CD10-PLAP and CD10-CD63 sEV counts didn't show a uniform gradient effect in UV and PV (Figure 8A).

2.5.7 The unique psEV profile of WWD-EOPE compared to NP and WWD-LOPE could be observed as early as the first trimester

To see if there was a gestational-age-related and disease-specific change in psEV, I quantified the counts of psEV in longitudinal (same patients) plasma samples from NP (n = 3), EOPE (n = 3) and LOPE (n = 4), from first trimester (10-12 weeks), second trimester (20-21 weeks) and third trimester (29-31 weeks), using three antibody pairs: CD10-PLAP, CD10-CD63 and CD63-PLAP. When counts in plasma from the three trimesters of each individual patient

were compared, none of the three combinations detected gestational age-related changes in counts with statistically significant differences (Figure 8B, 8C, 8D). However, counts of psEV as identified by all three coating and detection antibody pairs were elevated in WWD-EOPE compared to NP and WWD-LOPE as early as the first trimester. The high error bar observed might be due to the low sample size, but a clear separation between WWD-EOPE and NP or WWD-LOPE could still be observed. Therefore, I decided to increase the sample size to validate the above findings.

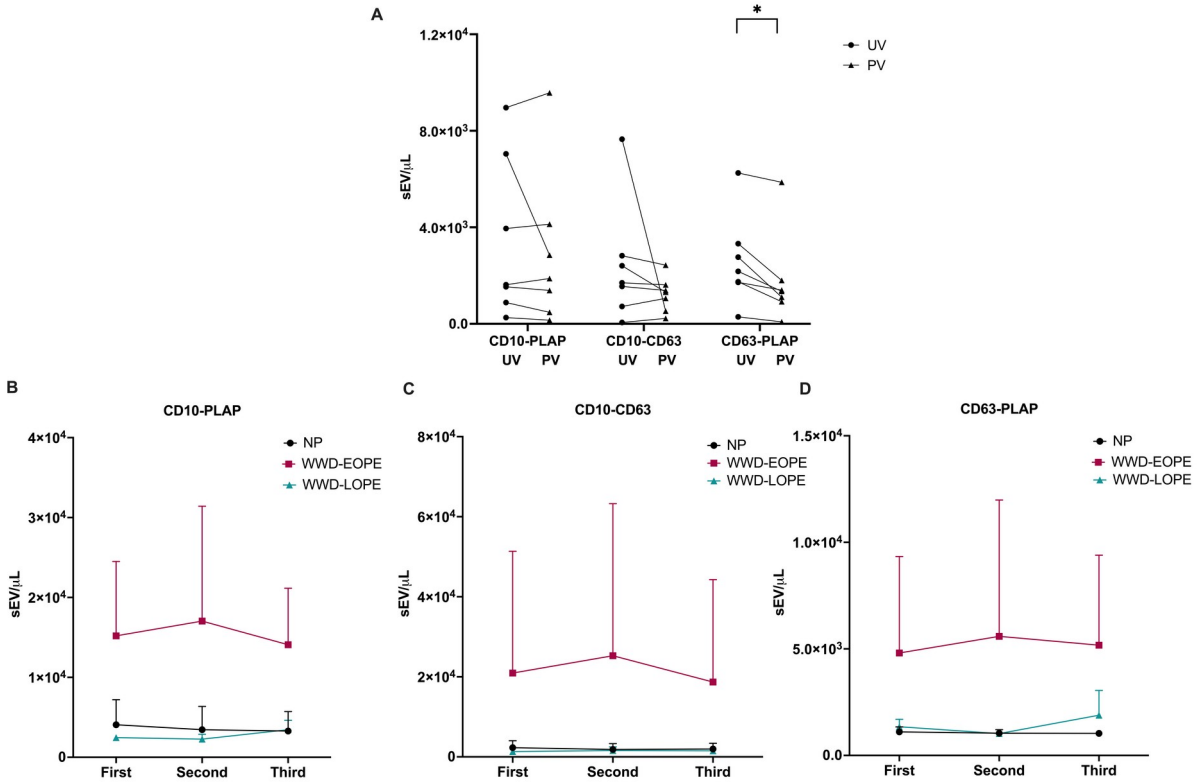


Figure 8. CD10-PLAP, CD10-CD63 and CD63-PLAP psEV counts in (A) paired peripheral vein (PV) and paired uterine vein (UV) from healthy pregnant women, n=7. psEV counts in longitudinal plasma samples from NP, WWD-EOPE and WWD-LOPE detected by (B) CD10-PLAP; (C) CD10-CD63; and (D) CD63-PLAP. Each data point represents the mean level of the group and the error bars were calculated by the standard deviation (SD). The y-axis represents the sEV counts/ml after background (BG) correction.

The patient information for the plasma samples is shown in Table 3. The average systolic and diastolic blood pressure was significantly higher among the WWD-EOPE (163/100) and WWD-LOPE (155/96.8) groups compared to NP (118.8/65.3). Likewise, there was a significant difference in proteinuria and gestation age at delivery for WWD-EOPE and WWD-LOPE compared to NP. Finally, all the WWD-EOPE babies were born preterm and none of NP or WWD-LOPE baby were born preterm. There was no difference in maternal age, weight, body mass index (BMI) and smoking status.

Characteristics	Normal Pregnancy	WWD-EOPE	WWD-LOPE	P Value
Sample size	3	3	4	
Maternal age years (mean ± SD)	26 ± 7.23	30.3 ± 7.23	26.2 ± 4.35	0.6533
Maternal weight kilograms (mean ± SD)	75.8 ± 24.2	69.1 ± 6.47	72.55 ± 1.97	0.8312
Maternal height centimetres (mean ± SD)	169.4 ± 5.31	169.1 ± 3.9	161.9 ± 8.8	0.3006
Body mass index kg/m-2 (mean ± SD)	26.7 ± 6.18	24.1 ± 1.77	27.8 ± 3.64	0.5420
Times of gravidity (mean ± SD)	1.7 ± 0.58	1.3 ± 0.58	2 ± 1.41	0.7061
Systolic blood pressure mmHg (mean ± SD)	113.3 ± 9.45	163.3 ± 15.28	155 ± 5.77	0.0011
Diastolic blood pressure	67 ± 6.24	100 ± 10	96.8 ± 3.77	0.0009

mmHg (mean ± SD)				
Proteinuria plus(es) (mean ± SD)	0	2.7 ± 1.15	3.3 ± 0.5	0.0013
Gestational age at delivery in weeks (mean ± SD)	39.7 ± 0.58	33 ± 2.65	38.5 ± 1.29	0.0037
Birth weight grams (mean ± SD)	3459.3 ± 352.1	1843.3 ± 491.74	3219.0 ± 673.49	0.0163
Preterm delivery (%)	0 (0)	3 (100)	0 (0)	0.0067
Smoking History	0/3	1/3	2/4	0.3564
Intrauterine growth restriction (IUGR) (%)	0 (0)	3 (100)	1 (25)	0.0321
Male gender (%)	2 (66.7)	0 (0)	3 (75)	0.1146

Table 3. Patient's demographics of the longitudinal plasma samples.

2.5.8 Counts of psEV detected by ExoCounter were highly consistent in serum and plasma samples from the same donor

Due to the limited availability of larger sizes of the first trimester plasma samples in the biobank, I next wanted to validate the above findings (Figure 8B & 8C & 8D) by using available serum samples. Before moving to serum samples to validate the results acquired from plasma samples. I compared the psEV counts detected in paired plasma and serum samples from 7 NP donors of the third-trimester pregnancy. The psEV counts detected by

CD63-PLAP in serum were similar to the counts in plasma in all 7 pairs (Figure 9). This indicates the psEV counts detected by ExoCounter were not influenced by the sample type.

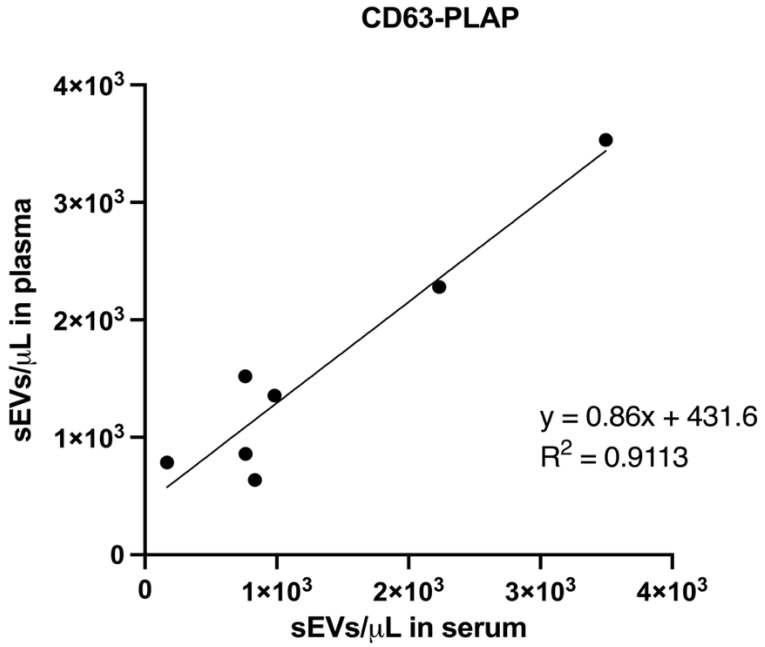


Figure 9. Correlation of CD63-PLAP psEV counts in serum and plasma from the 7 third trimester NP donors. The x-axis is the sEV/mL in serum and the y-axis is the sEV/ml in the plasma. The linear regression formula is $y = 0.86x + 431.6$ with $R^2 = 0.9113$.

2.5.9 Significant higher counts of CD10-PLAP and CD63-PLAP sEV were detected by ExoCounter in WWD-WOPE compared to WWD-LOPE and NP in the first trimester serum samples

Having found serum samples could be used as an alternative of plasma on ExoCounter, I have next analysed psEV in a collection of first-trimester serum samples, NP (n = 9), EOPE (n = 7) and LOPE (n = 8). Patients and controls were selected for matched BMI and parity. Only severe PE patients without HELLP syndrome were selected. Severe PE is defined according to the International Classification of Diseases (ICD) as blood pressure over

160/110 mmHg and required hospital admission [42]. Other patients' demographics and clinical characteristics are shown in Table 4.

Significantly higher psEV counts were found in the first-trimester serum samples from WWD-EOPE compared to NP detected by CD63-PLAP (P <0.01) and CD10-PLAP (P < 0.01, Figure 10A). There is no significant difference of psEV counts detected by CD10-CD63 from WWD-EOPE compared to NP. None of the three pairs, CD10-PLAP, CD10-CD63 and CD63-PLAP, showed significant differences between NP and WWD-LOPE in the first-trimester serum samples (Figure 10B).

Characteristics	Normal Pregnancy	EOPE	LOPE	P Value
Sample size	9	7	8	
Maternal age years (mean ± SD)	29 ± 8.78	28.1 ± 3	31.3 ± 6	0.6555
Body mass index kg/m-2 (mean ± SD)	25.0 ± 3.8	25.3 ± 3.3	24.0 ± 2.5	0.7126
Birth weight grams (mean ± SD)	3340 ± 394	1282.3 ± 390.2	3293.1 ± 669.5	<0.001
Smoking History	3/9	1/7	3/8	0.5784
Male sex (%)	3 (33)	1 (14)	5 (62.5)	<0.001

Table 4. Patient's information for serum samples.

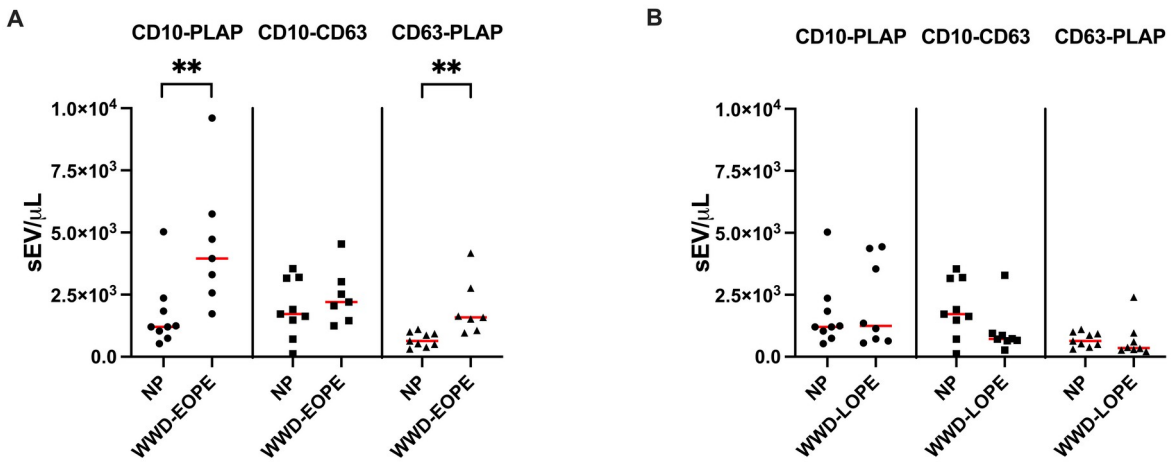


Figure 10. Counts of CD10-PLAP (circle dot), CD10-CD63 (square dots), and CD63-PLAP (triangle dots) psEV in the first trimester serum from (A) NP and WWD-EOPE; (B) NP and WWD-LOPE. For both figures, each dot represents an individual sample and the red line represents the median level of the group and ** denotes $P \leq 0.01$. The statistic test for both figures was carried using the Mann-Whitney test. The y axis represents the sEV counts after background (BG) correction.

2.6 Discussion & Future work

In this study, I have developed and optimized three assays to quantify and phenotype placental small EV (psEV) isolated from placental perfusion using the ExoCounter instrument. I have made adaptations to the assays to permit interrogation of psEV in plasma and serum samples. I found the ExoCounter assays 1) showed a wide linear range with high intra-organisation and inter-organisation reproducibility, 2) confirmed CD63 as the major tetraspannin associated with PLAP, (3) detected the previously identified gradient in psEV between the UV and PB; 4) identified significant differences between WWD-EOPE and NP in the first-trimester serum samples. To my best knowledge, this is the first study to show psEV counts by CD10-PLAP and CD63-PLAP differed significantly only between NP and WWD-EOPE but not between NP and WWD-LOPE. Most importantly, the differences can be detected as early as in the first trimester ((≤ 12 weeks) plasma or serum samples. Although higher PLAP-positive placental EV in EOPE plasma samples compared to LOPE and NP has been detected by ELISA in the third trimester's samples[34,45], here I expand previous observations and show differences are identified by ExoCounter assay in a small volume of unprocessed serum or plasma in the first trimester, thus providing a window of opportunity for early prophylaxis such as aspirin administration from 12 weeks of gestation.

Previous studies have reported placental EV in NP plasma increased with the advancing gestational age[22,46]. These results were not found in our study. The following reasons may explain the difference between my study and others. First, other studies have isolated placental particles prior to quantification (Table 5). The ultracentrifugation (UC) method they used in their studies can co-sediment unwanted soluble proteins and other non-EV materials[22,23,35,46]. It has been suggested that only a minority of EV could be isolated from plasma by UC[47]. Taken together, it may not be appropriate to compare data generated from

processed and un-processed samples. Secondly, the difference I saw between my study and other studies may be due to the size of the EV quantified. In my study, the physical structure of the discs selectively quantified placental EV no larger than 160nm. However, the size of placental EV from the previous studies varies from 50nm to 200nm[22,46] as detected by NTA (Table 5). Thirdly, the antibodies for placental EV quantification differ between studies. For other studies, the placental EV were quantified using anti-PLAP as the first antibody for ELISA[22,23,35,46]. While in my study, two pairs of antibodies, namely anti-CD63 and anti-PLAP were used to define not only their placental origin but also the expression of tetraspanins (Table 5). These more stringent EV quantification methods in my study may explain the difference between mine and other studies.

Study	Isolation Method	Particle Size	Quantification Method	Finding
Salomon et al[46]	Density Gradient Ultracentrifugation	50-200nm (NTA)	Anti-PLAP ELISA	Placental particles increase across gestation
Sarker et al[22]	Density Gradient Ultracentrifugation	98 ± 39nm (NTA)	Anti-PLAP ELISA	Placental particles increase from 6-12 weeks
Germain et al[23]	Ultracentrifugation	NM	Anti-PLAP ELISA	Placental particles increase across gestation
Goswami et al[35]	Ultracentrifugation	NM	Anti-PLAP ELISA	Placental particles increase across gestation

Table 5. Studies performed quantitative analysis of placental particles in maternal plasma from indicated gestational ages. NM indicated not mentioned.

I found the counts of CD10-PLAP psEV was significantly elevated in WWD-EOPE compared to NP serum from the first trimester (Figure 10A). CD10, also known as neprilysin, is a zinc metalloendopeptidase which is a pleiotropic inhibitor of several bioactive vasopeptides[48]. Pharmacological inhibition of CD10 has been proven to be an effective treatment in hypertension, which is a hallmark of preeclampsia[49]. Our group has previously shown higher CD10 activity in sEV released by preeclamptic placentas [38]. My current study thus far extended our previous observation and suggests CD10 may be involved in the development of EOPE many weeks before the onset of clinical features of disease. CD10 has been shown to have anti-angiogenic ability. I proposed that elevated CD10-PLAP psEV in EOPE plasma and serum, together with other well-known anti-angiogenic proteins including soluble fms-like tyrosine kinase (sFlt-1) and soluble endoglin (sEng); both of which appear much later in pregnancy, could play a role in maternal endothelial dysfunction seen in EOPE[50,51].

Using the uterine vein and paired peripheral vein samples, I have confirmed CD63-PLAP psEV were higher in uterine vein compared to peripheral blood (Figure 8A). This is consistent with other studies that PLAP-positive EV were higher in UV compared to PB [39,52]. However, the counts of CD10-PLAP and CD10-CD63 psEV didn't exhibit gradient differences (Figure 8A). This is possibly due to cells other than placental syncytial trophoblasts also contribute to CD10-positive sEV. Apart from placenta, CD10 has a variety of origins such as heart, kidney, lung, brain and adipose tissue [53-57]. The possible confounding of CD10-positive sEV from other tissues releasing into the blood might explain a lack of gradient difference observed here. Indeed, CD10-CD63 sEV were also identified in the plasma of non-pregnant women by ExoCounter (Figure 7D), supporting the presence of a high level of CD10-CD63 sEV in plasma samples from other tissues.

ExoCounter possesses several unique features which means it outperforms existing technologies in circulating placental EV quantification. First, it requires minimal sample processing. Other quantification methods which allow the interrogation of EV markers, such as fluorescence NTA and flow cytometry, are highly dependent on complicated sample processing. For example, the BD Influx flow cytometry can interrogate sEV subsets with fluorescent labelling, however, density gradient ultracentrifugation is recommended to separate the unbound dye during sample processing[58]. Fluorescence NTA showed high background signals with unprocessed samples, suggesting many non-EV particles were detected[59]. Complicated sample processing not only increases time required from processing samples to acquiring results, it is also likely to introduce procedure-operator-dependent biases. Secondly, the ExoCounter combines size exclusion with immunophenotyping, removing key confounders of each technique alone. For example, size exclusion approaches co-isolate chylomicrons and lipoproteins, which far outnumber psEV in plasma[60]. Conversely, immunophenotyping is hampered by co-isolation of protein targets which are not expressed on EV, such as soluble proteins and cell fragments. Thirdly the ExoCounter can interrogate two markers simultaneously, allowing us to combine markers of vesicles, tissue origin and disease, dramatically improving the richness of information. Fourthly the semi-automated setup of the ExoCounter reduces operator errors resulting in highly reproducible results (Figure 4B & 3C). Finally, the ExoCounter works with very small sample volumes, making it highly attractive for use in clinical practice and opening the possibility of simple sample acquisition (e.g. capillary blood sampling), which widens its applicability whilst reducing the cost of diagnostic sampling. The ExoCounter is a strong candidate for application in larger clinical studies.

In conclusion, this study demonstrated ExoCounter is a novel platform which permits quantitative (counts) and qualitative (two antigens) sEV analysis in minimally processed biological fluids. Distinct psEV profiles were detected by ExoCounter in early gestation (≤12 weeks) in WWD-EOPE compared to NP and WWD-LOPE. My results call for large-scale clinical study since the application of this assay might improve EOPE early diagnosis, patients risk stratification and early intervention.

2.7 Reference

1. van Niel G, D'Angelo G, Raposo G. Shedding light on the cell biology of extracellular vesicles. *Nat Rev Mol Cell Biol*. 2018;19:213-228. doi: 10.1038/nrm.2017.125
2. Muraoka S, Jedrychowski MP, Yanamandra K, Ikezu S, Gygi SP, Ikezu T. Proteomic Profiling of Extracellular Vesicles Derived from Cerebrospinal Fluid of Alzheimer's Disease Patients: A Pilot Study. *Cells*. 2020;9. doi: 10.3390/cells9091959
3. Guan F, Xiang X, Xie Y, Li H, Zhang W, Shu Y, Wang J, Qin W. Simultaneous metabolomics and proteomics analysis of plasma-derived extracellular vesicles. *Anal Methods*. 2021;13:1930-1938. doi: 10.1039/d1ay00060h
4. Erdbrügger U, Blijdorp CJ, Bijnsdorp IV, Borràs FE, Burger D, Bussolati B, Byrd JB, Clayton A, Dear JW, Falcón-Pérez JM, et al. Urinary extracellular vesicles: A position paper by the Urine Task Force of the International Society for Extracellular Vesicles. *J Extracell Vesicles*. 2021;10:e12093. doi: 10.1002/jev2.12093
5. Nakashiki S, Miuma S, Mishima H, Masumoto H, Hidaka M, Soyama A, Kanda Y, Fukushima M, Haraguchi M, Sasaki R, et al. Bile extracellular vesicles from end-stage liver disease patients show altered microRNA content. *Hepatol Int*. 2021;15:821-830. doi: 10.1007/s12072-021-10196-5
6. Han P, Bartold PM, Ivanovski S. The emerging role of small extracellular vesicles in saliva and gingival crevicular fluid as diagnostics for periodontitis. *J Periodontal Res*. 2022;57:219-231. doi: 10.1111/jre.12950
7. Hu Y, Thaler J, Nieuwland R. Extracellular Vesicles in Human Milk. *Pharmaceuticals (Basel)*. 2021;14. doi: 10.3390/ph14101050
8. Kaddour H, Panzner TD, Welch JL, Shouman N, Mohan M, Stapleton JT, Okeoma CM. Electrostatic Surface Properties of Blood and Semen Extracellular Vesicles: Implications of Sialylation and HIV-Induced Changes on EV Internalization. *Viruses*. 2020;12. doi: 10.3390/v12101117
9. Sharma P, Mesci P, Carromeu C, McClatchy DR, Schiapparelli L, Yates JR, 3rd, Muotri AR, Cline HT. Exosomes regulate neurogenesis and circuit assembly. *Proc Natl Acad Sci U S A*. 2019;116:16086-16094. doi: 10.1073/pnas.1902513116
10. Komaki M, Numata Y, Morioka C, Honda I, Tooi M, Yokoyama N, Ayame H, Iwasaki K, Taki A, Oshima N, et al. Exosomes of human placenta-derived mesenchymal stem cells stimulate angiogenesis. *Stem Cell Res Ther*. 2017;8:219. doi: 10.1186/s13287-017-0660-9
11. Raposo G, Nijman HW, Stoorvogel W, Liejendekker R, Harding CV, Melief CJ, Geuze HJ. B lymphocytes secrete antigen-presenting vesicles. *J Exp Med*. 1996;183:1161-1172. doi: 10.1084/jem.183.3.1161
12. Welker MW, Reichert D, Susser S, Sarrazin C, Martinez Y, Herrmann E, Zeuzem S, Piiper A, Kronenberger B. Soluble serum CD81 is elevated in patients with chronic hepatitis C and correlates with alanine aminotransferase serum activity. *PLoS One*. 2012;7:e30796. doi: 10.1371/journal.pone.0030796
13. Khan S, Jutzy JMS, Valenzuela MMA, Turay D, Aspe JR, Ashok A, Mirshahidi S, Mercola D, Lilly MB, Wall NR. Plasma-derived exosomal survivin, a plausible biomarker for early detection of prostate cancer. *PloS one*. 2012;7:e46737-e46737. doi: 10.1371/journal.pone.0046737

14. Li J, Sherman-Baust CA, Tsai-Turton M, Bristow RE, Roden RB, Morin PJ. Claudin-containing exosomes in the peripheral circulation of women with ovarian cancer. *BMC Cancer*. 2009;9:244-244. doi: 10.1186/1471-2407-9-244
15. Hill AF. Extracellular Vesicles and Neurodegenerative Diseases. *J Neurosci*. 2019;39:9269-9273. doi: 10.1523/jneurosci.0147-18.2019
16. Zhou H, Pisitkun T, Aponte A, Yuen PS, Hoffert JD, Yasuda H, Hu X, Chawla L, Shen RF, Knepper MA, et al. Exosomal Fetuin-A identified by proteomics: a novel urinary biomarker for detecting acute kidney injury. *Kidney Int*. 2006;70:1847-1857. doi: 10.1038/sj.ki.5001874
17. Zhou H, Cheruvanky A, Hu X, Matsumoto T, Hiramatsu N, Cho ME, Berger A, Leelahavanichkul A, Doi K, Chawla LS, et al. Urinary exosomal transcription factors, a new class of biomarkers for renal disease. *Kidney Int*. 2008;74:613-621. doi: 10.1038/ki.2008.206
18. Gurung S, Perocheau D, Touramanidou L, Baruteau J. The exosome journey: from biogenesis to uptake and intracellular signalling. *Cell Commun Signal*. 2021;19:47. doi: 10.1186/s12964-021-00730-1
19. Théry C, Witwer KW, Aikawa E, Alcaraz MJ, Anderson JD, Andriantsitohaina R, Antoniou A, Arab T, Archer F, Atkin-Smith GK, et al. Minimal information for studies of extracellular vesicles 2018 (MISEV2018): a position statement of the International Society for Extracellular Vesicles and update of the MISEV2014 guidelines. *J Extracell Vesicles*. 2018;7:1535750. doi: 10.1080/20013078.2018.1535750
20. Burton GJ, Jauniaux E. What is the placenta? *Am J Obstet Gynecol*. 2015;213:S6.e1, S6-8. doi: 10.1016/j.ajog.2015.07.050
21. Awoyemi T, Cerdeira AS, Zhang W, Jiang S, Rahbar M, Logenthiran P, Redman C, Vatish M. Preeclampsia and syncytiotrophoblast membrane extracellular vesicles (STB-EVs). *Clin Sci (Lond)*. 2022;136:1793-1807. doi: 10.1042/cs20220149
22. Sarker S, Scholz-Romero K, Perez A, Illanes SE, Mitchell MD, Rice GE, Salomon C. Placenta-derived exosomes continuously increase in maternal circulation over the first trimester of pregnancy. *Journal of Translational Medicine*. 2014;12:204. doi: 10.1186/1479-5876-12-204
23. Germain SJ, Sacks GP, Soorana SR, Sargent IL, Redman CW. Systemic Inflammatory Priming in Normal Pregnancy and Preeclampsia: The Role of Circulating Syncytiotrophoblast Microparticles. *The Journal of Immunology*. 2007;178:5949. doi: 10.4049/jimmunol.178.9.5949
24. Tersigni C, Furqan Bari M, Cai S, Zhang W, Kandzija N, Buchan A, Miranda F, Di Simone N, Redman CW, Bastie C, et al. Syncytiotrophoblast-derived extracellular vesicles carry apolipoprotein-E and affect lipid synthesis of liver cells in vitro. *J Cell Mol Med*. 2022;26:123-132. doi: 10.1111/jcmm.17056
25. Cronqvist T, Erlandsson L, Tannetta D, Hansson SR. Placental syncytiotrophoblast extracellular vesicles enter primary endothelial cells through clathrin-mediated endocytosis. *Placenta*. 2020;100:133-141. doi: 10.1016/j.placenta.2020.07.006
26. Göhner C, Plösch T, Faas MM. Immune-modulatory effects of syncytiotrophoblast extracellular vesicles in pregnancy and preeclampsia. *Placenta*. 2017;60 Suppl 1:S41-s51. doi: 10.1016/j.placenta.2017.06.004
27. Mol BWJ, Roberts CT, Thangaratinam S, Magee LA, de Groot CJM, Hofmeyr GJ. Pre-eclampsia. *Lancet*. 2016;387:999-1011. doi: 10.1016/s0140-6736(15)00070-7
28. Fox R, Kitt J, Leeson P, Aye CYL, Lewandowski AJ. Preeclampsia: Risk Factors, Diagnosis, Management, and the Cardiovascular Impact on the Offspring. *J Clin Med*. 2019;8. doi: 10.3390/jcm8101625

29. Lisonkova S, Joseph KS. Incidence of preeclampsia: risk factors and outcomes associated with early- versus late-onset disease. *Am J Obstet Gynecol*. 2013;209:544.e541-544.e512. doi: 10.1016/j.ajog.2013.08.019
30. Burton GJ, Redman CW, Roberts JM, Moffett A. Pre-eclampsia: pathophysiology and clinical implications. *Bmj*. 2019;366:l2381. doi: 10.1136/bmj.l2381
31. Poon LC, Shennan A, Hyett JA, Kapur A, Hadar E, Divakar H, McAuliffe F, da Silva Costa F, von Dadelszen P, McIntyre HD, et al. The International Federation of Gynecology and Obstetrics (FIGO) initiative on pre-eclampsia: A pragmatic guide for first-trimester screening and prevention. *Int J Gynaecol Obstet*. 2019;145 Suppl 1:1-33. doi: 10.1002/ijgo.12802
32. Hypertension in pregnancy: diagnosis and management. In: National Institute for Health and Care Excellence (NICE); 2019.
33. Salomon C, Guanzon D, Scholz-Romero K, Longo S, Correa P, Illanes SE, Rice GE. Placental Exosomes as Early Biomarker of Preeclampsia: Potential Role of Exosomal MicroRNAs Across Gestation. *J Clin Endocrinol Metab*. 2017;102:3182-3194. doi: 10.1210/jc.2017-00672
34. Pillay P, Maharaj N, Moodley J, Mackraj I. Placental exosomes and pre-eclampsia: Maternal circulating levels in normal pregnancies and, early and late onset pre-eclamptic pregnancies. *Placenta*. 2016;46:18-25. doi: 10.1016/j.placenta.2016.08.078
35. Goswami D, Tannetta DS, Magee LA, Fuchisawa A, Redman CW, Sargent IL, von Dadelszen P. Excess syncytiotrophoblast microparticle shedding is a feature of early-onset pre-eclampsia, but not normotensive intrauterine growth restriction. *Placenta*. 2006;27:56-61. doi: 10.1016/j.placenta.2004.11.007
36. Sammar M, Dragovic R, Meiri H, Vatish M, Sharabi-Nov A, Sargent I, Redman C, Tannetta D. Reduced placental protein 13 (PP13) in placental derived syncytiotrophoblast extracellular vesicles in preeclampsia - A novel tool to study the impaired cargo transmission of the placenta to the maternal organs. *Placenta*. 2018;66:17-25. doi: 10.1016/j.placenta.2018.04.013
37. Awoyemi T, Tannetta D, Zhang W, Kandzija N, Motta-Mejia C, Fischer R, Heilig R, Raiss S, Redman C, Vatish M. Glycosylated Siglec-6 expression in syncytiotrophoblast-derived extracellular vesicles from preeclampsia placentas. *Biochem Biophys Res Commun*. 2020;533:838-844. doi: 10.1016/j.bbrc.2020.09.081
38. Gill M, Motta-Mejia C, Kandzija N, Cooke W, Zhang W, Cerdeira AS, Bastie C, Redman C, Vatish M. Placental Syncytiotrophoblast-Derived Extracellular Vesicles Carry Active NEP (Neprilysin) and Are Increased in Preeclampsia. *Hypertension*. 2019;73:1112-1119. doi: 10.1161/hypertensionaha.119.12707
39. Motta-Mejia C, Kandzija N, Zhang W, Mhlomi V, Cerdeira AS, Burdujan A, Tannetta D, Dragovic R, Sargent IL, Redman CW, et al. Placental Vesicles Carry Active Endothelial Nitric Oxide Synthase and Their Activity is Reduced in Preeclampsia. *Hypertension*. 2017;70:372-381. doi: 10.1161/hypertensionaha.117.09321
40. Kabe Y, Suematsu M, Sakamoto S, Hirai M, Koike I, Hishiki T, Matsuda A, Hasegawa Y, Tsujita K, Ono M, et al. Development of a Highly Sensitive Device for Counting the Number of Disease-Specific Exosomes in Human Sera. *Clin Chem*. 2018;64:1463-1473. doi: 10.1373/clinchem.2018.291963
41. Dragovic RA, Collett GP, Hole P, Ferguson DJ, Redman CW, Sargent IL, Tannetta DS. Isolation of syncytiotrophoblast microvesicles and exosomes and their characterisation by multicolour flow cytometry and fluorescence Nanoparticle Tracking Analysis. *Methods*. 2015;87:64-74. doi: 10.1016/j.ymeth.2015.03.028

42. World Health Organization. ICD-10 revision. https://icd.who.int/browse10/2016/en#/O14.1.
43. Kabe Y, Sakamoto S, Hatakeyama M, Yamaguchi Y, Suematsu M, Itonaga M, Handa H. Application of high-performance magnetic nanobeads to biological sensing devices. *Anal Bioanal Chem*. 2019;411:1825-1837. doi: 10.1007/s00216-018-1548-y
44. Kenna JG, Major GN, Williams RS. Methods for reducing non-specific antibody binding in enzyme-linked immunosorbent assays. *J Immunol Methods*. 1985;85:409-419. doi: 10.1016/0022-1759(85)90150-4
45. Chen Y, Huang Y, Jiang R, Teng Y. Syncytiotrophoblast-derived microparticle shedding in early-onset and late-onset severe pre-eclampsia. *Int J Gynaecol Obstet*. 2012;119:234-238. doi: 10.1016/j.ijgo.2012.07.010
46. Salomon C, Torres MJ, Kobayashi M, Scholz-Romero K, Sobrevia L, Dobierzewska A, Illanes SE, Mitchell MD, Rice GE. A gestational profile of placental exosomes in maternal plasma and their effects on endothelial cell migration. *PLoS One*. 2014;9:e98667. doi: 10.1371/journal.pone.0098667
47. Baranyai T, Herczeg K, Onódi Z, Voszka I, Módos K, Marton N, Nagy G, Mäger I, Wood MJ, El Andaloussi S, et al. Isolation of Exosomes from Blood Plasma: Qualitative and Quantitative Comparison of Ultracentrifugation and Size Exclusion Chromatography Methods. *PLoS One*. 2015;10:e0145686. doi: 10.1371/journal.pone.0145686
48. Nalivaeva NN, Zhuravin IA, Turner AJ. Neprilysin expression and functions in development, ageing and disease. *Mech Ageing Dev*. 2020;192:111363. doi: 10.1016/j.mad.2020.111363
49. Yamamoto K, Rakugi H. Angiotensin receptor-neprilysin inhibitors: Comprehensive review and implications in hypertension treatment. *Hypertens Res*. 2021;44:1239-1250. doi: 10.1038/s41440-021-00706-1
50. Goodman OB, Jr., Febbraio M, Simantov R, Zheng R, Shen R, Silverstein RL, Nanus DM. Neprilysin inhibits angiogenesis via proteolysis of fibroblast growth factor-2. *J Biol Chem*. 2006;281:33597-33605. doi: 10.1074/jbc.M602490200
51. Carrasco-Wong I, Aguilera-Olguín M, Escalona-Rivano R, Chiarello DI, Barragán-Zúñiga LJ, Sosa-Macías M, Galaviz-Hernandez C, San Martín S, Gutiérrez J. Syncytiotrophoblast stress in early onset preeclampsia: The issues perpetuating the syndrome. *Placenta*. 2021;113:57-66. doi: 10.1016/j.placenta.2021.05.002
52. Knight M, Redman CW, Linton EA, Sargent IL. Shedding of syncytiotrophoblast microvilli into the maternal circulation in pre-eclamptic pregnancies. *Br J Obstet Gynaecol*. 1998;105:632-640. doi: 10.1111/j.1471-0528.1998.tb10178.x
53. Katsuda T, Oki K, Ochiya T. Potential application of extracellular vesicles of human adipose tissue-derived mesenchymal stem cells in Alzheimer's disease therapeutics. *Methods Mol Biol*. 2015;1212:171-181. doi: 10.1007/7651_2014_98
54. Fielitz J, Dendorfer A, Pregla R, Ehler E, Zurbrügg HR, Bartunek J, Hetzer R, Regitz-Zagrosek V. Neutral endopeptidase is activated in cardiomyocytes in human aortic valve stenosis and heart failure. *Circulation*. 2002;105:286-289. doi: 10.1161/hc0302.103593
55. Kaltenecker CC, Domenig O, Kopecky C, Antlanger M, Poglitsch M, Berlakovich G, Kain R, Stegbauer J, Rahman M, Hellinger R, et al. Critical Role of Neprilysin in Kidney Angiotensin Metabolism. *Circ Res*. 2020;127:593-606. doi: 10.1161/circresaha.119.316151
56. Carpenter TC, Stenmark KR. Hypoxia decreases lung neprilysin expression and increases pulmonary vascular leak. *Am J Physiol Lung Cell Mol Physiol*. 2001;281:L941-948. doi: 10.1152/ajplung.2001.281.4.L941

57. Yasojima K, McGeer EG, McGeer PL. Relationship between beta amyloid peptide generating molecules and neprilysin in Alzheimer disease and normal brain. *Brain Res*. 2001;919:115-121. doi: 10.1016/s0006-8993(01)03008-6
58. Nolte-'t Hoen EN, van der Vlist EJ, Aalberts M, Mertens HC, Bosch BJ, Bartelink W, Mastrobattista E, van Gaal EV, Stoorvogel W, Arkesteijn GJ, et al. Quantitative and qualitative flow cytometric analysis of nanosized cell-derived membrane vesicles. *Nanomedicine*. 2012;8:712-720. doi: 10.1016/j.nano.2011.09.006
59. Fortunato D, Mladenović D, Criscuoli M, Loria F, Veiman KL, Zocco D, Koort K, Zarovni N. Opportunities and Pitfalls of Fluorescent Labeling Methodologies for Extracellular Vesicle Profiling on High-Resolution Single-Particle Platforms. *Int J Mol Sci*. 2021;22. doi: 10.3390/ijms221910510
60. Johnsen KB, Gudbergsson JM, Andresen TL, Simonsen JB. What is the blood concentration of extracellular vesicles? Implications for the use of extracellular vesicles as blood-borne biomarkers of cancer. *Biochim Biophys Acta Rev Cancer*. 2019;1871:109-116. doi: 10.1016/j.bbcan.2018.11.006

Chapter 3

The functional studies of human podocytes treated with normal and preeclamptic small placental extracellular vesicles

Table of Contents

3.1 Abstract....129

3.2 Introduction....131

3.3 Aims....133

3.4 Methods....133

3.4.1 Human Subjects and Ethic Approval....133

3.4.2 Placenta perfusion and psEV isolation & characterisation....134

3.4.3 Western Blot....134

3.4.4 Podocyte Culture and Differentiation....134

3.4.5 PKH26 staining of psEV and time course assessment of internalisation of EV by podocyte via flow cytometry and confocal microscopy....135

3.4.6 F-actin staining....137

3.4.7 Podocyte Migration assay....137

3.4.8 Podocyte Adhesion assay....138

3.4.9 Podocyte Viability Assay....138

3.4.10 Podocyte RNA Extraction and quantitative polymerase chain reaction (qPCR)....139

3.4.11 ExoCounter....139

3.4.12 Isolation of Urine EV and Removal of Uromodulin....140

3.4.13 Isolation of red blood cell (RBC) EV by differential ultracentrifugation (UC)....142

3.4.14 Statistical Analysis....143

3.5 Results....144

3.5.1 NaCl is the better method to remove uromodulin in urine....144

3.5.2 The presence of psEV in urine from both NP and PE....146

3.5.3 Podocyte Differentiation....148

3.5.4 RBC sEV characterisation as control for the experiment....150

3.5.5 psEV internalisation by podocytes....151

3.5.6 The influence of psEV on podocytes upon internalisation....155

3.5.7 The mechanism of psEV influence podocytes migration and adhesion ability....157

3.6 Discussion & Future work....160

3.7 Reference....164

3.1 Abstract

Background: Circulating levels of placental extracellular vesicle (pEV) increase throughout gestation in normal pregnant (NP) women, and their levels are higher in preeclampsia (PE). Proteinuria is a common symptom in PE patients whose glomerular filtration barriers (GFB) have been damaged. I aim to detect the influence of placental small EV (psEV) from NP and PE on podocytes, a specialized renal cell that are involved in GFB maintenance.

Methods: NP (n=3) and PE (n = 3) psEV were isolated by dual-lobe placental perfusion and differential ultracentrifugation. psEV were characterised by western blot, nanoparticle tracking analysis (NTA) and transmission electron microscopy (TEM). In order to test if sEV could pass through the glomerular filtration barrier and interact with podocytes, urine sEV were isolated by ultracentrifugation and characterized by western blot, NTA and TEM. The presence of PLAP on urine sEV was confirmed via western blot and ExoCounter. The internalization of psEV by podocytes was assessed by flow cytometry, confocal microscopy and qPCR. Lastly, the effect of psEV from NP and PE on podocyte migration, cell viability, and adhesion capabilities were assessed.

Results: The presence of psEV in the urine were confirmed by western blot and ExoCounter assay. The internalization of psEV from NP and PE by podocytes, assessed by flow cytometry, showed a time and dose dependent manner. There was no significant difference in the number of psEV from NP and PE internalized by podocytes. psEV could transfer placenta-specific C19 miRNA cluster (miR-517a, miR-517c and miR-518b) into podocytes, and the level was higher in PE compared to NP. After the NP psEV treatment, the nephrin expression of podocytes was increased by 1.9-fold ($p<0.05$) and podocyte migration ability was upregulated by 1.2-fold compared to control ($p<0.05$). F-actin staining was enhanced

across the podocytes after NP psEV treatment. In contrast, PE psEV treatment showed no change in nephrin expression or podocyte migration ability compared to control. Additionally, podocyte adhesion ability was impaired, and F-actin appeared stressed (cortical ring formation) after PE psEV treatment.

Conclusion: The results here speculated the functions of NP psEV on podocyte might be enhancing nephrin expression and upregulating the migration ability to accommodate the higher filtration rate seen in pregnancy, while PE psEV may facilitate the reduced adhesion ability which might be contribute to the shedding of podocytes into the urine seen in PE.

3.2 Introduction

In normal pregnancy, a physiological increase in urine protein excretion is expected and significant protein excretion is defined as ≥ 300 mg per 24h[1,2]. This increased protein excretion is due to a 50% increased glomerular filtration rate (GFR) resulting from 30% - 80 % increase in blood volume passing glomerular and an altered tubular reabsorption[3,4]. In PE, a one-third reduction in GRF can be observed compared to NP controls[5], and proteinuria is often observed which indicates the injury of renal system is almost always involved[6,7]. However, the mechanism of the presence of proteinuria remains unclear. In kidney, glomerular filtration barrier (GFB) is responsible for preventing proteins leaking into urine[8]. GFB consists of three components including the fenestrated endothelial cells, podocytes, and a layer of basement membrane sandwiched between these two types of cells [8]. The basement membrane consisted of mixed glycoproteins secreted by both fenestrated endothelial cells and podocytes. Together they maintain the integrity and deliver the function of GFB. Detached and shed podocytes into urine, podocyturia, has been shown in PE and the increasing level of podocyturia is associated with the increasing level of proteinuria[9]. The barrier functions between podocytes are also impaired after treating the serum from PE patients and the effect can be reversed by vascular endothelial growth factor (VEGF)[10]. This suggests that PE is associated with both the loss and functional impairment of podocytes.

Throughout normal pregnancy, the level of pEV increases with the ongoing pregnancy which yields the highest number in the third trimester[11]. In PE, pEV increases compared to normal pregnancy and it is thought to be characteristic of PE since such an increase was not found in other placenta-related diseases, such as fetal growth restriction (FGR)[12]. The elevated pEV in PE has the ability to interact with different types of cells, such as endothelial cells[13], immune

cells[14,15] and hepatocytes[16], and induce functional changes. These changes may lead to disrupted immunoregulation[17], angiogenesis[18], signal transduction[19] and cell movement[20]. However, considering the high filtration rate of the kidney in pregnancy, how pEV influence glomerular filtration barrier, especially podocytes, remain unknown.

While the journey of EV from the bloodstream to podocytes involves crossing the GFB, several evidence suggests it can occur in vivo. First, after injecting fluorescence labelled EV into the circulation of a rat model, EV can be subsequently detected in the urine[21]. This suggests that podocytes, as part of the filtration process, might come into contact with EV. Though the exact mechanisms are understudied. Notably, for pEV, the fluorescence-labelled placenta EV can be detected in kidney tissues which implicate podocytes could potentially interact with circulating placenta EV[22]. It is also possible that the placental EV can be translocated by glomerular endothelial cells into the podocytes. This is supported by the evidence that when endocytosis takes place in endothelial cells, the cargo may undergo transcytosis across the endothelial cell to the underlying tissue[23]. However, given the complexity of the mechanisms dictating how molecules traverse the GFB – involving a dynamic interplay among glomerular endothelial cells, the basement membrane, and podocytes – further research is needed to elucidate the precise route EVs take through the GFB. This might enable small EV to pass through. In the pathological condition, the filtration slits of podocytes may widen, potentially allowing even larger EV to pass through[24]. Placenta EV has a variety range of size and certain placenta EV might be capable of traversing the GFB and entering the urine.

My hypothesis for this study was that placenta small sEV (psEV) could encounter podocytes and induce functional changes in podocytes. To investigate this, I have the following aims for this chapter.

3.3 Aims

The aims of this chapter are to:

1. Investigate the presence of psEV in the PE and NP urine samples to support the psEV passing through the GMB and encountering podocytes
2. Investigate the internalisation process of psEV by human differentiated podocytes.
3. Investigate the functional changes and the mechanism of podocytes caused by psEV from normal pregnancy and preeclamptic pregnancy.

3.4 Methods

3.4.1 Human Subjects and Ethic Approval

Our group obtained ethical approval from the Central Oxfordshire Research Ethics Committee C (REFS 07/H0607/74 & 07/H0606/148). I prospectively selected pregnant women undergoing elective caesarean sections before labour onset, from the maternity ward at the Women's Centre, John Radcliffe Hospital, Oxford. The research midwives obtained written informed consent before placenta collection from all participants. The placentas were subsequently collected from average (NP) and preeclamptic (PE) and perfused within 10 to 20 minutes of delivery. The normal pregnancy (NP) was defined as a singleton pregnancy with no history of preeclampsia, hypertensive disorders, or other complications in pregnancy. Patients with preeclampsia were defined as the co-occurrence of *de novo* hypertension (blood pressure >140/90 mmHg) and proteinuria (>300 mg/day) after week 20 of gestation

according to the criteria of the International Society for the Study of Hypertension in Pregnancy.

3.4.2 Placenta perfusion and psEV isolation & characterisation

The detailed placenta perfusion, psEV isolation by differential ultracentrifuge, psEV characterisation by western blot, nanoparticle tracking analysis (NTA) and transmission electron microscopy (TEM) can be found in Chapter 2.

3.4.3 Western Blot

Podocyte lysates were made using RIPA buffer (ThermoFisher, 89901) and the protein concentrations were determined using Bicinchoninic acid (BCA) assay (ThermoFisher, 23227). In brief, 20 μg of podocyte lysates were mixed with 4X Laemmli buffer with 5% β-Mercaptoethanol and diluted to 20 μL with distilled water. The sample mix was heated at 70°C for 10 mins before being loaded in 4%-12% SDS-PAGE 10 well gel (ThermoFisher, NP0321BOX) for electrophoresis and for transferring onto PVDF membranes (Bio-Rad, 1620177) afterwards. The membranes were then blocked for 1h in 5% skim milk in Tris-Buffered Saline with 0.1% Tween-20 (TBS-T, ThermoFisher) before incubated with the first antibody overnight at 4 °C. After further incubated with appropriate secondary antibody, enhanced chemiluminescence (ECL) (Thermo Fisher, 32106) was used and developed using a chemiluminescence film (Hyperfilm ECL, Merck, GE28-9068-35) in the dark room. The first antibodies used were nephrin (Abcam, ab58968), synaptopodin (Santa Cruz, sc-50459), podocin (Sigma, P0372), and WT-1 (Wilms' tumour 1, Santa Cruz, sc-393498).

3.4.4 Podocyte Culture and Differentiation

Immortalised human podocytes (gift from Prof. Saleem at University of Bristol) were cultured at 33°C in RPMI-1640 culture medium (Lonza LZBE12-702F) supplemented with

2% insulin-transferrin-selenium (Invitrogen 41400045), 10% fetal bovine serum (Sigma F7524) and 10 mL/L Penicillin-streptomycin (Sigma P4333) for growing and passaging. For differentiation, the immortalised podocytes were transferred to 37°C for 10 days until fully differentiated and the cells were ready for the experiments. To confirm podocyte differentiation, several key elements were examined: 1) podocytes' cell size becomes enlarged with the formation of digit-like foot process; 2) expression of podocytes differentiation markers including nephrin and synaptopodin should have increased; 3) expression of podocyte undifferentiation marker WT-1 should have reduced in differentiated status compared to non-differentiated status. The expression of the aforementioned markers was assessed by western blot.

3.4.5 PKH26 staining of psEV and time course assessment of internalisation of EV by podocyte via flow cytometry and confocal microscopy

psEV from NP and PE, and RBC-sEV were stained with PKH26 staining (Sigma, PKH26GL) according to the manufacturer's protocol. In brief, 200 μg sEV samples were diluted with diluent C till 1mL and incubated with 6 μL of PHK26 dye for 5mins at room temperature, which was followed by adding 2 mL of 10% BSA for quenching and topping the solution up with serum-free media. A 0.971M sucrose solution (Sigma, S1888) was added to the bottom of the ultracentrifuge tube before the sEV solution was transferred. The solution was centrifuged at 190,000g for 2hs at 4°C. The PKH26 stained small EV pellet was resuspended in 5ml of fPBS and transferred to Amicon 100kDa filter column (Sigma, UFC8100) and spun at 3,000g for 40mins to reduce the volume to 0.5ml. The stained sEV were aliquoted and frozen at -80 °C until further analysis.

Podocytes were transferred to 37 °C for 10 days to allow complete differentiation. The cell culture medium was changed every other day. Then podocytes were trypsinised and seeded at 0.2 x 10^6 cells/well on a 12-well plate. 20 μg/mL of sEV (determined by BCA assay) isolated from NP and PE placenta and RBCs were added to each well and incubated with podocytes for 2h, 4h and 6h. Podocytes were then washed with fPBS with 40 units/mL heparin (to wash away sEV bound to the outside of cells[25]) 3 times and detached by trypsin. After centrifugation at 1,300 rpm for 3mins, the cell pellet was washed with fPBS. The cell pellet was resuspended in 300 μL fPBS and half of it was analysed by flow cytometry (BD LSRII). CS&T beads (BD Biosciences) were used to calibrate the machine every time. An application setting was generated and applied for sample analysis.

The other half of the podocytes were applied on Cytospin (Shandon Cytospin 2). Podocytes were attached on slides (Fisherbrand Superfrost Plus Microscope Slides) after centrifugation at 800 rpm for 3mins. The podocytes were then fixed with 100 μL 4% paraformaldehyde (PFA, Alfa Aesar, J61899) for 20mins and washed with fPBS. After 30 mins blocking in blocking buffer (1% BSA and 0.3% triton-100 in fPBS), 100μL of anti-nephrin (1:50 dilution) (primary antibody) were applied to podocytes for 1h at room temperature. After washing with fPBS, the podocytes were incubated with anti-rabbit Alexa Fluor 488 (the secondary antibody, ThermoFisher, A21206, 1:100 dilution) for 1h, which was followed by fPBS wash again. Then, 7μL mounting medium with DAPI (Abcam, ab104139) was applied to the podocytes and covered by a coverslip and sealed with nail varnish. Podocytes were then visualised by confocal microscopy (PerkinElmer UltraVIEW spinning disc system), and images were captured and processed in Volocity acquisition software (Quorum Technologies).

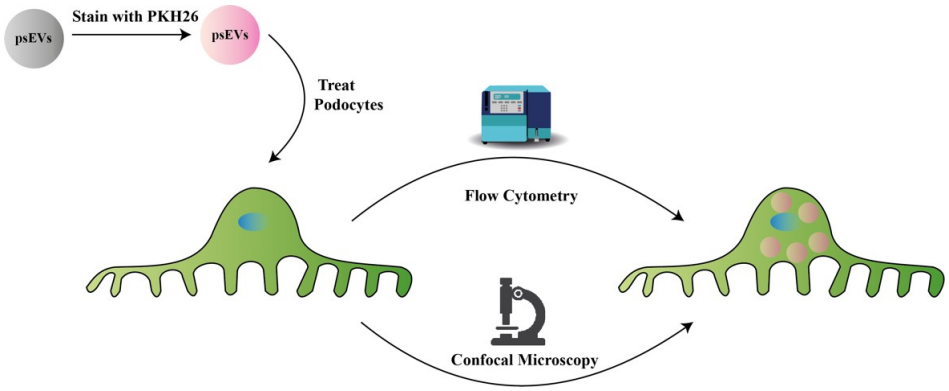


Figure 1. The illustration of the experimental methods to confirm the internalisation of psEV by human podocytes.

3.4.6 F-actin staining

Fully differentiated podocytes were trypsinised and seeded onto cell culture µ-Dish (ibidi, 81158). After settling overnight, fresh culture medium was added and podocytes were treated with either 20 µg/mL NP psEV or 20 µg/mL PE psEV for 6hs. Experimental controls include podocytes treated with fPBS or 20 µg/mL RBC-sEV. Treatment was stopped by removing the cell culture medium and washing with fPBS with 40 units/mL heparin 3 times. The cells were fixed with 100 µL 4% PFA for 20mins. After a wash in PBS to remove paraformaldehyde, blocking buffer (1% BSA and 0.3% triton-100 in fPBS) was added for 30mins, and this was followed by incubation with Phalloidin-iFluor 488 (ab176753) for 1h. Finally, mounting medium with DAPI (Abcam, ab104139) was added before visualisation on confocal microscopy.

3.4.7 Podocyte Migration assay

Fully differentiated podocytes were seeded at 2 x 10^4 cells/well on cell culture dish with 2-well insert (ibidi, 81176). After settled overnight, the inserts which are 500 µm in thickness were removed and either fPBS, or 20 µg/mL RBC-sEV, or 20 µg/mL NP psEV or 20 µg/mL

PE psEV were added. The brightfield pictures of the cells were captured with microscope (Olympus CKX53) with a 4x objective lens every 2hs from 0h (start of treatment) till 14h. Image J was used to analyse the results. The area of the gap between the cells was quantified by Image J and a graph showing the area of the gap versus time was created in Microsoft Excel. The gap was reducing slowly at the beginning and then entered a constant speed and finally slowed down again until the gap was fully covered by cells. The constant speed was used to determine the cell migration speed and it was calculated by the slope of the linear region of the migration curve. For data normalisation, the migration rate was divided by two times the length of the gap from the starting point (because the two cell fronts migrate towards each other) to calculate the cell front velocity (µm/hour). Each control and experimental condition were done in triplicates.

3.4.8 Podocyte Adhesion assay

Fully differentiated podocytes were seeded at 2 x 10^4 cells/well on 96 well plate (ThermoFisher, 167008) together with either fPBS, or 20 µg/mL RBC-sEV, or 20 µg/mL NP psEV or 20 µg/mL PE psEV were added to correspondent wells either as controls or experimental conditions. The cells were left for 12hs to adhere, and the non-adherent podocytes were washed away with PBS 2 times. The cells were then fixed with 100µL 4% PFA for 20mins at room temperature and stained with 0.1 % crystal violet (Sigma, C0775) for 1h at room temperature. After washing with distilled water 3 times, the 10% acetic acid solubilization solution (Merk, 100063) was added, and the absorbance was measured at 570nm using a plate reader (FluoStar Optima). Each control and experimental condition were done in triplicates.

3.4.9 Podocyte Viability Assay

CellTier-Glo Luminescent Cell Assay (Promega, G7571) was used for detecting podocyte viability influenced by psEV. This assay can determine the number of viable cells based on

quantitative measurement of ATP. In brief, fully differentiated podocytes were seeded at 2 x 10^4 cells/well on 96 well plate (ThermoFisher, 167008) with either fPBS, or 20 µg/mL RBC-sEV, or 20 µg/mL NP psEV or 20 µg/mL PE psEV were added to the correspondent wells. The experiments were stopped at 1h, 2hs and 6hs by adding 100 µL of the lysis buffer provided by the manufacturer. The luminescent signals were measured by a plate reader (FluoStar Optima). Each control and experimental condition were done in triplicates. The psEV from NP and PE and RBC-sEV were first tested with CellTier-Glo Luminescent Cell assay to check if they contained any ATP that could interfere with the assay.

3.4.10 Podocyte RNA Extraction and quantitative polymerase chain reaction (qPCR)

Fully differentiated podocytes were seeded on a 12-well plate at 0.2 x 10^6 cells/well and allowed for overnight adhesion. Then fresh cell medium was changed, and cells were treated with either fPBS, or 20 µg/mL RBC-sEV, or 20 µg/mL NP psEV or 20 µg/mL PE psEV. Cells were washed with fPBS containing heparin for 3 times at the end of 6hrs incubation. The total RNA of podocytes was extracted with miRNeasy Kits (QIAGEN) according to the manufacturer's protocol. The concentration and 260/280 ratio of RNA were determined by NanoDrop (NanoDrop 1000). The 260/280 of each sample higher than 1.9 was determined as an acceptable sample. For C19MC (mir-517-a, mir-517-c and mir-158b), cDNA from each sample was obtained by the TaqMan™ Advanced miRNA cDNA Synthesis kit (Applied Biosystems, A28007). For U6 (as reference microRNA), cDNA was obtained using TaqMan MicroRNA Reverse Transcription Kit (Applied Biosystems, 4366596). qPCR was done on Quant StudioTM 3 real-time PCR systems (Quant Studio™ Design and analysis software) using MicroAmp™ Optical 96-well reaction plate (N8010560) and optical adhesive film kit

(4313663), and TaqMan™ Gene Expression Assay employing the hydrolysis probe-based technology (Applied Biosystems, USA). The following settings were used: hold 50°C for 2 minutes, hold at 95°C for 20 seconds, followed by forty cycles of 95°C for 1 second and 60°C for 20 seconds. Quantitation cycles (Cq) values were generated automatically by the Quant Studio Design and Analysis desktop software.

3.4.11 ExoCounter

ExoCounter (JVCKENWOOD corp.) can capture and quantify sEV by sandwich immunoassay using disc and secondary antibodies conjugated to nanobeads. This assay allowed us to quantify sEV using a pair of two antibodies. In our current study, CD63 (sEV marker) and PLAP (syncytiotrophoblast marker) were chosen to quantify psEV in urines. Fresh spot urines from NP and PE pregnancies were spun at 1,500g for 10mins at room temperature to remove cells and debris. The urines were aliquoted in 5mL tubes and kept frozen at -80°C. An aliquot of frozen urine was defrosted before being applied to ExoCounter. This ExoCounter assay has five major steps. First, 90µL of anti-CD63 antibody (5µg/mL, Biolegend, 353014) was applied to the disc wells to coat for 1h at 37 °C. Next, 200µL of 0.1% Casein (Thermo Scientific, 37528) in PBS with 0.05% Tween-20 (Thermo Fisher) as blocking buffer was applied to block non-specific signal for 1h at room temperature. Then, 50µL of neat urine samples was applied to the wells and incubated for 2hs at 37 °C on an orbital shaker. Next, 50µL of bead-bound anti-PLAP antibody solution (20µg/mL) was applied to the disc for 90mins at 37 °C on an orbital shaker. Finally, after the washing and drying steps, the signals were read by the optical system using a Blu-ray laser device and counted as pulses by the pulse sensing circuit. Between each step, an automatic washer was used to remove the excess reagents and reduce non-specific binding. The washing buffer used was 0.05% Tween-20 in PBS (PBST). The washing program was set to

wash the disc with 300μL of PBST 3 times, and after this series, the disc was washed with 3,000μL PBST once followed by 3,000μL deionized water to minimise salt crystal formation.

3.4.12 Isolation of Urine EV and Removal of Uromodulin

In order to remove uromodulin, previously published methods including β-ME, NaCl and $ZnSO_4$ were tested with mild modification to maximise the removal. Fresh spot urine from NP was collected and spun at 1,500g to remove cells and debris. The urine pool from NP third-trimester urine (160 mL in total) was equally divided into 4 groups (40 mL in each group), namely control group (no treatment), β-ME group, NaCl group and $ZnSO_4$ group. For control group, the urine was centrifuged at 10,000g (10K) at 4 °C for 30mins (Beckman Coulter L80 ultracentrifuge and Sorvall TST28.39 swing-out rotor). The 10K pellet was resuspended in 40μL of fPBS and frozen at -80 °C. The supernatant after 10K spin was filtered with 0.22 μm syringe filter (MERCK, MPSLGVM33RS) and ultracentrifuged at 150,000g (150K) for 2hs for sEV isolation. The sEV pellet was resuspended in 40μL of fPBS and kept frozen until use. For β-ME group, after the first round of 10K spin, the pellet was resuspended in 2.5%β-ME in fPBS for 5mins with intermittent disturbance at room temperature to release the sEV trapped by uromodulin. The solution was topped up with fPBS for the second round of 10K spin. The 10K pellet was resuspended in 40ul fPBS and frozen at -80 °C until use. The supernatant of the first round (SN1) and the second round (SN2) of 10K spin were combined and was filtered with 0.22 μm syringe filter before spun at 150K. The resulting sEV pellet was resuspended in 40μL fPBS and frozen at -80°C until use. For NaCl or $ZnSO_4$ group, either 0.58M NaCl or 2mM ZnSO4 was added to an aliquot of urine for 2hs at room temperature. Then the urine was spun at 1,500g for 10mins to remove uromodulin. The supernatant was recovered and spun at 10K and the pellets were resuspended in 40μL fPBS and frozen at -80°C until use. The 10K supernatant was filtered through with 0.22μm

syringe filter before spun at 150K. The 150K pellet was resuspended in 40μL fPBS and frozen at -80°C until use. For each group, the same volume (35mL) of urine was used for the 10K spin to ensure sEV isolation started from the same amount of the original material. The same volume (20 μL) of isolated urine m/lEV and sEV from each group were applied on western blot. By doing so, differences observed at the end of sEV isolation is a reflection of method rather than the starting material. The protein concentration of the urine EV was determined using NanoOrange Protein Quantification Kit (N6666, ThermoFisher).

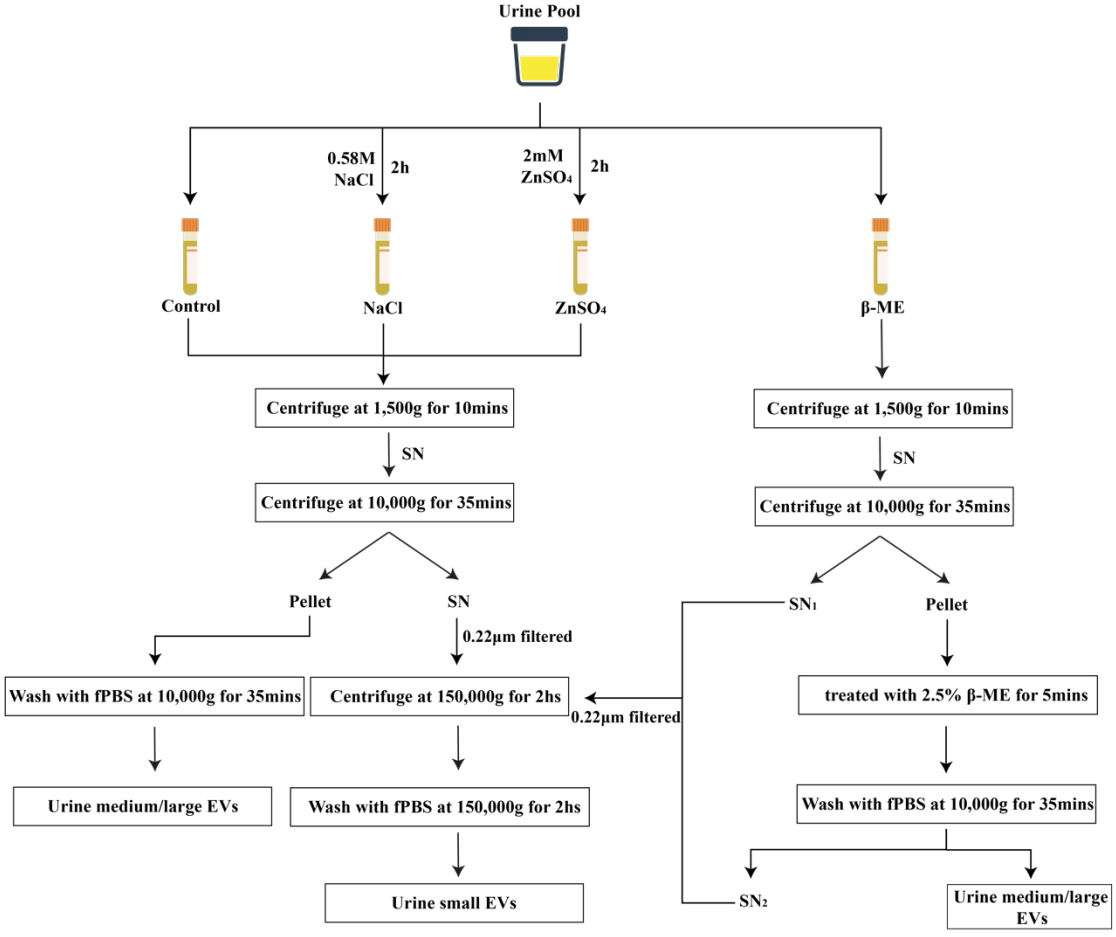


Figure 2. The illustration of the uromodulin removal plan. SN stands for supernatant.

3.4.13 Isolation of red blood cell (RBC) EV by differential ultracentrifugation (UC)

For RBC derived EV, fresh blood was obtained from pregnant women (n=3) using sodium citrate as an anticoagulant. Blood was centrifuged at 1,500g for 15mins at room temperature and the top plasma and buffy coat layer were discarded and the bottom RBC layer was transferred to a new tube and washed with fPBS 2 times. 2.5ml of RBCs were then transferred to a 50mL stimulation solution which was consist of 2mM $CaCl_2$ (Sigma, C5670) and 5μM calcium ionophore A23197 (Sigma, C7522) in 50ml of fPBS. After incubating overnight at 37 °C with consistent agitation, the stimulation was terminated by adding 500uL of 0.5M EDTA (Sigma, 324506) to the solution. The solution was centrifuged at 1,500g for 15mins at room temperature to remove RBCs. The supernatant was recovered and ultracentrifuged at 10,000g for 35mins for m/lEV isolation. The supernatant from the 10K spin was filtered by 0.22 μm syringe filter (MERCK, MPSLGVM33RS) and again ultracentrifuged at 150,000g for 2hs for RBC-sEV isolation.

3.4.14 Statistical Analysis

The statistical analysis was performed using built-in analysis algorism of GraphPad Prism 9. Continuous variables were compared using the Kruskal-Wallis test with Dunn's post-test and one-way ANOVA test with Tukey’s post-test was used according to the distribution of the data.

3.5 Results

3.5.1 NaCl is the better method to remove uromodulin in urine

I first wanted to see if there was PLAP signal in urine EV. If so then the detection of $PLAP^+$ sEV could be an indication of psEV could pass through the glomerular filtration barrier and enter into the urine. For this purpose, I have used two methods: the first method was to isolate urine EV and to investigate if PLAP signal was detected in isolated urine EV via western blot. The second method is to directly use neat urine on ExoCounter, a method to identify psEV from chapter 2, to see if PLAP was co-expressed with CD63 on urine sEV.

Uromodulin has been known to co-sediment with EV during low-speed centrifuge and entrap EV in its filaments[26]. Previously, β-ME, NaCl and $ZnSO_4$ were reported to be effective to remove uromodulin in urine during EV isolation[27-29]. I first tested which method was the best method to remove uromodulin and reduce the interference of uromodulin in the downstream analysis. Based on the western blot results, the expression EV markers including Alix, CD63, CD9 and syntenin could be detected for sEV. The expression of Alix and CD63 could be detected in m/lEV in the control, NaCl and $ZnSO_4$ group but not in the β-ME group (Figure

3). It is likely due to the antibodies for EV markers (Alix, CD63, CD9) requiring non-reducing condition while β-ME would disrupt the condition. The expression of EV markers was enriched for sEV rather than m/lEV, indicating the glomerular filtration process selectively let sEV pass. PLAP as the placenta marker could also be detected in urine sEV but not in m/lEV (Figure 3), suggesting the psEV passage from the GFB. Negative marker cytochrome c was not expressed on urine sEV or m/lEV (Figure 3). For uromodulin removal, β-ME group had the lowest uromodulin expression for m/lEV and NaCl group for sEV (Figure 3). The expression of EV' markers including Alix, CD63, CD9 and syntenin were not influenced by NaCl treatment (Figure 3). Therefore, NaCl treatment was decided to be the better method to reduce the uromodulin in urine sEV compared to no treatment (control group), β-ME or $ZnSO_4$ treated urines, while not interfering the expression of sEV markers, so NaCl was chosen to remove uromodulin in further urine sEV isolation.

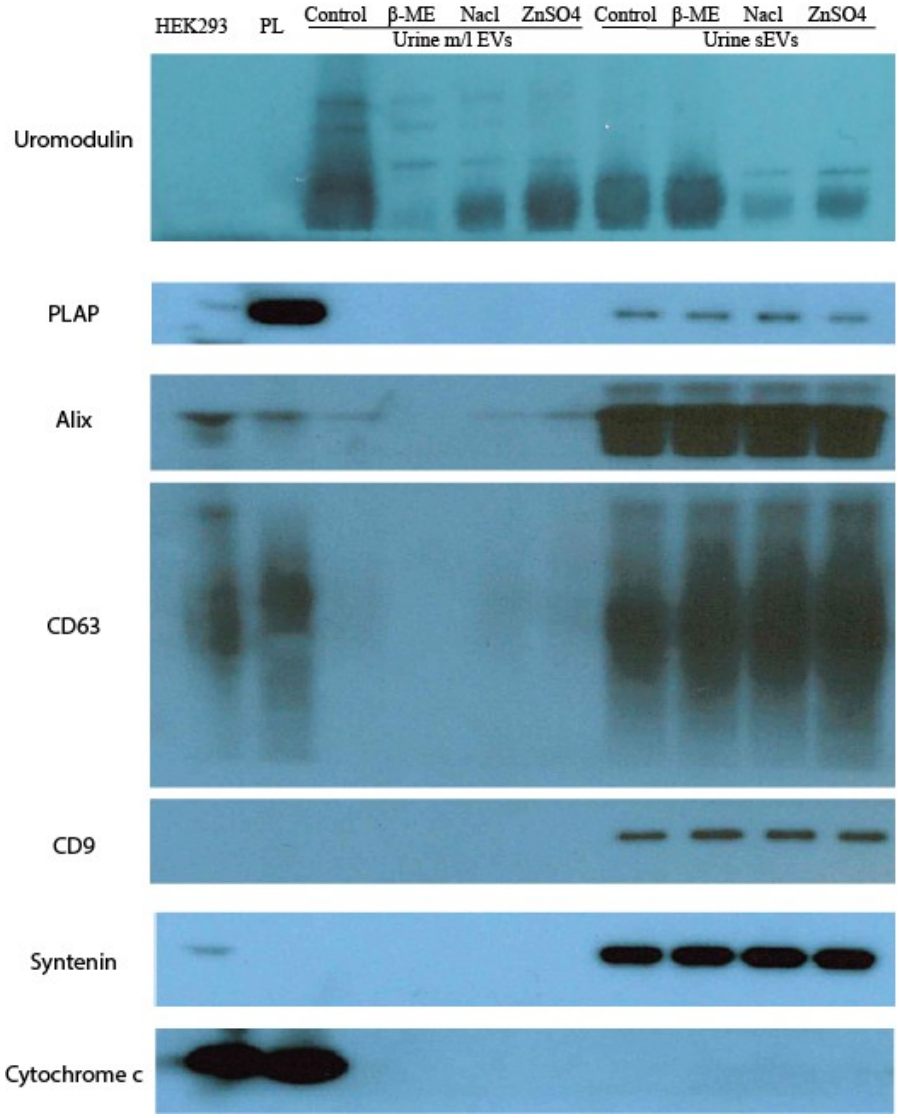


Figure 3. The different methods to remove uromodulin when isolating urine EV. The markers tested includes Alix (95kDa), CD63 (30-65kDa), uromodulin(75kDa), PLAP (66kDa), Syntenin (30kDa), CD9 (23kDa) and cytochrome c (10kDa). PL stands for placenta lysate. The presence of PLAP in HEK293 was due to the overload from the PL lane.

3.5.2 The presence of psEV in urine from both NP and PE

After I have confirmed the detection of PLAP on pooled NP urine sEV (Figure 3), I further characterised urine sEV isolated from NP and PE urine. Equal volumes of the isolated urine

sEV (20μL) from NP and PE were tested using western blot. Both NP and PE psEV expressed EV markers (CD63, CD9, Syntenin, Alix, TSG101), PLAP (the syncytiotrophoblast origin marker) and didn't express cytochrome C (negative control) (Figure 4A). The mean size distribution of urine sEV isolated via differential ultracentrifugation was (189.5± 1.4 nm) detected by NTA (Figure 4B). Urine sEV had a characteristic cup shape in negative staining shown by TEM (Figure 4C). These results indicated the presence of psEV in the urine.

Next, I used ExoCounter assay to check if psEV could be detected from minimally processed urines rather than isolated urine sEV. This device uses ELISA-like method to quantify the sEV number in biofluid using a set of two antibodies[30]. For this study, I used CD63 as capturing antibody and PLAP as beads antibody to detect the counts of psEV in urine samples (4 PE urines and 5 NP urines, Figure 4E). The quantification of psEV in urine was significantly higher when using CD63-PLAP antibodies compared to using fPBS as coating antibody, which represented the background signals of urine (Figure 4E). This again confirmed the presence of psEV in urine.

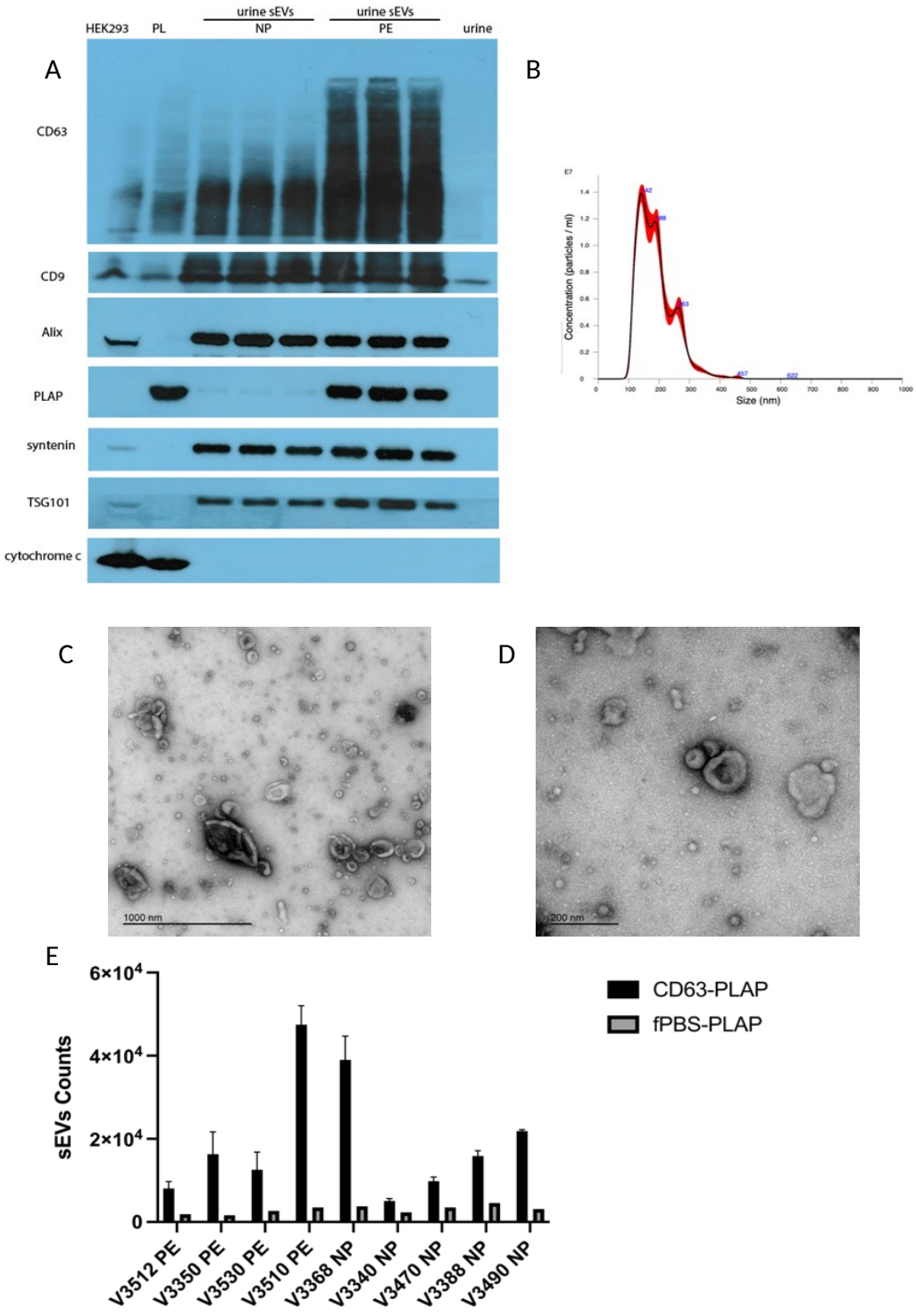


Figure 4. (A) Representative western blot characterisation of psEV in urine samples isolated from ultracentrifugation were characterized by western blot. PL indicates placenta lysate. HEL293 lysate as negative controls for PLAP and positive control for cytochrome C. (B) Representative characterization of urine sEV by NTA. (C) Representative pictures of sEV in urines characterized by TEM of higher magnification. Scale bar = 1000nm. (D)

Representative pictures of placental sEV in urines characterized by TEM at lower magnification. Scale bar = 2μm. (E) Quantification of CD63-PLAP psEV (dark bars) in 50μL of urine samples by ExoCounter. 4 PE urine samples and 5 NP urine samples were quantified. Grey bars are background (fPBS-PLAP) counts.

3.5.3 Podocyte Differentiation

After thermoswitch from 33°C to 37 °C, immortal podocytes stopped proliferation after 2 days and the cell diameter increased from (8 - 36) μm to (10 - 45) μm after 10 days (Figure 5A). The increase in cell size was also confirmed by F-actin staining (Figure 5B). After differentiation, podocytes changes from a round morphology to a big cell body with digit-like foot process under the light microscope (Figure 5C). The expression of podocyte differentiation markers nephrin and synaptopodin significantly increased by 1.9 folds and 38.8 folds respectively, and the expression of podocyte undifferentiated marker WT-1 significantly decreased to 0.3-fold, after 10 days of differentiation (Figure 5D). Based on these observations, I have confirmed the podocytes have differentiated after 10 days at 37 °C

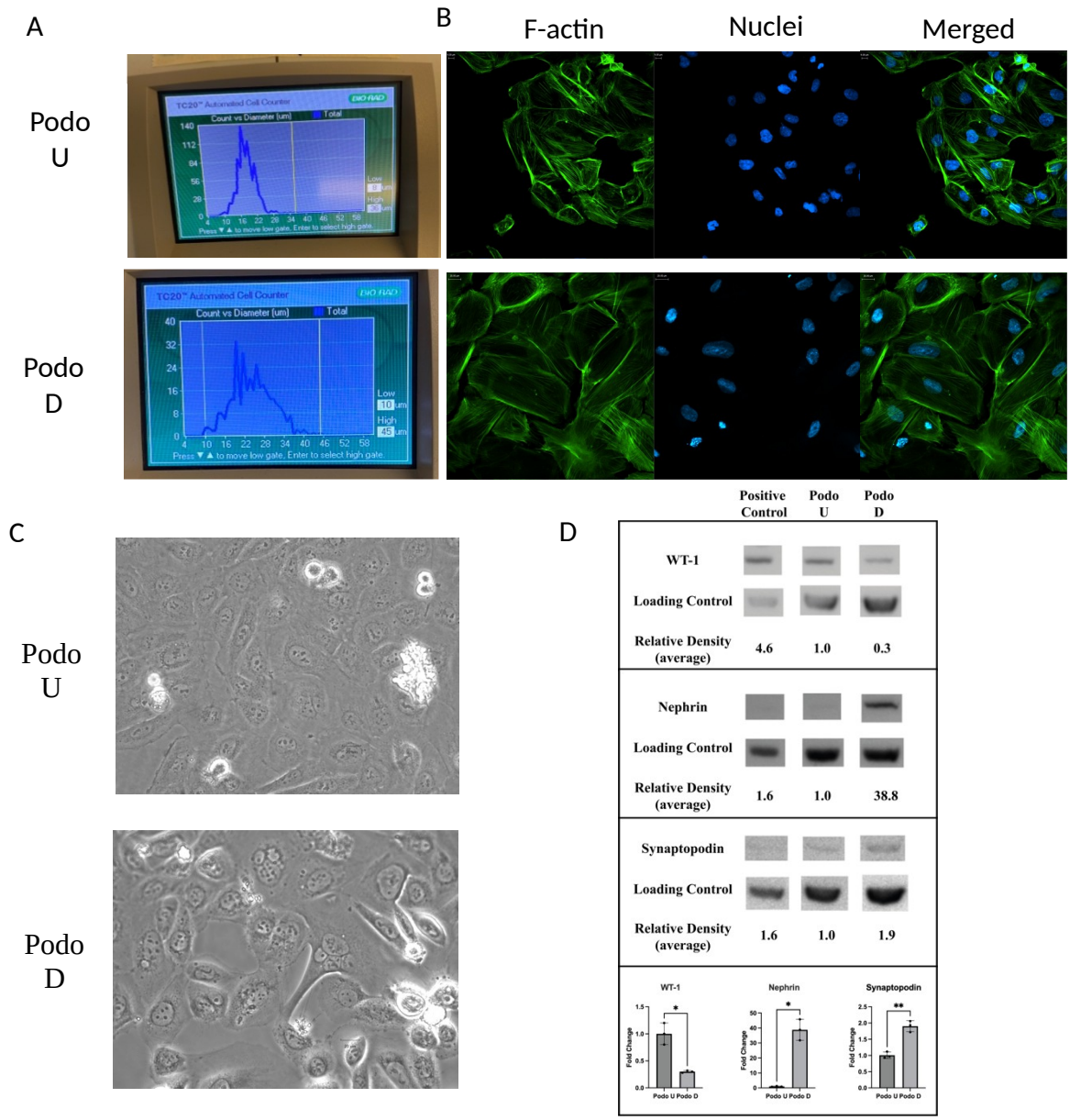


Figure 5. (A) The cell size distribution of undifferentiated podocytes and differentiated podocytes measured by TC20™ Automated Cell Counter. Podo U stands for undifferentiated podocytes, Podo D stands for differentiated podocytes. The lowest cell diameter is 8μm and the highest is 36μm for undifferentiated podocytes; the lowest cell diameter is 10μm and the highest is 45μm for differentiated podocytes. (B) The F-actin staining of undifferentiated and differentiated podocytes. The scale bar is 20μm. (C) The representative light microscope pictures of undifferentiated and differentiated podocytes. After differentiation, digit-like foot process can be observed (red arrow). (D) The expression of WT-1 (52kD), nephrin (85kD)

and synaptopodin (100kDa) of undifferentiated podocytes and differentiated podocytes. The loading control is β-actin. Positive control for WT-1 and synaptopodin is HEK293. Positive control for synaptopodin is testis lysate. The experiments were done using triplicate and the statistic difference was calculated using paired t-test. * denotes $p < 0.05$, ** denotes $p < 0.01$.

3.5.4 RBC sEV characterisation as control for the experiment

After confirmed the podocytes were differentiated after 10 days of thermoswitch, I next wanted to treat podocytes with psEV to detect its influence. But before that, I included another negative control, red blood cells sEV (RBC-sEV), to investigate if the functional changes of psEV on podocytes were mainly from psEV instead of other sEV. Considering the large volume of blood in the placenta, RBC-sEV would also be present in the psEV via isolation from placental perfusion. As a result, RBC-sEV would be an important negative control for the following functional studies. RBC-sEV was isolated by differential ultracentrifuge and the characterisation of isolated RBC-sEV was done by western blot, NTA and TEM. RBC-sEV expressed the characteristic sEV markers including CD63, TGS101 and syntenin by western blot (Figure 6A). RBC-sEV also expressed RBC origin marker CD235a and lack of the negative control cytochrome c (Figure 6A). The TEM showed RBC-sEV had a characteristic cup shape in negative staining (Figure 6B). The NTA showed RBC-sEV had a mean size of (146.4 ± 0.8nm) (Figure 6C).

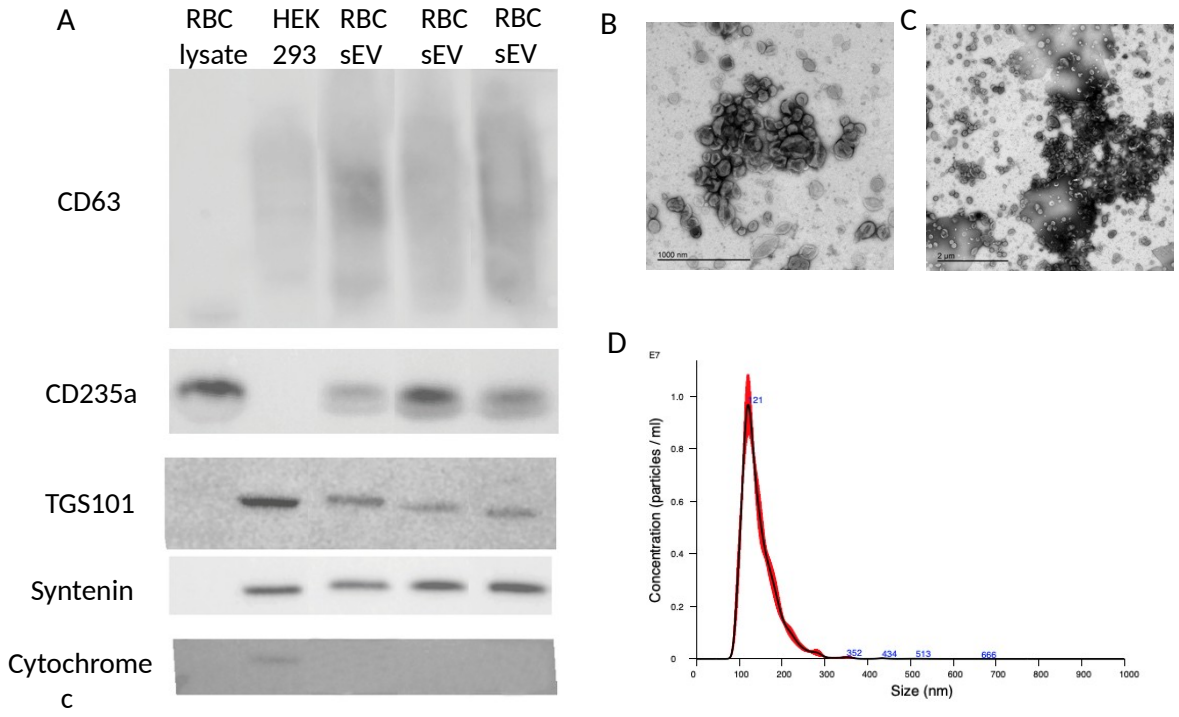


Figure 6. (A) RBC-sEV characterized by western blot. HEL293 lysate as negative controls for CD235a and positive control for cytochrome C, n= 3. (B) Representative pictures of RBC-sEV characterized by TEM of higher magnification. Scale bar = 1000nm. (C) Representative pictures of RBC-sEV characterized by TEM at lower magnification. Scale bar = 2um. (D) Representative characterization of RBC-sEV by NTA.

3.5.5 psEV internalisation by podocytes

After I have acquired RBC-sEV as negative control, I next wanted to investigate if psEV could be internalized by differentiated podocytes. First, after staining psEV with a fluorescent membrane dye named PKH26, I treated podocytes with stained psEV and podocytes were analysed via flow cytometry and confocal microscopy. By using flow cytometry, I observed the internalization of PKH26 stained psEV by podocytes could be seen at 30mins of treatment (data not shown) and the internalization accumulated via a dose and time-dependent manner (Figure 7A&B). There was no significant difference between the NP and PE psEV entering the podocytes (Figure 7A&B). The presence of PKH26-stained psEV in

podocytes was also confirmed by confocal microscopy (Figure 7C). The same methods were applied to investigate if RBC-sEV could enter podocytes to check if RBC-sEV could be a comparable negative control for psEV. Similar to psEV internalised by podocytes, the internalisation of PKH26-stained RBC-sEV was confirmed by confocal microscopy (Figure 8A). And the internalisation also showed a time-dependent manner by flow cytometry (Figure 8B & 8C & 8D).

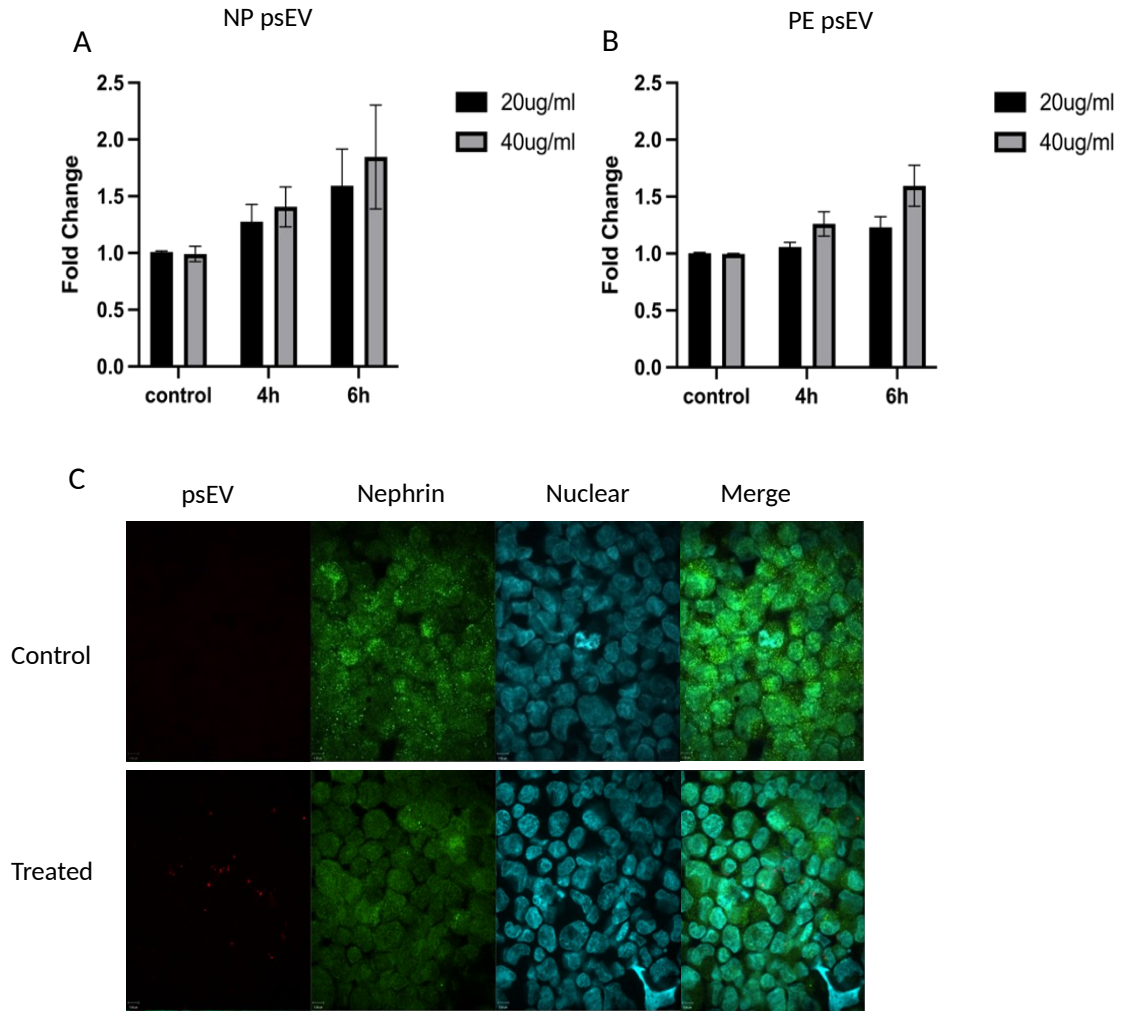


Figure 7. (A) The fold change of the mean intensity of PE-A of podocytes after treated with PKH26stained psEV isolated from NP placental perfusion detected by flow cytometry, n=3.

(B) The fold change of the mean intensity of PE-A of podocytes after treated with PKH26 stained psEV isolated from PE placental perfusion detected by flow cytometry, n=3. (C) Representative confocal microscope pictures of PKH26 stained psEV isolated from NP placental perfusion. Scale bar = 7μm, objective lens 20x.

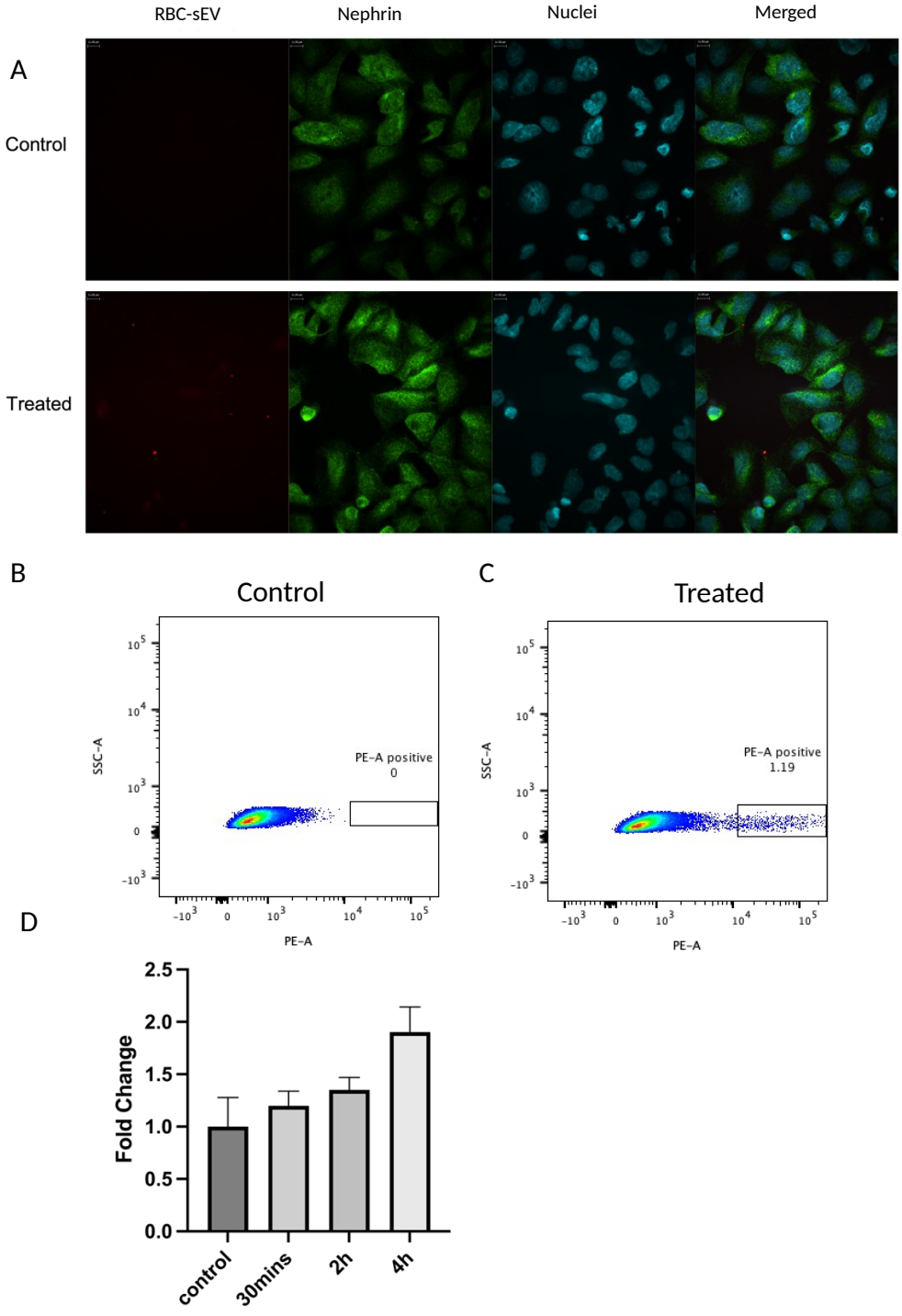


Figure 8. (A) Representative confocal microscope pictures of PKH26 stained RBC-sEV treated podocytes. Scale bar = 11µm, objective lens 40x. (B) The illustration of flow cytometry of untreated podocytes. (C) The illustration of flow cytometry of podocytes treated with PKH26 stained RBC-sEV for 4hs. The red box represents the podocytes that became fluorescent after internalised fluorescent RBC-sEV (1.19%). (D) The fold change of the mean intensity of PE-A of podocytes after treated with PKH26 stained RBC-sEV detected by flow cytometry, n=3. The error bar is standard deviation.

Next, I conducted additional experiments to test if psEV from NP and PE could enter podocytes. Chromosome 19 microRNA cluster (C19MC) has been shown to be exclusively expressed in the placenta, embryonic stem cells and certain cancers[31]. I reasoned C19MC may not be expressed by podocytes. Had pEV entered podocytes, detection of C19MC after but not before pEV treatment would be evidence as C19MC being transferred by pEV after their podocyte entering. In this experiment, I used RBC-sEV isolated from RBCs from pregnant women acting as another negative control together with fPBS to prove this effect was coming from psEV instead of other types sEV. As expected, I observed signals of miR-517a, miR-517c and miR-518b from podocytes after treated with NP psEV and PE psEV while no signal was observed from fPBS treated or RBC-sEV treated podocytes (Figure 9). Interestingly, the fold changes of miR-517c and miR-518b were significantly higher after PE psEV treatment compared to NP psEV treatment (Figure 9).

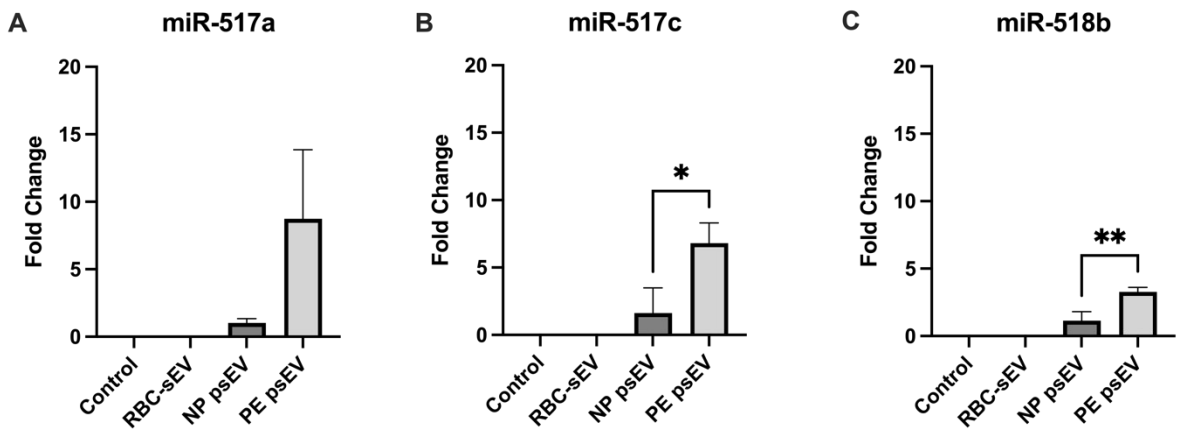


Figure 9. C19MC expression in human podocytes after psEV treatment. The expression of three placental C19MC including miR-517a (A), miR-517c (B) and miR-518b (C) were analysed by qPCR. The results were normalized to U6 expression of each sample and the delta-delta CT method was used to calculate the fold changes. The y-axis is the fold change (± SD) of miRNA expression. * denotes $P < 0.05$, ** denotes $P < 0.01$.

3.5.6 The influence of psEV on podocytes upon internalisation

After confirming psEV could enter podocytes, I next wanted to see the functional changes of podocytes as a result of psEV entering. Podocytes' adhesion ability is damaged in preeclampsia[9] and podocytes' migration can be altered in nephropathy[32]. Therefore, I investigated if podocytes' adhesion and migration ability after treatment with psEV from PE and PE. After treated NP psEV, the podocyte migration ability was upregulated, while the migration ability was not influenced by no treatment, RBC-sEV treatment or PE psEV (Figure 10A & 10B). In contrast, podocyte adhesion ability was significantly impeded after treatment with PE psEV compared to control (no treatment) ($P<0.05$, Figure 10C). Treatment with either RBC-sEV or NP psEV did not influence the podocytes' adhesion ability (Figure 10C). I next want to further confirm the altered migration and adhesion ability of podocytes were not from the changed cell viability. Indeed, after treating podocytes with RBC-sEV, NP psEV, PE psEV, the cell viability determined by ATP quantification, showed no significant

difference compared to control, irrespective of the incubation duration, from short incubation time (1h) to long incubation time (6h) (Figure 10D).

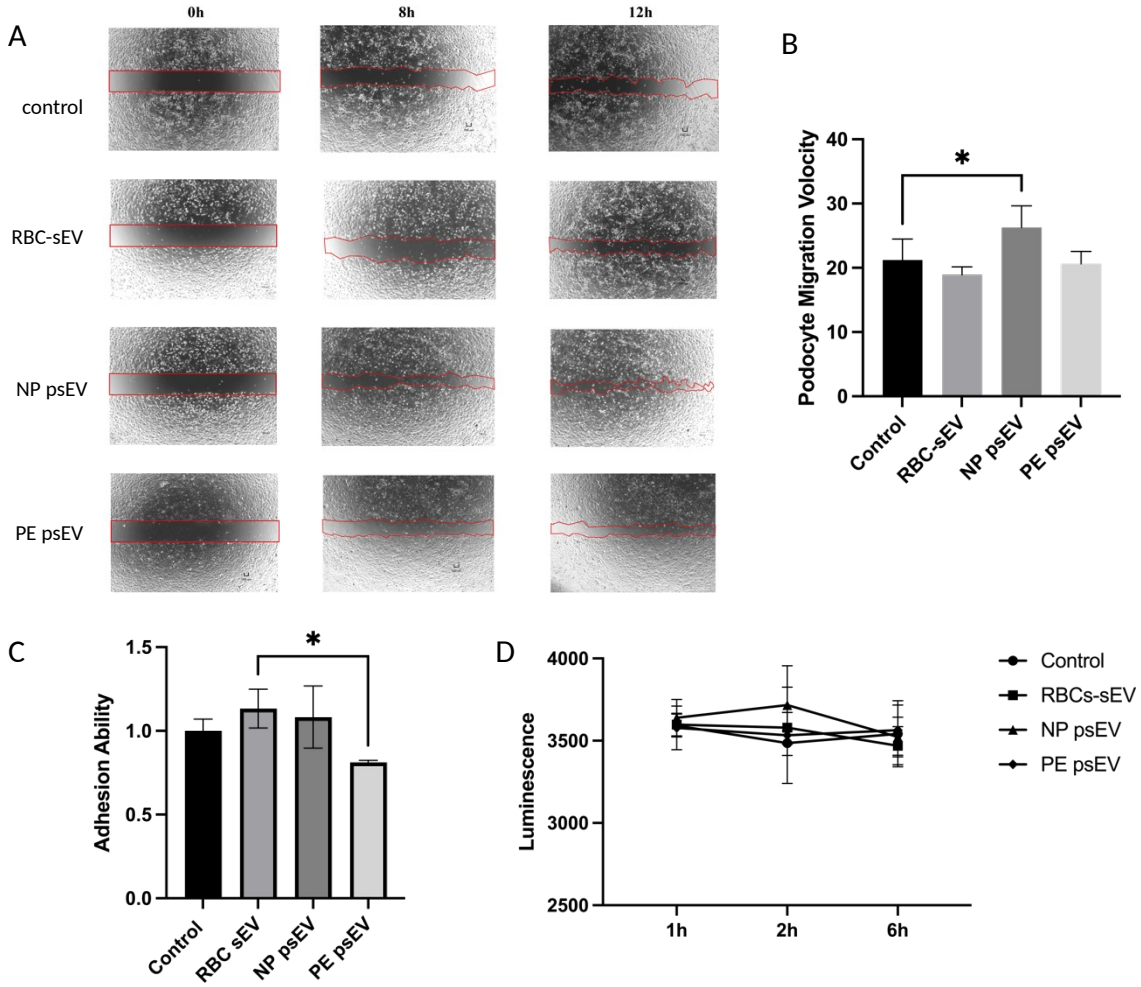


Figure 10. (A)The representative bright field pictures of podocyte migration after RBC-sEV, NP psEV and PE-sEV treatment compared to control for 0h, 8h and 12h. The area defined by the red line is the gap between the cells' front. The objective lens used was 5x. Images are representative of three independent experiments. (B) The podocytes migration velocity (μm/hour) in control, RBC-sEV, NP psEV and PE psEV treatment. (C) The adhesion ability of podocytes after treated with fPBS (n = 3), RBC-sEV (n = 3), NP psEV (n = 3) and PE psEV (n = 3). The y-axis represents the adhesion ability compared to control. * denotes P <

0.05. (D) The podocyte viability influenced by RBC-sEV, NP psEV and PE psEV. The x-axis represents the incubation time, and the y-axis represents the luminescence from ATP of the cells read by the plate reader (background corrected).

3.5.7 The mechanism of psEV influence podocytes migration and adhesion ability

Considering nephrin is at the central signalling pathway of podocyte migration and adhesion function[33,34], I next investigated if nephrin expression would be altered by psEV. Indeed, the NP psEV enhanced the nephrin expression by 1.9 folds after 1h treatment compared to control, while PE psEV didn't induce significant nephrin expression enhancement on podocyte compared to control (Figure 11A & 11B). Another important structure of podocytes to regulate their migration abilities is the F-actin cytoskeleton, a type of stress fibre [33], which could also be potentially influenced by psEV. In podocytes that were not treated (control) or treated with RBC-sEV, F-actin (stress fibre) was predominantly found around the cell membrane and scarce throughout each podocyte, with the stress fibres of different podocytes displaying a random orientation (Figure 11C). However, after treatment with NP psEV, the stress fibres within podocytes were markedly more prominent and organized, with a parallel alignment seen both within individual cells and between neighbouring cells (Figure 11C). Notably, podocytes that had been treated with PE psEV exhibited a classic F-actin reorganization, with the formation of a cortical ring structure observed (Figure 11C). Such F-actin reorganization is typically interpreted as a response of podocytes to stress or injury[35,36].

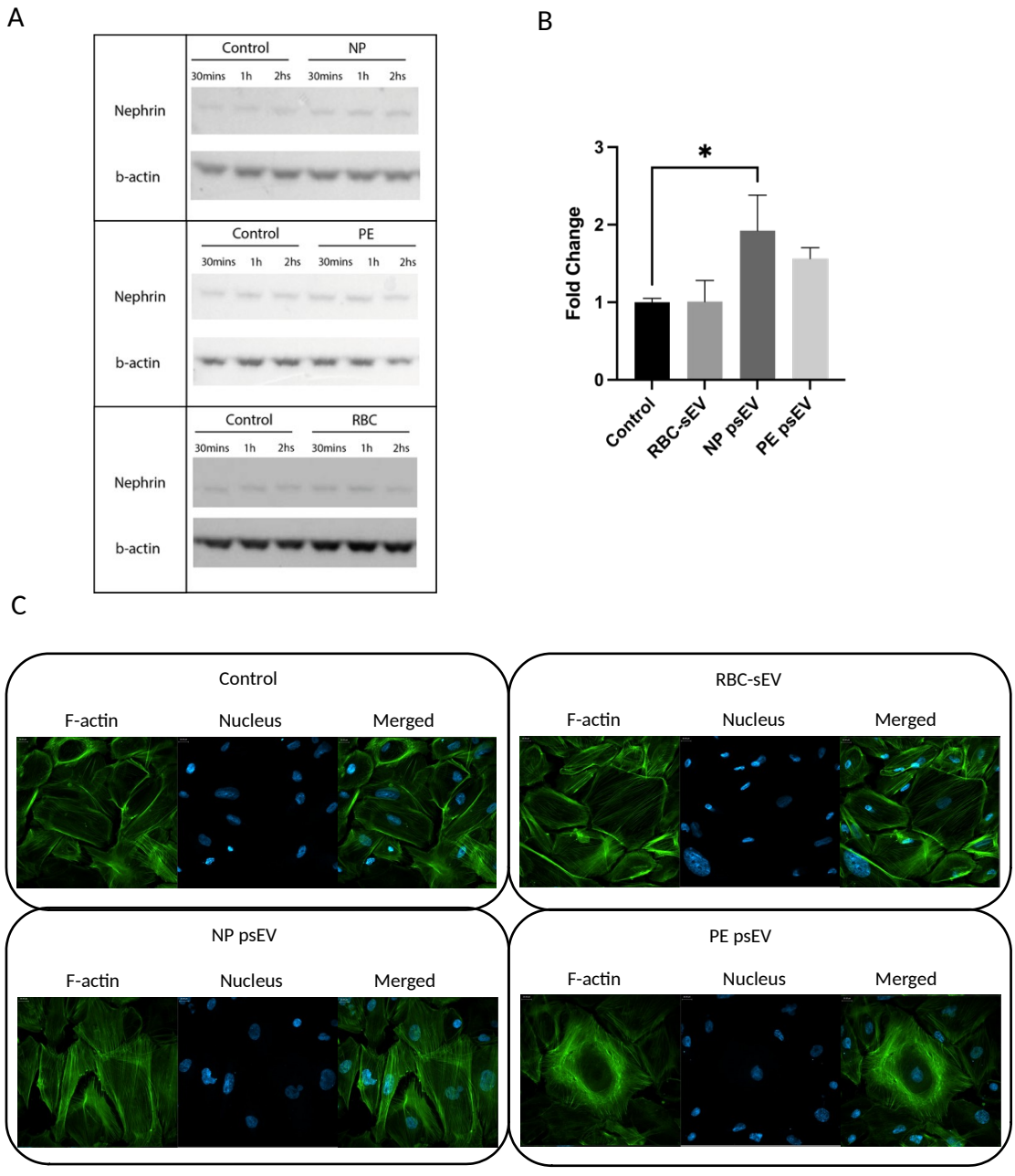


Figure 11. (A) The representative western blot results of the nephrin and β-actin expression of podocytes after RBC-sEV, NP psEV and PE psEV treatment compared to control (no treatment). (B) The comparison of nephrin expression of podocytes detected by western blot

after RBC-sEV, NP psEV and PE psEV 1h treatment compared to control. The nephrin expression was normalized to total protein loaded (ponceau red). (C) F-actin staining of podocytes after fPBS treatment or RBC-sEV (as control) where F-actin was heavily stained around the cell body but not across the cell body. F-actin staining of podocytes after NP psEV treatment where the enhanced F-actin across the podocytes cell body could be observed. F-actin staining of podocytes after PE psEV treatment where cortical ring formation of F-actin could be observed. The objective lens used was 20x. The scale bar is 20μm. * denotes $P < 0.05$.

3.6 Discussion & Future work

In this study, I first demonstrated the presence of psEV in urine which suggests psEV could pass through the glomerular filtration barrier (GFB) and encounter podocyte (Figure 4). Then I have shown the psEV isolated from placenta perfusion from NP or PE could enter podocytes in a dose and time-dependent manner (Figure 7). Upon internalisation, psEV could transfer placenta-specific C19MC into podocytes (Figure 9). Furthermore, the functions of podocyte influenced by psEV isolated from NP were different from PE. The psEV isolated from NP could enhance podocytes' movement ability (Figure 10A&B). This effect was possibly induced by the strengthened F-actin in the podocytes (Figure 11C) and the upregulated nephrin expression (Figure 11A&B). However, psEV isolated from PE did not enhance podocyte movement ability which was possibly due to the cortical ring formation of the stressed F-actin (Figure 11C). Additionally, the psEV from PE could inhibit podocytes' adhesion ability, which was not seen after NP psEV treatment (Figure 10C). This could result in a higher chance of podocytes relocating from GFB in PE.

The podocyte's movement ability has been the centre of topics for a long time. Both enhanced motility and reduced motility of podocyte can be seen in disease status which implies the fine regulation of mobility is the key to healthy podocytes[37,38]. In pregnancy, the renal blood flow increases 50-85% and the glomerular filtration rate (GFR) upregulates 40-65%[39]. The increased workload of the kidney implicates the enhanced GFB ability required to process the

hyperfiltration seen in pregnancy. In this study, the upregulated motility of podocytes after NP psEV treatment, which was not seen after PE STB-sEV or RBC sEV treatment, might be essential to counter the increased hemodynamic stresses under hyperfiltration on podocytes in NP (Figure 10A & 11B).

Under hyperfiltration, podocytes undergo extensive repairment and development which require robust actin cytoskeletal changes. During the static situation, the transversal stress fibres are seen in podocytes, after applying shear stress, the reinforcement of actin filaments can be observed and cells are still attached indicating the enhanced actin cytoskeleton is one of the key alterations when healthy podocytes counter the shear stress[40]. However, with the increased hemodynamic stress, the stress fibres are gradually lost, the cortical actin networks show up and finally the podocytes are detached and lost[40,41]. In this study, after NP psEV treatment, podocytes showed up enhanced stress fibre staining which indicated NP psEV might help to prepare the podocytes to counter the hemodynamic stresses during normal pregnancy by a strong actin cytoskeleton. While after PE psEV treatment, the stress fibre of podocytes was lost and the cortical actin network shows up (Figure 11C) which indicates the reduced ability of podocytes to counter the hemodynamic stress in PE. This current study has suggested that the psEV in the blood might be responsible for the stressed actin cytoskeleton seen in PE, expanding a previous observation which showed the serum from PE patients could induce the F-actin reorganization with cortical ring formation[42].

Nephrin of podocytes is responsible for assembling the protein complex important for regulating actin filament network and focal adhesion dynamics including lamellipodia formation[43,44]. When podocytes are injured, the nephrin expression together with the actin-associated fraction is progressively lost from the foot process[45]. Considering nephrin is

important for regulating the actin cytoskeleton of podocytes, the upregulated nephrin expression after NP psEV treatment (Figure 11A & 11B) might explain the upregulated motility in NP compared to PE (Figure 10A&10B). In contrast, PE psEV didn't induce such adequate nephrin expression and this might also explain the reduced adhesion ability of podocytes in PE (Figure 10C). Nephrin is essential for the induction of podocyte adhesion ability, which is important for maintaining the integrity of the glomerular barrier and the proper functioning of cell-matrix and cell-cell junctions[46,47]. The impaired adhesion ability of podocytes ultimately leads to the development of proteinuria, a prevalent symptom in PE.

The reduced expression of nephrin on podocyte in PE compared to normotensive or chronic hypertensive pregnancies has been well established using kidney tissue sections[48,49]. This suggests the inadequate nephrin expression might be associated with podocyte injury in PE. However, it is not clear if the reduced nephrin expression in podocytes in PE is mainly due to the shedding from the cell surface or if other mechanisms are also involved, such as reduced synthesis or increased degradation. Research data supports that the reduced nephrin expression in PE is due to the shedding of nephrin into the urine since the excessive nephrin excretion found in the urine of PE compared to NP[50-52] and the severity of proteinuria is highly correlated with the increased amount of nephrin excretion[53,54]. The synthesis of nephrin of podocytes is not influenced in PE compared to NP supported by the nephrin mRNA expression is not changed[55]. However in their study, podocytes were stimulated with the culture medium from glomerular endothelial cell treated with serum from PE instead of directly analysing from biopsy[55]. More evidence is needed to investigate the synthesis of the nephrin expression by podocytes in NP and PE. Finally, to my best knowledge, the degradation of nephrin on podocytes in PE has not been investigated yet. It would be

interesting to investigate the mechanism of nephrin expression on podocytes influenced by psEV.

C19MC as the largest human miRNA gene cluster is expressed almost exclusively in the placenta[56], and its expression can be also detected in tumors[57] and embryonic stem cells[58]. Interestingly, it has been shown the majority of miRNA in sEV released by human placental trophoblast cells is C19MC, which emphasizes the important roles of C19MC carried by sEV to the recipient cells[59]. It has been shown C19MC cluster was responsible for regulating target transcripts related to cell movement and selectively attenuate cell migration without affecting cell proliferation[60]. These results are consistent with the findings in our study that, the attenuated podocyte movement ability after the treatment by PE psEV compared to NP (Figure 10A&B) correlated with higher extent of C19MC been transferred into the podocytes (Figure 9).

Interestingly, either psEV from NP or PE didn't influence podocytes viability while the adhesion ability impaired after treated with PE psEV compared to NP psEV (Figure 10). These results implicated that PE psEV mainly impaired podocytes functions rather than induce the apoptosis of podocytes. Indeed, compared to NP, more podocytes shed into the urine in PE[61-63]. And these podocytes were alive and these cells could be subcultured for a long time[64]. This is in the line with our finding that adhesion ability of podocytes was impaired rather than viability after PE psEV treatment (Figure 10).

In conclusion, this study demonstrated psEV isolated from placental perfusion from NP and PE could be internalized by podocytes and influence podocyte functions. Podocyte migration ability was upregulated after NP psEV treatment which might be due to the reinforced actin

cytoskeleton F-actin rearrangement evidenced by enhanced F-actin staining and increased nephrin expression. In contrast, PE psEV treatment showed impaired podocyte adhesion ability and stressed actin cytoskeleton (cortical ring formation). These findings suggest that psEV released from placenta play important roles in the glomerular permeability barrier in pregnancy.

3.7 Reference

1. ACOG practice bulletin. Diagnosis and management of preeclampsia and eclampsia. Number 33, January 2002. *Obstet Gynecol*. 2002;99:159-167. doi: 10.1016/s0029-7844(01)01747-1
2. Fishel Bartal M, Lindheimer MD, Sibai BM. Proteinuria during pregnancy: definition, pathophysiology, methodology, and clinical significance. *Am J Obstet Gynecol*. 2022;226:S819-s834. doi: 10.1016/j.ajog.2020.08.108
3. Sturgiss SN, Dunlop W, Davison JM. 1 Renal haemodynamics and tubular function in human pregnancy. *Baillière's Clinical Obstetrics and Gynaecology*. 1994;8:209-234. doi: https://doi.org/10.1016/S0950-3552(05)80319-0
4. Ouzounian JG, Elkayam U. Physiologic Changes During Normal Pregnancy and Delivery. *Cardiology Clinics*. 2012;30:317-329. doi: https://doi.org/10.1016/j.ccl.2012.05.004
5. Moran P, Lindheimer MD, Davison JM. The renal response to preeclampsia. *Seminars in Nephrology*. 2004;24:588-595. doi: https://doi.org/10.1016/j.semnephrol.2004.07.008
6. Sudo M, Yoshita K, Ito Y, Imai N, Iino N, Narita I. Histopathological features of kidney and renal prognosis in patients with preeclampsia. *Pregnancy Hypertens*. 2021;25:75-80. doi: 10.1016/j.preghy.2021.05.015
7. Cornelis T, Odutayo A, Keunen J, Hladunewich M. The kidney in normal pregnancy and preeclampsia. *Semin Nephrol*. 2011;31:4-14. doi: 10.1016/j.semnephrol.2010.10.002
8. Nagata M. Podocyte injury and its consequences. *Kidney Int*. 2016;89:1221-1230. doi: 10.1016/j.kint.2016.01.012
9. Zhai T, Furuta I, Akaishi R, Ishikawa S, Morikawa M, Yamada T, Koyama T, Minakami H. Alteration of podocyte phenotype in the urine of women with preeclampsia. *Sci Rep*. 2016;6:24258. doi: 10.1038/srep24258
10. Henao DE, Cadavid AP, Saleem MA. Exogenous vascular endothelial growth factor supplementation can restore the podocyte barrier-forming capacity disrupted by sera of preeclamptic women. *J Obstet Gynaecol Res*. 2013;39:46-52. doi: 10.1111/j.1447-0756.2012.01889.x

11. Germain SJ, Sacks GP, Sooranna SR, Sargent IL, Redman CW. Systemic inflammatory priming in normal pregnancy and preeclampsia: the role of circulating syncytiotrophoblast microparticles. *J Immunol*. 2007;178:5949-5956. doi: 10.4049/jimmunol.178.9.5949
12. Goswami D, Tannetta DS, Magee LA, Fuchisawa A, Redman CW, Sargent IL, von Dadelszen P. Excess syncytiotrophoblast microparticle shedding is a feature of early-onset pre-eclampsia, but not normotensive intrauterine growth restriction. *Placenta*. 2006;27:56-61. doi: 10.1016/j.placenta.2004.11.007
13. Cronqvist T, Erlandsson L, Tannetta D, Hansson SR. Placental syncytiotrophoblast extracellular vesicles enter primary endothelial cells through clathrin-mediated endocytosis. *Placenta*. 2020;100:133-141. doi: 10.1016/j.placenta.2020.07.006
14. Zabel RR, Bär C, Ji J, Schultz R, Hammer M, Groten T, Schleussner E, Morales-Prieto DM, Markert UR, Favaro RR. Enrichment and characterization of extracellular vesicles from ex vivo one-sided human placenta perfusion. *Am J Reprod Immunol*. 2021;86:e13377. doi: 10.1111/aji.13377
15. Awoyemi T, Motta-Mejia C, Zhang W, Kouser L, White K, Kandzija N, Alhamlan FS, Cribbs AP, Tannetta D, Mazey E, et al. Syncytiotrophoblast Extracellular Vesicles From Late-Onset Preeclampsia Placentae Suppress Pro-Inflammatory Immune Response in THP-1 Macrophages. *Front Immunol*. 2021;12:676056. doi: 10.3389/fimmu.2021.676056
16. Tersigni C, Furqan Bari M, Cai S, Zhang W, Kandzija N, Buchan A, Miranda F, Di Simone N, Redman CW, Bastie C, et al. Syncytiotrophoblast-derived extracellular vesicles carry apolipoprotein-E and affect lipid synthesis of liver cells in vitro. *J Cell Mol Med*. 2022;26:123-132. doi: 10.1111/jcmm.17056
17. Göhner C, Plösch T, Faas MM. Immune-modulatory effects of syncytiotrophoblast extracellular vesicles in pregnancy and preeclampsia. *Placenta*. 2017;60 Suppl 1:S41-s51. doi: 10.1016/j.placenta.2017.06.004
18. Todorova D, Simoncini S, Lacroix R, Sabatier F, Dignat-George F. Extracellular Vesicles in Angiogenesis. *Circ Res*. 2017;120:1658-1673. doi: 10.1161/circresaha.117.309681
19. Gangoda L, Boukouris S, Liem M, Kalra H, Mathivanan S. Extracellular vesicles including exosomes are mediators of signal transduction: are they protective or pathogenic? *Proteomics*. 2015;15:260-271. doi: 10.1002/pmic.201400234
20. Sung BH, Parent CA, Weaver AM. Extracellular vesicles: Critical players during cell migration. *Dev Cell*. 2021;56:1861-1874. doi: 10.1016/j.devcel.2021.03.020
21. Cheng Y, Wang X, Yang J, Duan X, Yao Y, Shi X, Chen Z, Fan Z, Liu X, Qin S, et al. A translational study of urine miRNAs in acute myocardial infarction. *J Mol Cell Cardiol*. 2012;53:668-676. doi: 10.1016/j.yjmcc.2012.08.010
22. Tong M, Stanley JL, Chen Q, James JL, Stone PR, Chamley LW. Placental Nano-vesicles Target to Specific Organs and Modulate Vascular Tone In Vivo. *Hum Reprod*. 2017;32:2188-2198. doi: 10.1093/humrep/dex310
23. Simionescu M, Popov D, Sima A. Endothelial transcytosis in health and disease. *Cell and Tissue Research*. 2009;335:27-40. doi: 10.1007/s00441-008-0688-3
24. Tyagi I, Agrawal U, Amitabh V, Jain AK, Saxena S. Thickness of glomerular and tubular basement membranes in preclinical and clinical stages of diabetic nephropathy. *Indian J Nephrol*. 2008;18:64-69. doi: 10.4103/0971-4065.42336
25. Usman WM, Pham TC, Kwok YY, Vu LT, Ma V, Peng B, Chan YS, Wei L, Chin SM, Azad A, et al. Efficient RNA drug delivery using red blood cell extracellular vesicles. *Nat Commun*. 2018;9:2359. doi: 10.1038/s41467-018-04791-8

26. Musante L, Bontha SV, La Salvia S, Fernandez-Piñeros A, Lannigan J, Le TH, Mas V, Erdbrügger U. Rigorous characterization of urinary extracellular vesicles (uEVs) in the low centrifugation pellet - a neglected source for uEVs. *Sci Rep*. 2020;10:3701. doi: 10.1038/s41598-020-60619-w
27. Yao C, Chen X, Xu Y, Wang F, Ji J, Xu H, He J, Wang L, Li Y. Comparing pretreatment strategies to increase the yield and purity of human urinary extracellular vesicles. *J Chromatogr B Analyt Technol Biomed Life Sci*. 2022;1206:123359. doi: 10.1016/j.jchromb.2022.123359
28. Liu Z, Cauvi DM, Bernardino EMA, Lara B, Lizardo RE, Hawisher D, Bickler S, De Maio A. Isolation and characterization of human urine extracellular vesicles. *Cell Stress Chaperones*. 2018;23:943-953. doi: 10.1007/s12192-018-0902-5
29. Santucci L, Bruschi M, Del Zotto G, Antonini F, Ghiggeri GM, Panfoli I, Candiano G. Biological surface properties in extracellular vesicles and their effect on cargo proteins. *Sci Rep*. 2019;9:13048. doi: 10.1038/s41598-019-47598-3
30. Yokose T, Kabe Y, Matsuda A, Kitago M, Matsuda S, Hirai M, Nakagawa T, Masugi Y, Hishiki T, Nakamura Y, et al. O-Glycan-Altered Extracellular Vesicles: A Specific Serum Marker Elevated in Pancreatic Cancer. *Cancers (Basel)*. 2020;12. doi: 10.3390/cancers12092469
31. Mong EF, Yang Y, Akat KM, Canfield J, VanWye J, Lockhart J, Tsibris JCM, Schatz F, Lockwood CJ, Tuschl T, et al. Chromosome 19 microRNA cluster enhances cell reprogramming by inhibiting epithelial-to-mesenchymal transition. *Scientific Reports*. 2020;10:3029. doi: 10.1038/s41598-020-59812-8
32. Xu W, Ge Y, Liu Z, Gong R. Glycogen synthase kinase 3β dictates podocyte motility and focal adhesion turnover by modulating paxillin activity: implications for the protective effect of low-dose lithium in podocytopathy. *Am J Pathol*. 2014;184:2742-2756. doi: 10.1016/j.ajpath.2014.06.027
33. Faul C, Asanuma K, Yanagida-Asanuma E, Kim K, Mundel P. Actin up: regulation of podocyte structure and function by components of the actin cytoskeleton. *Trends Cell Biol*. 2007;17:428-437. doi: 10.1016/j.tcb.2007.06.006
34. Zha D, Chen C, Liang W, Chen X, Ma T, Yang H, Goor H, Ding G. Nephrin phosphorylation regulates podocyte adhesion through the PINCH-1-ILK-α-parvin complex. *BMB Rep*. 2013;46:230-235. doi: 10.5483/bmbrep.2013.46.4.270
35. Hsu HH, Hoffmann S, Endlich N, Velic A, Schwab A, Weide T, Schlatter E, Pavenstädt H. Mechanisms of angiotensin II signaling on cytoskeleton of podocytes. *J Mol Med (Berl)*. 2008;86:1379-1394. doi: 10.1007/s00109-008-0399-y
36. Tan R, Patni H, Tandon P, Luan L, Sharma B, Salhan D, Saleem MA, Mathieson PW, Malhotra A, Husain M, et al. Nef interaction with actin compromises human podocyte actin cytoskeletal integrity. *Exp Mol Pathol*. 2013;94:51-57. doi: 10.1016/j.yexmp.2012.06.001
37. Ito N, Sakamoto K, Hikichi C, Matsusaka T, Nagata M. Biphasic MIF and SDF1 expression during podocyte injury promote CD44-mediated glomerular parietal cell migration in focal segmental glomerulosclerosis. *Am J Physiol Renal Physiol*. 2020;318:F741-f753. doi: 10.1152/ajprenal.00414.2019
38. Majmundar AJ, Buerger F, Forbes TA, Klämbt V, Schneider R, Deutsch K, Kitzler TM, Howden SE, Scurr M, Tan KS, et al. Recessive NOS1AP variants impair actin remodeling and cause glomerulopathy in humans and mice. *Sci Adv*. 2021;7. doi: 10.1126/sciadv.abe1386
39. Helal I, Fick-Brosnahan GM, Reed-Gitomer B, Schrier RW. Glomerular hyperfiltration: definitions, mechanisms and clinical implications. *Nat Rev Nephrol*. 2012;8:293-300. doi: 10.1038/nrneph.2012.19

40. Friedrich C, Endlich N, Kriz W, Endlich K. Podocytes are sensitive to fluid shear stress in vitro. *Am J Physiol Renal Physiol*. 2006;291:F856-865. doi: 10.1152/ajprenal.00196.2005
41. Srivastava T, McCarthy ET, Sharma R, Cudmore PA, Sharma M, Johnson ML, Bonewald LF. Prostaglandin E(2) is crucial in the response of podocytes to fluid flow shear stress. *J Cell Commun Signal*. 2010;4:79-90. doi: 10.1007/s12079-010-0088-9
42. Tian J, Zhang L, Zhou Y, Xiao J, Li S, Chen Y, Qiao Z, Niu J, Gu Y. Angiotensin-(1-7) attenuates damage to podocytes induced by preeclamptic serum through MAPK pathways. *Int J Mol Med*. 2014;34:1057-1064. doi: 10.3892/ijmm.2014.1870
43. Venkatareddy M, Cook L, Abuarquob K, Verma R, Garg P. Nephrin regulates lamellipodia formation by assembling a protein complex that includes Ship2, filamin and lamellipodin. *PLoS One*. 2011;6:e28710. doi: 10.1371/journal.pone.0028710
44. Zhu J, Sun N, Aoudjit L, Li H, Kawachi H, Lemay S, Takano T. Nephrin mediates actin reorganization via phosphoinositide 3-kinase in podocytes. *Kidney Int*. 2008;73:556-566. doi: 10.1038/sj.ki.5002691
45. Yuan H, Takeuchi E, Taylor GA, McLaughlin M, Brown D, Salant DJ. Nephrin dissociates from actin, and its expression is reduced in early experimental membranous nephropathy. *J Am Soc Nephrol*. 2002;13:946-956. doi: 10.1681/asn.V134946
46. Lennon R, Randles MJ, Humphries MJ. The importance of podocyte adhesion for a healthy glomerulus. *Frontiers in endocrinology*. 2014;5:160-160. doi: 10.3389/fendo.2014.00160
47. Ristola M, Lehtonen S. Functions of the podocyte proteins nephrin and Neph3 and the transcriptional regulation of their genes. *Clinical Science*. 2013;126:315-328. doi: 10.1042/cs20130258
48. Zhao S, Gu X, Groome LJ, Wang Y. Decreased nephrin and GLEPP-1, but increased VEGF, Flt-1, and nitrotyrosine, expressions in kidney tissue sections from women with preeclampsia. *Reprod Sci*. 2009;16:970-979. doi: 10.1177/1933719109338630
49. Garovic VD, Wagner SJ, Petrovic LM, Gray CE, Hall P, Sugimoto H, Kalluri R, Grande JP. Glomerular expression of nephrin and synaptopodin, but not podocin, is decreased in kidney sections from women with preeclampsia. *Nephrol Dial Transplant*. 2007;22:1136-1143. doi: 10.1093/ndt/gfl711
50. Ozdemir F, Tayyar AT, Acmaz G, Aksoy H, Erturk G, Muhtaroglu S, Tayyar M. Comparison of blood and urine nephrin levels in preeclampsia and intrauterine growth retardation. *Pak J Med Sci*. 2016;32:40-43. doi: 10.12669/pjms.321.8865
51. Kostovska I, Tosheska Trajkovska K, Kostovski O, Labudovic D. Urinary Nephrin and Podocalyxin Levels as Predictors of Pre-eclampsia in High-Risk Pregnant Women. *Folia Med (Plovdiv)*. 2021;63:948-957. doi: 10.3897/folmed.63.e60055
52. Jung YJ, Cho HY, Cho S, Kim YH, Jeon JD, Kim YJ, Lee S, Park J, Kim HY, Park YW, et al. The Level of Serum and Urinary Nephrin in Normal Pregnancy and Pregnancy with Subsequent Preeclampsia. *Yonsei Med J*. 2017;58:401-406. doi: 10.3349/ymj.2017.58.2.401
53. Son GH, Kwon JY, Lee S, Park J, Kim YJ, Yun B, Park JH. Comparison of serum and urinary nephrin levels between normal pregnancies and severe preeclampsia. *Eur J Obstet Gynecol Reprod Biol*. 2013;166:139-144. doi: 10.1016/j.ejogrb.2012.10.011
54. Furuta I, Zhai T, Ishikawa S, Umazume T, Nakagawa K, Yamada T, Morikawa M, Minakami H. Association between nephrinuria, podocyturia, and proteinuria in women with pre-eclampsia. *J Obstet Gynaecol Res*. 2017;43:34-41. doi: 10.1111/jog.13180

55. Collino F, Bussolati B, Gerbaudo E, Marozio L, Pelissetto S, Benedetto C, Camussi G. Preeclamptic sera induce nephrin shedding from podocytes through endothelin-1 release by endothelial glomerular cells. *Am J Physiol Renal Physiol*. 2008;294:F1185-1194. doi: 10.1152/ajprenal.00442.2007
56. Bentwich I, Avniel A, Karov Y, Aharonov R, Gilad S, Barad O, Barzilai A, Einat P, Einav U, Meiri E, et al. Identification of hundreds of conserved and nonconserved human microRNAs. *Nature Genetics*. 2005;37:766-770. doi: 10.1038/ng1590
57. Flor I, Bullerdiek J. The dark side of a success story: microRNAs of the C19MC cluster in human tumours. *J Pathol*. 2012;227:270-274. doi: 10.1002/path.4014
58. Ren J, Jin P, Wang E, Marincola FM, Stroncek DF. MicroRNA and gene expression patterns in the differentiation of human embryonic stem cells. *J Transl Med*. 2009;7:20. doi: 10.1186/1479-5876-7-20
59. Donker RB, Mouillet JF, Chu T, Hubel CA, Stolz DB, Morelli AE, Sadovsky Y. The expression profile of C19MC microRNAs in primary human trophoblast cells and exosomes. *Mol Hum Reprod*. 2012;18:417-424. doi: 10.1093/molehr/gas013
60. Xie L, Mouillet J-F, Chu T, Parks WT, Sadovsky E, Knöfler M, Sadovsky Y. C19MC microRNAs regulate the migration of human trophoblasts. *Endocrinology*. 2014;155:4975-4985. doi: 10.1210/en.2014-1501
61. Aita K, Etoh M, Hamada H, Yokoyama C, Takahashi A, Suzuki T, Hara M, Nagata M. Acute and transient podocyte loss and proteinuria in preeclampsia. *Nephron Clin Pract*. 2009;112:c65-70. doi: 10.1159/000213083
62. White WM, Garrett AT, Craici IM, Wagner SJ, Fitz-Gibbon PD, Butters KA, Brost BC, Rose CH, Grande JP, Garovic VD. Persistent urinary podocyte loss following preeclampsia may reflect subclinical renal injury. *PLoS One*. 2014;9:e92693. doi: 10.1371/journal.pone.0092693
63. Craici IM, Wagner SJ, Bailey KR, Fitz-Gibbon PD, Wood-Wentz CM, Turner ST, Hayman SR, White WM, Brost BC, Rose CH, et al. Podocyturia predates proteinuria and clinical features of preeclampsia: longitudinal prospective study. *Hypertension*. 2013;61:1289-1296. doi: 10.1161/hypertensionaha.113.01115
64. Zhao S, Gu Y, Coates G, Groome LJ, Saleem MA, Mathieson PW, Wang Y. Altered nephrin and podoplanin distribution is associated with disturbed polarity protein PARD-3 and PARD-6 expressions in podocytes from preeclampsia. *Reprod Sci*. 2011;18:772-780. doi: 10.1177/1933719111398145

CHAPTER 4

Proteomics analysis of human podocytes treated with normal and preeclampsia placental small extracellular vesicle

Table of Contents

4.1 Abstract....171
4.2 Introduction....173
4.3 Aims....174
4.4 Methods....175
4.4.1 Proteomics experimental design....175
4.4.2 Data cleaning (distribution, missing value, normalization, imputation)....176
4.4.3 Differentially expressed proteins (DEPs) using outlier significance A/B test....176
4.4.4 Protein-protein interaction (PPI) and functional enrichment analysis....177
4.4.5 Western blot....178
4.4.6 Statistical Analysis....179
4.5 Results....180
4.5.1 The initial data cleaning....180
4.5.2 Data imputation....182
4.5.3 Principal component analysis (PCA) plot and cluster analysis....184
4.5.4 Differentially expressed proteins (DEPs)....186
4.5.5 Protein-protein-interaction (PPI) and functional enrichment analysis....193
4.5.6 DEPs validation through western blot....202
4.6 Discussion & Future work....205
4.7 References....210

4.1 Abstract

Background: Mass spectrometry offers a powerful means to explore the proteomic profiles of cells, which can be instrumental in studying systems biology. This chapter delves into the proteomic changes in human podocytes affected by placenta small extracellular vesicles (psEV) derived from NP and PE, potentially revealing mechanisms underlying podocyte functions in these conditions.

Methods: I conducted mass spectrometry on podocytes without any treatment, or treated with RBC-sEV, or treated with psEV from NP and PE placentas obtained through *ex vivo* dual lobe placenta perfusion. Using R, I analysed differentially expressed proteins (DEPs) bioinformatically in each group. The expression of DEPs were validated through western blot. Protein-protein interactions (PPIs) and functional enrichment analysis of DEPs were further examined using Cytoscape software via STRING analysis.

Results: Over 4,000 proteins were identified in each sample tested. Among these, 160 proteins were differentially expressed (adjusted p-value < 0.001) following NP psEV treatment and 197 proteins after PE psEV treatment, compared to the control group. Moreover, when directly comparing PE psEV treated podocytes to NP psEV treated podocytes, 206 proteins were differentially expressed (adjusted p-value < 0.001). Functional enrichment analysis revealed that DEPs in podocytes treated with NP psEV were associated with cellular component organization or biogenesis, intracellular transport, and mitochondrial functions. In contrast, DEPs in podocytes treated with PE psEV were involved in metabolic processes, nitrogen compound metabolic processes, and gene expression.

Conclusion: From the current proteomics analysis, the potentially responsible proteins are identified in podocytes that may involve in the adaption of podocytes in NP to deal with increased glomerular filtration rate. I also identified the potentially responsible proteins that may involve in the pathology of injured podocytes in PE. The DEPs found could be used in future studies to understand the renal pathology in PE.

4.2 Introduction

Preeclampsia (PE) is a leading cause of maternal and fetal death worldwide[1]. Renal function impairment, often manifested as proteinuria, is among the most common symptoms in PE[2]. Evidence has been suggested that more adverse maternal and fetal outcomes are seen in proteinuric PE compared to non-proteinuric PE[3,4]. The degree of proteinuria is positively correlated with the severity of PE, such that heavier proteinuria is linked to more adverse maternal and perinatal outcomes[5,6].

One of the reasons that women with preeclampsia develop proteinuria is due to the increased permeability of the glomerular filtration barrier (GFB). GFB is composed of glomerular endothelial cells, podocytes and a layer of basement membrane secreted by these two types of cells. Although the increased permeability can be caused by the injured endothelial cells or podocytes, the current evidence supports the concept that the underlying pathology of GFB permeability is damaged podocytes rather than endothelial cells. This is due to several reasons. First, though the endotheliosis of the endothelial cells, where the cells appear vacuolized and hypertrophic, is believed to be the hallmark in PE[7]. The endotheliosis also appears in normal pregnancy indicating that it is not PE specific[8-11]. Second, more evidence has highlighted that podocyturia, where an increased number of podocytes is found in urine, might be the main mechanism of GFB damage in PE. The presence of podocyturia distinguishes PE compared to gestational hypertension[12] and the level of podocyturia is associated with the severity of proteinuria[12]. This indicates the shedding of podocytes is one of the mechanisms of renal damage in PE. Interestingly, the increased shedding of podocytes in PE, as opposed to NP, does not result in a reduced number of these cells in the glomeruli when examined via renal biopsy[13]. This suggests that an elevated turnover rate of podocytes is a critical characteristic of podocyte injury in PE. Other than podocyturia, podocyte

effacement is often observed where podocytes gradually lose their morphology and spread out[14,15]. However, the findings are morphological where the underlying mechanism remains unclear.

In this chapter, I have focused on the influence of placental psEV on podocytes via a proteomics approach, hoping to identify potential molecular targets, mechanisms and processes. Furthermore, I attempted to find the potential regulatory mechanisms of the functional changes, especially the altered migration and adhesion ability which I determined in podocytes from Chapter 3.

4.3 Aims

The aims of this chapter are to:

1. Characterise the protein changes of podocytes after treatment with psEV from NP or PE using mass spectrometry.
2. Identify critical regulatory protein pathways, mechanisms, and networks of podocytes influenced by psEV from NP and PE using bioinformatics tools.
3. Identify potential biomarkers that can be targeted for improving podocytes function in PE

4.4 Methods

4.4.1 Proteomics experimental design

For this proteomics study, undifferentiated podocytes were transferred to 37°C for 10 days to permit full differentiation. Podocytes were then trypsinized and seeded onto a 12-well plate at 0.2 x 10^6 cells/well overnight to allow adhesion. Then, podocytes were washed with fPBS and treated with either fPBS , 20μg/mL RBC-sEV, 20μg/mL NP psEV or 20μg/mL PE psEV for 6 hours. Each treatment group was performed in triplicate. After stimulation, cells were washed with fPBS with 40 units/mL heparin (to wash away sEV bound to the outside of cells) 3 times and the cells were lysed with RIPA buffer (ThermoFisher, 89901) containing protease inhibitors (Roche, 1183617001) at the recommended concentration. The podocyte lysate protein concentration was determined using BCA assay (Bicinchoninic acid assay, ThermoFisher, 23227). The initial lysate quality check was done by Coomassie blue staining (ab119211) of the electrophoresis gel and the expression of podocyte marker nephrin via western blot. The podocyte lysate was then sent to the Target Discovery Institute in Oxford for mass spectrometry. The lysate was further fully digested using the suspension trapping (S-TRAP) method and run in the data-independent acquisition (DIA) mode using Orbitrap Fusion Lumos Tribrid Mass Spectrometer (ThermoFisher). In order to conveniently describe the 4 different treatment groups in the analysis, the control group, RBC-sEV, NP psEV, PE psEV treated podocytes groups were noted as the control group, the RBC group, the NP group and the PE group respectively in the following thesis.

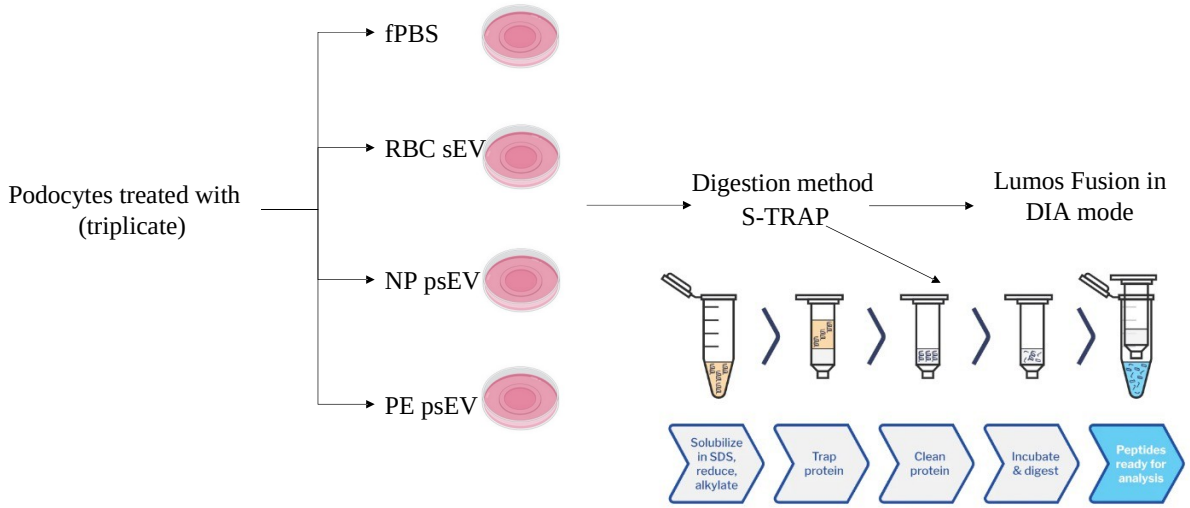


Figure 1. The illustration of proteomics study design.

4.4.2 Data cleaning (distribution, missing value, normalization, imputation)

After acquiring data from DIA software, the programming language R was used to further clean the data. Missing values from each sample were identified and only the proteins that were identified in all triplicates of at least one group were kept for downstream analysis. Subsequently, the data was examined for normal distribution and normalized before further analysis. Finally, the missing value for each group was imputed using either a random drawing from a distribution around the background intensity or a random drawing from a manually defined left-shifted distribution. The initial data cleaning process was done using an R package "DEP"[16]. After this, the data was ready for calculating p values to detect the differentially expressed proteins (DEPs). The principal component analysis (PCA) and the heatmap for cluster analysis was performed by using "DEP" package in R[16].

4.4.3 Differentially expressed proteins (DEPs) using outlier significance A/B test

The differentially expressed proteins (DEPs) were tested using a significance A/B test[17]. For this test, significance A and B were calculated to represent if a certain protein acted like an outlier in a normal distribution. In brief, an outlier significance score for log protein ratios

(significance A) was calculated. To create an estimate of the standard deviation (sd) of the main distribution, the 15.87, 50 and 84.13 percentiles were calculated as r_{-1}, r_0 and r_1 respectively. Accordingly, r_1-r_0 and r_0-r_{-1} are right and left side SD. A measurement for a ratio $r > r_0$ being significantly far away from the main distribution is the distance to r_0 measured in terms of the right sd (1). Similarly, a measurement for a ratio $r < r_{-1}$ being significantly far away from the main distribution is the distance to r_{-1} measured in terms of the left sd (2). The p-value was calculated using the significant outlier ratios (3). The Complementary Error function (ERFC) returns the complement of the Error function integrated between a given input value and infinity, and is used in mathematics and statistics for calculations involving Gaussian distributions. Given that the statistical variation in high-abundance proteins tends to be smaller than in low-abundance proteins, a similar ratio change in a high-abundance protein would be more significant than that in a low-abundance one. To correct this effect, significance B was introduced and calculated. Significance B was calculated in the same way as significance A, only the proteins were divided into 10 groups equally with each group having more than 400 proteins before calculating significance A. For this study, the figures were generated using significance B with a Benjamini-Hochberg corrected p-value with a threshold of 0.05.

$$z = \frac{r - r_0}{r_1 - r_0} \tag{1}$$

$$z = \frac{r_0 - r}{r_0 - r_{-1}} \tag{2}$$

$$significance\ A = \frac{1}{2}\, erfc\left(\frac{z}{\sqrt{2}}\right) \tag{3}$$

4.4.4 Protein-protein interaction (PPI) and functional enrichment analysis

The protein interaction network and functional enrichment analysis was performed using Cytoscape software with stingAPP[18]. In brief, the proteins from a list of up-regulated or down-regulated genes were interrogated using the STRING database. The species interrogated was homo sapiens and the interactions with an evidence score of 0.4 or greater were included. Subsequently, orphan proteins in the PPI network were pruned to generate a subnetwork consisting only of connected components (i.e. interacting genes and proteins). The largest subnetwork was then chosen, and the log fold change value and p-values were imported to the network. Finally, the built-in enrichment analysis of the STRING app was employed to assess the overrepresentation of upregulated or downregulated DEPs in each comparison group, specifically examining gene ontology: biological process (GO: BP) and the tissue distribution.

4.4.5 Western blot

The expression of DEPs was validated through western blot. In brief, HEK293 cell lysate worked as positive control for Tripartite Motif Containing 23 (TRIM23) and placental tissue lysates worked as positive control for PLAP and S100 calcium binding protein P (S100P). Cell lysates were made using RIPA buffer (ThermoFisher, 89901) and the protein concentrations were determined using Bicinchoninic acid (BCA) assay (ThermoFisher, 23227). 35μg of podocyte lysates were mixed with 4X Laemmli buffer with 5% β-Mercaptoethanol and diluted to 20μL with distilled water. The sample mix was heated at 70°C for 10mins before loading onto a 4%-12% SDS-PAGE 15-well gel (ThermoFisher, NP0323BOX) for electrophoresis. Proteins were transferred onto PVDF membranes (Bio-Rad, 1620177) using a semi-dry transfer system. The membranes were then blocked for 1h in 5**%** Blottto (2BScientific, AD-80402-500) in Tris-Buffered Saline with 0.1% Tween-20 (TBS-T, ThermoFisher) before incubation with primary antibody overnight at 4°C. The first

antibodies used were PLAP (1:200 dilution, in-house antibody), S100P (1:1000, Abcam, ab133554), TRIM23 (1:200, Santa Cruz, sc-135587). After further incubation with the appropriate secondary antibody for an hour, chemiluminescence (ECL) (Thermo Fisher, 32106) was used for signal enhancement and developed in a dark room (Hyperfilm ECL, Merck, GE28-9068-35). For quantification, the total protein of each lane was stained with Ponceau Red (Sigma, P7170) and each protein tested was normalised to the total protein and analysed by Image J.

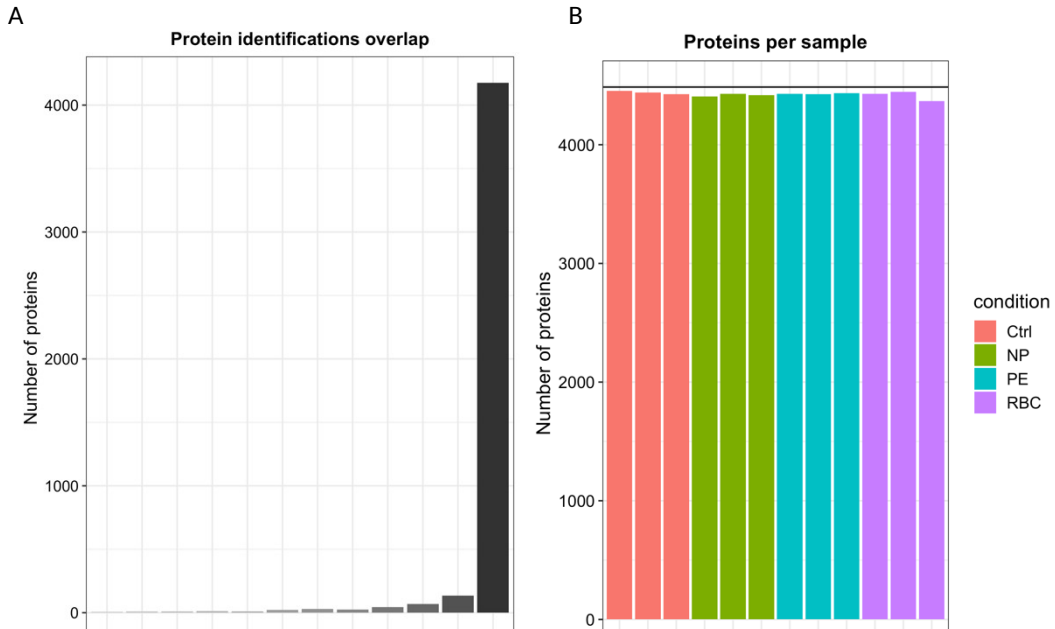
4.4.6 Statistical Analysis

The statistical analysis for the expression of proteins for validation via western blot was performed using built-in analysis algorithm of GraphPad Prism 9 using the Mann-Whitney test.

4.5 Results

4.5.1 The initial data cleaning

In each sample, over 4,000 proteins were identified, with most of these proteins being present in all 12 samples (Figure 2A). Initial data cleaning was carried out in two stages: filtering out missing values and data normalization. Firstly, proteins in each sample with excessive missing values were removed, retaining only proteins that were identified in all triplicates of at least one group. After filtering, all 12 samples maintained a similar number of proteins, with each still containing over 4,000 proteins (Figure 2B). Notably, the majority of retained proteins overlapped among the samples (Figure 2C). Most of the filtered data exhibited a normal distribution, with a few samples being positively skewed (Figure 2D, e.g., PE2). To eliminate any potential outlier effects, the data were normalized, and after transformation, the data distribution was confirmed to be normally distributed (Figure 2E).



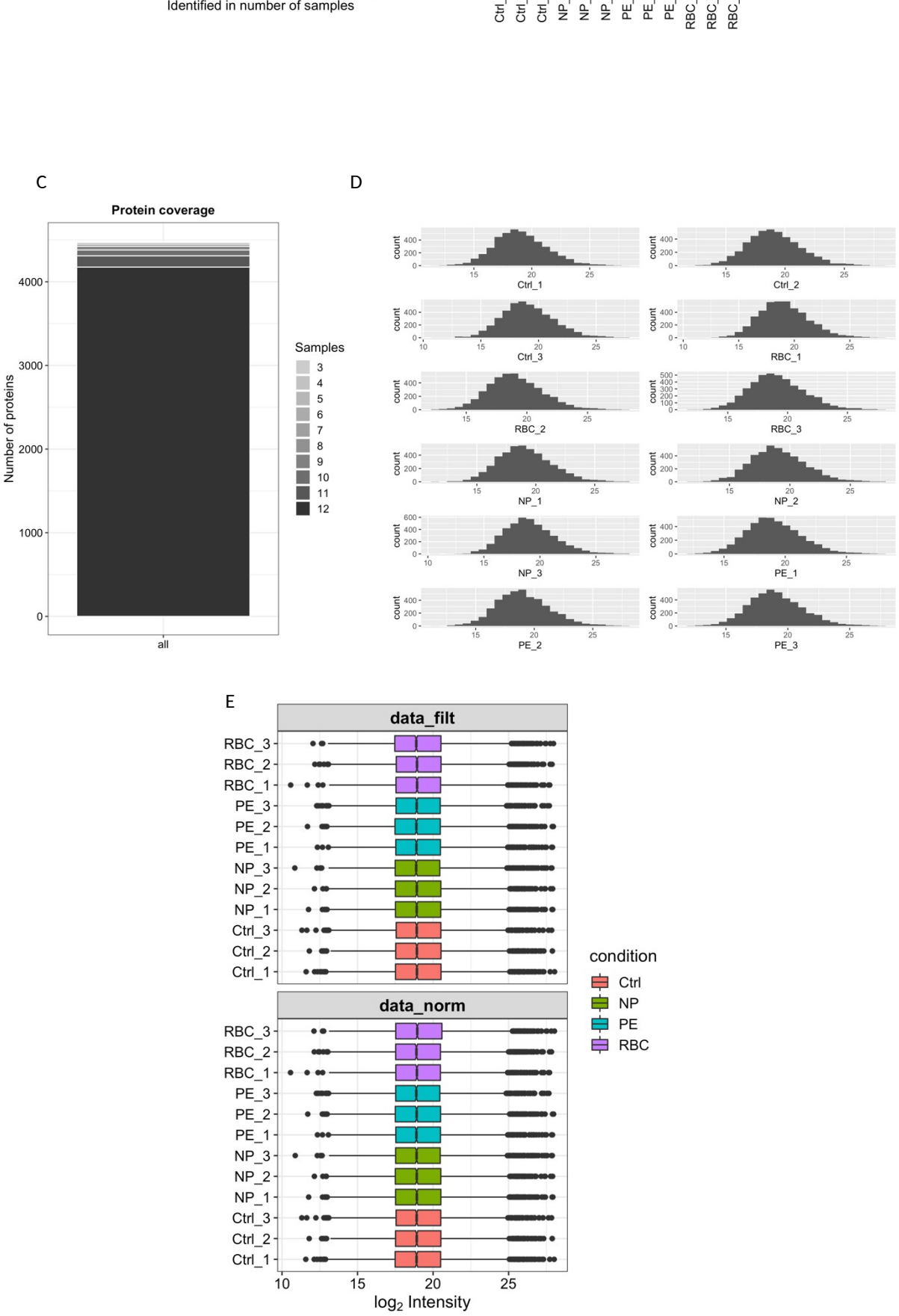
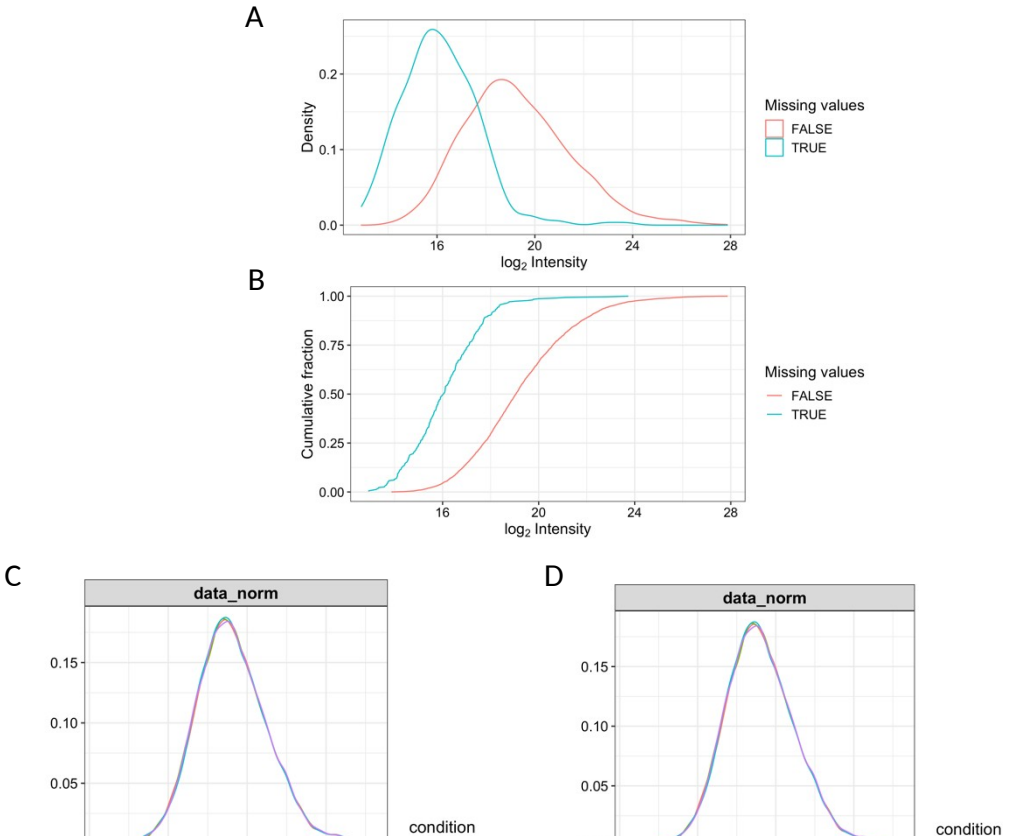


Figure 2. (A) The number of proteins identified in each sample. (B) The number of proteins left after filtering out missing values. (C) The protein identification overlaps between samples after filtering out missing values. (D) The distribution of log2 raw intensity of each sample. (E) The boxplot of data distribution before (data_filt) and after (data_norm) normalization.

4.5.2 Data imputation

Following normalization, the next step involved examining the distribution of missing values to determine the appropriate imputation method. Proteins with missing values exhibited, on average, lower log_2 intensities than non-missing values, suggesting that the missing values were at background levels (Figure 3A&B). Consequently, the data were missing not at random (MNAR), and a left-censored imputation method was employed. I tested the MinProb method, which carries out imputation using a left-censored Gaussian distribution defined by a centred minimal value and standard deviation (SD) (Figure 3C). The minimal value and SD were set to the default values of 1 and 1%, respectively. However, post-imputation, the data no longer followed a normal distribution (Figure 3C). Thus, I tried another imputation method that used a manually defined Gaussian distribution, set 1.8 SD apart with a width of 0.3 (Figure 3D). The data distribution after imputation was similar to the distribution before imputation and exhibited normal distribution (Figure 3D). Hence, this method was chosen for further analysis.



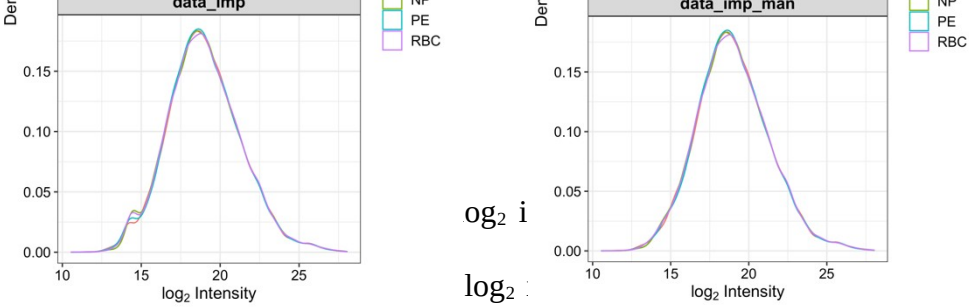
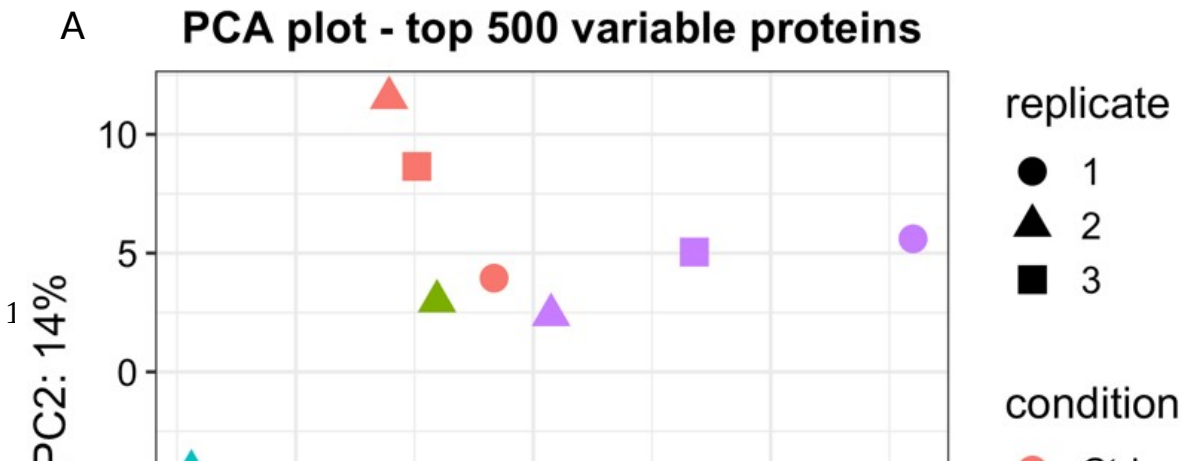


Figure og$_2$ i -missing values. log$_2$ -missing values. (C) The density distribution of data before (data_norm) and after (data_imp) imputation using random draws from a Gaussian distribution centred around a minimal value. (D) The density distribution of data before (data_norm) and after (data_imp_man) imputation using a manually defined left-shifted Gaussian distribution.

4.5.3 Principal component analysis (PCA) plot and cluster analysis

After initial data cleaning and imputation, PCA was performed to investigate potential batch effects among different treatment groups. The top 500 proteins, chosen based on the highest row (protein) variance, were used for analysis. Principal component 1 (PC1) accounted for 16.4%, and PC2 accounted for 14% variance. Control triplicates and RBC triplicates clustered well together and were distinguishable from NP triplicates and PE triplicates (Figure 4A). Subsequently, a heatmap was generated using k-means clustering (k = 6) to identify any proteins with similar behaviour in each treatment group (Figure 4B). Interestingly, SLC4A1 (solute carrier family 4 member 1) was significantly upregulated in the RBC group compared to the NP, PE, and control groups. SLC4A1 is located on red blood cell membranes, and its highly upregulated expression was observed only in the RBC group, suggesting that RBC-sEV had been internalized by podocytes (Figure 4B). Similarly, ALPP, the placental alkaline phosphatase (PLAP), was uniquely upregulated in the NP and PE groups, implying that psEV from NP and PE were internalized by podocytes (Figure 4B).



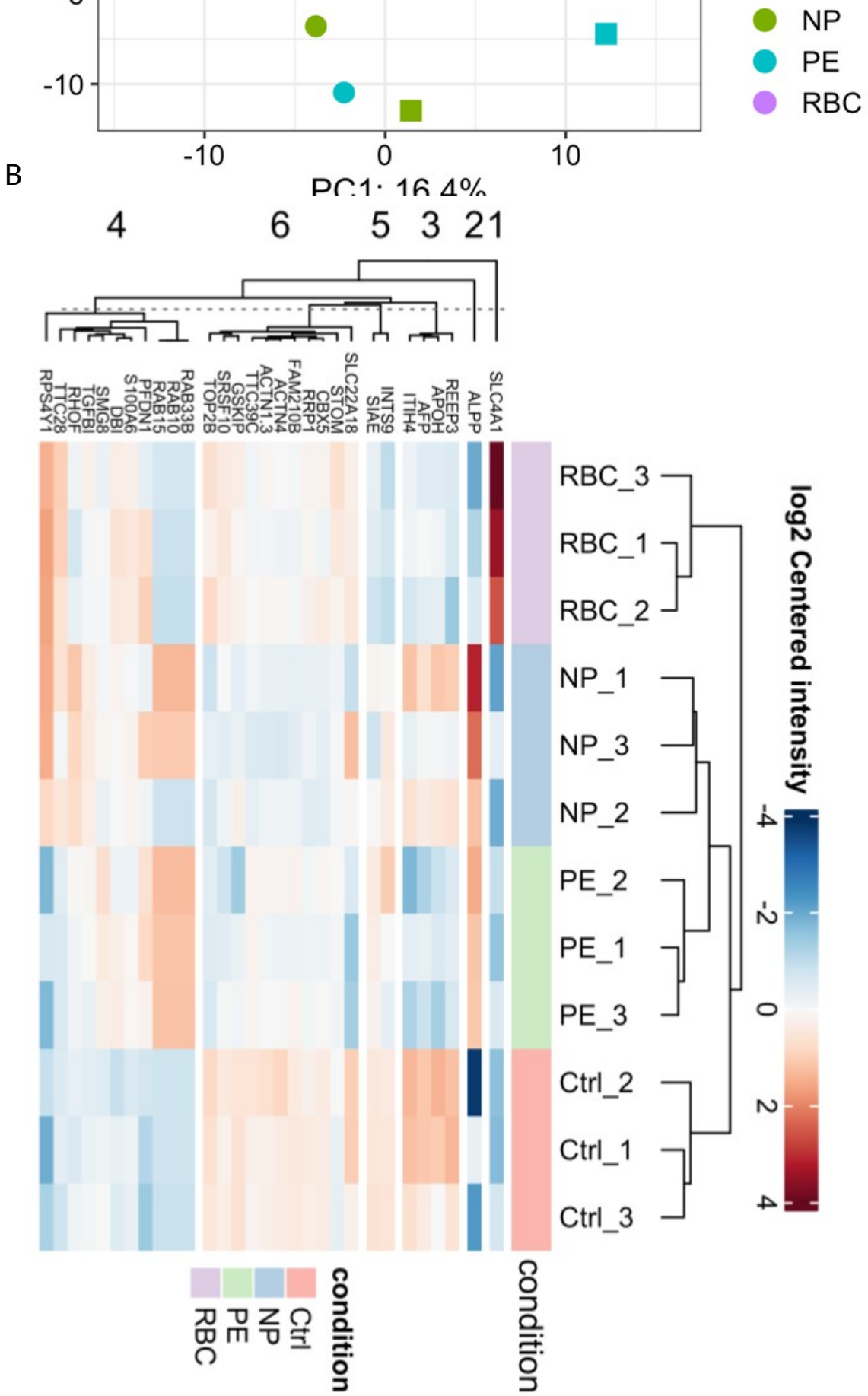
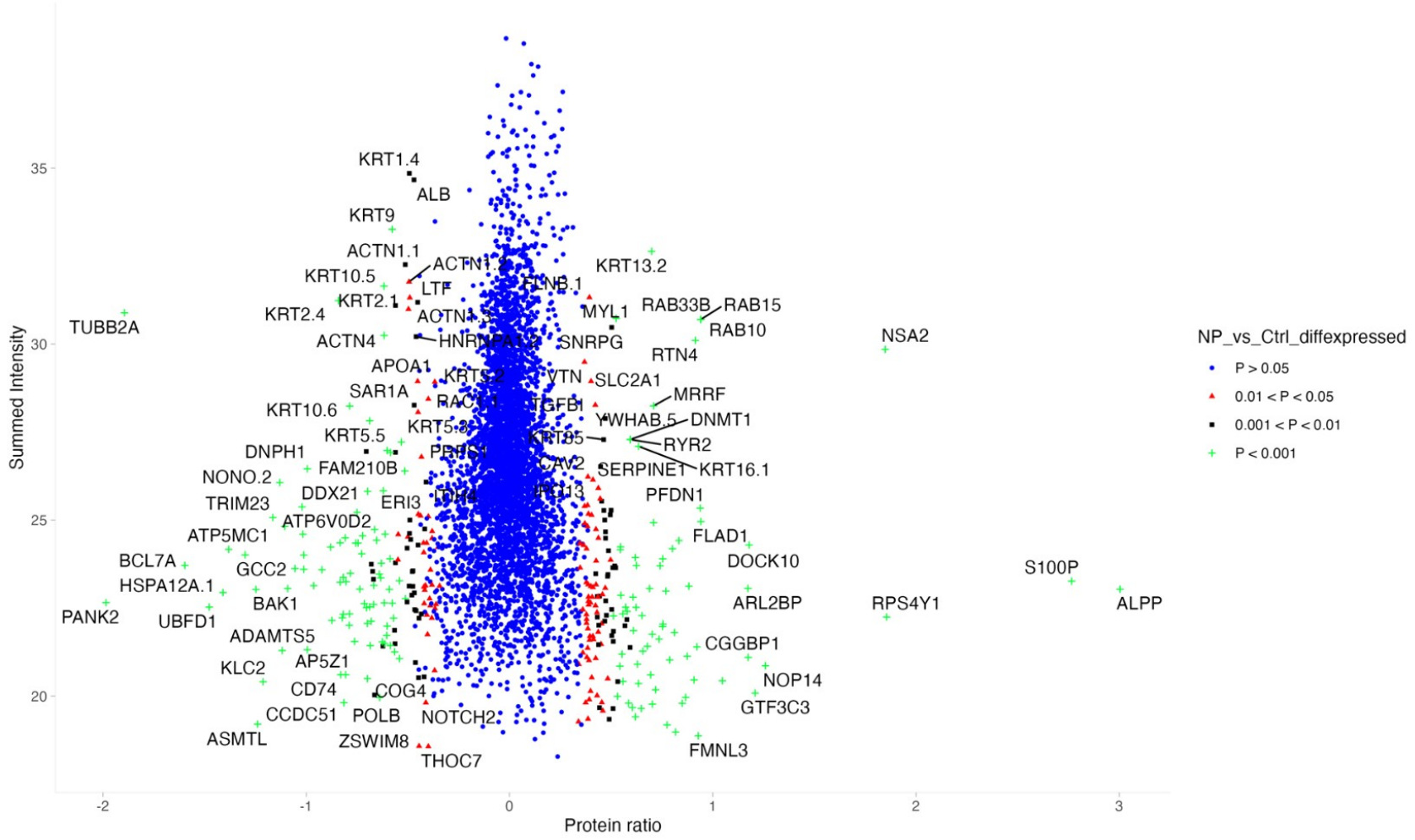
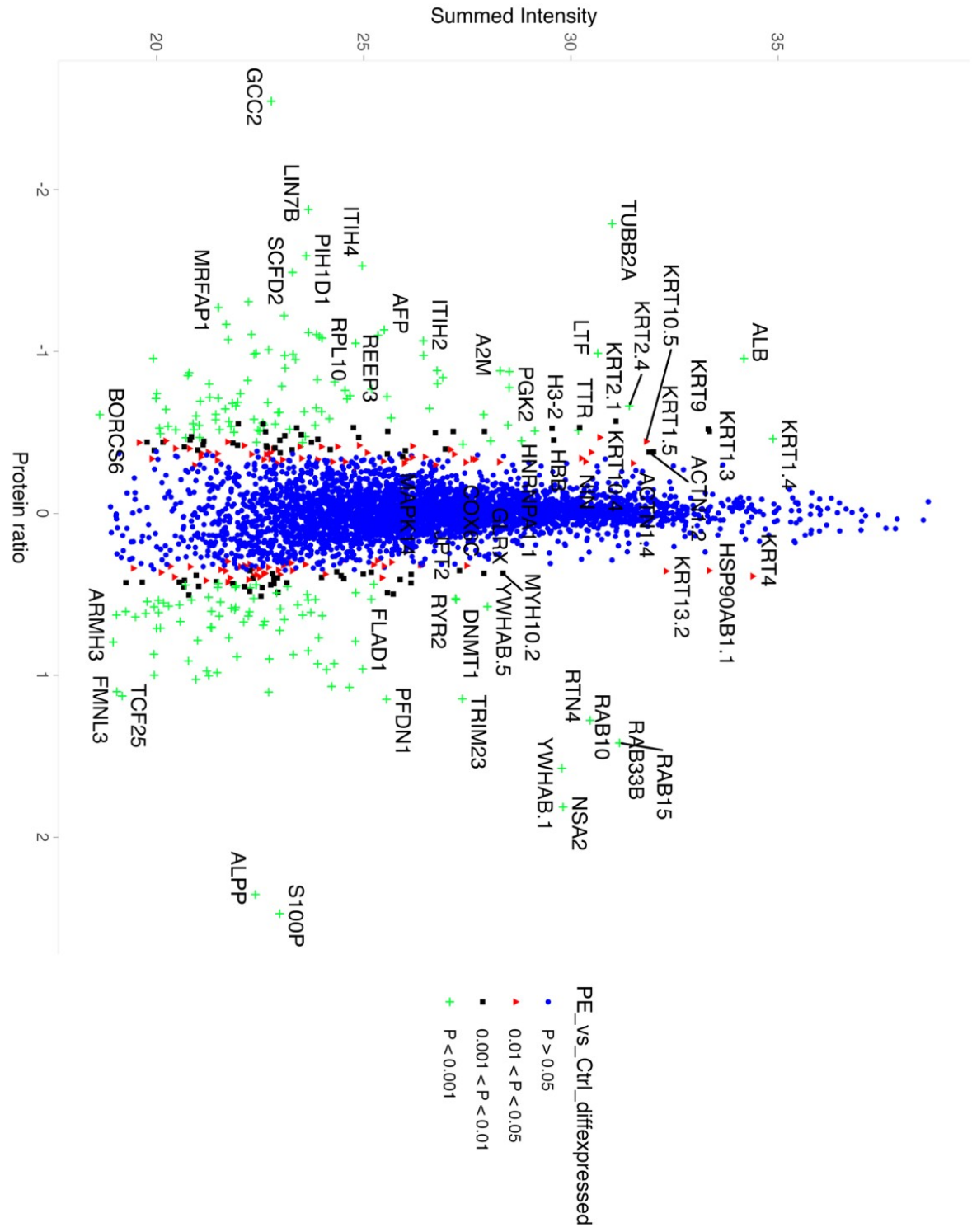

-10
-10
0
10
NP
PE
RBC
B
4
6
5
3
21
SLC4A1
ALPP
REEP3
APOH
AFP
ITIH4
INTS9
SIAE
SLC22A18
STOM
CBX5
RRP1
FAM210B
ACTN4
ACTN1.3
TTC39C
GSKIP
SRSF10
TOP2B
RAB33B
RAB10
RAB15
PFDN1
S100A6
DBI
SMG8
TGFBI
RHOF
TTC28
RPS4Y1
RBC_3
RBC_1
RBC_2
NP_1
NP_3
NP_2
PE_2
PE_1
PE_3
Ctrl_2
Ctrl_1
Ctrl_3
log2 Centered intensity
-4
-2
0
2
4
condition
RBC
PE
NP
Ctrl
condition

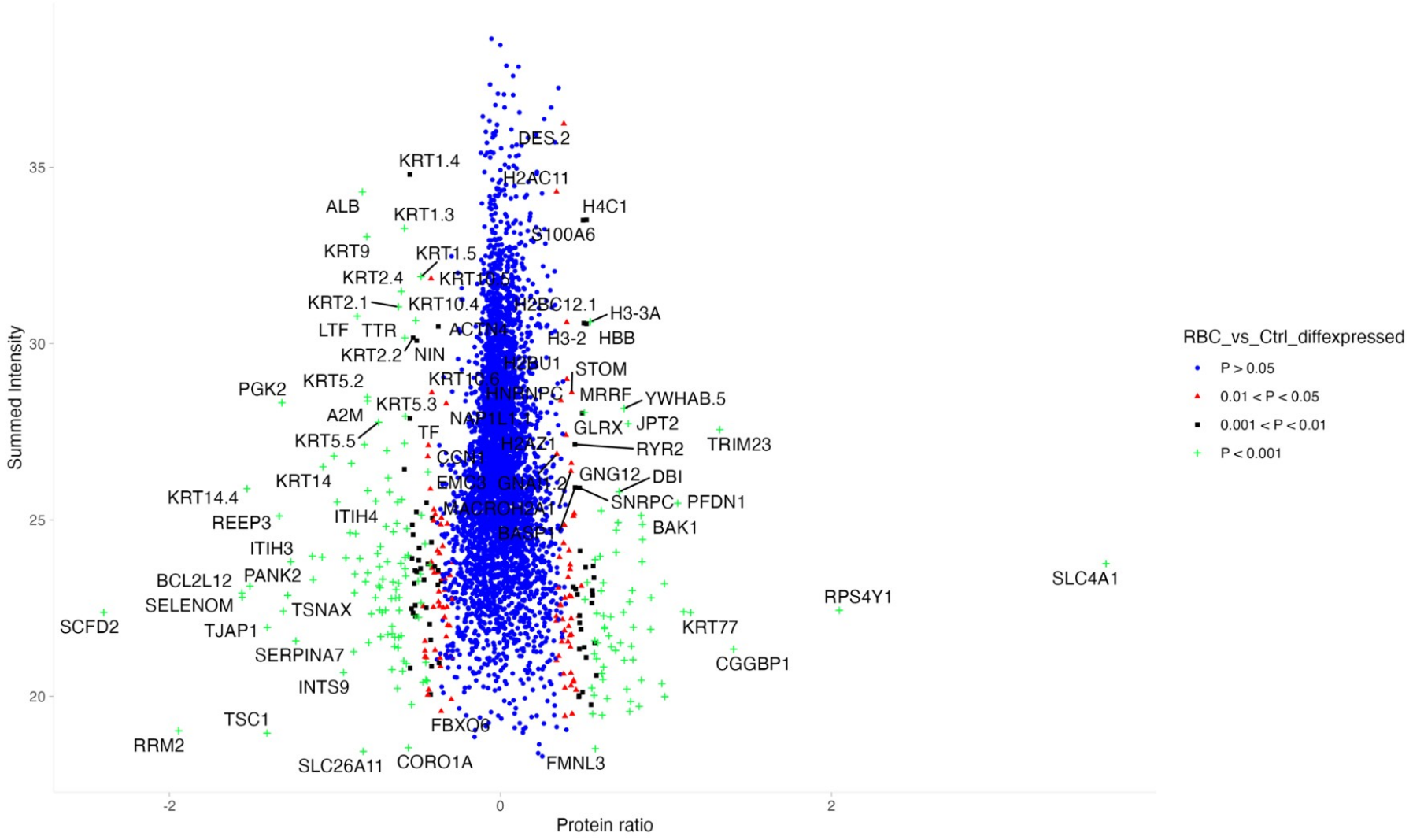
Figure 4. (A) The principal component analysis (PCA) plot of the top 500 proteins. (B) The cluster analysis for each treatment group. Red indicates the upregulated proteins and blue indicates the downregulated proteins.

4.5.4 Differentially expressed proteins (DEPs)

Subsequently, I examined whether there were any differentially expressed proteins in each treatment group compared to the control group. Among the over 4,000 proteins identified in each group, 160 proteins in the NP group (Figure 5A), 197 proteins in the PE group (Figure 5B), and 177 proteins in the RBC group (Figure 5C) were differentially expressed with an adjusted p-value < 0.001 when compared to the control group. Notably, I conducted a comparison between the NP and PE groups to identify DEPs that might potentially be responsible for the distinct podocyte functions observed in NP and PE pregnancies. In this comparison, 208 proteins (105 upregulated proteins, 103 downregulated proteins) were differentially expressed in the PE group with an adjusted p-value < 0.001 when compared to the NP group (Figure 5D).


Summed Intensity
Protein ratio
35
30
25
20
-2
-1
0
1
2
3
KRT1.4
ALB
KRT9
ACTN1.1
KRT10.5
LTF
KRT2.1
KRT2.4
ACTN4
TUBB2A
APOA1
SAR1A
KRT10.6
KRT5.5
DNPH1
FAM210B
NONO.2
DDX21
TRIM23
ATP6V0D2
ATP5MC1
BCL7A
GCC2
HSPA12A.1
BAK1
PANK2
UBFD1
ADAMTS5
KLC2
AP5Z1
CD74
COG4
CCDC51
POLB
NOTCH2
ASMTL
ZSWIM8
THOC7
KRT13.2
MYL1
RAB33B
RAB15
RAB10
RTN4
SNRPG
SLC2A1
MRRF
DNMT1
RYR2
KRT16.1
PFDN1
FLAD1
DOCK10
ARL2BP
CGGBP1
NOP14
GTF3C3
FMNL3
NSA2
RPS4Y1
S100P
ALPP
NP_vs_Ctrl_diffexpressed
P > 0.05
0.01 < P < 0.05
0.001 < P < 0.01
P < 0.001


Summed Intensity
20
25
30
35
Protein ratio
-2
-1
0
1
2
GCC2
LIN7B
SCFD2
PIH1D1
ITIH4
MRFAP1
RPL10
REEP3
AFP
BORCS6
ITIH2
A2M
PGK2
LTF
TTR
H3-2
HBB
TUBB2A
KRT10.5
KRT2.4
KRT2.1
KRT9
KRT1.5
KRT10.4
ACTN1.4
ALB
KRT1.3
KRT1.4
KRT4
HSP90AB1.1
KRT13.2
RAB15
RAB33B
RAB10
RTN4
YWHAB.1
NSA2
MYH10.2
YWHAB.5
DNMT1
TRIM23
RYR2
PFDN1
FLAD1
ARMH3
FMNL3
TCF25
ALPP
S100P
PE_vs_Ctrl_diffexpressed
P > 0.05
0.01 < P < 0.05
0.001 < P < 0.01
P < 0.001


Summed Intensity
35
30
25
20
-2
0
2
Protein ratio
DES.2
KRT1.4
H2AC11
ALB
KRT1.3
H4C1
S100A6
KRT9
KRT1.5
KRT2.4
KRT10.6
KRT2.1
KRT10.4
H2BC12.1
H3-3A
LTF
TTR
ACTN4
H3-2
HBB
KRT2.2
NIN
H2BU1
STOM
PGK2
KRT5.2
KRT10.6
HNRNPC
MRRF
YWHAB.5
KRT5.3
A2M
NAP1L1.1
GLRX
JPT2
KRT5.5
TF
H2AZ1
RYR2
TRIM23
CCN5
GNG12
DBI
KRT14
EMC3
GNAI2
KRT14.4
SNRPC
PFDN1
MACROH2A1
REEP3
ITIH4
BAK1
BASP1
ITIH3
BCL2L12
PANK2
SLC4A1
RPS4Y1
SELENOM
TSNAX
SCFD2
TJAP1
KRT77
SERPINA7
CGGBP1
INTS9
TSC1
FBXO6
RRM2
SLC26A11
CORO1A
FMNL3
RBC_vs_Ctrl_diffexpressed
P > 0.05
0.01 < P < 0.05
0.001 < P < 0.01
P < 0.001

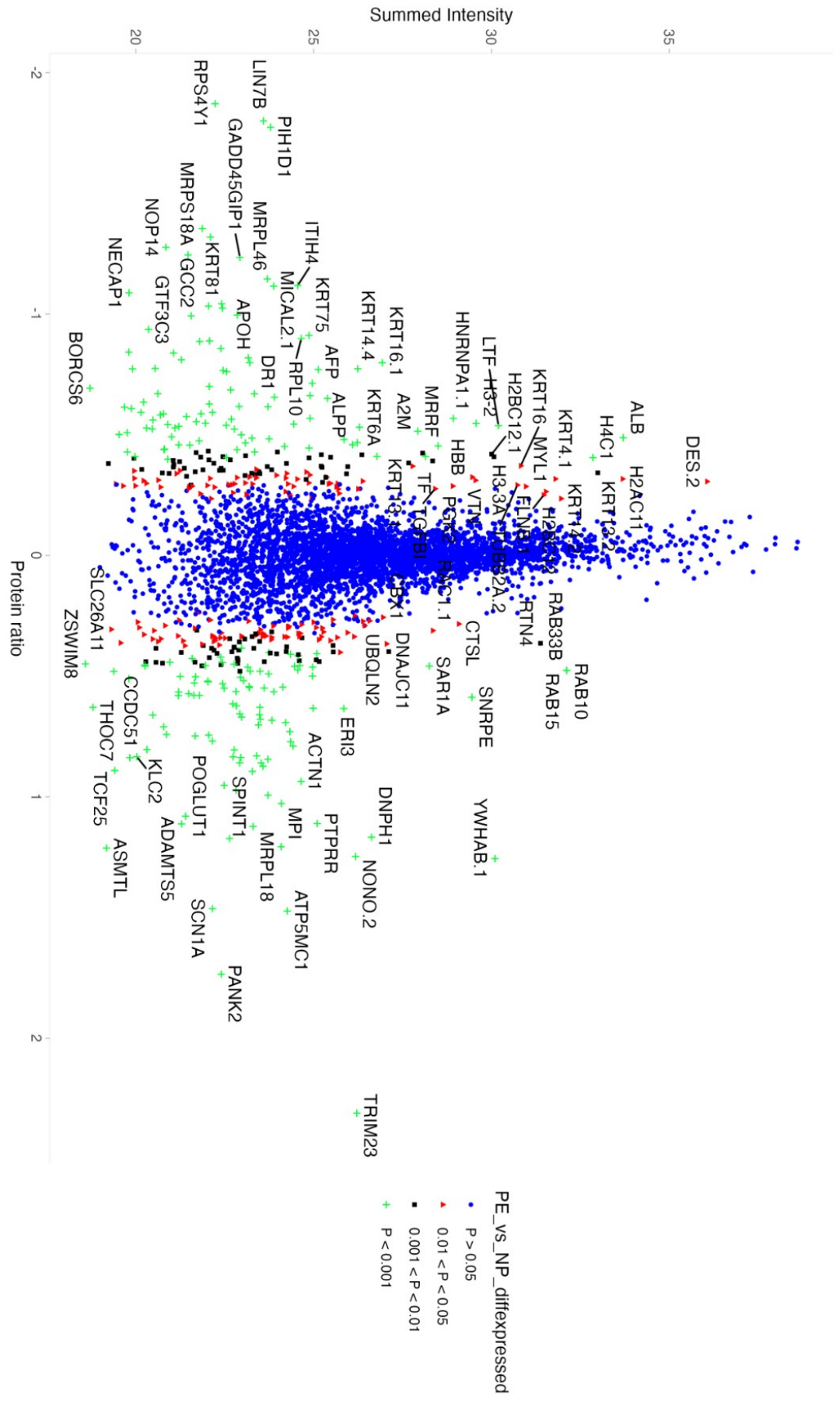

Summed Intensity
Protein ratio
PE_vs_NP_diffexpressed
P > 0.05
0.01 < P < 0.05
0.001 < P < 0.01
P < 0.001
DES.2
ALB
H2AC11
H4C1
KRT13.2
KRT4.1
KRT16
MYL1
H2BC12.1
LTF
H3-2
HNRNPA1.1
HBB
VIM
PGK2
TF
TGFBI
KRT10.1
KRT16.1
A2M
MRRF
KRT14.4
KRT6A
ALPP
AFP
KRT75
ITIH4
MICAL2.1
RPL10
DR1
APOH
MRPL46
GADD45GIP1
PIH1D1
LIN7B
RPS4Y1
KRT81
MRPS18A
GCC2
GTF3C3
NOP14
NECAP1
BORCS6
ZSWIM8
SLC26A11
THOC7
TCF25
CCDC51
KLC2
ASMTL
ADAMTS5
POGLUT1
SCN1A
PANK2
SPINT1
MRPL18
ATP5MC1
MPI
PTPRR
NONO.2
DNPH1
ERI3
ACTN1
YWHAB.1
SNRPE
CTSL
SAR1A
UBQLN2
DNAJC11
CBX1
RAC1.1
RTN4
RAB33B
RAB15
RAB10
TRIM23

Figure 5. (A) The volcano plot of DEPs in NP group compared to control group. (B) The volcano plot of DEPs in PE group compared to the control group. (C) The volcano plot of DEPs in the RBC group compared to the control group. (D) The volcano plot of DEPs in the PE group compared to the NP group. For all figures, the blue dots represent adjusted p-value> 0.05, red triangles represent 0.01 < adjusted p-value < 0.05, black squares represent 0.001 < adjusted p-value < 0.01, and green crosses represent adjusted p-value < 0.0001. The x-axis is the fold changes of the two comparison groups, where the fold change was calculated by the difference of mean log intensity of the two comparison groups. The y-axis is the summed log intensity of the two comparison groups.

For all comparison groups, the top 10 DEPs, ranked by their fold changes, are listed in Table 1. In the NP group compared to the control group, the most upregulated proteins included two placenta-enriched proteins—placental alkaline phosphatase (PLAP) and S100 calcium-binding protein P (S100P)—and three ribosome function-related proteins: ribosomal protein S4 Y-linked 1 (RPS4Y1), NSA2 ribosome biogenesis factor (NSA2), and NOP12 nucleolar protein (NOP14). Simultaneously, the most downregulated proteins included pantothenate kinase 2 (PANK2), Tubulin beta 2A class IIa (TUBB2A), and BAF chromatin remodeling complex subunit (BCL7A).

In the PE group compared to the control group, the most upregulated proteins also encompassed the two placenta-enriched proteins PLAP and S100P, as well as the ribosome function-related protein NSA2. Additionally, Tyrosine 3-monooxygenase/tryptophan 5-monooxygenase activation protein beta (YWHAB) was upregulated. The most downregulated proteins included GRIP and coiled-coil domain containing 2 (GCC2) and Lin-7 homolog B (LIN7B).

In the RBC group compared to the control group, the most upregulated proteins featured one RBC-enriched protein SLC4A1, one ribosomal protein RPS4Y1, and one nuclear protein CGG triplet repeat binding protein 1 (CGGBP1). Meanwhile, the most downregulated proteins consisted of Sec1 family domain containing 2 (SCFD2), ribonucleotide reductase regulatory subunit M2 (RRM2), and BCL2-like 12 (BCL2L12).

Lastly, in the PE group compared to the NP group, the most upregulated proteins included Tripartite motif containing 23 (TRIM23), PANK2, and ATP synthase membrane subunit c locus 1 (ATP5MC1). The most downregulated proteins comprised RPS4Y1, LIN7B, and PIH1D1.

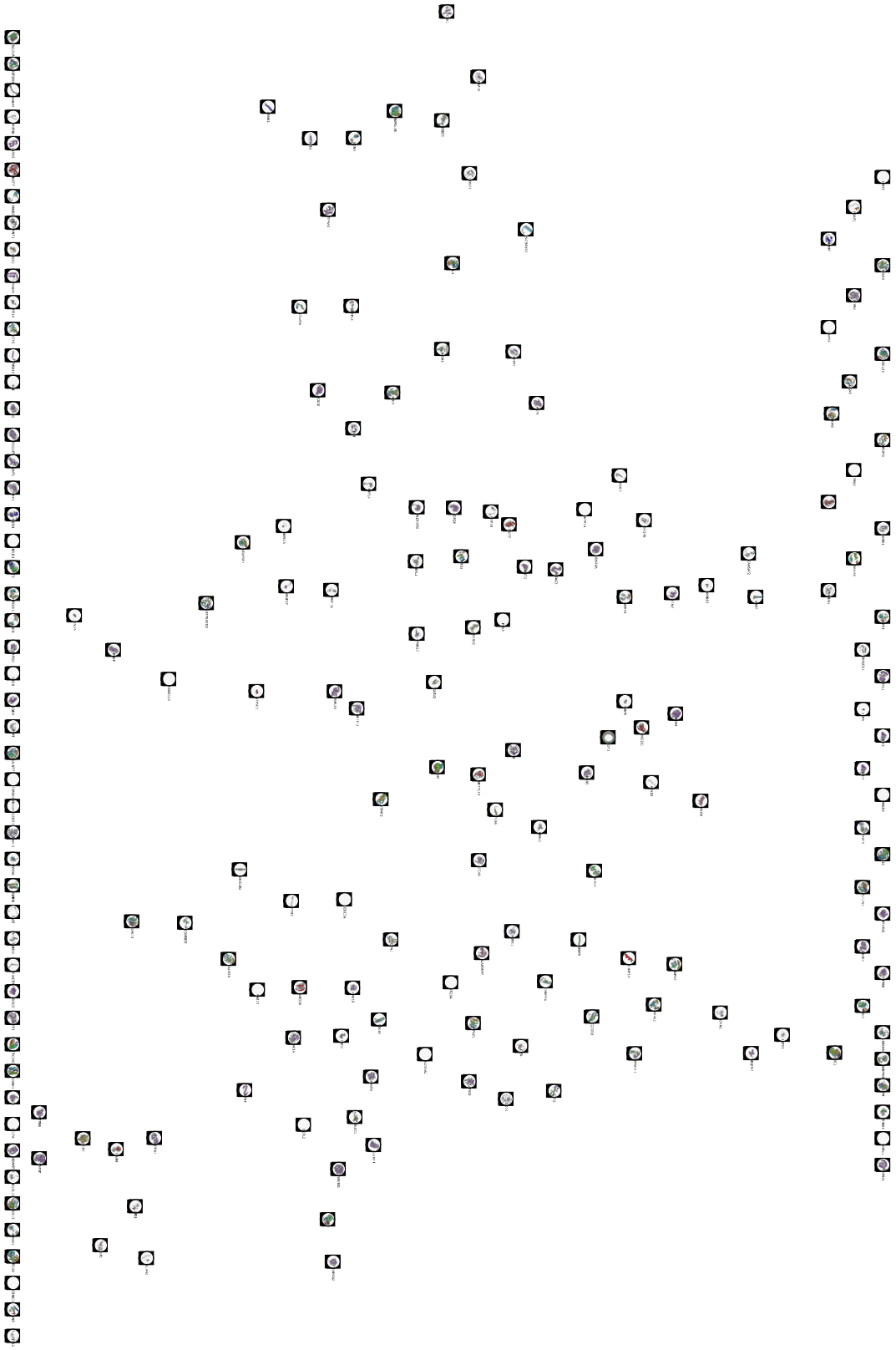
	Protein	Symbol	Fold Change	adjusted p value
NP_vs_Ctrl	Placental alkaline phosphatase	ALPP	3.003513183	5.0512E-117
	S100 calcium binding protein P	S100P	2.765605075	1.90504E-90
	Ribosomal protein S4 Y-linked 1	RPS4Y1	1.855245727	2.02527E-34
	NSA2 ribosome biogenesis factor	NSA2	1.848297099	4.05211E-42
	NOP14 nucleolar protein	NOP14	1.259088031	2.56718E-20
	Pantothenate kinase 2	PANK2	-1.98517578	2.29881E-50
	Tubulin beta 2A class Iia	TUBB2A	-1.894320906	3.21058E-37
	BAF chromatin remodeling complex subunit	BCL7A	-1.597116496	2.20227E-23
	Ubiquitin family domain containing 1	UBFD1	-1.477196491	4.83967E-14
	Heat shock protein family A (Hsp70) member 12A	HSPA12A	-1.409478882	2.86421E-18
PE_vs_Ctrl	S100 calcium binding protein P	S100P	2.471192639	1.26518E-72
	Placental alkaline phosphatase	ALPP	2.353101519	4.84878E-68
	NSA2 ribosome biogenesis factor	NSA2	1.814076897	3.727E-39
	Tyrosine 3-monooxygenase/tryptophan 5-monooxygenase activation protein beta	YWHAB	1.573429938	1.89033E-31
	RAB10, member RAS oncogene family	RAB10	1.417466127	1.39856E-24
	GRIP and coiled-coil domain containing 2	GCC2	-2.545505197	6.9793E-102
	Lin-7 homolog B, crumbs cell polarity complex component	LIN7B	-1.877046428	1.68885E-67
	Tubulin beta 2A class IIa	TUBB2A	-1.78770562	3.53755E-50
	PIH1 domain containing 1	PIH1D1	-1.591369022	1.01855E-39
	Inter-alpha-trypsin inhibitor heavy chain 4	ITIH4	-1.528841644	1.26429E-44
PE_vs_NP	Tripartite motif containing 23	TRIM23	2.310661565	4.58937E-80
	Pantothenate kinase 2	PANK2	1.734684528	2.7285E-61
	ATP synthase membrane subunit c locus 1	ATP5MC1	1.47283101	6.68968E-29
	Sodium voltage-gated channel alpha subunit 1	SCN1A	1.463245631	7.07403E-36
	Tyrosine 3-monooxygenase/tryptophan 5-monooxygenase activation protein beta	YWHAB	1.25607489	4.48123E-21
	Ribosomal protein S4 Y-linked 1	RPS4Y1	-1.871390206	6.139E-74
	Lin-7 homolog B	LIN7B	-1.799879038	4.14608E-59
	PIH1 domain containing 1	PIH1D1	-1.773879004	2.77729E-77
	Mitochondrial ribosomal protein S18A	MRPS18A	-1.354393136	3.75065E-28
	Keratin 81	KRT81	-1.318366843	4.77417E-32
RBC_vs_Ctrl	Solute carrier family 4 member 1	SLC4A1	3.658177103	1.4296E-176
	Ribosomal protein S4 Y-linked 1	RPS4Y1	2.046409456	5.43056E-44
	CGG triplet repeat binding protein 1	CGGBP1	1.408270648	9.17984E-23
	Tripartite motif containing 23	TRIM23	1.324635627	2.11171E-15
	Keratin 77	KRT77	1.149253544	2.84013E-15
	Sec1 family domain containing 2	SCFD2	-2.396743458	4.79992E-71
	Ribonucleotide reductase regulatory subunit M2	RRM2	-1.943575472	2.62222E-46
	BCL2 like 12	BCL2L12	-1.562214264	1.70034E-26
	Selenoprotein M	SELENOM	-1.560499715	7.9487E-46
	Keratin 14	KRT14	-1.531554762	1.7552E-25

Table 1. Top ten DEPs ranked by fold changes in NP group compared to the control group (red), PE group compared to the control group (blue), PE group compared to NP group (purple), and RBC group compared to the control group (black).

4.5.5 Protein-protein-interaction (PPI) and functional enrichment analysis

Upon identifying the DEPs in each comparison group, my next goal was to examine any potential PPIs among these DEPs and conduct a functional enrichment analysis to better understand their roles. To achieve this, DEPs in each comparison group with an adjusted p-value < 0.05 were analysed using the STRING app in Cytoscape. Taking the PE group

compared to the NP group as an example, most DEPs exhibited PPIs with one another, while only a few proteins had no connections (orphan proteins) or limited connections with proteins in the same group (Figure 6A). A similar trend was observed in other comparison groups, where most DEPs had PPIs (data not shown). Subsequently, the largest subnetwork of PPIs was chosen and visually represented with color-coding based on their fold changes (Figure 6B). Interestingly, the mitochondrial large ribosomal subunit protein UL 18m (MRP18) exhibited significant upregulation within the network and occupied a central position with five interactions (Figure 6B). Additionally, the small nuclear ribonucleoprotein polypeptide E (SNPPE) and DNA-directed RNA polymerase II subunit RPB11-a (POLR2J) demonstrated strong interactions with other upregulated proteins, with SNPPE showing 9 connections and POLR2J exhibiting 10 connections, underlining the crucial roles of these two proteins (Figure 6B).



B

Figure 6. (A) PPIs of DEPs (adjusted $p < 0.05$) in PE group compared to NP group. The color-coded nodes are PPIs within the largest subnetwork. The grey color-coded nodes are either orphan proteins or proteins with few interactions. (B) The largest subnetwork of PPIs of DEPs (adjusted $p < 0.05$) in PE group compared to NP group. The nodes were colour-

coded so that higher fold change appeared dark red and lower fold changes appeared light orange.

In order to further understand the roles of proteins in the largest subnetwork, I performed an enrichment analysis for gene ontology: biological process (GO: BP). The function of gene ontology: biological process (GO:BP) is to categorize and describe the biological processes and pathways that genes are involved in, providing valuable insights into the functional roles and relationships of genes within specific biological contexts. For the NP group compared to the control group, 57 GO: BP terms were overrepresented for upregulated proteins and 10 for downregulated proteins. For the PE group compared to the control group, 37 GO: BP terms were overrepresented for upregulated proteins and 81 for downregulated proteins. For the PE group compared to the NP group, 41 GO: BP terms were overrepresented for upregulated proteins and 94 for downregulated proteins. For the RBC group compared to the control group, 40 GO: BP terms were overrepresented for upregulated proteins and 13 for downregulated proteins. For simplicity, the top 5 GO: BP terms, ranked by adjusted p-value for all comparisons, can be found in Figure 7.

When compared to podocytes not treated with small EV, those exposed to NP psEV demonstrated changes in protein expression involved in cellular component organization or biogenesis, intracellular transportation, and mitochondrial functions (Figure 7). In contrast, podocytes treated with PE psEV, in comparison to NP, displayed differences in protein expression related to metabolic processes, nitrogen compound metabolism, and gene expression (Figure 7).

Interestingly, among the 57 overrepresented GO: BP terms for upregulated proteins in the NP group compared to the control group, the term, wound healing process, was identified, which

includes 6 proteins—RAB3A, E1, VTN, FGA, F2, and FGG (Table 3). These proteins may contribute to the increased podocyte migration ability observed after NP psEV treatment in Chapter 3. Similarly, when comparing the PE group directly to the NP group, 12 downregulated DEPs were identified in the wound healing process, including APOH, COL1A1, FGB, FGA, DST, F2, PLEC, A2M, HBB, ANXA6, SERPINC1, and PIK3R1. These downregulated DEPs could explain why the increased podocyte migration ability is observed only after NP psEV treatment, rather than after PE psEV treatment. Two proteins were overlapped in these two comparisons which were FGA and F2.

Among the 81 overrepresented GO: BP terms for downregulated DEPs in the PE group compared to the control group, 3 GO: BP terms involved cell-cell/tight junction assembly. Cell-cell/tight junction proteins play a crucial role in podocyte adhesion ability by facilitating the formation and maintenance of strong adhesive contacts between neighboring cells, ensuring tissue integrity and stability[19]. Within these 3 GO:BP terms, 9 proteins were identified: KRT14, ACTN4, DSG1, MPP5, CLDN1, EPB41L3, DLG1, ACTN2, and LSR (Table 4). These proteins may be responsible for the reduced podocyte adhesion ability observed after PE psEV treatment in Chapter 3.

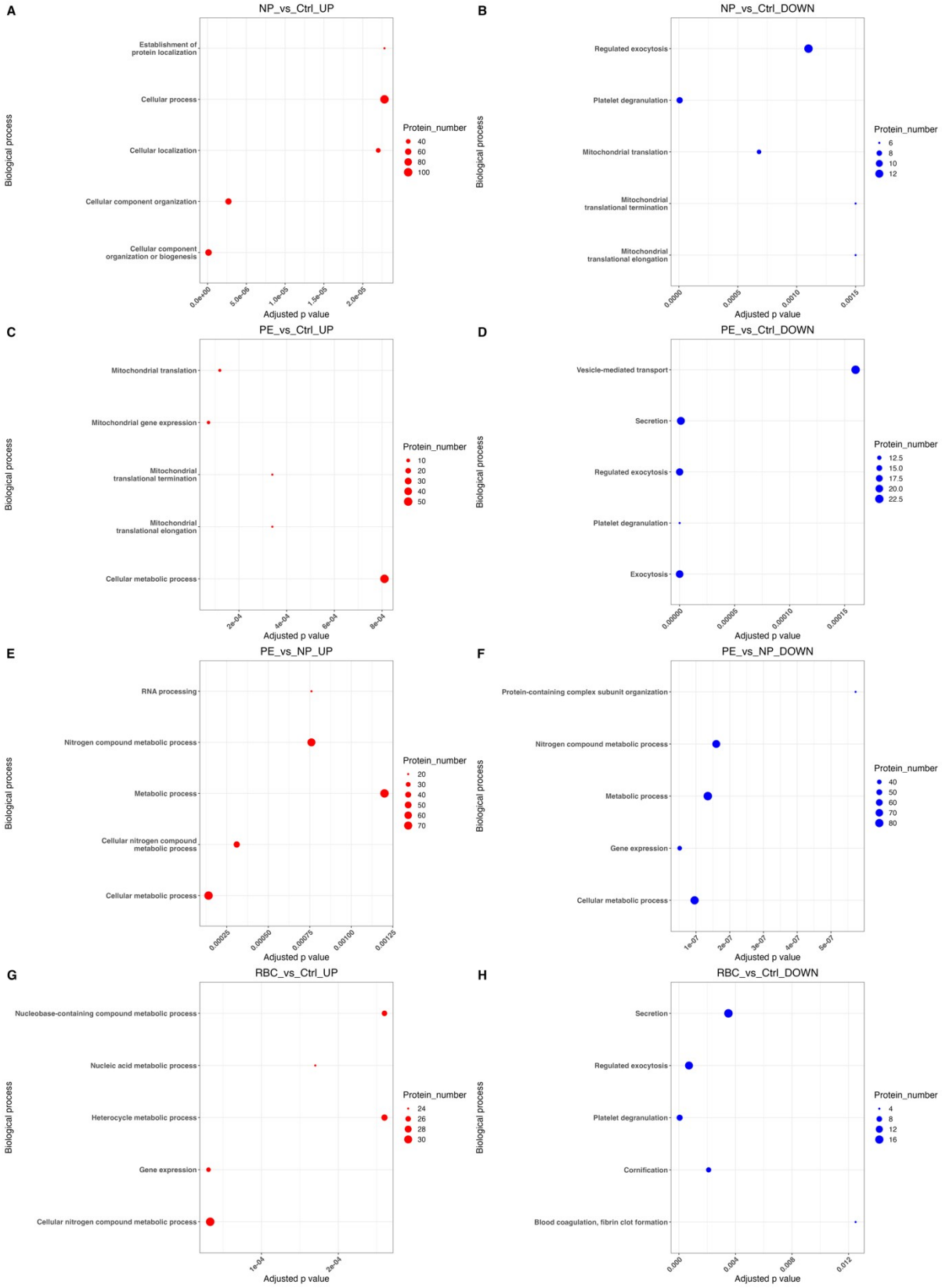


Figure 7. The top 5 functionally enriched proteins in gene ontology: biological process (GO: BP) in each comparison group. (A) The top 5 biological processes (BP) identified using

upregulated DEPs from NP psEV treated podocytes compared to non-treated podocytes. (B) The top 5 BP identified using downregulated DEPs from NP psEV treated podocytes compared to non-treated podocytes. (C) The top 5 BP identified using upregulated DEPs from PE psEV treated podocytes compared to non-treated podocytes. (D) The top 5 BP identified using downregulated DEPs from PE psEV treated podocytes compared to non-treated podocytes. (E) The top 5 BP identified using upregulated DEPs from PE psEV treated podocytes compared to NP psEV treated podocytes. (F) The top 5 BP identified using downregulated DEPs from PE psEV treated podocytes compared to NP psEV treated podocytes. (G) The top 5 BP identified using upregulated DEPs from RBC-sEV treated podocytes compared to non-treated podocytes. (H) The top 5 BP identified using downregulated DEPs from RBC-sEV treated podocytes compared to non-treated podocytes.

Proteins	Name	Function
RAB3A	Ras-related protein Rab-3A	Small GTP-binding protein
SERPINE1	Plasminogen activator	Acts as a regulator of cell migration, independently of its role as protease inhibitor
VTN	Vitronectin	The protein encoded by this gene functions in part as an adhesive glycoprotein. Differential expression of this protein can promote either cell adhesion or migration as it links cells to the extracellular matrix through a variety of ligands.
FGA	Fibrinogen alpha chain	During the early stages of wound repair to stabilize the lesion and guide cell migration during re-epithelialization
F2	Prothrombin	Functions in blood homeostasis, inflammation and wound healing
FGG	Fibrinogen gamma chain	Dunctions during the early stages of wound repair to stabilize the lesion and guide cell migration during re-epithelialization.

Table 3. The 6 upregulated DEPs overrepresented in the GO: BP wound healing process term in the NP group compared to the control group

Description	Adjusted p -value	No. of proteins in terms	Proteins
Cell-cell junction assembly	8.30E-04	7	ACTN4|DSG1|MPP5|CLDN1|EPB41L3|DLG1|LSR
Cell junction assembly	0.001	9	KRT14|ACTN4|DSG1|MPP5|CLDN1|EPB41L3|DLG1|ACTN2|LSR
Tight junction assembly	0.0027	5	ACTN4|MPP5|CLDN1|DLG1|LSR

Table 4. The GO: BP terms in the PE group compared to the control group involves cell/tight junction assembly.

I then aimed to examine the distribution of DEPs in tissues, particularly focusing on whether they originated from the placenta. The goal was to identify proteins in psEV that were transferred from the placenta to podocytes after psEV treatment that may have impact on podocytes. Intriguingly, using an adjusted p-value < 0.05, for the NP group compared to the control group, 16 upregulated DEPs were found to be enriched in the placenta (Figure 8). The top 3 proteins, ranked by fold changes, were reticulon 4 (RTN4), versican (VCAN), and prefoldin subunit 5 (PFDN5). Furthermore, directly comparing PE psEV treated podocytes to NP psEV treated podocytes, 21 downregulated DEPs in this comparison group were identified in the placenta (Figure 9). This suggests a potential deficiency in the transfer of these proteins from PE psEV to podocytes, which could contribute to the observed downregulated podocyte functions in PE.

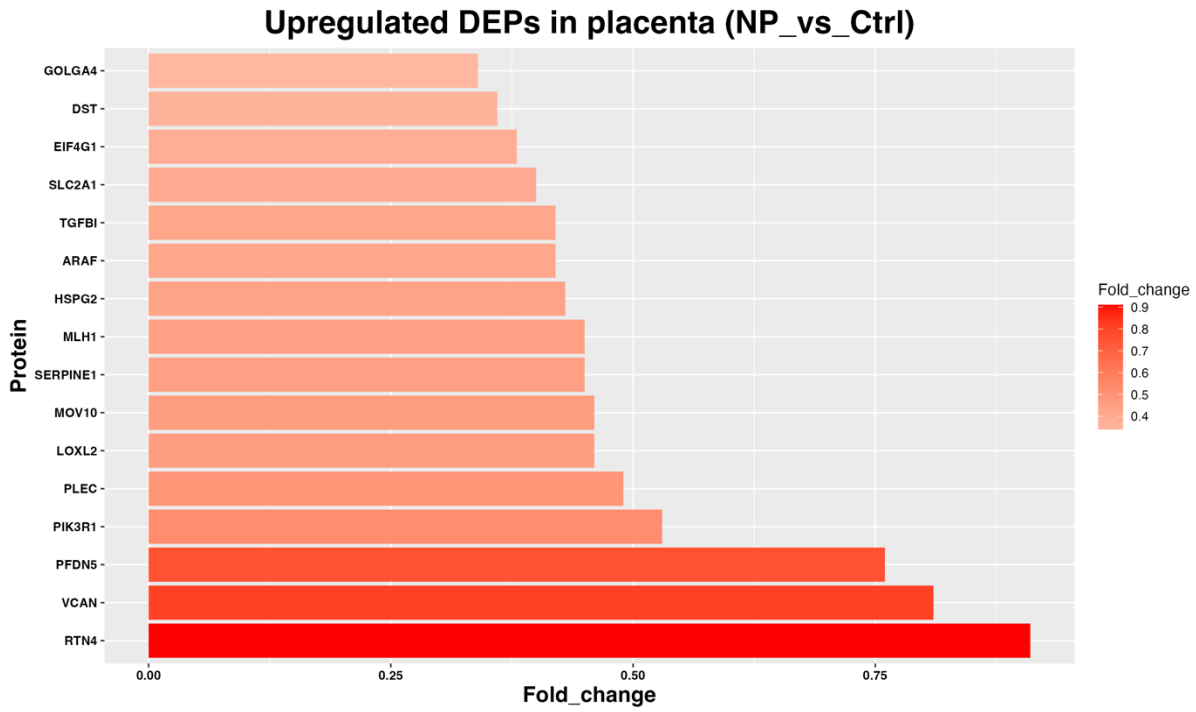


Figure 8. The 16 upregulated DEPs in the NP psEV treated podocytes compared to the control group are located at the placenta. The x-axis is Log_2 fold change of comparing NP psEV treated podocytes to podocytes with no treatment (the control group). The y-axis is the protein name.

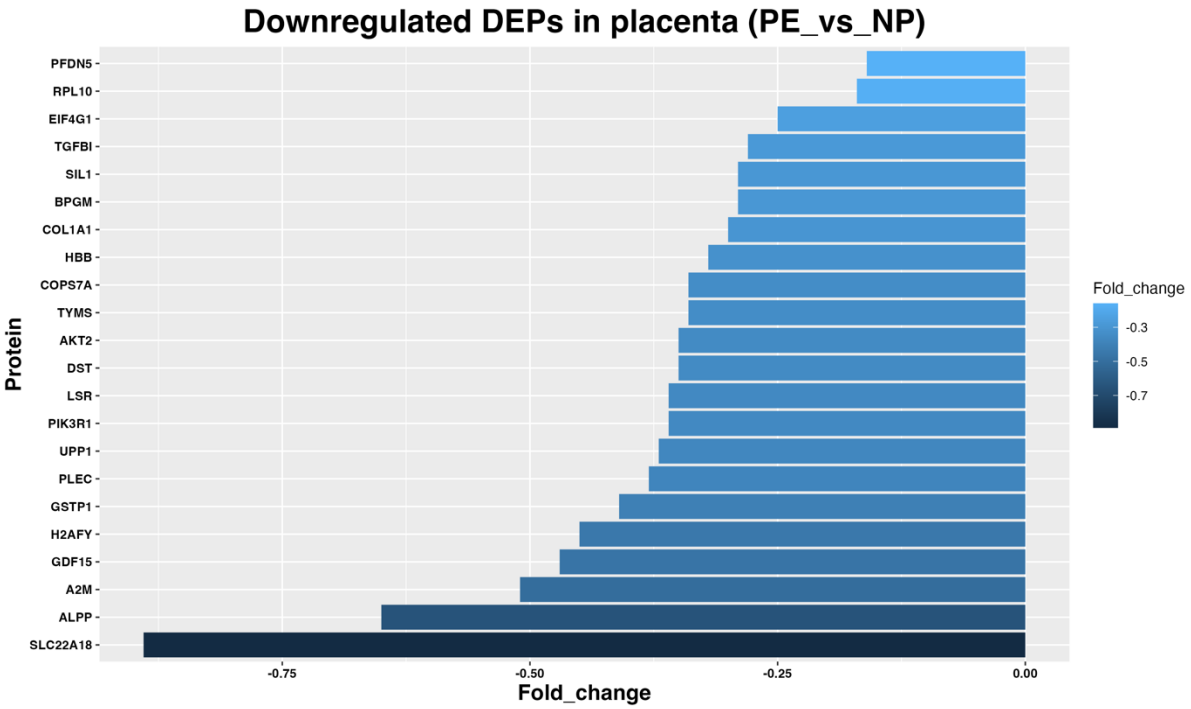


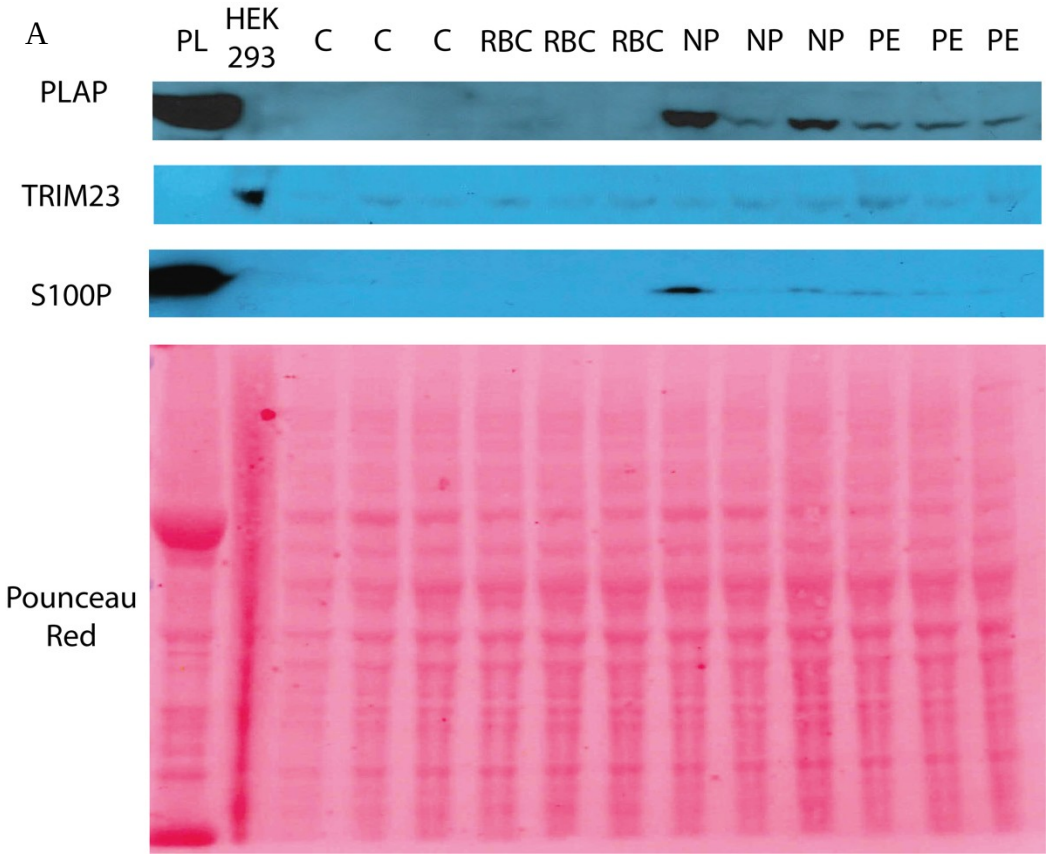
Figure 9. The downregulated DEPs in the PE psEV treated podocytes compared to the NP psEV treated podocytes that were located at the placenta.

4.5.6 DEPs validation through western blot

After conducting the above bioinformatic analysis, three DEPs proteins were selected for further validation. PLAP and S100P were chosen due to being the top two DEPs in NP psEV and PE psEV treated podocytes compared to the control (Table 1), and their presence in podocytes after being treated with psEV could suggest internalisation of psEV. The expression of PLAP and S100P was observed in both NP and PE psEV treated podocytes, with varying levels of expression indicating different amounts of psEV internalised (Figure 10 A & B). This also suggests that psEV may contain S100P and to my best knowledge, the presence of S100P on psEV has not been previously reported, making it potentially intriguing for future investigation.

Another DEP tested was TRIM23, which was the top one DEPs in PE psEV treated podocytes compared to NP psEV treated podocytes (Table 1, fold change = 2.3). TRIM23, an important member of TRIM family, is a unique TRIM protein that possesses both E3 ubiquitin ligase and GTPase enzymatic activities, participating in multiple cell signalling pathways[20]. TRIM23 was expressed in podocytes without any EV treatment, as well as in RBC-sEV and NP and PE psEV treated podocytes (Figure 10A). There was a trend that the level of TRIM23 expression was higher in PE psEV treated podocytes, but not significantly different from NP psEV treated podocytes (p = 0.1, Figure 10B).

A



B

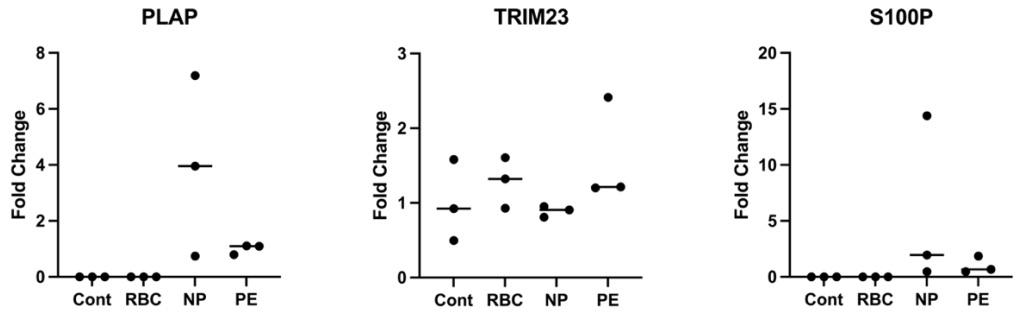


Figure 10. (A) The western blot results of PLAP (66 kDa), Trim23 (64 kDa), S100P (10 kDa) and the ponceau red (represents total protein) for the control podocytes (C), RBC-sEV treated podocytes (RBC), NP-psEV treated podocytes (NP) and PE-psEV treated podocytes (PE). PL denotes placenta lysate and is the positive control for PLAP and S100P. HEK293 cell lysate is the positive control for TRIM23. (B) The same results from (A) were analysed by Image J. For TRIM23, the fold change was normalised to the control group. For PLAP and S100P, the fold change was normalised to the PE-psEV treated group. The statistical analysis comparing NP and PE psEV treated podocytes was done using the Mann-Whitney test.

4.6 Discussion & Future work

This study represents the first proteomics analysis of podocytes influenced by normal and preeclamptic placental small extracellular vesicle (psEV), providing insight into potential biomarkers and mechanisms for investigating podocyte function under normal pregnancy (NP) and preeclampsia (PE). Out of over 4,000 identified proteins, analysis of differentially expressed podocyte proteins revealed distinct biological processes responsible for podocyte function under non-pregnant, NP, and PE conditions. Notably, when compared to podocytes not treated with small EV, those exposed to NP psEV demonstrated changes in protein expression involved in cellular component organization or biogenesis, intracellular transportation, and mitochondrial functions. In contrast, podocytes treated with PE psEV, in comparison to NP, displayed differences in protein expression related to metabolic processes, nitrogen compound metabolism, and gene expression. Intriguingly, the analysis of these differentially expressed proteins has highlighted potential drivers for the observed enhancement of podocyte migration following NP psEV treatment, as well as the diminished adhesion ability after PE psEV treatment, as previously detailed in Chapter 3.

Compared to the control, there were 6 upregulated DEPs that might be responsible for the upregulated podocyte migration ability following treatment with NP psEV (Table 3). Among these 6 DEPs, two proteins have been extensively studied. Ras-related protein Rab-3A (RAB3A) is a synaptic vesicle protein which belongs to the Rab family of guanosine triphosphate (GTP) hydrolases[21]. Its effector is Rabphilin-3A which binds to RAB3A in its

GTP-bound state and this complex is important for Ca^{2+}-dependent neurotransmitter release and the correct docking of synaptic vesicles to their target membrane[21]. This complex also plays a role in regulating the actin cytoskeleton, and both RAB3A and rabpilin-3A are exclusively present in podocytes in the kidney[22,23]. Knockout of RAB3A has been shown to result in podocyte damage and proteinuria[24]. Another DEP that has been studied is plasminogen activator inhibitor 1 (SERPINE1). SERPINE1 can regulate the actin cytoskeleton via α actinin 4 (ACTN4) of podocyte [25]. Dynamic modulation of ACTN4 and actin interactions is required for podocyte functions[26]. It is possible that the placenta releases psEV in NP that can regulate the expression of RAB3A and SERPINE1 on podocytes and further influence the actin cytoskeleton. In contrast, inadequate expression of RAB3A and SERPINE1 in PE may lead to podocyte damage and proteinuria.

Podocyte adhesion ability is crucial for proper podocyte function, and reduced adhesion ability is a hallmark of preeclampsia with proteinuria[12]. Epithelial cells, including podocytes, rely on cell-cell adhesions to their neighbours to bear the mechanical stresses and exert their barrier functions[27]. Loss of cell-cell adhesion molecules can result in the loss of glomerular barrier integrity and subsequent proteinuria. There were 9 downregulated DEPs involved in the regulation of cell-cell junction assembly and tight junction assembly after PE psEV treatment (Table 4), and several of them have shown their importance in podocyte adhesion. ACTN4 interacts with integrins and is required for podocyte adhesion through recruiting SH2-containing protein tyrosine phosphatase 2 (Shp2) and activation of Rho-associated protein kinase 2 (ROCK2)[28,29]. Erythrocyte membrane protein band 4.1 like 3 (EPB41L3) can be detected in the podocyte integrin adhesion complexes using mass spectrometry[30]. And EPB41L3 interacts with F-actin and the lack of its expression can lead to impaired cell adhesion[31]. Desmoglein 2 (DGS2), an integral component of desmosomes, interacts with

desmosomal cadherin desmocollin-2 and other classical cadherins such as E-cadherin and N-cadherin[32]. However, DGS2 is not expressed on mature podocytes, suggesting DGS2 may not play an important role in podocyte adhesion[33]. Claudin-1 (CLND1) belongs to the claudin family of proteins and it is important for determining the podocyte cell junction fate by facilitating silt diaphragm transition to tight junction[34]. CLND1 expression is lost after podocyte maturation based on animal studies, such as mice[35]. However, its expression and functions in the human podocytes have not been fully elucidated.

Ribosomal protein S4 Y-linked 1 (RPS4Y1). RPS4Y1 was 1.8-fold upregulated after NP psEV treatment and 2-fold upregulated after RBC-sEV treatment when compared to the control group. However, the expression of RPS4Y1 was downregulated in podocytes after PE psEV treatment when compared to the NP psEV treatment. The inadequate expression of RPS4Y1 might play an important role in podocyte injury in PE. According to THE HUMAN PROTEIN ATLAS (https://www.proteinatlas.org/ENSG00000129824-RPS4Y1), RPS4Y1 is expressed in various tissues which include the placenta and the kidney, and the level is higher in the placenta. Therefore, it is hard to conclude if the upregulated expression of RPS4Y1 is due to the direct transfer from the placenta via psEV or originated from the podocytes via psEV stimulation. Evidence suggests that the expression of RPS4Y1 is upregulated in preeclamptic placentas when compared to normal pregnancy[36]. However, the lack of upregulated RPS4Y1 expression after PE psEV treated podocytes might be due to several reasons. First, though RPS4Y1 is upregulated in the PE placenta, its expression in psEV is still unknown. The difference of RPS4Y1 expression in podocytes after psEV treatment might the consequence of the RPS4Y1 different levels in psEV. Second, the change of RPS4Y1 expression might be triggered by other mechanisms of psEV treatment rather than directly being transferred into the podocytes. While the function of RPS4Y1 is not very clear,

evidence suggests it may involve in the regulation of cell migration and epithelial-mesenchymal transitions (EMTs)[36], which are mechanisms that can lead to lead to podocyte dysfunction and proteinuria[37]. The current study is the first one to address RPS4Y1 might be involved in the mechanism of podocyte injury in PE.

In this current study, I demonstrated the effective internalisation of psEV derived from PE and NP into the podocytes by detecting the presence of placenta-enriched/specific proteins such as PLAP and S100P, in treated podocytes. Investigating the effects of introducing high levels of these placenta-enriched proteins into podocytes could be intriguing. Alkaline phosphatase placental type (ALPP) is also known as placental alkaline phosphatase (PLAP) is highly and mainly expressed on placenta syncytiotrophoblast[38]. Its expression increases throughout the pregnancy and adequate expression serving as an indication of a healthy foetus[38-40]. PLAP is a type of alkaline phosphatase that hydrolyses various monophosphate esters[41]. Though the three-dimensional structure and function domains of PLAP has been well described before, the biological functions of PLAP are still not clear[42]. Of the four different genes encoding the alkaline phosphate (intestinal, placental, germ cell, and nonspecific tissue types), the human kidney contains tissue with non-specific alkaline phosphatase (TNAP) and it is expressed mainly in tubules not in glomeruli[43,44]. No evidence suggests that podocytes express TNAP. Investigating the effects of introducing nearly 3-fold higher PLAP into podocytes via psEV could be intriguing. Another placenta-enriched protein, S100 calcium binding protein P (S100P), was also upregulated in podocytes after being treated with psEV. The expression of S100P is almost exclusive in the placenta and plays a crucial role in regulating the implantation window during pregnancy[45,46]. It can also stimulate cell migration[47], potentially contributing to the increased podocyte migration ability observed after NP psEV treatment. Interestingly, compared to NP, 24 downregulated DEPs were enriched in the placenta after being treated with PE psEV (Figure 9). These DEPs might be

responsible for the inadequate adaptation of podocytes in PE due to insufficient signalling from the placenta.

TRIM23 is a unique TRIM protein that possesses both E3 ubiquitin ligase and GTPase enzymatic activities[20]. E3 ubiquitin ligase is important for ubiquitination, a post-translational modification that affects various cellular processes, such as protein degradation, DNA repair and signal transduction[48]. The GTPase enzymatic activities of TRIM23 can stimulate GTP hydrolysis and are important in cargo recruitment and autophagy[20]. This is the first study that demonstrates the presence of TRIM23 on podocytes and suggests that its expression could be impacted by psEV (Figure 10B). Though the presence and functions of TRIM23 on podocytes have not been studied, other TRIM proteins which contain E3 ubiquitin ligase have provided insights into renal functions. For example, TRIM31, an E3 ubiquitin ligase, serves as an important regulator in hypertensive nephropathy by inhibiting the TGF-β1 signalling pathway[49]. Similarly, TRIM18, also an E3 ubiquitin ligase, modulates the signal transducer and activator of transcription 3 (STAT3) signalling pathway, promoting renal epithelial-mesenchymal transition[50]. Exploring whether TRIM23 influenced podocytes through similar pathways and its roles under the influence of psEV would be interesting.

In conclusion, I have identified the significantly differentially expressed proteins of podocytes after being treated with psEV from NP and PE. Some of the DEPs are transferred from the placenta while others might be originated from podocytes. These DEPs play a role in the changes observed in the migration, adhesion and metabolic ability of podocytes, offering potential mechanistic pathways that help decipher the mechanisms of renal damage in PE.

4.7 References

1. Rana S, Lemoine E, Granger JP, Karumanchi SA. Preeclampsia. *Circulation Research*. 2019;124:1094-1112. doi: doi:10.1161/CIRCRESAHA.118.313276
2. Cornelis T, Odutayo A, Keunen J, Hladunewich M. The kidney in normal pregnancy and preeclampsia. *Semin Nephrol*. 2011;31:4-14. doi: 10.1016/j.semnephrol.2010.10.002
3. Homer CS, Brown MA, Mangos G, Davis GK. Non-proteinuric pre-eclampsia: a novel risk indicator in women with gestational hypertension. *J Hypertens*. 2008;26:295-302. doi: 10.1097/HJH.0b013e3282f1a953
4. Page EW, Christianson R. Influence of blood pressure changes with and without proteinuria upon outcome of pregnancy. *American Journal of Obstetrics and Gynecology*. 1976;126:821-833. doi: https://doi.org/10.1016/0002-9378(76)90671-2
5. Genest DS, Dal Soglio D, Girard S, Rey E. Association between proteinuria and placental pathology in preeclampsia: A retrospective study. *SAGE Open Med*. 2021;9:20503121211058053. doi: 10.1177/20503121211058053
6. Bramham K, Poli-de-Figueiredo CE, Seed PT, Briley AL, Poston L, Shennan AH, Chappell LC. Association of proteinuria threshold in pre-eclampsia with maternal and perinatal outcomes: a nested case control cohort of high risk women. *PLoS One*. 2013;8:e76083. doi: 10.1371/journal.pone.0076083
7. Gaber LW, Spargo BH, Lindheimer MD. Renal pathology in pre-eclampsia. *Baillieres Clin Obstet Gynaecol*. 1987;1:971-995. doi: 10.1016/s0950-3552(87)80045-7
8. Stillman IE, Karumanchi SA. The Glomerular Injury of Preeclampsia. *Journal of the American Society of Nephrology*. 2007;18:2281. doi: 10.1681/ASN.2007020255
9. Fishel Bartal M, Lindheimer MD, Sibai BM. Proteinuria during pregnancy: definition, pathophysiology, methodology, and clinical significance. *Am J Obstet Gynecol*. 2022;226:S819-s834. doi: 10.1016/j.ajog.2020.08.108
10. Dong X, Gou W, Li C, Wu M, Han Z, Li X, Chen Q. Proteinuria in preeclampsia: Not essential to diagnosis but related to disease severity and fetal outcomes. *Pregnancy Hypertension: An International Journal of Women's Cardiovascular Health*. 2017;8:60-64. doi: https://doi.org/10.1016/j.preghy.2017.03.005
11. Mateus J, Newman R, Sibai BM, Li Q, Barton JR, Combs CA, Guzman E, Boggess KA, Gyamfi C, von Dadelszen P, et al. Massive Urinary Protein Excretion Associated with Greater Neonatal Risk in Preeclampsia. *AJP Rep*. 2017;7:e49-e58. doi: 10.1055/s-0037-1601866
12. Craici IM, Wagner SJ, Bailey KR, Fitz-Gibbon PD, Wood-Wentz CM, Turner ST, Hayman SR, White WM, Brost BC, Rose CH, et al. Podocyturia predates proteinuria and clinical features of preeclampsia: longitudinal prospective study. *Hypertension*. 2013;61:1289-1296. doi: 10.1161/hypertensionaha.113.01115
13. Penning ME, Bloemenkamp KW, van der Zon T, Zandbergen M, Schutte JM, Bruijn JA, Bajema IM, Baelde HJ. Association of preeclampsia with podocyte turnover. *Clin J Am Soc Nephrol*. 2014;9:1377-1385. doi: 10.2215/cjn.12811213

14. Zhao S, Gu X, Groome LJ, Wang Y. Decreased nephrin and GLEPP-1, but increased VEGF, Flt-1, and nitrotyrosine, expressions in kidney tissue sections from women with preeclampsia. *Reprod Sci*. 2009;16:970-979. doi: 10.1177/1933719109338630
15. Garg P. A Review of Podocyte Biology. *Am J Nephrol*. 2018;47 Suppl 1:3-13. doi: 10.1159/000481633
16. Zhang X, Smits AH, van Tilburg GB, Ovaa H, Huber W, Vermeulen M. Proteome-wide identification of ubiquitin interactions using UbIA-MS. *Nat Protoc*. 2018;13:530-550. doi: 10.1038/nprot.2017.147
17. Cox J, Mann M. MaxQuant enables high peptide identification rates, individualized p.p.b.-range mass accuracies and proteome-wide protein quantification. *Nat Biotechnol*. 2008;26:1367-1372. doi: 10.1038/nbt.1511
18. Shannon P, Markiel A, Ozier O, Baliga NS, Wang JT, Ramage D, Amin N, Schwikowski B, Ideker T. Cytoscape: a software environment for integrated models of biomolecular interaction networks. *Genome Res*. 2003;13:2498-2504. doi: 10.1101/gr.1239303
19. Eftekhari A, Vahed SZ, Kavetskyy T, Rameshrad M, Jafari S, Chodari L, Hosseiniyan SM, Derakhshankhah H, Ahmadian E, Ardalan M. Cell junction proteins: Crossing the glomerular filtration barrier in diabetic nephropathy. *Int J Biol Macromol*. 2020;148:475-482. doi: 10.1016/j.ijbiomac.2020.01.168
20. Sparrer KMJ, Gableske S, Zurenski MA, Parker ZM, Full F, Baumgart GJ, Kato J, Pacheco-Rodriguez G, Liang C, Pornillos O, et al. TRIM23 mediates virus-induced autophagy via activation of TBK1. *Nat Microbiol*. 2017;2:1543-1557. doi: 10.1038/s41564-017-0017-2
21. Takai Y, Sasaki T, Shirataki H, Nakanishi H. Rab3A small GTP-binding protein in Ca(2+)-dependent exocytosis. *Genes Cells*. 1996;1:615-632. doi: 10.1046/j.1365-2443.1996.00257.x
22. Kato M, Sasaki T, Ohya T, Nakanishi H, Nishioka H, Imamura M, Takai Y. Physical and functional interaction of rabphilin-3A with alpha-actinin. *J Biol Chem*. 1996;271:31775-31778. doi: 10.1074/jbc.271.50.31775
23. Rastaldi MP, Armelloni S, Berra S, Li M, Pesaresi M, Poczewski H, Langer B, Kerjaschki D, Henger A, Blattner SM, et al. Glomerular podocytes possess the synaptic vesicle molecule Rab3A and its specific effector rabphilin-3a. *Am J Pathol*. 2003;163:889-899. doi: 10.1016/s0002-9440(10)63449-9
24. Marelja Z, Simons M. Filling the Gap: Drosophila Nephrocytes as Model System in Kidney Research. *J Am Soc Nephrol*. 2019;30:719-720. doi: 10.1681/asn.2019020181
25. Zhao X, Khurana S, Charkraborty S, Tian Y, Sedor JR, Bruggman LA, Kao HY. α Actinin 4 (ACTN4) Regulates Glucocorticoid Receptor-mediated Transactivation and Transrepression in Podocytes. *J Biol Chem*. 2017;292:1637-1647. doi: 10.1074/jbc.M116.755546
26. Michaud JL, Hosseini-Abardeh M, Farah K, Kennedy CR. Modulating alpha-actinin-4 dynamics in podocytes. *Cell Motil Cytoskeleton*. 2009;66:166-178. doi: 10.1002/cm.20339
27. Braga VM. Cell-cell adhesion and signalling. *Curr Opin Cell Biol*. 2002;14:546-556. doi: 10.1016/s0955-0674(02)00373-3
28. Dandapani SV, Sugimoto H, Matthews BD, Kolb RJ, Sinha S, Gerszten RE, Zhou J, Ingber DE, Kalluri R, Pollak MR. Alpha-actinin-4 is required for normal podocyte adhesion. *J Biol Chem*. 2007;282:467-477. doi: 10.1074/jbc.M605024200
29. Tseng CC, Zheng RH, Lin TW, Chou CC, Shih YC, Liang SW, Lee HH. α-Actinin-4 recruits Shp2 into focal adhesions to potentiate ROCK2 activation in podocytes. *Life Sci Alliance*. 2022;5. doi: 10.26508/lsa.202201557

30. Randles MJ, Lausecker F, Humphries JD, Byron A, Clark SJ, Miner JH, Zent R, Humphries MJ, Lennon R. Basement membrane ligands initiate distinct signalling networks to direct cell shape. *Matrix Biol*. 2020;90:61-78. doi: 10.1016/j.matbio.2020.02.005
31. Wang J, Song J, An C, Dong W, Zhang J, Yin C, Hale J, Baines AJ, Mohandas N, An X. A 130-kDa protein 4.1B regulates cell adhesion, spreading, and migration of mouse embryo fibroblasts by influencing actin cytoskeleton organization. *J Biol Chem*. 2014;289:5925-5937. doi: 10.1074/jbc.M113.516617
32. Fuchs M, Kugelmann D, Schlegel N, Vielmuth F, Waschke J. Desmoglein 2 can undergo Ca(2+)-dependent interactions with both desmosomal and classical cadherins including E-cadherin and N-cadherin. *Biophys J*. 2022;121:1322-1335. doi: 10.1016/j.bpj.2022.02.023
33. Garrod DR, Fleming S. Early expression of desmosomal components during kidney tubule morphogenesis in human and murine embryos. *Development*. 1990;108:313-321. doi: 10.1242/dev.108.2.313
34. Gong Y, Sunq A, Roth RA, Hou J. Inducible Expression of Claudin-1 in Glomerular Podocytes Generates Aberrant Tight Junctions and Proteinuria through Slit Diaphragm Destabilization. *J Am Soc Nephrol*. 2017;28:106-117. doi: 10.1681/asn.2015121324
35. Ohse T, Chang AM, Pippin JW, Jarad G, Hudkins KL, Alpers CE, Miner JH, Shankland SJ. A new function for parietal epithelial cells: a second glomerular barrier. *Am J Physiol Renal Physiol*. 2009;297:F1566-1574. doi: 10.1152/ajprenal.00214.2009
36. Chen X, Tong C, Li H, Peng W, Li R, Luo X, Ge H, Ran Y, Li Q, Liu Y, et al. Dysregulated Expression of RPS4Y1 (Ribosomal Protein S4, Y-Linked 1) Impairs STAT3 (Signal Transducer and Activator of Transcription 3) Signaling to Suppress Trophoblast Cell Migration and Invasion in Preeclampsia. *Hypertension*. 2018;71:481-490. doi: 10.1161/hypertensionaha.117.10250
37. Li Y, Kang YS, Dai C, Kiss LP, Wen X, Liu Y. Epithelial-to-mesenchymal transition is a potential pathway leading to podocyte dysfunction and proteinuria. *Am J Pathol*. 2008;172:299-308. doi: 10.2353/ajpath.2008.070057
38. Okamoto T, Seo H, Mano H, Furuhashi M, Goto S, Tomoda Y, Matsui N. Expression of human placenta alkaline phosphatase in placenta during pregnancy. *Placenta*. 1990;11:319-327. doi: 10.1016/s0143-4004(05)80223-1
39. Adeniyi FA, Olatunbosun DA. Origins and significance of the increased plasma alkaline phosphatase during normal pregnancy and pre-eclampsia. *Br J Obstet Gynaecol*. 1984;91:857-862. doi: 10.1111/j.1471-0528.1984.tb03697.x
40. Uyanikoglu H, Turp AB, Hilali NG, Incebiyik A. Serum endothelin-1 and placental alkaline phosphatase levels in placenta percreta and normal pregnancies. *J Matern Fetal Neonatal Med*. 2018;31:777-782. doi: 10.1080/14767058.2017.1297412
41. Sharma U, Pal D, Prasad R. Alkaline phosphatase: an overview. *Indian J Clin Biochem*. 2014;29:269-278. doi: 10.1007/s12291-013-0408-y
42. Millán JL. Alkaline Phosphatases : Structure, substrate specificity and functional relatedness to other members of a large superfamily of enzymes. *Purinergic Signal*. 2006;2:335-341. doi: 10.1007/s11302-005-5435-6
43. Pfleiderer G, Mössner E, Schenk R. Alkaline phosphatase isoenzymes in human kidney and urine, immunohistochemical, immunological and biochemical characterization. *Histochemistry*. 1984;80:145-148. doi: 10.1007/bf00679988
44. Buchet R, Millán JL, Magne D. Multisystemic functions of alkaline phosphatases. *Methods Mol Biol*. 2013;1053:27-51. doi: 10.1007/978-1-62703-562-0_3

45. Zhang D, Ma C, Sun X, Xia H, Zhang W. S100P expression in response to sex steroids during the implantation window in human endometrium. *Reprod Biol Endocrinol*. 2012;10:106. doi: 10.1186/1477-7827-10-106
46. Prica F, Radon T, Cheng Y, Crnogorac-Jurcevic T. The life and works of S100P - from conception to cancer. *Am J Cancer Res*. 2016;6:562-576.
47. Du M, Wang G, Ismail TM, Gross S, Fernig DG, Barraclough R, Rudland PS. S100P dissociates myosin IIA filaments and focal adhesion sites to reduce cell adhesion and enhance cell migration. *J Biol Chem*. 2012;287:15330-15344. doi: 10.1074/jbc.M112.349787
48. Toma-Fukai S, Shimizu T. Structural Diversity of Ubiquitin E3 Ligase. *Molecules*. 2021;26. doi: 10.3390/molecules26216682
49. Zhang J, Cao L, Wang X, Li Q, Zhang M, Cheng C, Yu L, Xue F, Sui W, Sun S, et al. The E3 ubiquitin ligase TRIM31 plays a critical role in hypertensive nephropathy by promoting proteasomal degradation of MAP3K7 in the TGF-β1 signaling pathway. *Cell Death Differ*. 2022;29:556-567. doi: 10.1038/s41418-021-00874-0
50. Chen Q, Gao C, Wang M, Fei X, Zhao N. TRIM18-Regulated STAT3 Signaling Pathway via PTP1B Promotes Renal Epithelial-Mesenchymal Transition, Inflammation, and Fibrosis in Diabetic Kidney Disease. *Front Physiol*. 2021;12:709506. doi: 10.3389/fphys.2021.709506

CHAPTER 5

Final Discussion

Table of Contents

5.1 Final summary....216
5.2 Limitations....218
5.3 Future studies....219
5.4 A step forward....221
5.6 Final discussion....229
5.7 Reference....230

5.1 Final summary

In this thesis, I investigated several aspects related to placental small extracellular vesicle (psEV): 1) the levels of psEV in normal pregnant and preeclamptic women from the first to the third trimester quantified by a novel EV quantification device called ExoCounter; 2) the effects of psEV on renal functions through podocytes view in normal pregnant and preeclamptic women; 3) the bioinformatic identification of proteins responsible for influencing podocyte functions by psEV from normal pregnant and preeclamptic women.

Chapter 1 provides a comprehensive review of the literature on extracellular vesicles, preeclampsia, and renal functions in normal pregnancy and preeclampsia. This chapter summarizes the current understanding of the biogenesis of EV and their uptake by recipient cells. Additionally, I examined common and innovative EV isolation and characterization methods. Furthermore, it delves into the renal functions and pathology observed in both normal pregnant individuals and those with preeclampsia, exploring the potential mechanisms through which placenta-derived EV may impact the integrity of the glomerular filtration barrier.

Chapter 2 investigates the diagnostic potential of psEV in early-onset preeclampsia patients (EOPE) using a novel device called ExoCounter. I compared the levels of three pairs of psEV markers—CD10-CD63, CD10-PLAP, and CD63-PLAP—in normal pregnancy (NP), late-onset preeclampsia (LOPE), and EOPE. Interestingly, the levels of CD10-PLAP and CD63-PLAP psEV were elevated from the first trimester of pregnancy in EOPE compared to NP. These findings offer potential mechanisms for implementing prophylactic measures such as aspirin therapy for EOPE patients before the disease manifests.

Chapter 3 primarily focuses on the impact of psEV on renal cells, specifically human podocytes. This began with determining whether psEV can pass through the glomerular filtration barrier and interact with podocytes. After confirming this, I employed three different methods (flow cytometry, imaging, qPCR) to verify the internalization of psEV by podocytes in vitro. psEV from NP increased nephrin expression, migration ability, and enhanced cytoskeleton staining in podocytes, suggesting improved podocyte function in NP. In contrast, psEV from PE did not enhance nephrin expression and migration ability, while adhesion ability was impaired, suggesting diminished podocyte function in PE.

Chapter 4 utilizes bioinformatics to analyse proteomic changes in podocytes influenced by psEV. The presence of placental proteins (e.g., PLAP and S100P) in podocytes further confirmed the internalization of psEV by podocytes by mass spectrometry and western blot. Additionally, proteins potentially responsible for enhanced podocyte migration ability after NP psEV treatment (e.g., RAB3A and SERPINE1) and reduced podocyte adhesion ability after PE psEV treatment (e.g., ACTN4 and EPB41L3) were identified. These responsible proteins offer new insights into the pathology of podocytes in preeclampsia.

In conclusion, I have explored the roles of psEV in maternal circulation, focusing on their impact on renal functions in NP and PE. These findings provide insight into the pathology of psEV in PE and guidance for early intervention in PE.

5.2 Limitations

There are several limitations of the current studies.

First, the sample size is small. For the ExoCounter study in Chapter 2, I examined serum from 9 NP, 7 EOPE and 8 LOPE patients. Increasing the sample size is challenging due to several factors. First, the incidence rate of EOPE and LOPE is low, with EOPE occurring in 0.38% and LOPE in 5% of all pregnancies[1]. Second, the study required sample collection before the onset of the disease. This necessitated collecting samples at the beginning of gestation and then retrospectively identifying the appropriate samples after delivery. The number of samples I could use was limited by the biobank's availability. For the podocyte study in Chapters 3 and 4, I examined 3 psEV samples from NP perfusion and 3 psEV samples from PE perfusion. The number of perfusion samples is limited by placental availability and the perfusion success rate. PE placentas are smaller with thinner blood vessels compared to NP placentas, making PE placenta perfusion more challenging.

Second, the experiments investigating the influence of PE and NP psEV on podocytes were *in vitro*, which may not accurately reflect *in vivo* podocyte behaviour. Additionally, the podocytes used were immortalized and transfected with a temperature-sensitive SV40 construct, potentially behaving differently than in vivo podocytes. It is crucial to determine whether the *in vitro* findings in this thesis can be replicated in an *in vivo* system. Apart from *in vivo* systems, organoids are another popular approach for studying the pathology of psEV on podocytes.

Third, a co-culture system of podocytes with glomerular endothelial cells might better represent the *in vivo* glomerular filtration barrier (GFB). To maintain the barrier functions,

podocytes continuously work with glomerular endothelial cells, and cross-communication is essential. Investigating the influence of psEV on a co-culture system of glomerular endothelial cells and podocytes could yield interesting insights.

5.3 Future studies

There are several directions for the future studies of this current thesis.

First, regarding the findings of higher CD10-PLAP and CD63-PLAP psEV counts in EOPE patients compared to NP from the first trimester in Chapter 2, it is desirable to recruit more patients and increase the sample size through multicentre collaboration. If these findings can be validated in large cohort studies, incorporating early pregnancy psEV detection could help doctors identify high-risk pregnancies and implement prophylactic measures. Additionally, it would be intriguing to explore whether the elevated psEV counts found in blood samples can also be detected in urine samples from EOPE patients. Comparing blood and urine profiles may reveal the population of psEV absorbed by the maternal system, potentially shedding light on the pathology of PE.

Second, as mentioned in the limitations, investigating the findings in an in vivo system or using 3D spheroids, which better mimic in vivo conditions than 2D culture systems, would be interesting. Conducting in vivo experiments with animals can be expensive, time-consuming, and labour-intensive. Consequently, a 3D culture system appears to be a suitable alternative since it can more closely resemble the physiological conditions observed in vivo.

Third, I have identified potential key proteins that may play a crucial role in regulating podocyte functions after being treated with NP and PE psEV, particularly those associated with podocyte migration and adhesion abilities. Conducting knockdown or knockout experiments in future studies could offer more insights into the functions of these proteins.

Lastly, incorporating glomerular endothelial cells into future research would be valuable. Since psEV first interact with glomerular endothelial cells in circulation, it is essential to comprehend the overall impact of psEV on both glomerular endothelial cells and podocytes as a more comprehensive system.

5.4 A step forward

3D culture is a promising approach for studying cell functions, and a 3D co-culture system that includes both glomerular endothelial cells (GEnCs) and podocytes is crucial for examining the glomerular filtration barrier (GFB). To this end, I have already begun establishing a 3D co-culture renal system that incorporates both GEnCs and podocytes. In this system, both podocytes and GEnCs were treated with NanoShuttle-PL beads (Greiner Bio-One) to magnetize the cells by electrostatically attaching them to the cell membrane. Cell spheroids can then be formed under the magnetic force (Figure 1). In this system, introducing one type of cell first and another type later allows for the manual adjustment of cell positions in the final spheroid formation. For instance, by adding podocyte first and then adding GEnCs subsequently to the system, spheroids with podocytes on the inside and GEnCs on the outside can be created (Figure 1). As observed in brightfield microscope images, these co-culture renal spheroids gradually transform from loose spheroids to condensed ones over 10 days of differentiation (Figure 2).

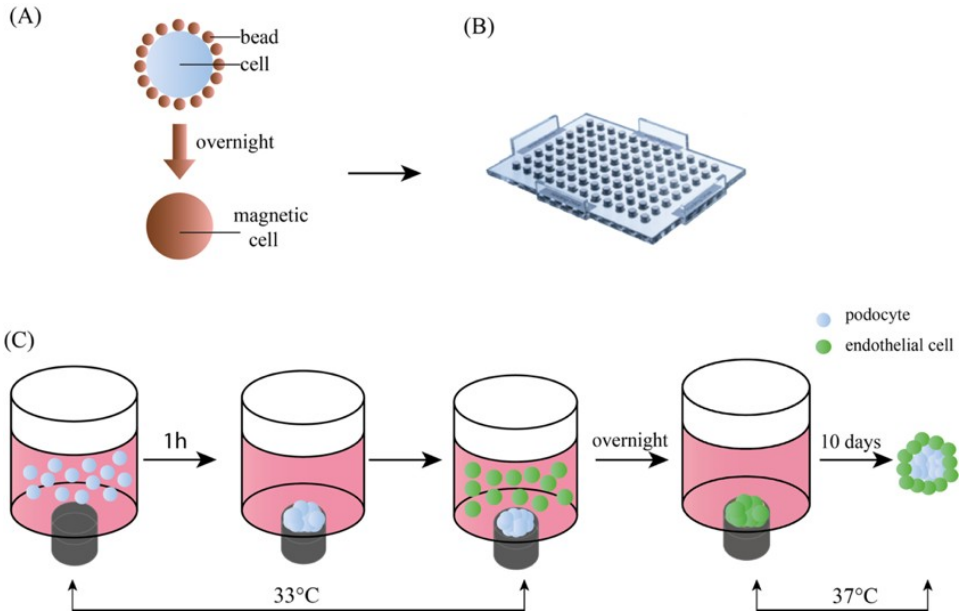


Figure 1. (A) The schematic illustration of the magnetic 3D cell formation. Cells are electrostatically coated with magnetic beads overnight. The cells are then trypsinized and seeded on the 96-well plate with the magnet (B) underneath. (C) The illustration of forming podocytes inside and GEnCs outside spheroids. The magnetised podocytes are first seeded to form spheroids, and after 1h's settling down, the magnetised GEnCs are slowly added to cover the outside of the podocytes. The initial co-culture spheroids formation is carried under 33°C and after the formation, the spheroids are transferred to 37°C to allow the differentiation.

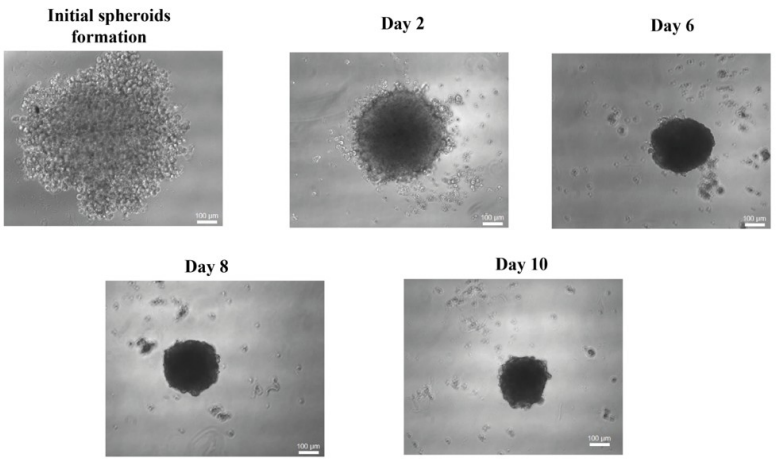


Figure 2. The representative brightfield microscope pictures of the renal co-culture spheroids formation from undifferentiated status to 10 days' differentiation. The spheroids were formed as podocytes inside and GEnCs outside.

Subsequently, I aimed to further investigate the composition of renal spheroids after formation and differentiation using podocyte and GEnC-specific markers through immunocytochemistry. To carry out this experiment, I first needed to identify representative markers for podocytes and GEnCs and ensure they would not exhibit cross-expression. I selected synaptopodin, nephrin, WT-1, and podocin as podocyte-specific markers, and CD31 as the GEnC-specific marker. After checking the expression of these makers on GEnCs and podocytes, I found CD31 was exclusively expressed in GEnCs, with no expression found in podocytes (Figure 3A). However, all the podocyte-specific markers were expressed in GEnCs, indicating podocyte contamination in the GEnC population (Figure 3A).

Given that CD31 effectively distinguished podocytes from GEnCs, I then examined the GEnCs population stained with CD31 to identify any population lacking CD31 expression which could indicate contamination by podocytes. Interestingly, flow cytometry analysis revealed the presence of three distinct populations: dim-CD31, medium-CD31, and bright-CD31 (Figure 3B). Through cell sorting, I isolated the bright-CD31 population (representing GEnCs) and investigated whether this population still exhibited podocyte-specific markers. Although the bright-CD31 population continued to express synaptopodin and nephrin, WT-1 and podocin were absent. Given that WT-1 expression is typically low in differentiated podocytes, podocin was ultimately chosen as the podocyte-specific marker.

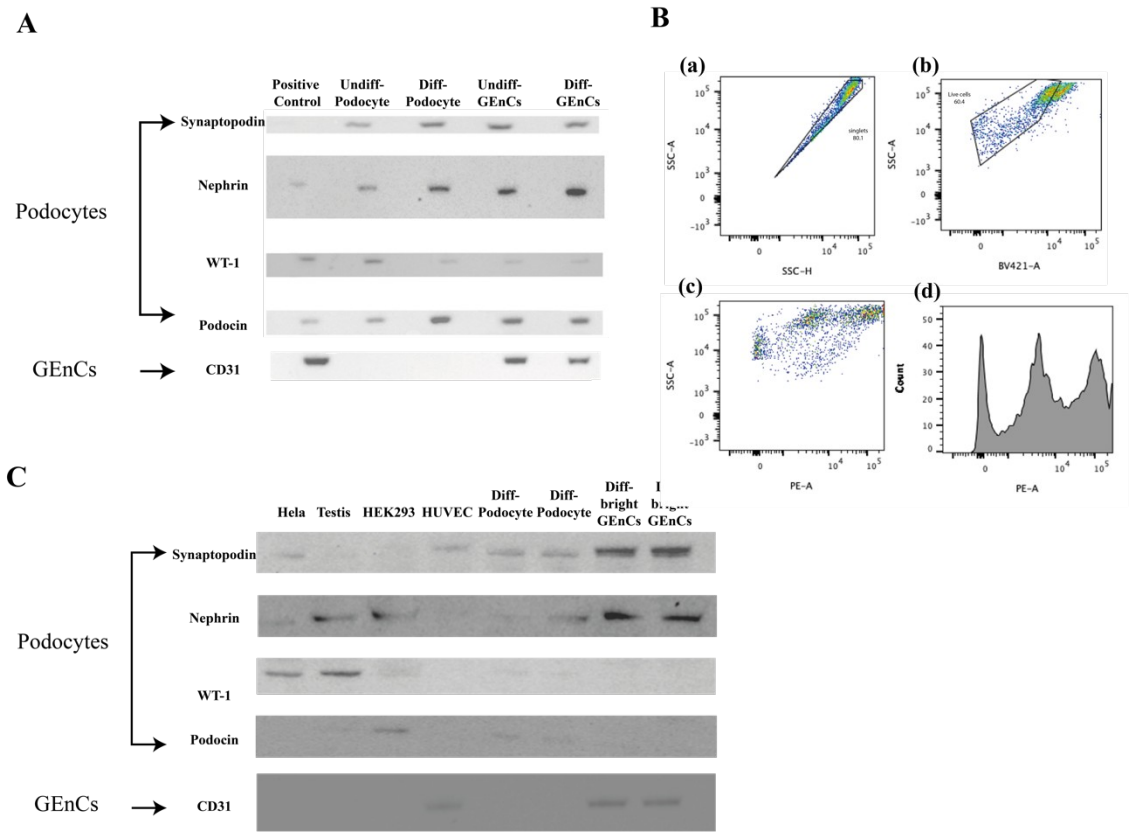


Figure 3. (A) The expression of podocyte-specific and GEnCs-specific markers on undifferentiated podocytes (undiff-podocyte), differentiated podocytes (diff-podocyte), undifferentiated GEnCs (undiff-GEnCs) and differentiated GEnCs (diff-GEnCs). (B) The GEnCs population was stained with CD31 (PE) and Live-dead-cell staining (BV421-A). The singlets of GEnCs were first gated (a), following by gating the live cells (b), and finally 3 populations of GEnCs (dim, medium and bright) were identified (c). The same results of the histogram were in (d). (C) The expression of podocyte-specific and GEnCs-specific markers on differentiated podocytes and differentiated GEnCs after cell sorting. The positive control for synaptopodin was Hela cell lysate, the positive control for Nephrin, WT-1 and podocin were HEK293 cell lysate and testis tissue lysate, the positive control for CD31 was HUVEC cell lysate.

After verifying that podocin was a suitable marker for podocytes and CD31 for GEnCs, I proceeded to stain the complete spheroids using these two markers to understand their structures. I constructed two types of spheroids. The first type (GEnCs-in) involved forming GEnC spheroids initially and then adding podocytes on the outside. This design was considered more physiological, as podocytes naturally surround and wrap around GEnCs in vivo. The second type (Podo-in) involved forming podocyte spheroids first and then adding GEnCs on the outside. This type was constructed because, when treating the renal coculture spheroids with psEV, the psEV would first encounter the GEnCs, better mimicking the actual in vivo situation. For simplicity, I will refer to the first type of spheroids as GEnCs-in spheroids and the second type as Podo-in spheroids in the following thesis.

Interestingly, after 10 days of differentiation and staining these two types of spheroids with CD31, podocin, and DAPI, I observed a well-defined spheroid/round structure of GEnCs (red) encircled by podocytes (green) in the GEnCs-in spheroid (Figure 4A). However, in the Podo-in spheroid, I did not observe a distinct podocyte round structure (green) at the centre of the spheroid surrounded by GEnCs (red). Instead, I noticed GEnCs (red) moving toward the centre of the spheroids and a mixture of podocytes and GEnCs (red + green = yellow) on the outer part of the spheroids (Figure 4B). These results suggested that GEnCs prefer to be surrounded by podocytes after differentiation, which more closely resembles the in vivo system. Even when GEnCs were initially placed on the outside of podocytes, they tended to move inwards as differentiation progressed.

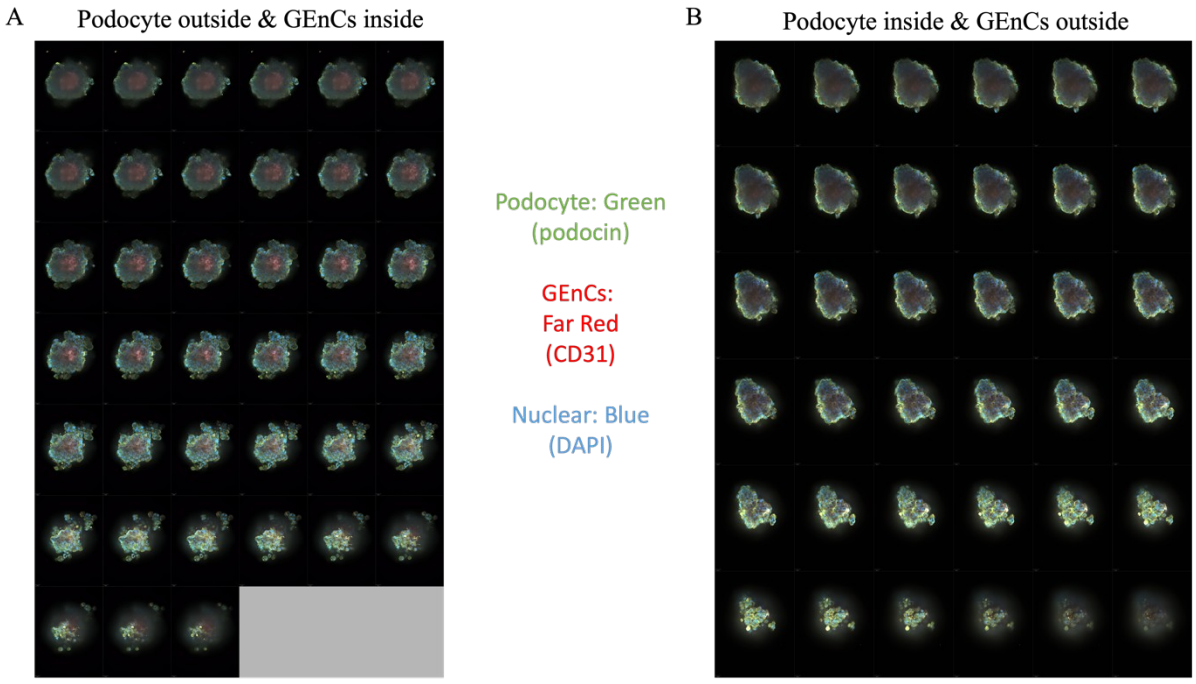


Figure 4. The representative z-stack confocal microscope picture of the whole spheroid after 10 days of differentiation. (A) The initial spheroids formation was done by forming GEnCs spheroids first and then adding podocytes to the outside of the spheroids. (B) The initial spheroids formation was done by forming podocytes spheroids first and then adding GEnCs to the outside of the spheroids. The green colour is podocin which represents podocytes, the far-red colour is CD31 which represents GEnCs, the blue colour is the nuclear stained with DAPI. Each z-stack image was 1mm deeper than the previous one.

After examining the complete staining of these two types of spheroids, I wanted to further investigate whether the GEnCs-in spheroids could more accurately represent the GFB by forming characteristic structures such as blood vessel lumens. I performed cryosectioning on the GEnCs-in spheroids, and the cell morphology appeared different compared to the 2D culture (Figure 5A). Upon staining with DAPI, I observed several lumens without cells (Figure 5B, indicated by the red arrows). Further staining the sections with CD31 revealed continuous staining that formed blood vessel lumen-like structures (Figure 5C). These

findings suggested that GEnCs-in spheroids have the potential to closely resemble the *in vivo* appearance of the GFB.

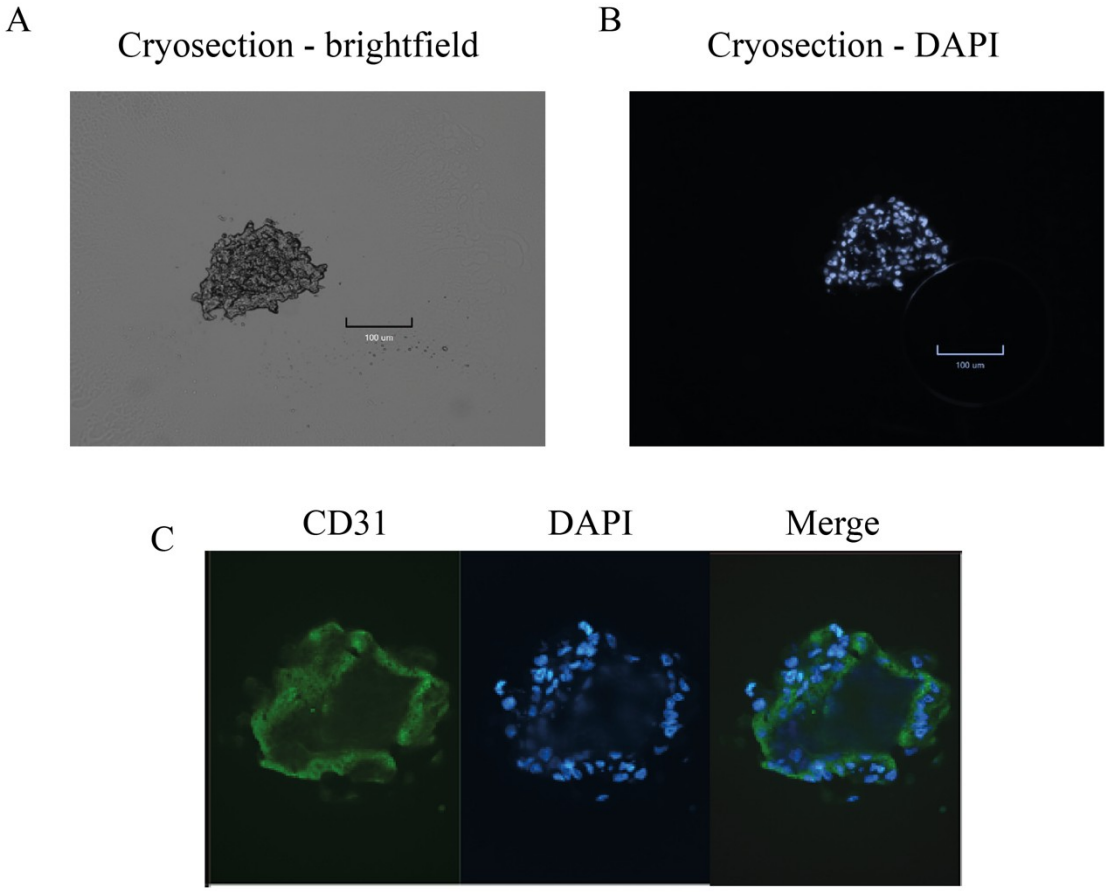


Figure 5. The representative brightfield image of the cryosection of the GEnCs-in spheroids (A) and with the DAPI staining (B), the lumen formed without cells were indicated by the red arrows. (C) The CD31 (green) and DAPI (blue) staining of the section. The section is 3mm thick.

In summary, I have demonstrated that GEnCs-in spheroids are potentially a more reliable model for representing the GFB compared to Podo-in spheroids. Notably, GEnCs-in spheroids have shown the capability to form structures resembling blood vessel lumens post-formation. However, it's important to consider the possibility that this structure may have emerged due to cell death in the central region of the spheroids. Further investigation is

warranted to fully understand this phenomenon. These spheroids have additional advantages, such as allowing the differentiation of podocytes and GEnCs together, which increases the likelihood of creating the basement membrane in the GFB. Moreover, this culture system enables the spheroids to produce their own extracellular matrix, rather than manually introducing it, as in other Matrigel-based 3D culture system[2].

There are other important aspects of GEnCs-in spheroids that can be tested in future research to determine if their performance surpasses that of 2D culture. For instance, it is crucial to evaluate basement membrane formation between GEnCs and podocytes. The permeability of the spheroids can also be assessed to determine if they accurately represent the *in vivo* GFB. Methods for evaluating spheroid permeability have been developed[3]. Other cell-specific functions, such as podocyte degradation of albumins, can also be assessed[4]. More importantly, the transcriptomics and proteomics profile of the spheroids can be compared to the GFB isolated from the human tissue.

There are, however, several technical challenges must be addressed before using GEnCs-in spheroids for testing the effects of psEV. For example, the inaccessibility of psEV treatment to GEnCs by simply adding psEV to the spheroid culture medium is a concern. As GEnCs are located in the inner core of GEnCs-in spheroids, any treatment applied through the culture medium will first interact with podocytes, deviating from the in vivo system. This can be overcome by micro-injection of psEV directly to the lumen of the spheroids[5]. However, this invasive approach may cause non-negligible damage to the spheroids. Using other 3D culture systems with the accessibility to lumen could be an alternative solution. For instance, the microfluidic system 3D culture systems[6] or culture cells using a scaffold[7] may enable easy access to the lumen surface.

5.6 Final discussion

The research conducted in this thesis has contributed to a deeper understanding of psEV in preeclampsia. I have demonstrated the diagnostic potential of psEV in preeclampsia and provided comprehensive methods to achieve this goal. Additionally, I have investigated the effects of NP and PE psEV on podocyte functions, which may shed light on future therapeutic targets aimed at improving maternal and fetal outcomes. Lastly, I have examined the feasibility of a 3D co-culture system involving glomerular endothelial cells and podocytes, with the hope that this work will serve as a solid foundation for further research.

5.7 Reference

1. Lisonkova S, Joseph K. Incidence of preeclampsia: risk factors and outcomes associated with early-versus late-onset disease. *American journal of obstetrics and gynecology*. 2013;209:544. e541-544. e512.
2. Habanjar O, Diab-Assaf M, Caldefie-Chezet F, Delort L. 3D Cell Culture Systems: Tumor Application, Advantages, and Disadvantages. *Int J Mol Sci*. 2021;22. doi: 10.3390/ijms222212200
3. Cho CF, Wolfe JM, Fadzen CM, Calligaris D, Hornburg K, Chiocca EA, Agar NYR, Pentelute BL, Lawler SE. Blood-brain-barrier spheroids as an in vitro screening platform for brain-penetrating agents. *Nat Commun*. 2017;8:15623. doi: 10.1038/ncomms15623
4. Carson JM, Okamura K, Wakashin H, McFann K, Dobrinskikh E, Kopp JB, Blaine J. Podocytes Degrade Endocytosed Albumin Primarily in Lysosomes. *PLOS ONE*. 2014;9:e99771. doi: 10.1371/journal.pone.0099771
5. Puschhof J, Pleguezuelos-Manzano C, Martinez-Silgado A, Akkerman N, Saftien A, Boot C, de Waal A, Beumer J, Dutta D, Heo I, et al. Intestinal organoid cocultures with microbes. *Nat Protoc*. 2021;16:4633-4649. doi: 10.1038/s41596-021-00589-z
6. Lee HN, Choi YY, Kim JW, Lee YS, Choi JW, Kang T, Kim YK, Chung BG. Effect of biochemical and biomechanical factors on vascularization of kidney organoid-on-a-chip. *Nano Converg*. 2021;8:35. doi: 10.1186/s40580-021-00285-4
7. Wang Y, Gunasekara DB, Reed MI, DiSalvo M, Bultman SJ, Sims CE, Magness ST, Allbritton NL. A microengineered collagen scaffold for generating a polarized crypt-villus architecture of human small intestinal epithelium. *Biomaterials*. 2017;128:44-55. doi: https://doi.org/10.1016/j.biomaterials.2017.03.005

Appendix

List of Publications

Published Papers

- **Jiang S**, Zhang W, Cao Q, Rahbar M, Cooke W, Ono M, Fujimaki K, Saito A, Itonaga M, Oda K, Redman C, Vatish M. ExoCounter Assays Identify Women Who May Develop Early-Onset Preeclampsia From 12.5 µL First-Trimester Serum by Characterizing Placental Small Extracellular Vesicles. Hypertension. 2023 May 25. doi: 10.1161/HYPERTENSIONAHA.123.20907. Epub ahead of print. PMID: 37226734.
- Awoyemi T, Cerdeira AS, Zhang W, **Jiang S**, Rahbar M, Logenthiran P, Redman C, Vatish M. Preeclampsia and syncytiotrophoblast membrane extracellular vesicles (STB-EVs). Clin Sci (Lond). 2022 Dec 22;136(24):1793-1807

Submitted Patent

- **Jiang S**, Vatish M, Zhang W, Ono M, Fujimaki K, Saito A, Itonaga M, Oda K. (2023). First trimester prediction of early-onset preeclampsia by quantifying small extracellular vesicles from plasma and serum via ExoCounter using CD63, CD10 and placental alkaline phosphatase as specific biomarkers. UK Intellectual Property Office.

Submitted Manuscript

- Awoyemi T, **Jiang S**, Bjarakadottir, Rahbar M, Lognetherian P, Fischer, Colette G, Zhang W, Cerdeira S, Redman C, and Vatish M. Identification of novel preeclampsia biomarkers through protemics anaylsis of placenta derived extracellular vesicles. AJOG (submitted in April 2023)

Conference Abstracts

- **Jiang S**, Chen Q, et al. Characterisation of urine small extracellular vesicles from normal pregnancy and early-onset preeclampsia. 2nd Virtual Symposium on Urinary Extracellular Vesicles-uEVs 2023
- **Jiang S**, Awoyemi T, et al. The Influence of normal and preeclamptic syncytiotrophoblast extracellular vesicles on Human podocytes. Kidney Week, American Society of Nephrology, 2022
- **Jiang S**, Awoyemi T, et al. Syncytiotrophoblast Extracellular Vesicles Can Be Internalized by Podocytes and Influence Their Functions. 13th International Podocyte Conference, University of Manchester 2021